Immune and microbiota contributions to age-related intestinal decline

JEANETTE ALCARAZ

Immune and microbiota contributions to age-related intestinal decline

Jeanette Alcaraz

Submitted in accordance with the requirements

for the degree of Doctor of Philosophy

Department of Biosciences

Durham University

April 2022

Abstract

Deterioration of the innate immune system is generally accepted as a hallmark of aging. As a consequence of immune dysregulation, the host is not able to reliably fight infection or retain a symbiotic relationship with gut microbes. Individuals diagnosed with immune-related pathologies demonstrate gut microbial imbalances, or dysbiosis, as well as a decline in immune cell function. Additionally, aging significantly contributes to immune cell decline. Studies in adult *Drosophila melanogaster* have reported age-related dysbiosis as a primary driver of immune dysfunction. The objective of this thesis is to better understand how specific physiological changes, namely microbial imbalance, and immune dysfunction, along the aging intestine affect gut and host health. Here, my data demonstrates that the consequences of chronic immune activation, in particular microbial imbalance and changes in immune cell number and function, are closely associated with immune-induced intestinal permeability. This adds weight to recent published work across multiple model organisms that highlights the key role of intestinal barrier loss as a driver of age-related decline. Detailed insight into the immune factors that drive intestinal barrier loss and how this drives age-associated decline in immune function, for example changes in macrophages, could lead to the development of immune-targeted antiaging therapies.

Table of Contents

List of Figures

List of Tables

List of Abbreviations

A. pas	*Acetobacter pasteurianus*
act	Actin
AiP	apoptosis-induced proliferation
AJs	adherens junctions
Alpha	Alphaproteobacteria
AMP	antimicrobial peptide
arm	armadillo
BBG	big bang gene
BODIPY	Boron-dipyrromethene dyes
bsk	basket
CCR	copper cell region
da	daughterless
DAP	diaminopimelic acid-type peptidoglycan
DE-cad	Drosophila E-Cadheren
Dipt/Dpt	diptericin
Dlg-1	Discs Large-1
Dome	domeless
Dros/Drs	drosomycin
DUOX	Dual Oxidase
E. coli	*Escherichia coli*
EB	enteroblast
EC	enterocyte
EE	enteroendocrine
EGF	epidermal growth factor
EGFR	epidermal growth factor receptor
FACS	fluorescence-activated cell sorting
FISH	fluorescence in situ hybridization
Gamma	*Gammaproteobacteria*
GMR	glass multiplier reporter
GS	GeneSwitch
hml	hemolectin
HOCl	hypochlorous acid
IMD	Immune Deficiency Pathway
IPT	ion transport protein
ISC	intestinal stem cell
Jak/STAT	Janus Kinase/Signal Transducer and Activator of Transcription
JNK	Jun N-terminal Kinase
kune	Kune-Kune
L. plant.	*Lactobacillus plantarum*
LB	Luria-Bertani agar
MAGUK	*membrane-associated guanylate kinase*

MARCM	mosaic analysis with a repressible cell marker
MRS	De Man, Rogosa and Sharpe agar
NADPH	reduced nicotinamide adenine dinucleotide phosphate
NF-kB	nuclear factor kB
Non-SMF	non-Smurf
NOX	NADPH oxidase
PBS	phosphate buffered saline
pck	Pickel
Pdm1/nub	POU-domin homeobox transcription factor/nubbin
PGRP	Peptidoglycan Recognition Protein
PH3	phosphorylated histone-3
puc	puckered
pyd	polychaetoid
rel	relish
rho	rhomboid
ROS	Reactive Oxygen Species
rpr	reaper
RU-486	mifepristone
sinu	Sinuous
SJs	septate junctions
SMF	Smurf
Sox21a	SRY-box 21a
srp	serpent
ssk	snakeskin
Su[H]	notch-suppresor of hairless
TCJ	tricellular junction
tk	tachykinin
Tsp2A	tetraspanin2A
TURD	The Ultimate Reader of Dung
UAS	Upstream Activating Sequence
upd	Unpaired
ZO-1	zonula adherens-1

Declaration

I hereby attest that the works included in this thesis are original and were performed by me as part of my doctoral training and degree. Where any exception exists, it has been clearly marked. Work previously performed during my Master of Science Degree at the University of California, Los Angeles is summarized in Chapter 3 of this dissertation. It has been clearly distinguished from my doctoral work and was included as it gives foundational context for my PhD project at Durham University. The complete citation for my referenced Master of Science thesis is as follows:

Alcaraz, J. (2016). Microbiota and immune contributions to age-related intestinal decline. UCLA. ProQuest ID: Alcaraz_ucla_0031N_14798. Merritt ID: ark:/13030/m5vq7q89. Retrieved from https://escholarship.org/uc/item/0mh6n0z1

Funding

My doctoral work was funded by the Durham Doctoral Studentship (DDS).

Acknowledgments

I'd like to begin by thanking my supervisor, Rebecca Clark. It has been a privilege to work beside and learn from you for the better part of a decade. Thank you for trusting me with all-things science, it gave me the courage to trust myself. I'd also like to thank my secondary supervisors, David Doupé and David Weinkove. To David Doupé thank you for always being so generous with your time and support. To David Weinkove thank you for welcoming me to Durham with a smile and for all your kindness over the years.

To fellow founding member of Lab 20, Abbi Abigail. There are few people who will ever understand this journey, I can't tell you how grateful I am to have shared it with you.

My experience at Durham would not have been the same without past members of the Weinkove group - Sushmita, Claire and Kasia. To Sush, thank you for being my safe place in the department, for all the chocolate, hugs, and encouragement. To Claire and Kasia, my daisy roses, thank you for adopting me into the Kirkwood family, and rejuvenating my spirit with dinners, dancing, and lots of laughs.

Thank you to my partner in life, Car. My love, I am writing this and here in large part because of your unwavering love and support. Thank you for the 4 a.m. drives to the lab, for sitting with me for hours when I only had to 'pop in for a bit', for helping me navigate this experience from start to finish. Bees and Trees forever.

Last, but certainly not least, I'd like to thank my entire family. Your love has gotten me here. Especially to Kosa and Keek, thank you for being so wonderfully weird, for accepting and unconditionally loving and supporting me. This win is for all of us!

Chapter 1: Thesis Introduction

1.1 Microbiota and immune contributions to age-related intestinal decline

The human microbiota encompasses populations of microorganisms that live on and in human organ systems. Importantly, a large proportion of the microbiota lies in the digestive tract. Gut microbes facilitate beneficial, and necessary, metabolic and protective processes within their host (Sommer and Bäckhed, 2013). Deregulation of gut microbial load has been correlated with inflammatory disorders and changes in intestinal physiology (Sommer and Bäckhed, 2013). There are several factors which can influence gut microbiota composition in mammalian systems (Bischoff, 2016, Claesson et al., 2012). For example, mild or extended use of antibiotics can drastically change microbial populations in the gut. Importantly, physiological aging is an evolutionarily conserved process where intestinal bacterial load and composition changes in invertebrates (Clark et al., 2015, Guo et al., 2014) and humans alike (Claesson et al., 2012, Claesson et al., 2010). Both naturally occurring and lifestyle-related changes in microbial composition are critically important. Natural physiological changes, such as aging, and lifestyle decisions, such as diet and exercise, can facilitate critical changes in microbial composition. Thus, regulation of microbial populations is highly important, as bacteria help to maintain organismal health.

Recently, the human microbiome has become an intriguing and highly sought area of research. The Human Microbiome Project has paved the way for science to start asking pertinent questions regarding mammals' invaluable symbiotic community (Heintz and Mair, 2014, Cho and Blaser, 2012). Apart from pathogens, it is widely accepted that host microbes are beneficial to overall physiology. Human studies have revealed that microbes affect host physiology and directly contribute to the pathophysiology of aging (Heintz and Mair, 2014). However, microbes are often classified as either pathogenic or symbiotic (Heintz and Mair,

2014). By categorizing most gut microbes as commensal (neutral) researchers may be able to better understand how the microbial environment, and microbes themselves, can facilitate aging interventions. However, bacterial mechanisms inside mammals remain to be well understood. Microbial colonization, alongside microbial changes, are difficult to characterize and define in vivo (Heintz and Mair, 2014). Mammalian models and human systems prove to be challenging study systems, due to their complexity. For these reasons, ascertaining causal mechanisms becomes technically difficult and expensive in higher order organisms (Cho and Blaser, 2012). Thus, the fruit fly, *Drosophila melanogaster*, provides an avenue through which the relationship between host, microbiome, and age-related pathologies can be studied intricately and simply.

Currently, we understand that age-related changes in gut microbiota are a primary source of immune activation in flies and in humans (Clark et al., 2015, Claesson et al., 2012). However, the cause-effect relationships between microbiota dynamics, immune activity, and changes in intestinal health remain unknown. This introduction chapter aims to consolidate and discuss research findings pertaining to age-related intestinal decline, microbial imbalance, and age-related immune activation which ultimately lead to organismal decline. Although not comprehensive, studies discussed will facilitate a general understanding of the chosen model organism and findings that have aided in understanding host-microbe homeostasis. Taken together, the studies discussed here will highlight current understandings in the field of aging and future work still needed to further understand microbial and immune pathway dynamics. Future experimental findings may help facilitate the development of interventions which delay age-related decline.

1.1.1 The fly as a model for host-microbe interactions

The power of *D. melanogaster* as a model organism comes from its genetic tractability, a simple but variable microbiome, and its relatively short lifespan. Although less complex than mammalian model systems, *Drosophila* still possesses homologous immune and metabolic pathways, receptors, and morphological traits consistent with those of higher order organisms. The bacterial communities inhabiting the *Drosophila* intestine fall into three major cohorts: Firmicutes, and the alpha and gamma classes of phyla Proteobacteria (Erkosar et al., 2013). These phyla are found in both flies and humans. Much like we see in humans, fly gut microbiota is also very dynamic and subject to change between differing environments, diets, and genetic backgrounds (Clark et al., 2015, Sommer and Bäckhed, 2013, Scott et al., 2013, Claesson et al., 2012, Ren et al., 2007). The ease and diversity of techniques afforded with *Drosophila*, allows for mechanistic research findings to be further tested in mammalian model systems.

1.1.2 Dietary effects on bacterial populations

Diet has a massive impact on microbiota composition. Human clinical trials have shown that from birth, formula versus breast-feeding dictates infant development of gut microbe communities (Roger and McCartney, 2010). Studies in the elderly population have also shown that living environment dictates diet (Claesson et al., 2012). Elderly individuals living in long-term assisting housing are more likely to show decreased diversity in microbiota, later correlated with an increase in inflammation (Claesson et al., 2012). In the fly, differences in diet and husbandry between labs can lead to confounding results in similar assays (Corby-Harris et al., 2007). For example, studies in the fly have shown that *Acetobacter* and *Lactobacillus* ratios change when fly medium contains differing amounts of sugar versus protein (Ridley et al., 2012, Wong et al., 2011, Kamareddine et al., 2020). These

results highlight the potential for microbial change to occur in flies in an analogous manner to humans. For these reasons, researchers should reasonably control for external impacts on the microbiome. Interpretations of data should consider diet other environmental effects – especially between different groups studying similar age-related pathologies (Heintz and Mair, 2014).

1.1.3 Bacterial population effects on lifespan

Gut microbes have been shown not to be required for fly survival (Bakula, 1969). There are, however, distinct differences in fly transcriptome in the presence and absence of bacteria – with bacteria heavily regulating differentiation of hormone-secreting enteroendocrine cells (Broderick et al., 2014). Intestinal microbiota contributes much to fly metabolism, especially during early life when bacteria are more balanced (Bonfini et al., 2016). It is with age that bacterial imbalance (or dysbiosis) occurs, triggering immune activation, resulting in compromised intestinal health.

There are inconsistent results in the *Drosophila* literature regarding whether microbial presence is beneficial or not to fly lifespan. For example, Brummel et al. have shown that axenic culture during development and antibiotic treatment during adulthood increases mortality (Brummel et al., 2004); while Ren et al. showed that similar microbe ablation techniques had no lifespan trade-off on adult flies (Ren et al., 2007). By contrast, other groups have shown that microbe ablation indeed extends adult fly lifespan – regardless of when flies are made germ-free (Clark et al., 2015, Lee et al., 2019). Clark et al. show that axenic flies and flies antibiotic-treated from day 0, 10, 20, or 30 of adulthood all result in lifespan extensions when compared to age-matched controls (Clark et al., 2015). Supplementary information from Clark and colleagues further indicates that observed lifespan extensions are more prevalent in *Canton-S* flies compared to *w[1118]* flies.

Thus, differences in fly genotype, sex, and diet between studies may account for inconsistencies in results more so than the actual timing of microbial ablation itself.

Still, similar work in mice involving microbe ablation show that old germ-free mice live longer than conventionally reared counterparts (Thevaranjan et al., 2018). The differences in whether removing microbes or not is beneficial may depend on which founding microbes were cultured during development. For example, mice associated with segment filamentous bacteria were shown to elicit chronic inflammation, leading to age-associated decline. Importantly, segment filamentous bacteria are not found in humans (Sommer and Bäckhed, 2013). Further, clinical trials involving individuals who had reached maximum human lifespan (>100 years old) were shown to have microbial patterns similar to those of 20- to 40-year-olds (Biagi et al., 2010). Centenarians, or individuals living over 100 years of age, may be able to circumvent chronic inflammation associated with aging via changes in intestinal bacterial cohorts (Biagi et al., 2010).

1.1.4 Host: microbe interactions and the intestinal barrier

It is important to consider how much we can extrapolate from research findings pertaining to microbiota driven age-related decline. Although the fly, mouse, and human share homologous components, it is difficult to say if all research findings could be translated to therapeutic and/or preventative targets to delay age-related decline in the human population. As an example of how work in the fly can contribute to our understanding of microbiota roles in age-related decline, we can consider work focusing on age-related loss of intestinal barrier function. Rera et al. initially characterized loss of barrier function in the aging fly, referring to flies exhibiting a leaky gut phenotype as *Smurfs* (the Smurf assay and phenotype are detailed further in Section 2.3). Smurf proportion increases as a function of age, with almost all flies losing intestinal barrier function by the end of the lifespan (Rera et al., 2012).

Intestinal barrier function reliably predicts imminent death and correlates with increases in immune marker expression (Rera et al., 2012). Following this work, Clark et al. showed how barrier dysfunction was preceded and followed by significant changes to the population of intestinal microbiota (Clark et al., 2015). Results from Clark and colleagues further corroborated how intestinal permeability and dysbiosis work in synchrony to drive mortality. Importantly, Clark et al. findings were later supported in murine models of immune dysfunction (Clark et al., 2015, Thevaranjan et al., 2018).

The current published sequence of events in aging *Drosophila* is a follows (1) higher bacterial load and changes in microbial composition (Broderick et al., 2014) (2) loss of epithelial integrity drives further dysbiosis (Clark et al., 2015) (3) bacterial imbalance and loss of gut epithelial integrity further presents as ISC hyperproliferation (Buchon et al., 2009a, Guo et al., 2014) culminating in fly death (summarized in Figure 1.1). Taken together these works demonstrate the importance of the intestinal barrier in maintaining age-related health and the value of work in the fly in addressing the complex interplay between the microbiota, intestinal homeostasis, and immune function in the context of aging.

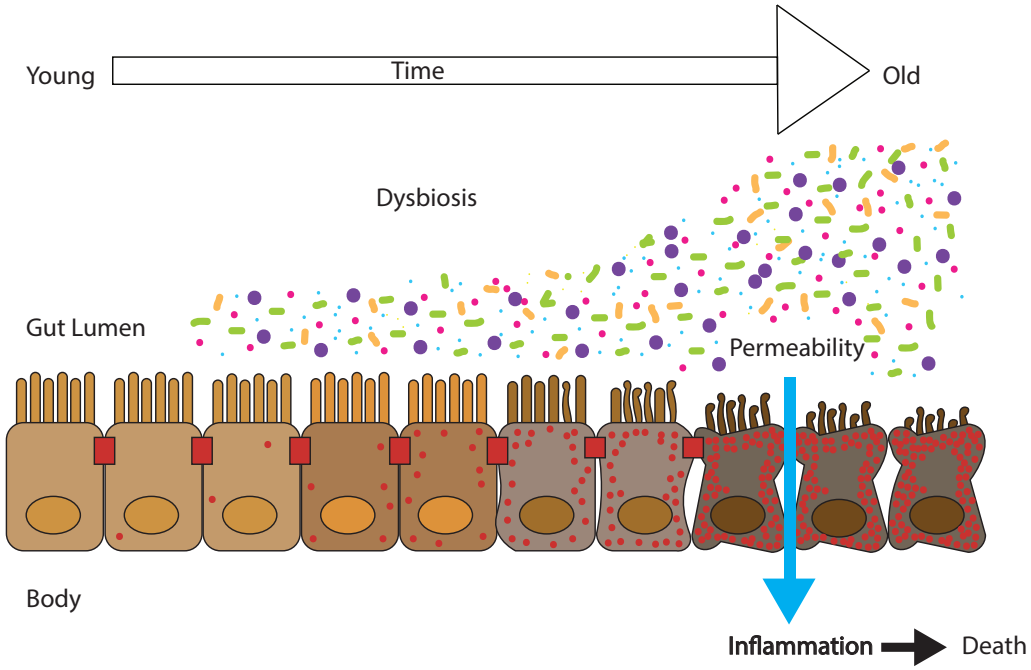

Figure 1.1: Representation of age-related intestinal decline

1.2 Immune system control of commensal microbes

In vertebrates and invertebrates alike, the immune system is largely responsible for shaping and maintaining the commensal population (Sompayrac, 2016, Thaiss et al., 2016). The importance of host-microbe symbiosis was realized in mammalian health when the absence of immune recognition of microbiota resulted in host decline (Slack et al., 2009, Rakoff-Nahoum et al., 2004). Notably, effects of innate immunity on microbial populations are a concerted effort between several mechanisms and pathways. For example, in addition to protecting the host from commensal over-proliferation, the immune system may be aiding bacteria during periods of ecological stress or pathogenic invasion (Bäckhed et al., 2012). A study involving mice suggested that sugars could be added to epithelia by white blood cells during periods of infection-induced starvation. Fucosylated proteins were shed into the intestinal lumen so commensal bacteria could retain a source of energy (Pickard et al., 2014). Importantly, when maintaining commensal control, the immune system must maintain a balance between resistance (direct resistance of microbial overgrowth) and tolerance (repair

to limit stress damage) in order to maintain host-microbe interactions (Chakrabarti et al., 2012). Tolerance mechanisms implemented by the host include regular turnover of epithelial cells along the intestine through controlled stem cell proliferation. Maintenance of mechanical barriers such as the monolayer of gut epithelia and the peritrophic matrix further facilitates symbiotic interactions between host and microbe populations. Fly studies have shown that damage, due to commensal deregulation, should be kept to a minimum by ensuring that immune and repair mechanisms work in tandem (Chakrabarti et al., 2012, Buchon et al., 2009b).

1.2.1 Why is it that commensals cannot always be controlled?

The immune system may not always be able to circumvent physiological stressors. This leads to an imbalance in gut microbiota, also referred to as dysbiosis (Thaiss et al., 2016, Thaiss et al., 2014). Bacterial load and composition change in the aging intestine (Claesson et al., 2010). The mechanism through which commensals begin to change is still poorly understood. Some potential hypotheses for microbe-associated ageing pathologies include microbes that may become virulent under specific conditions, a shift in bacterial metabolite excretion due to shifting bacterial communities, or bacterial desensitization to innate immunity. Additionally, immune deregulation increases with age (Broderick, 2016, Clark et al., 2015, Guo et al., 2014, Claesson et al., 2012, Buchon et al., 2009b). How immune responses regulate commensals with age is also poorly understood. Defining how the immune system can regulate its tolerance with age, such that it can continue to protect the organism without leading to host decline, may help circumvent age-associated immune deregulation. Current literature can answer, in part, some of these questions. The following sections will highlight the importance of the fly immune response, particularly regarding intestinal immunity.

1.2.2 The fly immune response

Drosophila melanogaster lacks an adaptive immune response; however, this invertebrate maintains a cohesive and relatively simple set of immune pathways. In mammals and flies, the innate immune system is largely able to sense bacteria along the intestinal epithelia via pattern-recognition receptors (PRRs) (Thaiss et al., 2016). These receptors are responsible for relaying information to the host regarding pathogen presence and/or microbial presence around tissues (Thaiss et al., 2016). In the fly there are two major immune pathways through which PRR information is relayed, the Toll and Immune Deficiency (IMD) pathways. There are homologs of each pathway found in the human immune system, however the IMD pathway itself is insect specific (Silverman and Maniatis, 2001). This section, however, will focus on the IMD pathway because studies have overwhelmingly looked at the role of IMD activity in intestinal immunity. The specific PRRs of the IMD pathway are called peptidoglycan recognition proteins (PGRPs). Most organisms, be it invertebrate or vertebrate, will contain these immune proteins, as they have been conserved through evolutionary time (Gupta, 2008). Although PGRPs are conserved and are involved in mediating bacterial responses, all PGRPs are not equal in function. *Drosophila* has one of the largest arrays of PGRP subtypes, 13 genes spliced into 19 different proteins (Werner et al., 2000). IMD pathway activation, via PGRP-LC sensing of gram-negative bacteria, leads to up-regulation of nuclear transcription factor Relish (Chu and Mazmanian, 2013). Collectively, Relish family transcription factors are called Nuclear Factor Kappa B (NF-kB) (Hedengren et al., 1999). NF-kB cell signaling results in antimicrobial peptide (AMP) expression (Chu and Mazmanian, 2013). AMPs will generally target pathogen-driven infection. However, AMP transcriptome analysis has been shown to correlate with regenerative and protective mechanisms (Buchon et al., 2009a). Regulatory factors of the IMD pathway include Caudal, which blocks AMP gene promoter regions, and Pirk, which prevents PGRP-LC from

integrating on the cell membrane (Chu and Mazmanian, 2013, Beutler, 2004). Other regulatory proteins include PGRP-LB and PGRP-SC. By degrading circulating peptidoglycan from bacterial cell walls, PGRP-LB and PGRP-SC help regulate and maintain immune responses at basal levels in the presence of commensal microbes (Zaidman-Rémy et al., 2006). Defense mechanisms in the *Drosophila* gut include: release of reactive oxygen species (ROS) via an NADPH oxidase called Dual Oxidase (DUOX) (Ha et al., 2005), intestinal peritrophic matrix which maintains the integrity of epithelial cells by preventing damage from toxins (Kuraishi et al., 2011, Buchon et al., 2009b), and expression of AMPs (Buchon et al., 2009a).

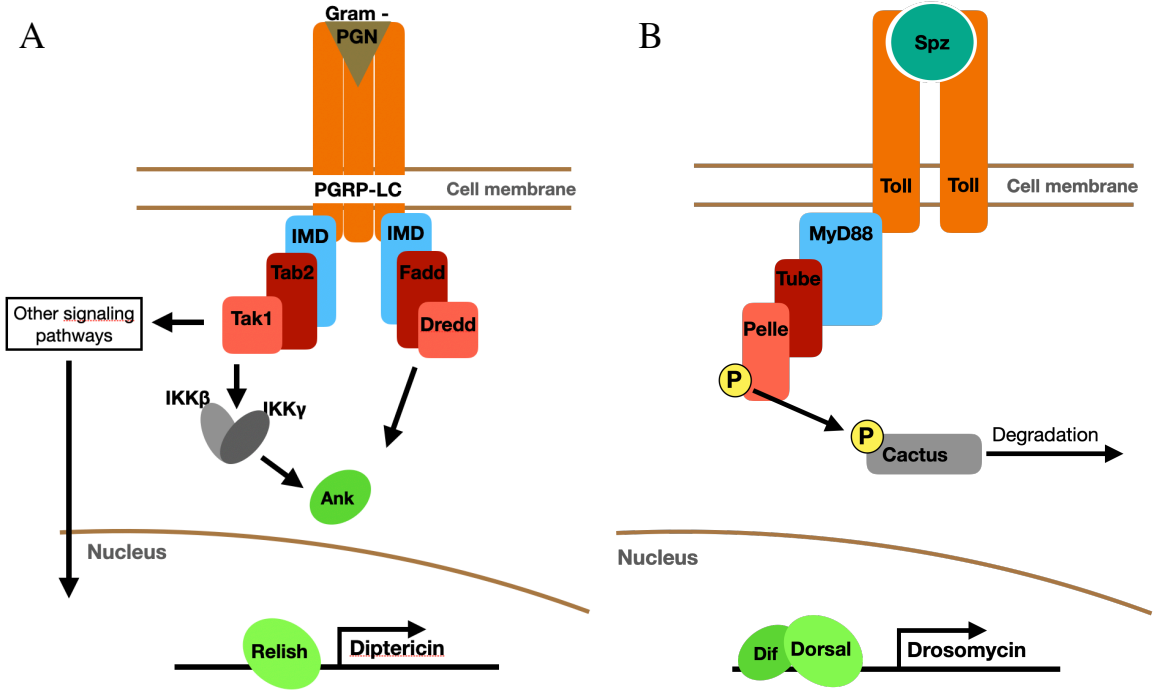

Figure 1.2: IMD and Toll pathways in Drosophila melanogaster

1.2.3 Bacterial feedback on innate immune homeostasis

To effectively protect the host, the immune system must be able to distinguish between harmful and commensal bacteria. The immune system must also be able to discriminate between live and dead bacteria to prevent over activity. Neyen et al. provide a mechanism for

how the immune system is able to down-regulate immune activation to circumvent the increase in mortality associated with unregulated immune responses (Neyen et al., 2016). Neyen et al. made use of *Drosophila*'s capacity to recognize the bacterial cell wall component, diaminopimelic-acid (DAP)-type peptidoglycans (PGNs), via IMD PGRPs (Neyen et al., 2016). To elucidate the mechanism by which the immune system discriminates between live and dead bacteria, Neyen first established AMP expression levels in the presence of mono versus polymeric PGN. Polymeric PGN, stemming from dead bacteria, led to a faster immune resolution rate. Neyen et al. found that dead versus live bacterial recognition lies in a variable exon region of the PGRP-LC receptor gene. This exon creates an alternative cytosolic tail variant of PGRP-LC, called regulatory PGRP-LC or rLC. Data suggest that the cytosolic tail characteristic of rLC facilitates immune dampening via rLC mediated endocytosis and ESCRT (endosomal sorting complexes required for transport)-dependent degradation of PGRP-LC2 (Neyen et al., 2016). An interesting follow-up study to expand on these findings could include age-related increases in bacterial load and what that does to expression of rLC. i.e., could overexpression of rLC regulate, or at least help modulate, microbial imbalance and the effects of dysbiosis?

Innate immune homeostasis is also facilitated via Homeobox gene, Caudal. By regulating immune system levels, the homeostatic relationship between gut and host is maintained. Ryu et al. show that Caudal (Cad) is necessary to maintain beneficial levels of AMP activity in the fly gut (Ryu et al., 2008a). Interestingly, findings show that Cad-RNAi (RNA interference) flies experience significant apoptosis of gut epithelial cells coupled with increased mortality (Ryu et al., 2008a). These findings corroborate the importance of immune regulation in maintaining intestinal homeostasis. AMP over-expression in the gut, due to Cad RNAi, leads to changes in commensal microbiota. Without Cad regulation, *Gluconobacter morbifer* (G707) becomes a dominant and pathogenic member of the commensal population.

G707 facilitates cell apoptosis in the intestines of germ-free mice, with and without Cad regulation. Similarly, Lee et al. found that gnotobiotic flies inoculated with *G. morbifer* generated constitutive ROS production, coupled with intestinal cell death (Lee et al., 2013b). *G. morbifer* mutants unable to produce uracil did not induce constitutive ROS production and reduced cell death. This mutation was also sufficient to rescue fly lifespan (Lee et al., 2013b). Although G707 was pathogenic under Cad RNAi, authors did not address the natural age-related changes in the commensal population. In other words, would unperturbed animals still experience an age-related increase in G707? Taken together, these studies provide data that suggests the regulation of innate immunity prevents deleterious bacterial populations from arising, as well as increased epithelial turnover, resulting in rescued animal lifespan.

1.2.4 When is a commensal not a commensal?

Sequencing work in non-Smurf flies specifically identifies commensal bacterial strains that when overgrown may be causing pathology in the fly. Identified bacteria are from Acetobacteraceae and Lactobacillaceae Families and have previously been shown to increase immediately following barrier dysfunction (Clark et al., 2015). Since these bacterial Families are largely categorized as commensal symbionts, the sharp increase in number may present an environment for commensal pathogenesis. For example, known commensal Genus Lactobacillus has been reported to act as a pathogen with age (Fast et al., 2018b, Fast et al., 2020, Ferguson et al., 2020). Specific bacterial metabolites (e.g., uracil, acetate, and cholera toxins) have all been shown to be involved in mechanisms that mediate imbalance between immunity responses and bacterial microbes (Fast et al., 2020, Ferguson et al., 2020, Kim, 2020, Lee et al., 2013a). In other words, dramatic overgrowth of commensal bacteria can induce pathology despite not being traditional pathogens themselves.

Published literature has shown how commensal species may evolve into opportunistic pathogens when out of balance (Fast et al., 2018a, Fast et al., 2018b, Lee et al., 2013a, Ryu et al., 2008b). Pathobionts, or symbionts capable of inducing disease, cause intestinal and host decline in the fly (Fast et al., 2018a). Further indirect contributions to intestinal homeostasis include bacteria to pathogen communication. Fast and colleagues have shown that in flies inoculated with select Lactobacillus and Acetobacter species, epithelial regeneration was prevented upon introduction of pathogen *Vibrio cholerae* (Fast et al., 2018a). In other words, flies were more susceptible to infection in the presence of known commensals. In a follow-up publication, authors showed that commensals facilitate the cholera toxin-mediated inhibition of epithelial renewal (Fast et al., 2020). These results underscore the importance and diversity of species - species interactions, and the complex nature of their impact on host intestinal physiology.

1.3 The importance of intestinal homeostasis

Intestinal homeostasis refers to the balance of cell loss and cell regeneration. Of note, there's apparent interplay between microbial dynamics, the immune response, and cellular homeostasis mechanisms that are important for age related health. In the fly, gut intestinal stem cells (ISCs) are the only dividing cells. ISCs indirectly give rise to two differentiated cell types: enteroendocrine cells (EE) and enterocytes (EC) (Micchelli and Perrimon, 2006). Increases in cell turnover lead to the accumulation of intestinal epithelial cells, as is seen in the aging organism. Over-proliferation of cells may facilitate loss of barrier function (Guo et al., 2014). The relationship between intestinal dysplasia/hyperplasia and barrier permeability is currently unclear.

1.3.1 Intestinal barrier function

The intestine as a barrier is also an integral part of immune function. The role of a gene called Big Bang Gene (BBG) has been elucidated as being part of a septate junction scaffold. Septate junctions, the fly equivalent of mammalian tight junctions, between gut epithelial cells are meant to regulate paracellular flow (Anderson and Van Itallie, 2008). In the absence of BBG, junctions become loose and disorganized. This in turn triggers chronic and deleterious activation of immune responses (Bonnay et al., 2013, Ryu et al., 2008a). Mutation in the BBG gene leads to gut epithelial inflammation and an increase in mortality (Bonnay et al., 2013). By making the fly gut germ-free, via antibiotic treatment, inflammation is dampened, and lifespan is rescued. BBG mutants are still able to induce expression of AMPs, thus the innate immune response against bacteria is still elicited. However, the overall role of septate junction integrity is part of the epithelial defense mechanism. These data, and others (Salazar et al., 2018), suggest that maintaining immune tolerance and immune response is also mediated, in part, by intact junction proteins. Intestinal homeostasis is an indirect measure of how well the immune system is regulating commensal microbe populations. When new epithelial cells regularly replace the old, the organism can avoid dysplasia, or the over proliferation of cells leading to abnormally large organs/tissues. Thus, immune deregulation may consequently lead to loss of intestinal homeostasis via loss of commensal control or vice versa.

1.3.2 Intestinal homeostasis facilitates commensal control

Thus far, studies have corroborated that the aging fly intestine is characterized by loss of intestinal immune homeostasis resulting in barrier dysfunction (Clark et al., 2015, Guo et al., 2014, Rera et al., 2012, Buchon et al., 2009b). Characterizing mechanisms behind commensal homeostasis are of equal importance for health and survivorship of the organism. Recent

data suggest that commensal homeostasis is facilitated by compartmentalization of the intestine (Li et al., 2016). Intestinal copper cells provide a stable acidic region in the fly midgut, partitioning commensals and keeping bacterial levels low in the posterior region of the intestine. Findings show that disruption of copper cells drives immune activation and ISC proliferation, ultimately leading to dysbiosis (Li et al., 2016). However, the initial cause of loss of copper cell remains to be elucidated. Age-related immune deregulation may have effects on commensals or intestinal physiology rendering the intestine less acidic and more alkaline. Questions remain regarding compartmentalization effects on general bacterial populations, bacterial communication and how those changes are affecting healthspan and intestinal homeostasis.

1.3.3 Pathogenic infection drives overactivation of immune tolerance mechanisms

Studies discussed have revealed that infection increases stem cell proliferation and gut repair. Adding to this literature, Chakrabarti and colleagues instigated infection in the fly to better understand how pathogenic bacteria disrupt gut homeostasis. Work aimed to uncover the relative contributions of host damage due to pathogen exposure versus collateral damage from the host's pathogen response (Chakrabarti et al., 2012). Chakrabarti et al. infected *Drosophila* with *Pseudomonas entomophila* and found that this pathogenic bacterial strain is associated with a block in antimicrobial peptide translation (Chakrabarti et al., 2012). Results suggest that bacteria-induced repression of protein synthesis could facilitate mechanisms of pathogenesis as well as deregulation of the immune response.

While overactivation of stress pathways in the presence of a pathogens are usually helpful – e.g., an increase in production of reactive oxygen species to combat pathogenesis (Chakrabarti et al., 2012) – overactivation also contributes to pathogenesis in a feedforward manner. Future studies may include looking at how the fly responds to introduction of a

pathogen at different ages. The focal question remains, how can intestinal homeostasis be preserved such that the organism retains its health and deters age-related decline?

1.3.4 Interplay between immune responses, the microbiota and intestinal homeostasis

A recent study has shown the importance of maintaining homeostasis between innate immunity and intestinal epithelia with age. Data suggest an interaction between *FOXO*, an insulin-signaling transcription factor, and IMD pathway regulator *PGRP-SC*. Upon increase in *PGPR-SC* activity in ECs, data show a decrease in dysbiosis and dysplasia. Thus, leading to a decrease in mortality, but only in conventionally reared flies (Guo et al., 2014). Intestinal tissue damage increases with age, independent of bacteria (Guo et al., 2014). Loss of barrier function is also seen in late life of axenic flies (Clark et al., 2015). Bacteria may be necessary in the maintenance of intestinal-immune homeostasis. Guo et al. alludes to immune system effects on commensals in the gut with age. However, more is needed to uncover how age-related immune activation may be leading to dysbiosis or how dysbiosis may be leading to immune activation with age.

1.4 Thesis aims and objectives

This thesis aims to answer the following question, what is the etiology of age-associated inflammation on intestinal decline? To answer this question, experimental works will focus on differentiating between age-related changes in immune activation versus bacterial changes, as well as characterizing immune activation consequences on microbial communities during aging. Generations of sterile flies and/or flies containing defined populations of bacteria will be used in conjunction with genetic manipulations to better understand the crosstalk existing between innate immune markers and microbial species.

1.4.1 Thesis Objectives

- Impact of forced immune activation on intestinal microbiota – Recapitulation of age-associated intestinal decline
- Impact of immune activation alone on intestinal epithelial integrity and cell-turnover homeostasis
- Validation of primary immune induction in the gut versus secondary systemic immune activation
- Consequences of intestinal barrier dysfunction on fly immune cells or hemocytes (hereafter referred to as phagocytic macrophage cells).

Chapter 2: Materials and Methods

Details of suppliers found in this thesis are listed below in Table 2-1.

Table 2-1: List of chemicals and suppliers used in the course of this thesis

Chemical	**Supplier**	**Catalogue Number**
Flystuff *Drosophila* Agar Type II	SLS	FLY1020
Flystuff Inactive Dry Yeast	SLS	FLY1062
D-Glucose monohydrate	Melford	G0802.5000
Sucrose	Melford	S0809.5000
Flystuff Cornmeal Yellow	SLS	FLY1110
Flystuff Tegosept	SLS	FLY1136
Propionic Acid	Sigma	P5561
FD&C Blue Dye No. 1	Fiorio Colori	42090
Bromophenol Blue Sodium Salt	Sigma	B5525
Mifepristone - Cayman Chemicals	Cambridge Bioscience	CAY10006317
Rifamycin	Sigma	R8626
Ampicillin	Sigma	A9518
Tetracycline	Sigma	87128
Sodium Hypochlorite	Sigma Aldrich	425044
Apple Juice	Tesco	Good quality/No additives
Sainsbury's Fast Action Dried Yeast Sachets	Sainsbury's	N/A
Sodium Chloride	Melford	S0520.1000
Triton X-100	Sigma	X100-500ML
Trizol	Fisher Scientific	12044977
Sodium Acetate Solution (3 M), pH 5.2	Thermofisher	R1181
Chloroform: Isoamyl alcohol 24:1	Sigma	C0549
Glycogen, RNA grade	Fisher Scientific	11873933
DNase I, RNase-free (1 U/μL)	Thermofisher	EN0521
Random Hexamer Primers	Fisher	10580091
Thermo Scientific™ RiboLock RNase Inhibitor	Fisher	11581505
Thermo Scientific™ RevertAid™ Reverse Transcriptase	Fisher	10161310
dNTP Set 100 mm Solutions	Thermofisher	R0181
Power SYBR green PCR master mix	Fisher Scientific	10658255
Paraformaldyhyde, 16%, 2x10 ml	Fisher	11490570
Normal Goat Serum, 2 ml	Fisher	10658654
Bovine Serum Albumin, 100g	Fisher	12737119

Invitrogen™ DAPI (4',6-Diamidino-2-Phenylindole, Dihydrochloride)	Fisher Scientific	10184322
VECTASHIELD® Antifade Mounting Medium	Vector Laboratories	H-1000
Staphylococcus aureus (Wood strain without protein A) BioParticles™ , Alexa Fluor™ 488 conjugate	ThermoFisher Scientific	S23371
Staphylococcus aureus (Wood strain without protein A) BioParticles™ , Alexa Fluor™ 594 conjugate	ThermoFisher Scientific	S23372
Halocarbon oil 27	Sigma-Aldrich	H8773

2.1 *Drosophila* melanogaster husbandry

2.1.1 General fly stock maintenance

Non-experimental fly stocks were housed in narrow polypropylene vials (95 mm height, 25 mm diameter) containing 8 ml of standard cornmeal medium. These flies were kept at room temperature (~22°C) and/or in an 18°C incubator, without control for fly circadian rhythm or humidity. Stock flies were transferred to new medium every 3-4 weeks at 18°C and each vial was checked thoroughly for contamination and viability. When a fly stock was required for experimental purposes, the respective fly line would be transferred to a new 8 ml vial and placed in a humidified and temperature-controlled incubator (25°C,12hr on/off light cycle, 60% humidity) for further expansion.

2.1.2 Experimental fly maintenance

Experimental flies were housed in vials with a population density of approximately 30 flies per vial. Vials were kept in a humidified and temperature-controlled incubator (25°C,12hr on/off light cycle, 60% humidity) for the entirety of the lifespan experiment and were only removed for sample collection or imaging at specific timepoints. In the event that temperature-sensitive lines were used to control transgene induction (discussed further in

section 2.2), flies were raised at 18°C to inhibit transgene expression. To induce transgene expression, flies were shifted to 29°C. Flies in both experimental and control cohorts were transferred onto new medium every two to three days throughout the lifespan. On these days, flies were scored for death if they were being used for longevity assays.

2.1.3 Fly media preparation

2.1.3.1 Standard and sterile cornmeal media

Standard cornmeal medium was prepared by mixing 1% (wt/vol) agar, 3% (wt/vol) yeast, 1.9% (wt/vol) sucrose, 3.8% (wt/vol) dextrose, 9.1% (wt/vol) cornmeal and water at 90% of the final volume. Non-sterile medium contained the following two preservatives: 15% Nipagin in ethanol and an acid mixture containing propionic acid and phosphoric acid. Stock solution of the acid mix was as previously described (Lewis, 1960). Cornmeal medium preparation was as previously described (Demerec, 1994a). Under axenic conditions, standard medium, vials and stoppers were autoclaved for 15 minutes at 121°C. No preservatives were added to sterile medium.

2.1.3.2 Blue media

Blue medium was prepared by adding FD&C blue dye no.1 at a concentration of 2.5% (wt/vol) to standard medium. Under axenic conditions, blue medium was autoclaved for 15 minutes at 121°C. Bromophenol-blue medium was prepared by mixing 0.5% (wt/vol) Bromophenol-blue sodium salt with standard medium.

2.1.3.3 RU486 media

The synthetic steroid mifepristone, or RU486, was added to standard media to induce GeneSwitch activity. RU486 powder was dissolved in ethanol to create a 20 mg/ml stock solution. RU486 stock solution was then added to cooled standard medium. Final

concentrations of the two RU486 doses used were 25 µg/ml and 50 µg/ml. Control standard medium contained an equivalent volume of ethanol alone.

2.1.3.4 Antibiotic media

Antibiotic (AB+) medium was prepared by adding tetracycline (1% wt/vol), rifamycin (1% wt/vol), and ampicillin (0.5% wt/vol) to standard medium. Control medium (AB-) was prepared by adding ethanol (2.5% wt/vol) to standard medium. Note, standard medium was cooled to < 60°C prior to adding antibiotic cocktail.

2.1.4 Virgin collection and sex-sorting flies

During experimental sorting adult flies were anesthetized using low levels of carbon dioxide gas. Low levels of CO_2 cover a range between 4-6 liters per minute as measured by The Flowbuddy™ flow regulator. Only female flies were used in experimentation. Female flies store sperm from previous mating events prior to egg fertilization (Demerec, 1994a), therefore virgin female flies were collected to ensure the correct genotype of progeny. Temperature cycling was used to slow development and delay mating. To begin virgin collection, culture bottles of our desired line were cleared of any eclosed adult flies at the end of the day and placed at 18°C. Flies were allowed to eclose overnight for no more than 16 hours. Adult virgin females were collected the following morning based on appearance and placed into separate vials containing 8 ml of standard cornmeal medium. When compared to the dark coloration of older and mated female flies, virgin flies are larger, translucent and have a dark spot on the abdomen (Demerec, 1994a). After morning collection, virgin only vials were kept at 18°C. Culture bottles were left at room temperature and virgins were collected again in the afternoon and evening. After 3 days of morning and evening collections, or once sufficient virgins were collected, virgins were allowed to mature at 25°C

for 24 hours to facilitate efficient mating. Male flies were then introduced to virgin females at a ratio of 3♀ : 1♂.

2.1.5 Generating Axenic and Gnotobiotic Flies

2.1.5.5 Axenic (germ-free) flies

To collect axenic embryos of the correct genotype, virgin females were collected as detailed above in section 2.1.4 and flipped into fresh vials along with males at a ratio of 5♀ : 2♂. Flies were allowed to mate in fresh vials at 25°C for 24 hours to increase mating frequency prior to being flipped into large embryo collection cages (cylindrical acrylic containers which accommodate 100 mm petri dishes on the bottom and are fused with stainless steel mesh at the top). The apple juice agar plates placed on the bottom of the cages were prepared by mixing 1% (wt/vol) agar and good quality apple juice without additives i.e., 100% pressed apple juice, not from concentrate. Once dry, plates were stored at 4°C for a maximum of 4-5 days and allowed to reach room temperature prior to use. Flies were added to individual embryo cages to total ~700/cage (5♀ : 2♂). A minimum of two cages were setup per genotype per experiment. Flies were allowed to acclimatize in embryo cages for at least 48 hours prior to embryo collection. Apple juice plates were replaced twice per day, morning, and evening. A small amount of yeast paste (live yeast with deionized water added to form a smooth paste) was added to each plate during each transfer to induce greater oviposition rate. Embryos were collected from an overnight egg-lay between 14-16 hours. The embryos were gently dislodged from the apple juice plates using a soft-bristled paint brush and deionized water. Embryos were collected in a sterile mesh container (0.4um diameter) and further washed with deionized water

In a laminar flow cabinet, washed embryos were then dechorionated in 2% sodium hypochlorite for 3 minutes, followed by a rinse with approximately 200 ml of sterile 1 x PBS.

Embryos were then transferred from the mesh container to a 50 ml Falcon Tube using sterile 0.7% NaCl, 0.1% Triton-X solution. Embryos were then allowed to settle out of solution and 20 µl of resuspended embryo solution was aliquoted into vials containing 8 ml of sterile standard medium. Seeded vials were then transferred from the laminar flow hood into a 25°C, 12hr on/off light cycle, 60% humidity incubator. After 10 days of development, progeny was allowed to eclose for 24-36 hours. Prior to sorting female axenic flies, all necessary equipment was sterilized with strong bleach and/or 80% ethanol and allowed to dry overnight in a sterile environment. Flies were then sorted, under light CO_2 anesthetic, with sterilized equipment next to an open flame.

Throughout the course of the lifespan, axenic flies were transferred onto new medium next to an open flame to minimize contamination. To test for continued sterility throughout the course of the experiment, samples were taken from soiled fly vials and plated on bacterial agar. Briefly, in a laminar flow cabinet 500 µl of sterile 1 x PBS was added to soiled vials, of which 200 µl was placed into a sterile microcentrifuge tube. Once fly media debris settled to the bottom of the microcentrifuge tube, the solution was then dispensed across MRS, yeast/glucose and LB agar plates in 15 µl aliquots. Culture plates were kept in a laminar flow hood overnight to dry and where then placed at 37°C and 30°C respectively. After 24 hours, plates were inspected under a light microscopy for any bacterial colony formation. As an additional sterile control, bacterial genomic DNA was isolated from whole fly samples and processed as detailed below in Section 2.5.

2.1.5.6 Gnotobiotic flies

Gnotobiotic flies were generated by associating sterile embryos (detailed in section 2.1.5.1) with a specific bacterial strain(s) during development. Adult progeny would then develop with a defined bacterial population. Bacterial solutions were prepared as follows: Individual cultures of *Lactobacillus plantarum*, *Escherichia coli* Keio wild-type, and *Acetobacter*

pasteurianus were grown over 48 hours. Cultures were then centrifuged at 850 g for 5 minutes, supernatant was removed, and the bacterial pellet was resuspended in sterile 1 x PBS. 24-hours prior to embryo collection (detailed in section 2.1.5.1) vials containing 8 ml of sterile cornmeal medium were evenly inoculated with a bacterial solution equal to $3x10^6$ CFU/vial. Previous work in the lab correlated specific optical density (OD) measurements with bacterial CFU values, thus allowing for a standard CFU/vial. Briefly, a single OD600 value, around 0.2, was measured for each bacterial strain using a spectrophotometer. The bacterial solution was then serially diluted 1:5 and plated on respective bacterial agar. Following incubation, colonies were counted from a single dilution sample and this dilution factor was used to calculate CFU/mL. Vials inoculated with bacteria were then seeded with sterile embryos. In order to maintain the integrity of the bacterial population introduced, adult gnotobiotic progeny were handled as though axenic, see Section 2.1.5.1 for handling of axenic adult flies. Thus, controlling for potential exposure to extraneous bacteria.

2.2 *Drosophila melanogaster* Stocks and Genetic Crosses

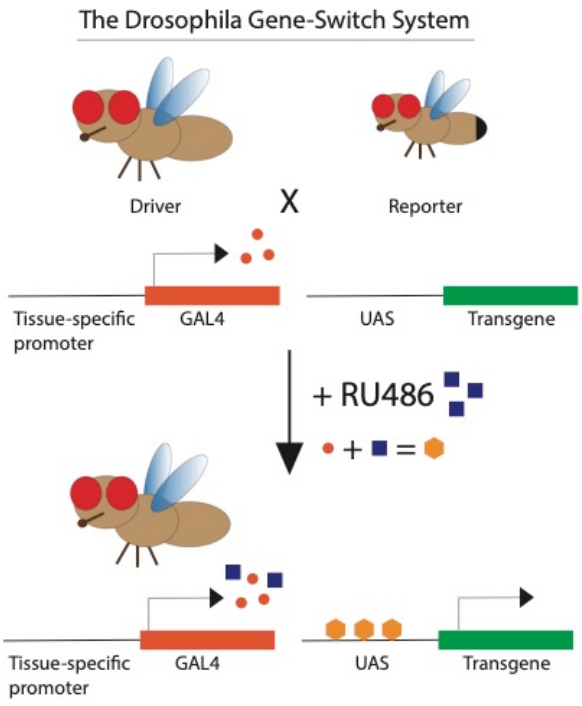

Figure 2.1: Mechanism for inducing constitutive immune activation in the fly

Drug-inducible Gal-4^{GeneSwitch} used throughout this thesis to drive expression of transgenes of interest. Table 2-2, found at the end of this chapter, shows a complete list of transgenic fly stocks used during this thesis.

Briefly, GeneSwitch refers to the following: a combination of the yeast GAL4 protein that targets a chosen upstream activating sequence (UAS) and a tissue-specific promoter region, which will sit upstream and control localized expression of the transgene. UAS transgene expression is restricted to a specific site via GeneSwitch activity; expression is then controlled temporally in the presence of steroid hormone, RU-486 (mifepristone) (Osterwalder et al., 2001).

2.3 Smurf Assay – Testing Barrier Integrity

As described previously (Rera et al., 2012), a non-invasive blue dye feeding assay was used in order to assess changes in intestinal barrier function with age. Flies eliciting a 'leaky gut' phenotype turn blue, due to blue medium escaping from the gut, these blue flies have been termed Smurfs. For the Smurf assay, ~240 experimental female flies (8 vials of 30 flies each) were placed on blue medium for a period of 24 hours. Flies were then scored as Smurfs when Blue Dye No. 1 was visible anywhere outside of the digestive tract. Blue fly cuticle is detectable to the human eye, as such a magnifying light was used to score Smurfs from outside of the vial without having to anesthetize the flies. Notably, the degree of 'Smurf-ness' correlates with mortality rate. The Smurf phenotype is continuous and can range from light blue to navy blue. When scoring and collecting Smurf samples, care was taken to consistently take flies with a similar cyan-blue hue. Post-scoring, flies were transferred onto fresh non-dyed medium. Under axenic conditions, flies were placed on sterile medium before, during and after scoring.

2.4 Fecal Plate Assay

2.4.1 Fecal plate preparation

Fecal plates for analysis were prepared as described previously (Cognigni et al., 2011). Briefly, only non-Smurf flies (identified as described in section 2.3) were used in the fecal plate assay. Flies were then placed into vials containing non-sterile Bromophenol-blue medium for 24 hours to ensure all flies would excrete pH sensitive feces. To preserve the chemical integrity of the bromophenol blue salt, Bromophenol-blue medium was not made sterile. As an indicator of pH, exposure to high autoclave temperature and pressure were subject to compromise the integrity of this solvent. Flies involved in fecal spot analysis were placed into small petri dishes with a wedge of Bromophenol-blue medium in groups of ten based on condition. There were 10 total plates per condition making a total of 100 flies per condition. Flies were allowed to excrete onto petri dish surfaces (lid and bottom) for 24 hours. Flies were sterile up until the experimental time point and were removed from their respective experimental cohort after completion of the assay. At the end of the experiment, flies and medium were removed from the plates, which were retained for imaging.

2.4.2 T.U.R.D analysis

A high-resolution image of each plate was obtained with an Epson Perfection V200 scanner at 1200 dpi. Images were later cropped with FIJI imaging software and analyzed with The Ultimate Reader of Dung (T.U.R.D) as previously described (Wayland et al., 2014). Default settings were changed in T.U.R.D to minimize fecal plate artifact and optimize fecal spot annotations: Block Size = 65, Offset = 8, Minimum = 25, Maximum = 1000, Brush Size = 1.

2.5 Genomic DNA Isolation

2.5.1 PowerSoil® DNA isolation kit (MoBio Lab, Inc.)

The PowerSoil DNA Isolation Kit (MoBio) was used to extract DNA from whole-fly bacterial samples. Prior to following the manufacture's protocol, flies were surface sterilized in 70% ethanol for 5 minutes followed by two rinses in sterile 1 x PBS (as previously published (Ren et al., 2007)). Fly samples were then homogenized in 150 µl of PowerSoil bead tube solution using a motor pestle. Fly homogenate was then returned to the PowerSoil bead tube, and the remainder of the manufacture's protocol was followed.

2.5.2 Genomic DNA extraction – Bead protocol

A transition was made away from using pre-packaged DNA isolation kits due to cost and concerns over contamination as kits were not sterile. The new genomic DNA extraction protocol implemented was a bead-based method. Whole flies were first surface sterilized as described above. Sterile flies were then homogenized in buffer at a volume of 100 µl per fly. Lysis buffer was sterile 1xTE, 1% triton X-100 with proteinase K added at 1:100 volume just before use. Lysate was incubated at 55ºC for 1.5 hours. Following incubation, homogenate was transferred to sterile screw cap tubes containing 0.4 grams of 100-micron low binding silica beads from OPS diagnostics. Samples were vortexed at max speed for 10 minutes. Prior to use, beads in each tube were sterilized as described for surface sterilization of flies. After removal of the ethanol, beads were washed three times with sterile water. After vortexing, samples were centrifuged briefly, and the homogenate transferred to the original microcentrifuge tube. Samples were further incubated for 1.5 hours at 55ºC and finally for 10 minutes at 95ºC.

2.6 RNA Extraction and cDNA Synthesis

2.6.1 Gut dissection protocol

For intestinal sample collection flies were first lightly anesthetized with CO_2 then dissected on a pre-cooled 9-well glass plate, in 20 µl of ice-cold sterile 1 x PBS. Sample collection from gut dissections included the crop and gut tissue starting from the proventriculus, the point at which the crop diverges, to the rectal papilla. Care was taken to collect the same amount of tissue for each sample. Dissected guts were placed in microcentrifuge tubes containing 100 µl of TRIzol. Gut samples were then homogenized using a motor pestle and left at room temperature for 10 minutes prior to storage at -80°C.

2.6.2 RNA extraction – Invitrogen™ TRIzol™ protocol

RNA extractions were completed following the manufacturers protocol, reagents listed in Table 2-1. Briefly, gut samples stored at -80°C (collected as described in section 2.6.1) were first incubated for 10 minutes at room temperature. Phase separation of the sample followed by adding 20 µl of chloroform to each microcentrifuge tube. Samples were shaken by hand vigorously, incubated for 3 minutes at room temperature and centrifuged at 12,000 g. The aqueous phase from each sample was then transferred to a clean microcentrifuge tube. Precipitation steps for each sample involved the addition of 3M Sodium Acetate at 10% volume of the aqueous phase. RNA-grade Glycogen was then added, followed by equal parts volume of room temperature isopropanol. Pelleted RNA was then stored under 75% ethanol at -80°C.

2.6.3 cDNA synthesis – ThermoFisher protocol

cDNA synthesis was completed following the manufacturers protocol, reagents listed in Table 2-1. Briefly, ethanol was first removed from RNA pellets stored at -80°C, RNA pellets

in microcentrifuge tubes were allowed to dry, and molecular H_2O was added to each sample, followed by a 10-minute incubation at 55°C. Resuspended RNA was then DNase treated, followed by a 30-minute incubation at 37°C. To remove DNase, EDTA was then added to each sample followed by a 10-minute incubation at 65°C. Random Hexamer Primers (0.2 mg/ml) were then added to each sample followed by a 5-minute incubation at 70°C. After cooling samples on ice, each RNA sample was then reverse transcriptase treated, followed by a 10-minute incubation at room temperature, a 1-hour incubation at 37°C, and a 10-minute incubation at 70°C.

2.7 Quantitative Polymerase Chain (qPCR) Reaction

qPCR was performed with *Power* SYBR™ Green master mix on a Bio-Rad CFX Connect Real-Time PCR Detection System. Cycling conditions are as previously published (Clark et al., 2015). Either 4.5 µl bacterial DNA or 1 µl of *Drosophila* cDNA sample, were used in a 10 µl master mix with 5 µl of Power SYBR™ Green and 0.25 µl of left and right resuspended primer, respectively. Molecular grade water made up the remaining volume. To compare amplification across conditions and between time-points, all calculated gene expression values were normalized to the value of the loading control gene, *Actin 5C*. All primer sequences used can be found below in Table 2-3.

2.8 Intestinal Cell Staining and Imaging

For immunofluorescence, guts were dissected in ice cold 1 x PBS, transferred to clean ice cold 1 x PBS with added 16% paraformaldehyde (making 4% final concentration of fixative) and fixed for 30 minutes, rinsed in PBST (1 x PBS containing 0.5% Triton X-100), then incubated with primary antibodies (1:500 anti-PH3, 1:500 anti-Prospero, and 1:1,000 anti-GFP) in PBST plus 1% bovine serum albumin (BSA). Primary antibodies were revealed with

Alexa 488 or Alexa 594-coupled anti- mouse antibodies, and nuclei were stained with 4',6-diamidino-2-phenylindole (DAPI). Guts were then mounted linearly onto microscope slides containing a small amount of VECTASHIELD® Antifade Mounting Medium. Coverslips were delicately applied, and a small amount of nail varnish was used to seal the edges. Posterior midguts were imaged using a 40x oil lens on a Leica SP5 LSCM SMD: Tandem Scanner confocal microscope. PH3-positive cells were tally counted along the length of the entire gut using a 40x oil lens on a Zeiss Axiovert 200M Apotome.

2.9 Sequencing and Analysis

Genomic DNA samples from whole flies were prepared as described above. Next generation sequencing and analysis in MEGAN software completed as previously published (Clark et al., 2015). Indexed paired end libraries were prepared by Rebecca Clark, PhD. Bioinformatics work was completed by David Dolan, PhD. Taxonomic analysis in MEGAN5 was completed as part of the PhD work presented in this thesis.

2.10 Live-Imaging of Aging Hemocytes

Whole female flies were put on blue media for 12-24 hours prior to time of imaging. Flies were briefly anesthetized with CO_2 under a light microscope and scored as either non-Smurf or Smurf and segregated into separate vials with media. Flies were allowed to recover prior to being lightly anesthetized a second time – this time flies were mounted on a 24x60x0.15 mm rectangular coverslip loaded with a small droplet of Loctite Superglue. After allowing for the glue to become tacky, forceps were used to arrange the dorsal side of the whole fly in the glue. Care was taken to ensure wings were not covering the dorsal cuticle.

Flies were then imaged at 10x magnification on a Zeiss LSCM 880 with Airyscan (or Zeiss 880). Z-stacks of the dorsal thorax and abdomen were obtained for each imaged fly.

Flies were imaged in batches of 2-3 at a time to control for fly stress experienced from being stuck in glue. The depth of sampling on the Zeiss 880 for adult female *Drosophila* was approximately 7 and 6 microns for the fly thorax and abdomen, respectively. Z-stacks were later compressed into max intensity projections in FIJI and processed using the following steps for each image: ROI (region of interest) selections were maintained across experiments > images cropped >'3D object counter' (built-in FIJI macro).

2.11 Hemocyte Extraction and Total Cell Counts

Hemolymph was extracted from whole adult female flies and fluorescent hemocytes counted as previously published in Bosch et al. 2019. Cells were quantified under a Leica M165FC Stereo Microscope.

2.12 Hemocyte Phagocytosis Assay

2.12.1 Microinjection protocol

Microinjections were carried out using adult female flies at various time points throughout the adult fly lifespan. Flies were placed on blue media for 12-24 hours prior to injections, all flies were scored as non-Smurf prior to injection. An Eppendorf electronic microinjector, the FemtoJet® was used to inject flies. Injector pressure was set to 3 PSI with injection time set between 0.1-0.3 seconds depending on needle bore diameter. 62nL of reconstituted BioParticle™ solution (diluted 1:10 in sterile 1 x PBS before use) was injected into each fly. Needle calibration was continuously measured through the duration of the experiment – ensuring injection volume between flies remained consistent. Injection volume was validated using a small petri dish filled with halocarbon oil and mineral oil (enough to cover the bottom of the petri dish). The volume of solution ejected was measured by injecting 1 x PBS into mineral oil and measuring droplet diameter using a graticule. The microinjection apparatus

was routinely calibrated between injections (approximately every 10 injections) to ensure consistent volume. Needles were pulled from borosilicate glass capillaries using a micropipette puller (Sutter instrument, P-1000), using program number 37. Needle tips were broken using fine forceps to create a larger bore. Flies were injected between the thorax and abdomen, into the hemocoel (body cavity of the fly).

2.12.2 Imaging protocol and analysis

For phagocytosis assays 1-2 flies were injected at a time, in 10–15-minute increments. Flies were allowed to recover for approximately 30 minutes before being mounted and imaged. Flies were glued to coverslips as described above. Total time from injection to image completion never exceeded more than one hour. Between and within timepoints total time from injection to end of imaging in individual flies was kept as consistent as possible. Needles were reloaded and calibrated every 30 minutes, only 2-3 flies were ever injected with the same needle. Confocal microscope settings were reused for every time point. Colocalization event analysis was completed following a previously published protocol for the method 'Squassh', or segmentation and quantification of subcellular shapes (Rizk et al., 2014).

2.13 Statistical Analysis

Survival curve analysis was completed using the log-rank test in GraphPad Prism software. To determine whether the Smurf proportion between the drug-induced and uninduced control groups was significantly different a binomial distribution test was run using R statistical software (v 3.1.2). Statistical significance for fecal images was computed using the Mann-Whitney U rank test in T.U.R.D and cross referenced with a secondary built-in rank test in R. Significant differences in gene expression values between time points were analyzed using a

two-sided Wilcoxon Test in R. Pairwise comparisons between macrophage number with age were also analyzed using a two-sided Wilcoxon Test in R. For hemocyte colocalization data, data were analyzed as previously described in Rizk et al. 2014. Briefly, changes in colocalization events were tested for age related differences using a One-way ANOVA/Kruskal-Wallis Test. For all boxplots shown Boxplots display the first and third quartile, with the horizontal bar at the median. On bar graphs, error bars show mean and standard error of the mean (SEM).

Table 2-2: Transgenic fly stocks used in the course of this thesis

Stock #	Designation	Source or Reference	Identifiers	Additional Information
1	w[1118]	BDSC	RRID: BDSC_58688	Inserted element P{{y[+t7.7] w[+mC]=UAS-GGGGCC.36}attP40
2	w[1118]; If/SM6a; TM2/TM6c,Sb[1]	BDSC	RRID: BDSC_3704/5687	
3	w[1118];; TM2/TM6c,Sb[1]	BDSC	RRID: BDSC_5906	
4 *	lethal/FMK; Gla/SM6a			Gift of Nick Brown
5 *	w[1118] daughterless-GeneSwitch	Tricoire et al., 2009	RRID: FlyBase_FBtp0057039	Gift of David W. Walker
6	y,w;; Ti-GeneSwitch-2	Kabil et al., 2011		Gift of David W. Walker
7	w[1118]; $S_1$106-GeneSwitch	Roman et al., 2001	RRID: BDSC_8151	Gift of David W. Walker
8 *	10759-2-GeneSwitch	Poirier et al., 2008		Gift of David W. Walker
9	w; actin-GeneSwitch-255B	Ford et al., 2007	RRID: FlyBase_FBtp0021868	Gift of David W. Walker
10	w; 5966-GeneSwitch	Clark et al., 2015	RRID: FlyBase_FBti0150384	Gift of David W. Walker
11 *	w 5961-GeneSwitch	Rera et al., 2011	RRID: FlyBase_FBti0150383	Gift of David W. Walker
12	y[1],w[*];; ELAV-GeneSwitch	Osterwalder et al., 2001	RRID: BDSC_43642	Gift of Haig Keshishian
13 *	actin5C-GeneSwitch/FM7	Andjelković et al., 2016		Gift of Scott Pletcher
14	w[1118]; S32-GeneSwitch	BDSC; Poirier et al., 2008	RRID: BDSC_8527	Inserted element P{w[+mW.hs]=Switch1}bun[Switch1.32]
15	w[*]; 4073-GeneSwitch	BDSC; Nicholson et al., 2008	RRID: BDSC_62084	Inserted element P{w[+mW.hs]=Switch2}GSG4073
16	w[1118]; HmlΔGal4,UAS-2xeGFP	Sinenko and Mathey-Prevot, 2004		Gift of Marc Dionne
17	w[1118];; daw-Gal4 / TM6c,Sb[1]	Clark et al., 2011		Gift of Marc Dionne

18	w[1118];daw[NP4661]/SM6a; [HmlΔ-dsRed]/TM6c,Sb[1]	Clark et al., 2011		Gift of Marc Dionne
19	w[1118];; crq-Gal4/TM6c,Sb[1]	Woodcock et al., 2015		Gift of Marc Dionne
20	w;; dpp-Gal4.blk/TM6c,Sb[1]	BDSC	RRID: BDSC_1553	Inserted element P{w[+mW.hs]=GAL4-dpp.blk1}40C.6
21	w[1118]; GMR-Gal4/CyO	BDSC	RRID: BDSC_9146	Inserted element P{GMR-GAL4.w[-]}2
22	w[1118]; c564	BDSC	RRID: BDSC_6982	Inserted element P{w[+mW.hs]=GawB}c564
23 *	tubulin-Gal80(ts); tubulin-Gal4/TM6B, Tb[1]			Gift of David Doupé
24 *	If/SM6a; tubulin-Gal80(ts)/TM6c,Sb[1]	Perrimon Lab		Gift of David Doupé
25 *	tubulin-Gal80(ts)/FM7; myo1AGal4, UAS-GFP	Karpowicz, Perez, and Perrimon, 2010		Gift of David Doupé
26	w; c564-Gal4; tubulin-Gal80(ts)	Woodcock et al., 2015		Gift of Marc Dionne
27	w[1118]; UAS-PGRP Lca	Clark et al., 2015		Gift of David W. Walker
28	w[1118]; UAS-Toll[10b]	Clark et al., 2015		Gift of David W. Walker
29	w; UAS-2xeGFP/[SM6a]	BDSC	RRID: BDSC_6874	Gift of Marc Dionne
30	y[1]w[1118];; UAS-hep[CA]	BDSC	RRID: BDSC_6406	Inserted element P{w[+mC]=UAS-hep.CA}4
31	w; UAS-hep IR	VDRC	RRID: FlyBase_FBgn0010303; VDRC_109277	
32	w; UAS-ssk RNAi	Yanagihashi et al., 2012		Gift of Mikio Furuse
33	w[1118];; srpHemo-3xmCherry/TM6c,Sb[1]	Gyoergy et al., 2018		Gift of Daria Siekhaus
34	w[1118]; HmlΔ-dsRed/SM6a	Clark et al., 2011		Gift of Marc Dionne
35	GMR-Gal4/CyO; TM2 / TM6c, Sb [1]	This Study	Component lines detailed above	
36	If/SM6a; TIGS	This Study	Component lines detailed above	
37	HmlΔ-dsRed/SM6a; TIGS/TM6c,Sb[1]	This Study	Component lines detailed above	
38	If/SM6a; srpHemo3xmCherry/TIGS	This Study	Component lines detailed above	
39	UAS PGRP LCa / fmk ; Gla / sm6a	This Study	Component lines detailed above	

40	UAS PGRP LCa ; Hml-GFP / sm6a	This Study	Component lines detailed above
41	UAS-PGRP LCa ; HML∆ds-Red / sm6a	This Study	Component lines detailed above
42	lethal / fmk ; Hml-GFP / sm6a	This Study	Component lines detailed above
43	lethal / fmk ; Hml∆dsRed / sm6a	This Study	Component lines detailed above
44	; HML∆ds-Red / sm6a ; TM2/TM6c,Sb1	This Study	Component lines detailed above
45	; IF/sm6a ; srp 3xmCherry/TM6c,Sb1	This Study	Component lines detailed above
*Genotype information is as complete as published record will allow			

Table 2-3: List of primer sets used in the course of this thesis

Gene Name	Forward Sequence	Reverse Sequence	Reference
Actin 5C	TTGTCTGGGCAAGAGGATCAG	ACCACTCGCACTTGCACTTTC	Clark et al., 2015
Drosomycin	GTACTTGTTCGCCCTCTTCG	CTTGCACACACGACGACAG	
Diptericin	ACCGCAGTACCCACTCAATC	CCCAAGTGCTGTCCATATCC	
Unpaired-3	GCAAGAAACGCCAAAGGA	CTTGTCCGCATTGGTGGT	
DE-Cad	GACGAATCCATGTCGGAAAA	TCACTGGCGCTGATAGTCAT	
Delta	AGTGGGGTGGGTGTAGCTTT	GCTGTTGCTGCCAGTTTTG	
Notch	GAATTTGCCAAACACCGTTC	ACCGACACTTGTGCAGGAA	
Pickel	GCTCTCGCTTACCATCATCC	TACGGCCAAAAACATGAACA	
Kune-kune	AGGTTGTGGGCTCTGTTTTC	ATCCCGAGAATCTCCTTTGG	
Sinuous	CATTGAATTGCATAAACTTCAGCTA	GCGGAGTTTCGCTTACCTT	
Polychetoid	TGAATCGAGAGGCAACTTCTT	TTCTCGCGGGACAGACTC	
Discs Large-1	AGAGTCGCGATGAGAAGAATG	GCTGGTGCTGCTCACAACT	
Bacilli	CGACCTGAGAGGGTAATCGGC	GTAGTTAGCCGTGGCTTTCTGG	
Alpha	CCAGGGCTTGAATGTAGAGGC	CCTTGCGGTTCGCTCACCGGC	

Gamma	GGTAGCTAATACCGCATAACG	TCTCAGTTCCAGTGTGGCTGG	
16S V1F/V2R	AGAGTTTGATCCTGGCTCAG	CTGCTGCCTYCCGTA	Claesson et al., 2010
Hemolectin	TTGCCTATCCCACCTGTTGT	AGGAAACGGGTAAACAAGATGA	This study
Reaper	TCGATTTCTACTGCAGTCAAGG	GAGTAAACTAAAATTGGGTGGGTGT	This study

Chapter 3: Inflammation drives age-related physiological decline

3.1 Introduction

Tolerance mechanisms include regeneration and protection of epithelial tissues. These mechanisms keep immune activity at a basal state, allowing for the survival and healthy proliferation of commensal bacterial species. Fly studies have shown that intestinal damage can be kept to a minimum by ensuring that immune and repair mechanisms work in tandem (Chakrabarti et al., 2012, Buchon et al., 2009b). However, with age the delicate balance between immune tolerance and regulation becomes skewed. Studies in the adult fly have repeatedly shown the importance of immune regulation in maintaining intestinal homeostasis (Marra et al., 2021, Fast et al., 2020, Shin et al., 2019, Wang and Xia, 2018, Broderick et al., 2014, Liu and Jin, 2017, Regan et al., 2013). Multiple works have corroborated findings that constitutive immune activation results in over proliferation and pathogenesis of bacteria originally present in the commensal population, such as Alphaproteobacterial species *Gluconobacter morbifer* (Lee et al., 2013b, Roh et al., 2008, Ryu et al., 2008b). Findings from the Walker group later showed that gut permeability increases as a direct correlate of age. Age-related intestinal decline is associated with an increase in inflammatory markers, epithelial disruption, and reliably predicts death (Rera et al., 2012). Guo and colleagues further corroborated that chronic activation of gut immunity can sensitize flies to bacterial infection and shorten lifespan (Guo et al., 2014). Using the *Drosophila* Gal4/UAS system, PGRP-SC2 (a negative regulator of IMD signaling) was overexpressed in enterocytes along the adult fly intestine (Guo et al., 2014). By increasing expression of peptidoglycan scavenger PGRP-SC2, Guo et al. show that levels of IMD marker diptericin decreased, resulting in reduced dysbiosis and intestinal stem cell proliferation. In other words, prolonged bacterial and epithelial homeostasis with age

resulted in increased lifespan (Guo et al., 2014). These works collectively indicate how promotion of gut health improves host/commensal interactions, resulting in extended intestinal homeostasis and decreased mortality.

Evidence suggests that intestinal decline occurs because of dysbiosis. However, the question remains, what event causes commensal dysbiosis? Guo and colleagues did not show how or why bacteria were changing, only that age-associated changes in insulin signaling caused deregulation of humoral immunity, associated with an increased bacterial load. Clark and colleagues further showed that there are distinct and substantial changes in bacterial composition before and after loss of intestinal barrier function (Clark et al., 2015). By eliminating Smurf-induced dysbiosis, the authors revealed that rapid lifespan decline was a consequence of bacterial imbalance. While Clark et al. were able to extend lifespan in post-Smurf germ-free flies, these flies still exhibited persistent barrier dysfunction.

Immune system dynamics and microbe relationships seem to be mostly studied from the effects on epithelial cells. However, there may be proceeding aspects of this mechanism that are yet to be understood. For example, how are gut epithelial cells able to defend against immunity/bacteria-induced dysplasia? Work carried out during the completion of my Master of Science (M.Sc.) degree aimed to further understanding the consequential role of innate immunity on changes associated with intestinal decline. The data summarized in Section 3.1.1.2 were completed during my master's in the Walker Lab at the University of California, Los Angeles. These findings are presented here as they provide important foundational context for work done throughout the course of this doctorate. Key assays, including mortality, Smurf counts, and bacterial works were repeated in the Clark Lab at Durham University to assure robustness of data. Master's work will be clearly indicated and referenced respectively.

3.1.1 Master of Science Thesis Findings – Immune activation drives physiological decline

3.1.1.1 Drosophila melanogaster's innate immune system – in brief

In adult *Drosophila*, intestinal immunity is largely regulated by two nuclear factor κB (NF-κB) signaling pathways – the immune deficiency (IMD) and Toll pathways (Hetru and Hoffmann, 2009). Together, IMD and Toll maintain epithelial integrity and regulate production of antimicrobial peptides (AMPs). The *Drosophila* intestine is regionalized by foregut, midgut, and hindgut, with each respective locale having distinct physiological properties. Immune responses are also highly regionalized, with Toll pathway activity being present in the foregut and hindgut and IMD pathway activity being present throughout the whole gut, especially the midgut (Dutta et al., 2015). For the experiments conducted, spaciotemporal expression of genes associated with these NF- κB pathways in the fly intestine were used to determine how closely immune-induced changes mimic age-induced changes. To recapitulate intestinal inflammation in the fly, the drug-inducible GeneSwitch-UAS transgene expression system was used with the driver line 5966-GS. This provided a means for temporal control of immune activation. Specifically, 5966-GS is expressed in fly intestinal progenitor cells, enteroblasts, and post-mitotic absorptive cells, enterocytes (Mathur et al., 2010) as well as other tissues (see Chapter 5).

3.1.1.2 Summary of Master of Science Thesis Findings

Previous data from my M.Sc. show that immune activation hastens organismal decline, as displayed by increased loss of intestinal barrier function and increased death rate (Table 3.1). These findings are consistent with previously published work indicating that age-associated increases in immune activity are linked to accelerated rates of barrier dysfunction (Clark et al., 2015, Salazar et al., 2018).

Identification of changes in intestinal physiology requires non-invasive assays which allow for in vivo study without sacrificing the animal. The Ultimate Reader of Dung (T.U.R.D) provides a means to study age-related changes in gut physiology by analyzing the fecal output of live flies (Cognigni et al., 2011, Wayland et al., 2014). By adding a non-toxic bromophenol blue salt to fly media, fecal deposits were monitored in IMD, and Toll activated cohorts (assay detailed in Section 2.4). M.Sc. data show IMD and Toll activation significantly increase fecal deposit hue, or color, indicating greater alkalinity in the gut. Fecal deposit concentration, number, and individual excrement area were also impacted by immune activation (Table 3.1). Using fecal read out as a proxy for intestinal function, these data suggest that intestinal immune activation drives changes in intestinal physiology.

Utilizing bacterial DNA extracted from whole flies and universal primers to the bacterial 16s rRNA gene, total bacterial load was examined in immune activated flies. After only ten days of immune activation, there is a two-fold increase in whole-fly non-Smurf internal bacterial load (Table 3.1). Indicating that immune activation, in the presence of intact intestinal epithelia, drives substantial microbial changes. Similarly, Toll activation is sufficient to significantly increase bacterial load (Table 3.1). These data show that intestinal immune activation drives dysbiosis regardless of chronological age and barrier status.

To further characterize how microbial populations may have changed in immune activated flies, samples were run against taxon-specific primers to discern potential changes in proportions of bacterial classes. IMD activation significantly increased Bacilli and Alphaproteobacteria proportions in the whole fly (Table 3.1). Toll activation significantly increased Alphaproteobacteria proportions and increased Bacilli proportions (Table 3.1). Taxon-specific findings indicate that bacterial composition is adversely

affected by immune activation.

These same DNA extractions would later be used for in-depth taxonomic analysis through next generation, or 'shotgun', sequencing for PhD work at Durham.

No.	M.Sc. Thesis Experiment	IMD Activation	Toll Activation
1	Mortality	↑	↑
2	Barrier Dysfunction	↑	↑
3	Fecal Deposit pH	↑	↑
4	Fecal Deposit Concentration	↑	↓
5	Fecal Deposit Area	↑	↓
6	Fecal Deposit Number	↓	↓
7	Total Bacterial (β) Load	↑	↑
8	Alpha Taxon β Load	↑	↑
9	Gamma Taxon β Load	–	–
10	Bacilli Taxon β Load	↑	–

Table 3-1: Summary Table of M.Sc. Thesis Findings

All immune activation experiments occurred in conventionally reared 5966-GS > UAS-PGRP-LCa and 5966-GS > UAS-Toll^{10b} non-Smurf, female flies, immune induced from day 10 of adulthood. Downward arrows (↓) indicate immune-induced decreases in the measured phenotype i.e., a decrease in fecal deposit number, or fewer excrements, were observed upon IMD and Toll activation. Upward arrows (↑) indicate immune-induced increases in the measured phenotype i.e., an increase in mortality, or more death, was observed upon IMD and Toll activation. A dash (-) indicates no observed immune-induced change in the measured phenotype. Detailed methods for each experiment can be found in the following sections of this thesis: 2.1, 2.3-2.5, and 2.7.

3.1.2 Relating my M.Sc. data to my PhD work

Although there are minor differences between how IMD and Toll activation impact intestinal physiology with age, M.Sc. data robustly show that constitutive immune activation significantly impacts intestinal physiology, resulting in whole organism decline. Immune activation appears to mimic the same physiological decline associated with age. Data suggests that both IMD and Toll activation lead to significant disruptions in digestive transit which manifests as changes in fecal output and increased intestinal pH. Concurrent with other published works (Buchon et al., 2009a, Buchon et al., 2009b, Ryu et al., 2008b), my M.Sc. data also showed dysbiosis associated with constitutive immune activation.

Collectively my M.Sc. findings provided a foundation for more detailed hypotheses regarding how immune dysregulation drives loss of intestinal homeostasis. Much of this introduction pertains to correlative data that establish a baseline characterization of how immune activation affects intestinal and whole organism physiology. Shortly after submission of my M.Sc. thesis, Dantoft and colleagues published work corroborating many of my own findings up to this point (Dantoft et al., 2016). An important methodological difference between Dantoft et al. and myself includes the genetic background of *Drosophila* used. The authors mutated immune repressor *Nubbin* (also known as *Pdm1*) which was sufficient to induce expression of NF-κB-like transcription factor *Rel*. Constitutive IMD activation was thus indirectly driven in the male fat body and midgut ECs. This led to dysbiosis, specifically increases in Acetobacteraceae and Bacilli bacterial populations. Dantoft and colleagues also fed antibiotics to *Nubbin* mutants and observed a lifespan increase, similar to lifespan extension effects reported by Clark and colleagues (Clark et al., 2015). By mutating *Nubbin*, however, the authors were also effecting transcription of other genes (Dantoft et al., 2013). The authors were likely also driving barrier dysfunction and loss of tissue function simultaneously. Consideration is needed for how *Nubbin* deletion in ECs may result in accelerated epithelial disruption. Indeed, the authors may just be profiling changes associated with barrier dysfunction (Clark et al., 2015, Rera et al., 2012).

An important distinction between my work and other published findings is that here conscious effort was taken to separate non-Smurf from Smurf flies. The importance of identifying and characterizing Smurfs separately is paramount in discerning the impact of immune activation without the confounding effects of loss of barrier function – a phenotype which has consistently shown disproportionate levels of immune expression (Clark et al., 2015, Rera et al., 2012). This point becomes increasingly important when

considering that constitutive immune activation drives barrier dysfunction, whereby up to 50% of the induced population is Smurf by midlife (Alcaraz, 2016).

3.1.3 Aim and Objectives

The focal question remains, what is the etiology of age-associated intestinal inflammation? The aim of this chapter is to establish the relative contributions of immune activation and loss of barrier function to intestinal and organismal decline. I hypothesized that immune induction from young age would continue to mimic age-related decline and show loss of tissue homeostasis.

Objectives for this chapter: To answer the question of whether immune activation alone is sufficient to drive the physiological changes seen with age or whether immune activation acts via its impact on barrier function, I compare age-induced and immune-induced phenotypes.

I will assess the effect of immune activation on:

- Bacterial load and composition – both prior to and following loss of barrier function
- Markers of intestinal integrity, stress, and regeneration, prior to the visible loss of barrier function defined by the Smurf phenotype

All data presented from this point forward are original findings from my Ph.D.

3.2 Intestinal immune activation drives bacterial dysbiosis in a species-specific manner

3.2.1 Acetobacteraceae expansion is driven by IMD pathway activation

To detect effects of constitutive immune activation on microbial composition a metagenomics approach was taken. The same DNA extractions used during my M.Sc. to quantify immune-induced effects on bacterial load were also used for in-depth taxonomic analysis through next generation, or 'shotgun', sequencing. MEGAN software was used to assign the resulting sequences to respective NCBI taxonomy. Only IMD activated early, and mid-life samples were sequenced. Importantly this work was carried out in non-Smurf flies.

Sequencing analysis revealed that bacterial species composition changes upon sustained activation of the IMD pathway. Figure 3.1 shows summarized reads of the taxonomic classification Family at two separate time points, day 10 and day 20. Unlike assigned reads, summarized reads show the number of taxa assigned to the Family level as well as higher classifications i.e., *Genus* and *species*. The proportion of taxa changes substantially between day 20 control and immune activated flies. Namely, Acetobacteraceae increases from zero summarized reads in the uninduced control to an average of 3488 reads across replicate samples in drug induced 20-day old flies (Figure 3.1). The bacterial Family Lactobacillaceae also increases from 227 summarized reads in uninduced controls to 384 summarized reads in immune activated flies. Relative to uninduced control flies; Family summarized reads pertaining to Enterobacteriaceae, Burkholderiaceae and Anaplasmataceae decreased in immune activated flies at 20-days-old (Figure 3.1). Summarized reads were available for six species of bacteria, two of which changed significantly between control and immune activated flies (Figure 3.2). Both *Commensalibacter intestine* and *Lactobacillus antri*, parts of the Acetobacteraceae and

Lactobacillaceae Families respectively, increased significantly in IMD activated flies (Figure 3.2).

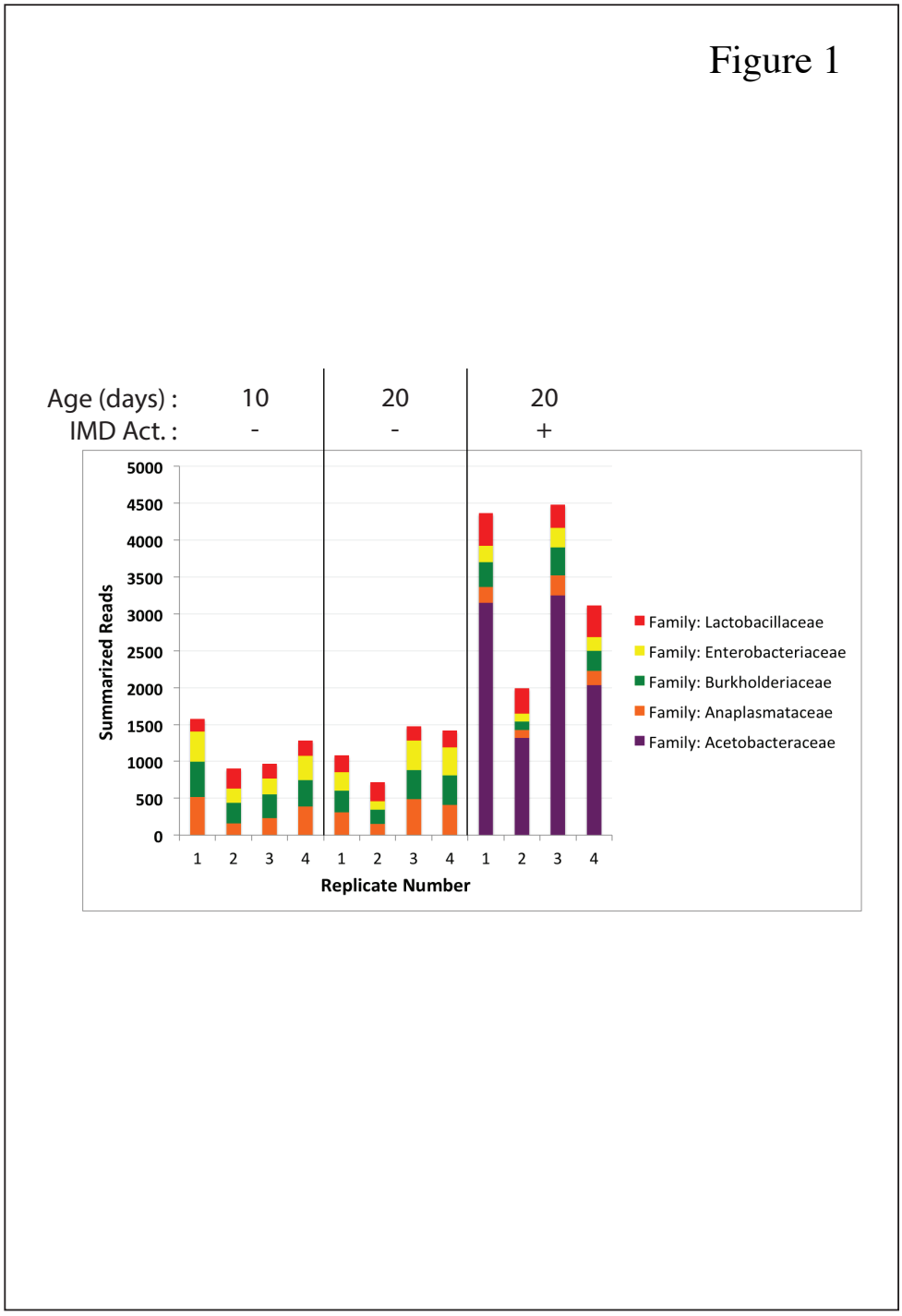

Figure 3.1: Acetobacteraceae expansion is driven by IMD activation

Total number of summarized counts for the Family taxonomic classification. Next generation sequencing was completed in 5966GS > UAS-PGPR-LCa non-Smurf female flies. Family units are sorted according to color; figure legend shows which color corresponds with each Family unit. Each column represents a biological replicate, n = 4 replicates of five surface-sterilized whole flies. Sequencing samples originate from master's work but were sequenced and analyzed as part of my doctoral work.

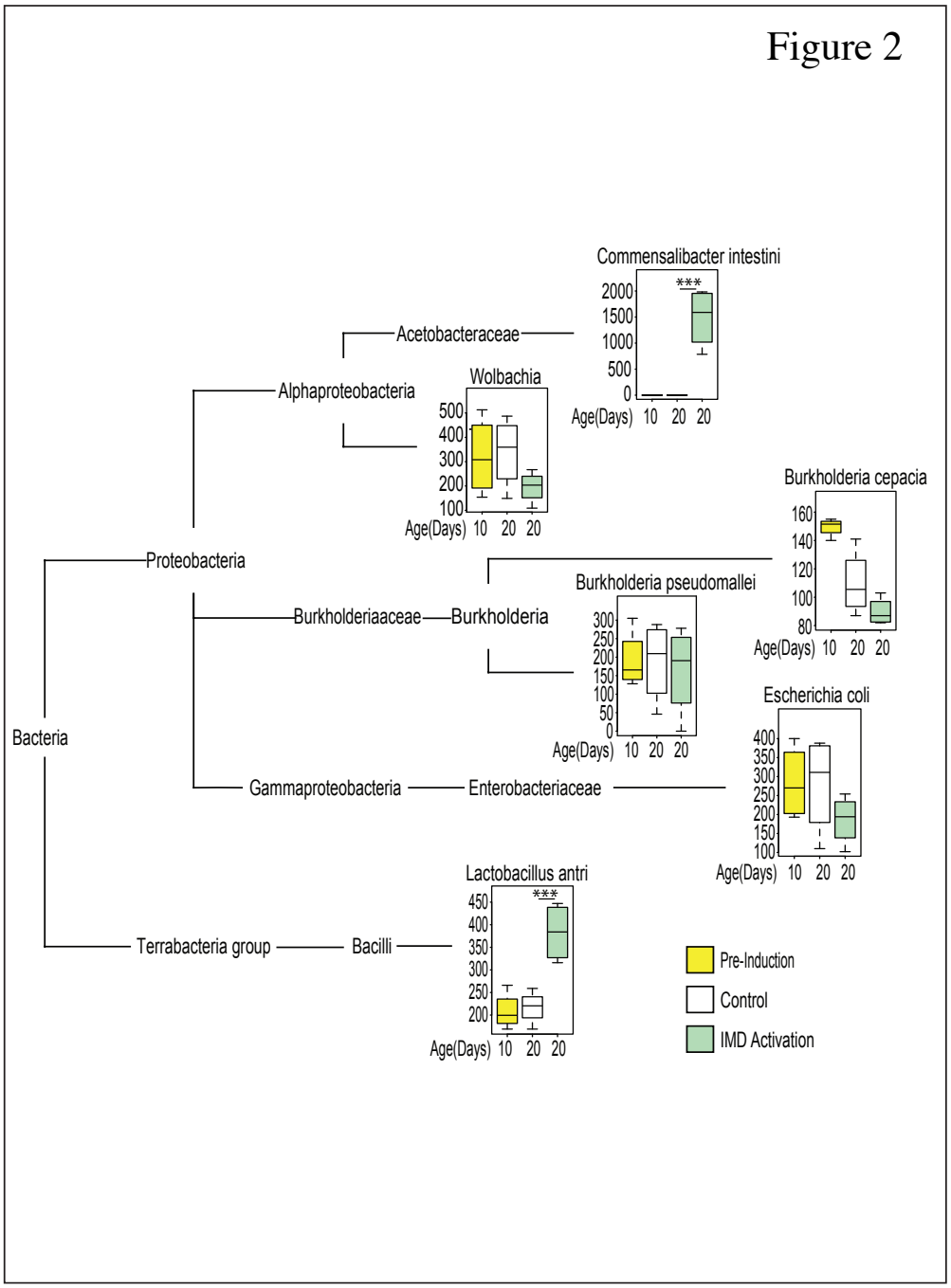

Figure 3.2: Immune activation significantly changes expression of specific bacterial species

Taxonomic tree representing a simplified list of the classifications Phyla, Class, Order, Family, Genus and Species as identified in sequencing analysis. Summarized reads are shown for six Species in immune activated and control *5966GS > UAS-PGPR-LCa* non-Smurf whole female flies. n = 4 replicates of 5 surface-sterilized whole flies Boxplots display the first and third quartile, with the horizontal bar at the median, y-axis = summarized reads. p-value <0.001 = *** in Wilcoxon Test, only significant changes shown.

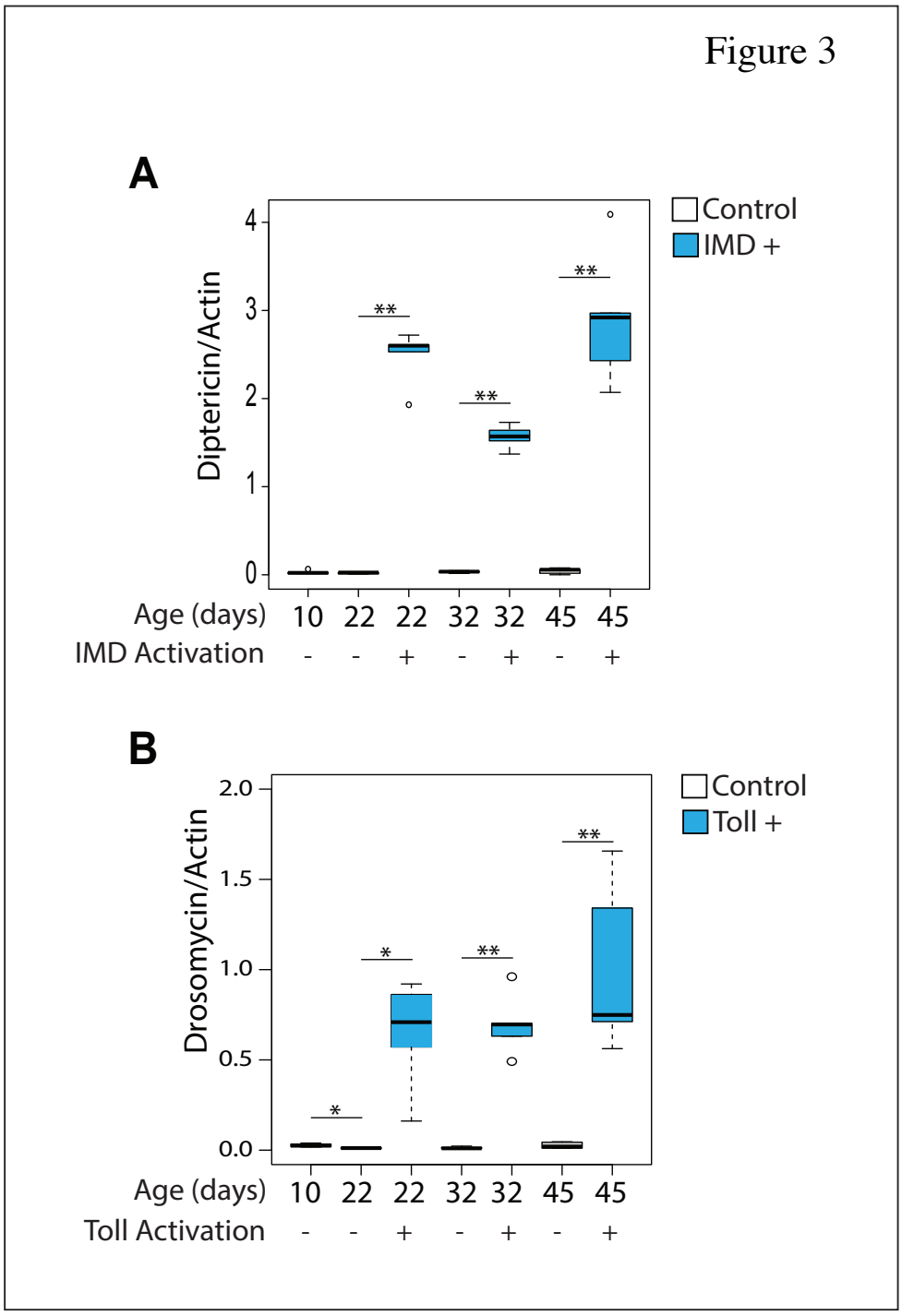

Figure 3.3: Validation of immune pathway activation

Diptericin (IMD associated AMP) and drosomycin (Toll associated AMP) gene expression. Assayed by RT-qPCR from dissected intestines of *5966GS > UAS-PGRP-LCa* (A) and *UAS-Toll 10b* (B) in immune activated and control non-Smurf female flies induced from day 10 of adulthood. n = 5 replicates of five intestines. p-value <0.05 = *, <0.01 = ** in Wilcoxon Test, only significant changes shown.

3.2.2 Validation of immune pathway activation

Upregulation of the IMD pathway was achieved through overexpression of the membrane receptor PGRP-LCa. As the upstream receptor for the IMD pathway, PGRP-LCa directly regulates expression of the antimicrobial peptide (AMP), diptericin (Hetru and Hoffmann, 2009). Similarly, the Toll Pathway was induced using constitutively active Toll. Activation of the Toll receptor regulates expression of the AMP Drosomycin (Hetru and Hoffmann, 2009). To validate the upregulation of IMD and Toll immune pathways, associated AMPs were quantified by RT-qPCR. Drug-induced lines for PGRP-LCa and Toll showed a significant increase in Diptericin and Drosomycin, respectively (Figure 3.3 A-B).

3.3 Immune activation drives dysbiosis in immune-induced Smurf flies

To validate M.Sc. findings from the Walker Lab in California, lifespan, Smurf counts, and bacterial load assays were repeated at the start of my doctoral training in Durham. IMD and Toll activation findings were reproducible, with significant increases in mortality and Smurf number upon immune activation. Next, internal fly bacterial load was reassessed using the same M.Sc. protocol previously used (detailed in Section 2.5.1). In addition to non-Smurf samples, Smurf samples were collected for comparison. The working hypothesis was that immune-induced barrier dysfunction would result in even greater variability of bacterial composition.

Using universal primers to the bacterial 16s rRNA gene, total bacterial load was examined in immune activated flies at 10, 20, and 30 days of age. Increases in bacterial load results were greatest in immune-induced Smurfs (Figure 3.4 A-B). Loss of barrier function, driven by immune activation, consistently showed dysbiosis of the internal fly. In contrast to my M.Sc. data, shown above, bacterial load changes were not observed in

immune activated non-Smurfs, neither at mid- nor late life (Figure 3.4 A-B). There was, however, a small nonsignificant increase in Toll activated non-Smurfs (Figure 3.4 B).

3.3.1 Immune activation drives dysbiosis in reconstituted flies

To better understand bacterial interactions and major effector bacterial species, flies were reconstituted with taxa known to be commonly associated with *Drosophila* (methods detailed in Section 2.1.5). Gnotobiotic or re-associated flies are a standard in the field to further elucidate the impact/role of bacteria on the gut (Bonfini et al., 2016). During reassociation, fly guts are typically reassociated with one or more of five bacterial species from Acetobacteraceae and Lactobacillaceae Families (Chandler et al., 2011). Gnotobiotic flies were exposed to equal CFU of *Acetobacter pasteurianus, Lactobacillus plantarum*, and *Escherichia coli*. These commensal species are known to populate invertebrate and vertebrate species alike (Pais et al., 2018). IMD and Toll activation were then induced, and samples taken at 10-days old and 20-days old.

Dysbiosis is induced even in the presence of limited commensal populations. IMD activation increases bacterial load in immune-induced mid-life Smurf flies (Figure 3.5 A). Toll activation significantly increases bacterial load in non-Smurf and Smurf immune activated flies (Figure 3.5 B). Taxon-specific primer runs show an increase in Alphaproteobacterial and Bacilli levels in IMD and Toll activated Smurf flies (Figure 3.6 A-B, Figure 3.7 A-B). Together, these data suggest that Alpha and Bacilli bacterial classes contribute to immune-induced increase in bacterial load (Figure 3.5). Toll activation increases Alpha and Bacilli levels equally in both non-Smurf and Smurf reconstituted flies (Figure 3.6 B, Figure 3.7 B). IMD activated flies showed no changes in Gammaproteobacterial levels (Figure 3.7 A). These data show that IMD activation drives

dysbiosis via intestinal barrier loss. Toll activation drives dysbiosis upon induction regardless of barrier status.

3.3.2 Immune activation drives dysbiosis in monoassociated flies

To establish if one bacterial taxon was responsible for an increase in bacterial load upon immune activation, flies were re-associated with one of the following three species: *Acetobacter pasteurianus (A. pas)*, *Lactobacillus plantarum (L. plant.)*, and *Escherichia coli (E. coli)*. Even with single species re-association immune-induced loss of barrier function shows significant increases in bacterial load.

Monoassociation with *A. pas*. showed increased bacterial load in IMD activated Smurf flies (Figure 3.5 A). *A. pas*. also showed significantly increased bacterial load in Toll activated Smurfs and non-Smurfs flies (Figure 3.5 B). Further functional analysis was completed by running *A. Pas*. monoassociated samples against Alphaproteobacterial (Alpha) primers. IMD activated Smurf flies showed a non-significant increase in Alpha levels (Figure 3.6 A). Toll activated non-Smurf flies showed a significant increase in Alpha levels (Figure 3.6 B). There was an even greater significant increase in alpha levels for Toll activated Smurf flies (Figure 3.6 B).

Monoassociation with *L. plant*. significantly increased bacterial load in IMD activated Smurf flies (Figure 3.5 A), and in Toll activated non-Smurf flies (Figure 3.5 B). Further functional analysis was completed by running *L. plant*. monoassociated samples against Bacilli primers. IMD and Toll activated Smurf flies showed a significant increase in Bacilli levels (Figure 3.7 A-B). Toll activated non-Smurf flies also showed a non-significant increase in Bacilli levels (Figure 3.7 B).

Monoassociation with *E. coli* showed significantly increased bacterial load in Toll activated non-Smurf and Smurf flies (Figure 3.5 B). Further functional analysis was

completed by running *E. coli* monoassociated samples against Gammaproteobacterial (Gamma) primers. Toll activated non-Smurfs and Smurfs showed a significant increase in Gamma levels (Figure 3.8). Data pertaining to the effects of monoassociation with *E. coli* on IMD activated flies is not shown due to a lack of bacterial colonization. Potential colonization issues will be interpreted further in this chapter's discussion, Section 3.5.1.

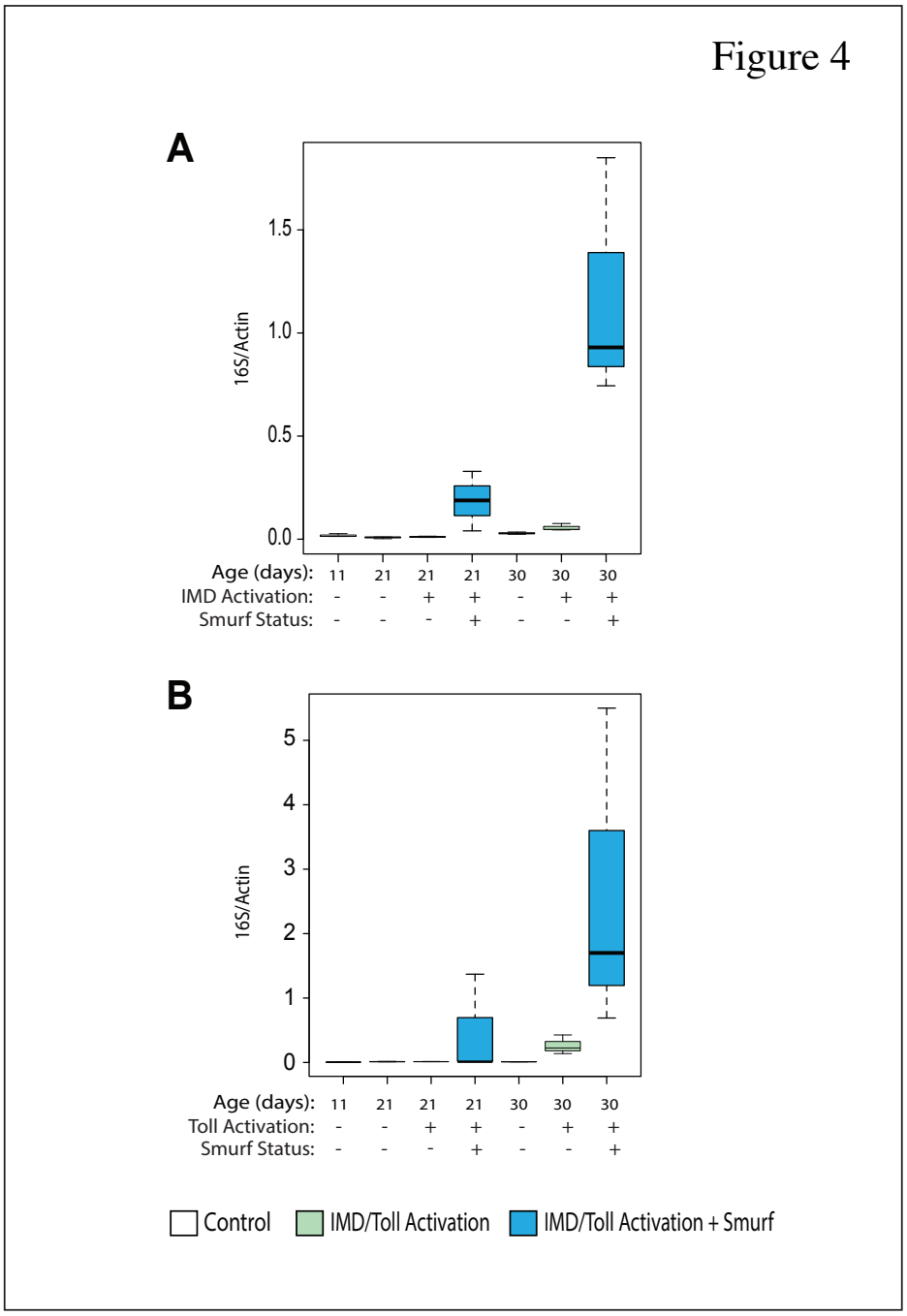

Figure 3.4: Immune activation increases total bacterial load in Smurf flies

Bacterial levels assayed by RT-qPCR of 16S with universal primers in immune activated and control non-Smurf female flies. *5966GS > UAS-PGRP Lc* (A) and *5966GS > UAS-Toll10b* (B). n = 5 replicates of five surface-sterilized whole flies. No statistically significant differences in Wilcoxon Test.

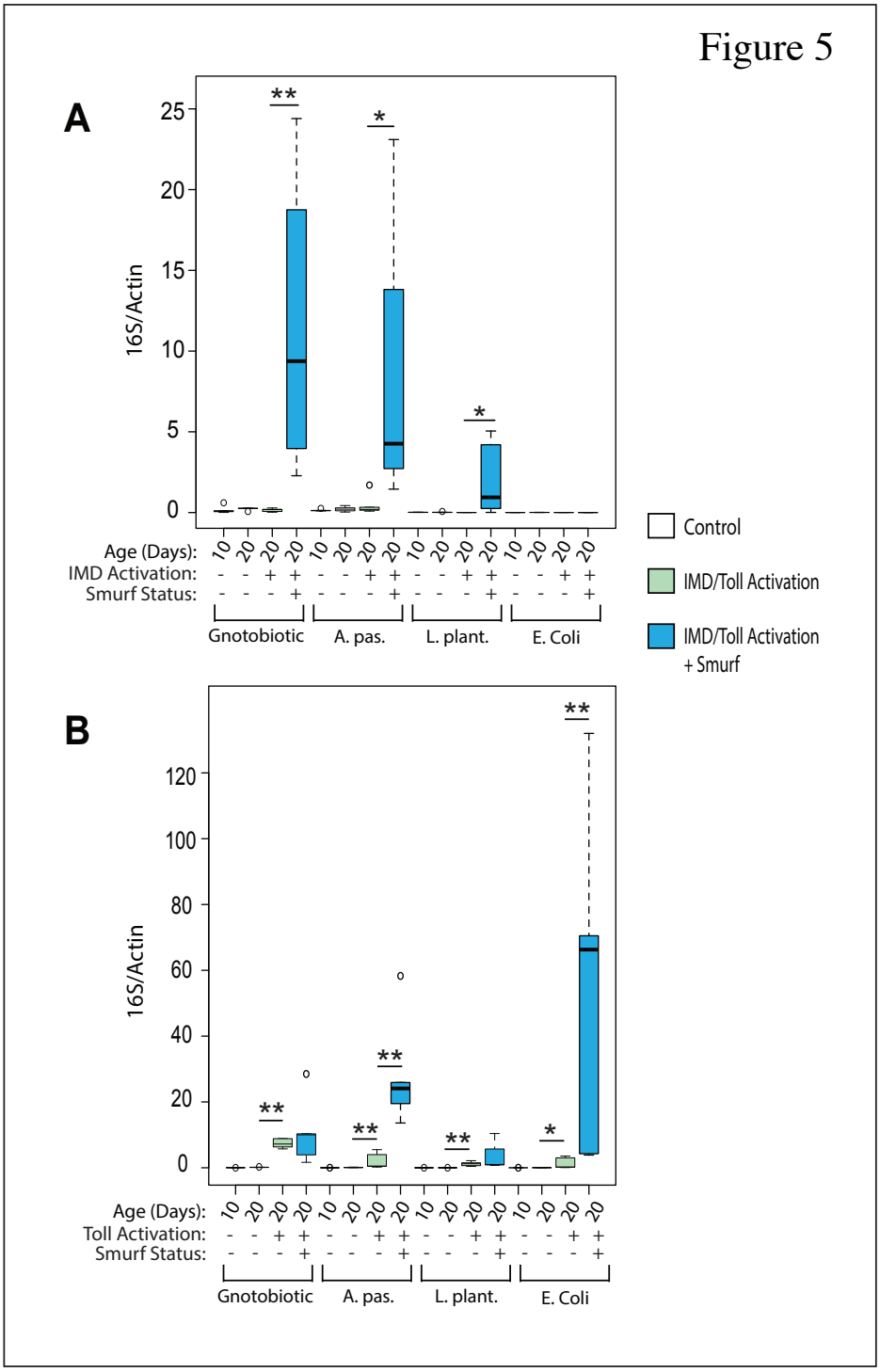

Figure 3.5: Immune activation drives dysbiosis in reconstituted flies

Bacterial levels assayed by RT-qPCR of 16S with universal primers in immune activated and control non-Smurf and Smurf female flies. *5966GS > UAS-PGRP-LCa* (A) and *UAS-Toll10b* (B) immune induced from day 10 of adulthood. n = 5 replicates of five surface-sterilized flies. p-value <0.05 = *, <0.01 = ** in Wilcoxon Test, only significant changes shown. A.pas. = Acetobacter *pasteurianus*, L. plant. = Lactobacillus *plantarum*, E. Coli = Escherichia *coli*

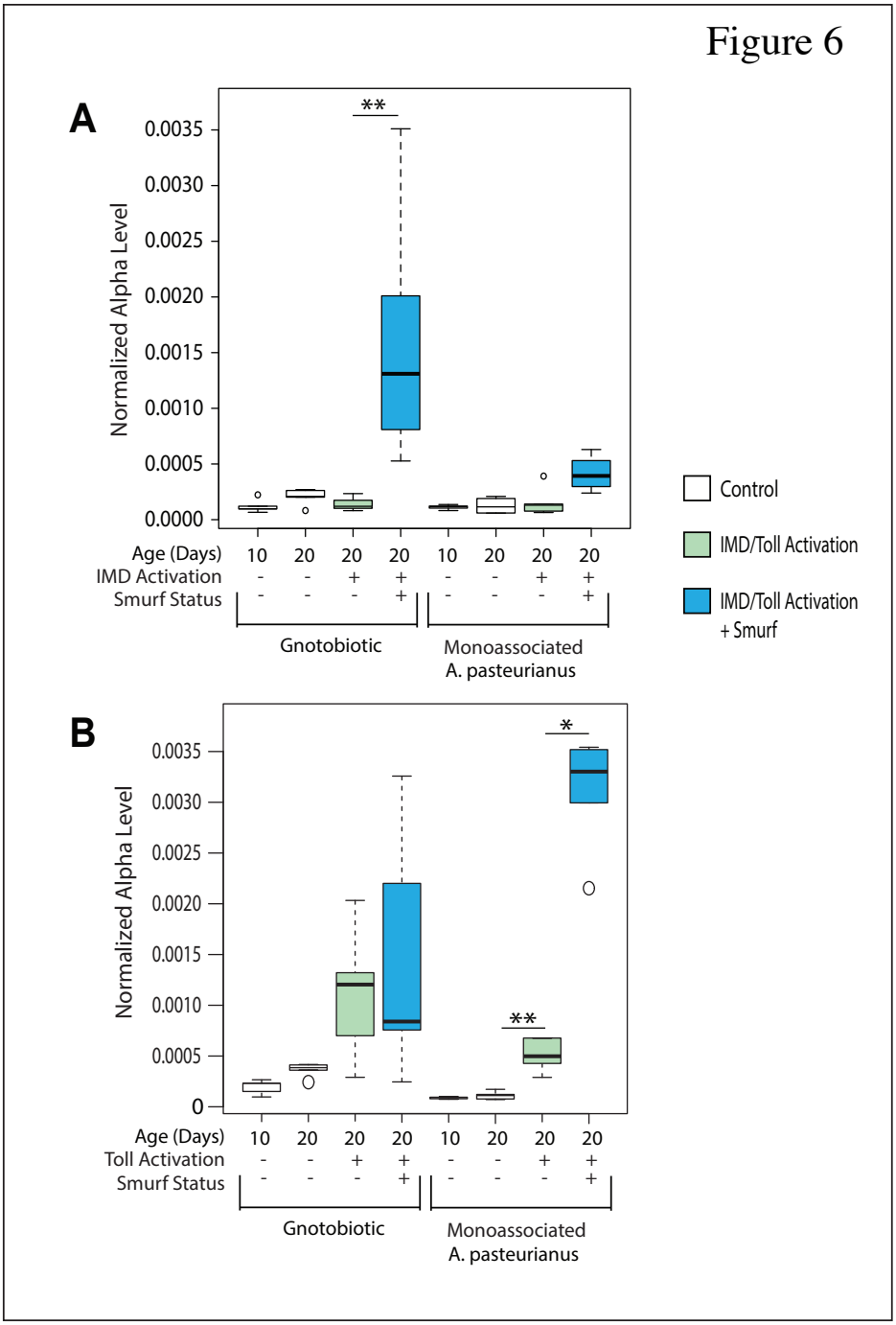

Figure 3.6: Immune activation impacts Alphaproteobacteria Class in reconstituted flies

Bacterial levels assayed by taxon-specific RT-qPCR of the Alpha16S rRNA gene in immune activated and control non-Smurf and Smurf female flies. *5966GS > UAS-PGRP LCa* (A) and *UAS-Toll10b* (B) immune activated from day 10 of adulthood. n = 5 replicates of five surface-sterilized flies. p-value <0.05 = *, <0.01 = ** in Wilcoxon Test, only significant changes shown.

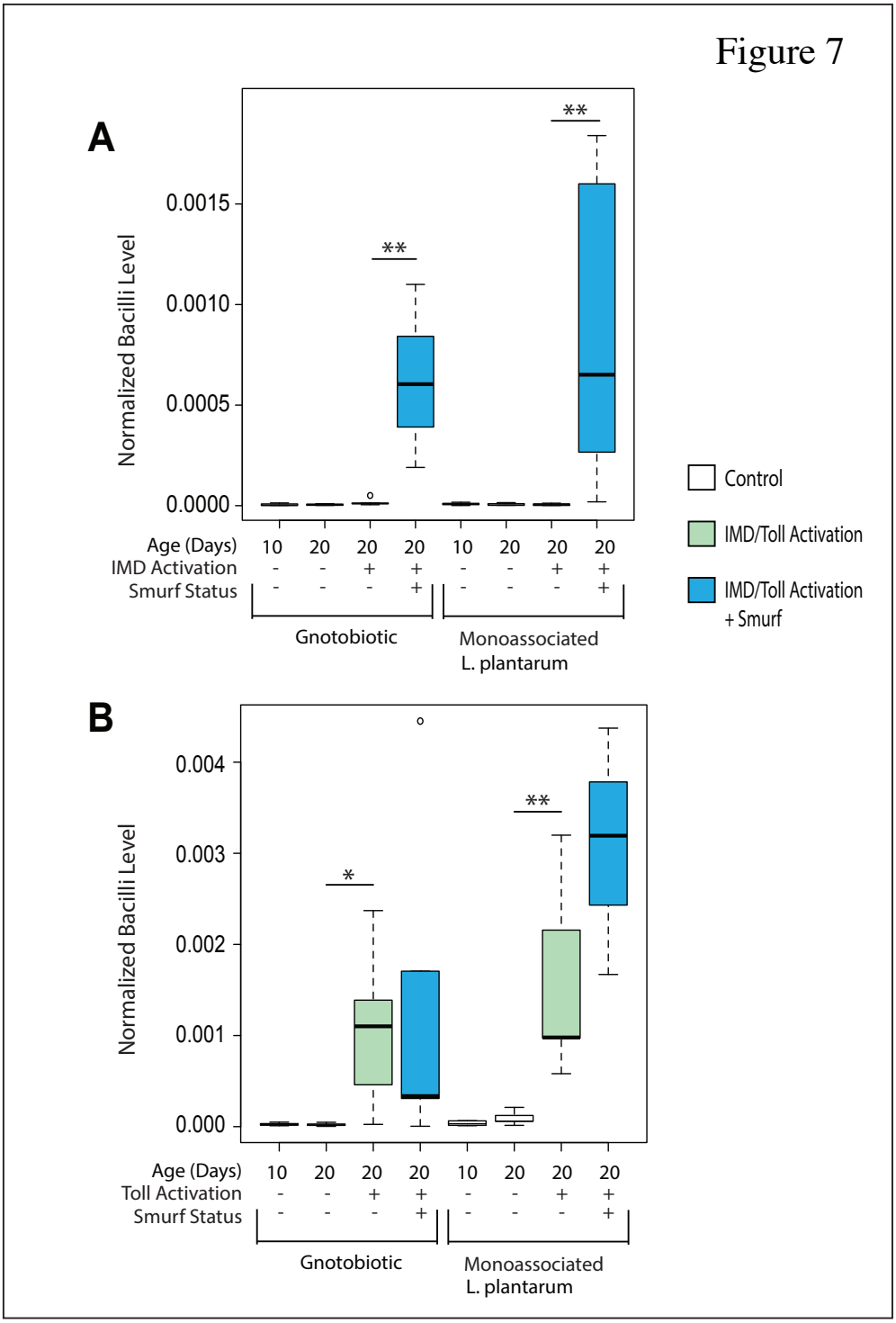

Figure 3.7: Immune activation impacts Bacilli Class in reconstituted flies

Bacterial levels assayed by taxon-specific RT-qPCR of the Bacilli 16S rRNA gene in immune activated and control non-Smurf and Smurf female flies. *5966GS > UAS-PGRP LCa* (A) and *UAS-Toll10b* (B) immune activated from day 10 of adulthood. n = 5 replicates of five surface-sterilized flies. p-value <0.05 = *, <0.01 = ** in Wilcoxon Test, only significant changes shown.

Figure 8

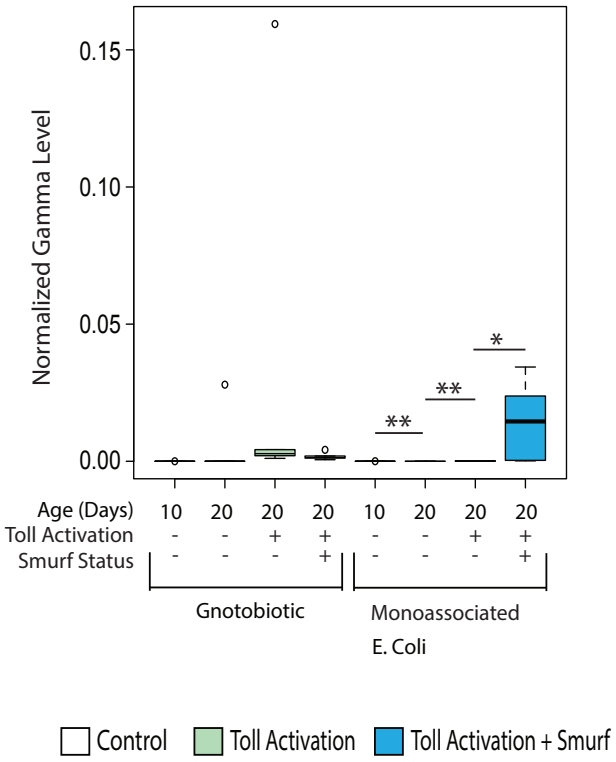

Figure 3.8: Toll activation impacts Gammaproteobacteria Class in reconstituted flies

Bacterial levels assayed by taxon-specific RT-qPCR of the Gamma 16S rRNA gene in immune activated and control non-Smurf and Smurf female flies. *5966GS > UAS-Toll10b* immune activated from day 10 of adulthood. n = 5 replicates of five surface-sterilized flies. p-value <0.05 = *, <0.01 = ** in Wilcoxon Test, only significant changes shown.

3.4 Intestinal immune activation drives loss of epithelial integrity and promotes dysplasia

To further characterize immune-induced effects on age-associated intestinal decline, expression of an array of intestinal epithelial markers were quantified. These markers include junctional proteins and immune pathway ligands and extracellular matrix components - all of which form a network to maintain homeostasis. Expression was quantified by RT-qPCR from dissected intestines throughout fly lifespan. Time points were based on immune activated lifespans i.e., early (10-days old), mid (20-days old), and late (30-days old) life. Importantly, these intestines were dissected from non-Smurf flies, or flies that still retained barrier function on the day of dissection. The scoring and segregation of flies maintaining barrier function allowed for data analysis and interpretation based on immune-induced effects on gene expression without the added confounding factor of loss of barrier function.

3.4.1 Immune activation drives misexpression of adherens junction genes

The working hypothesis was that epithelial junction expression may be directly perturbed by immune pathways associated with the gut.

Adherens junctions (AJs) help maintain cell polarity in the adult fly gut and are key regulators of cell-cell communication by modulating Notch signaling. Importantly, there are a set of canonical proteins associated with AJs that are responsible for establishing polarity in epithelial tissues. AJs sit apically along the lateral membrane of epithelial cells; however, the adult fly midgut is organized in opposite orientation (Tepass et al., 2001, Chen et al., 2018). Expression of *Drosophila* E-Cadherin (DE-Cad) and polychaetoid were assayed to determine immune-induced effects on AJs. DE-Cad is a transmembrane protein

localized in the Zonula Adheren domain of the plasma membrane. Polychaetoid encodes ZO-1, a cytoplasmic protein which binds to DE-Cad (Figures 3.9 C, 3.10 C).

Control and IMD/Toll activated flies all show age-related increases in DE-Cad gene expression (Figure 3.9 A-B). IMD and Toll activation do not change DE-Cad expression, however there are slight non-significant increases in late life (Figure 3.9 A-B). IMD activation significantly increases polychaetoid expression (Figure 3.10 A). By contrast, Toll activation significantly decreases polychaetoid expression during mid-life (Figure 3.10 B).

3.4.2 Immune activation drives misexpression of septate junction genes

Septate junctions (SJs) in the fly are responsible for restricting flow of digestive enzymes and potential pathogens between intestinal epithelial cells, promoting transcellular movement through the cell membrane. The transepithelial seal created by SJs is analogous to the mammalian tight junction. Transmembrane proteins of the claudin family form the stable SJ core complex, which sits basal to the AJ, except in the midgut where they sit apical to the AJ (Chen et al., 2018). Here, I look at expression of claudin proteins – Pickel (also known as Megatrachea), Sinuous, and Kune-Kune (Figures 3.11 C, 3.12 C, 3.13 C). Expression of tumor-suppressor gene Discs Large-1 (Dlg) was also quantified. Discs Large-1 is a membrane-associated guanylate kinase (MAGUK) which is located on the cytoplasmic face of SJs (Figure 3.14 C). Dlg is required for proper localization of the SJ core complex as well as regulating cell proliferation.

Pickel expression is non-significantly upregulated by IMD activation at mid-life, and significantly downregulated by Toll activation at mid-life (Figure 3.11 A-B). Sinuous expression is unchanged by IMD activation, and significantly downregulated by Toll activation (Figure 3.12 A-B). Kune-kune expression is significantly upregulated by IMD

activation at mid- and late life and is significantly downregulated by Toll activation at midlife (Figure 3.13 A-B). Together, these data show immune activation impacts expression of claudin protein genes. Discs Large-1 expression is significantly upregulated by IMD activation in late life, and significantly downregulated by Toll activation during mid-life (Figure 3.14 A-B). IMD activation mostly impacts junction gene expression during late life by increasing transcript level. Toll activation mostly impacts expression during mid-life by decreasing transcript level.

3.4.3 Immune activation may drive dysplasia via Jak/STAT pathway

3.4.3.1 IMD activation drives JNK-induced upregulation of apoptotic marker

The effects of IMD activation on epithelial decline were further assayed by quantifying apoptotic gene expression. The Jun N-terminal Kinase (JNK) pathway branches out from the IMD pathway and is responsible, in part, for cell proliferation and apoptosis resulting from tissue damage due to stress (Pinal et al., 2019). JNK phosphorylation activates transcription of reaper, a pro-apoptotic gene. Reaper expression is significantly upregulated by IMD activation during late life (Figure 3.15).

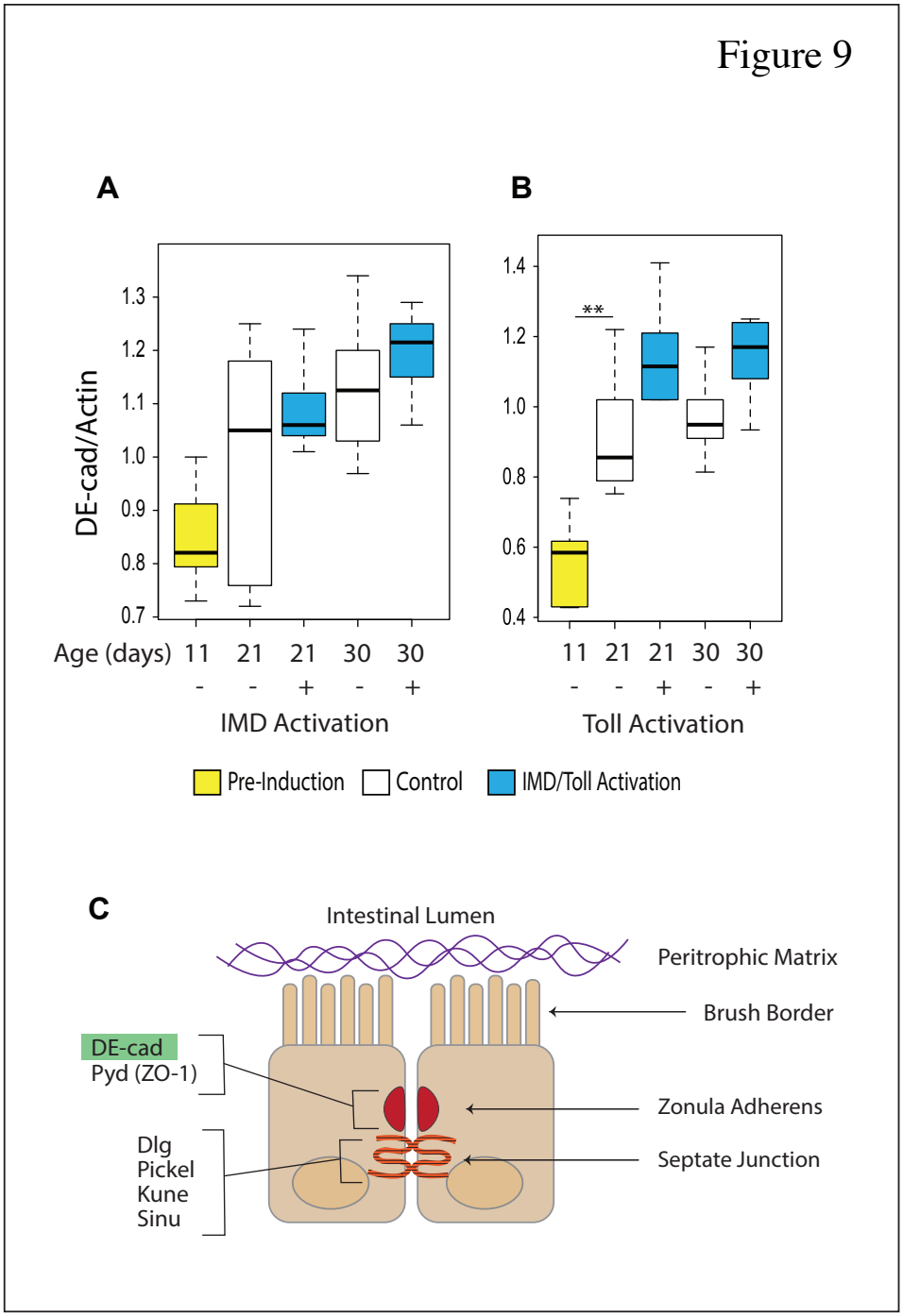

Figure 3.9: Immune activation drives misexpression of adherens junction gene DE-cad

Quantification of *Drosophila* E-Cadherin (DE-cad) mRNA levels. Gene expression assayed by RT-qPCR from dissected intestines; non-Smurf female flies immune activated from day 10 of adulthood and uninduced controls. *5966GS > UAS-PGRP LCa* (A) and *UAS-Toll10b* (B). n = 6 replicates of five intestines. p-value <0.01 = ** in Wilcoxon Test, only significant changes shown. Cartoon depicting epithelial cell organization and respective localization of junction-associated protein DE-cad (C).

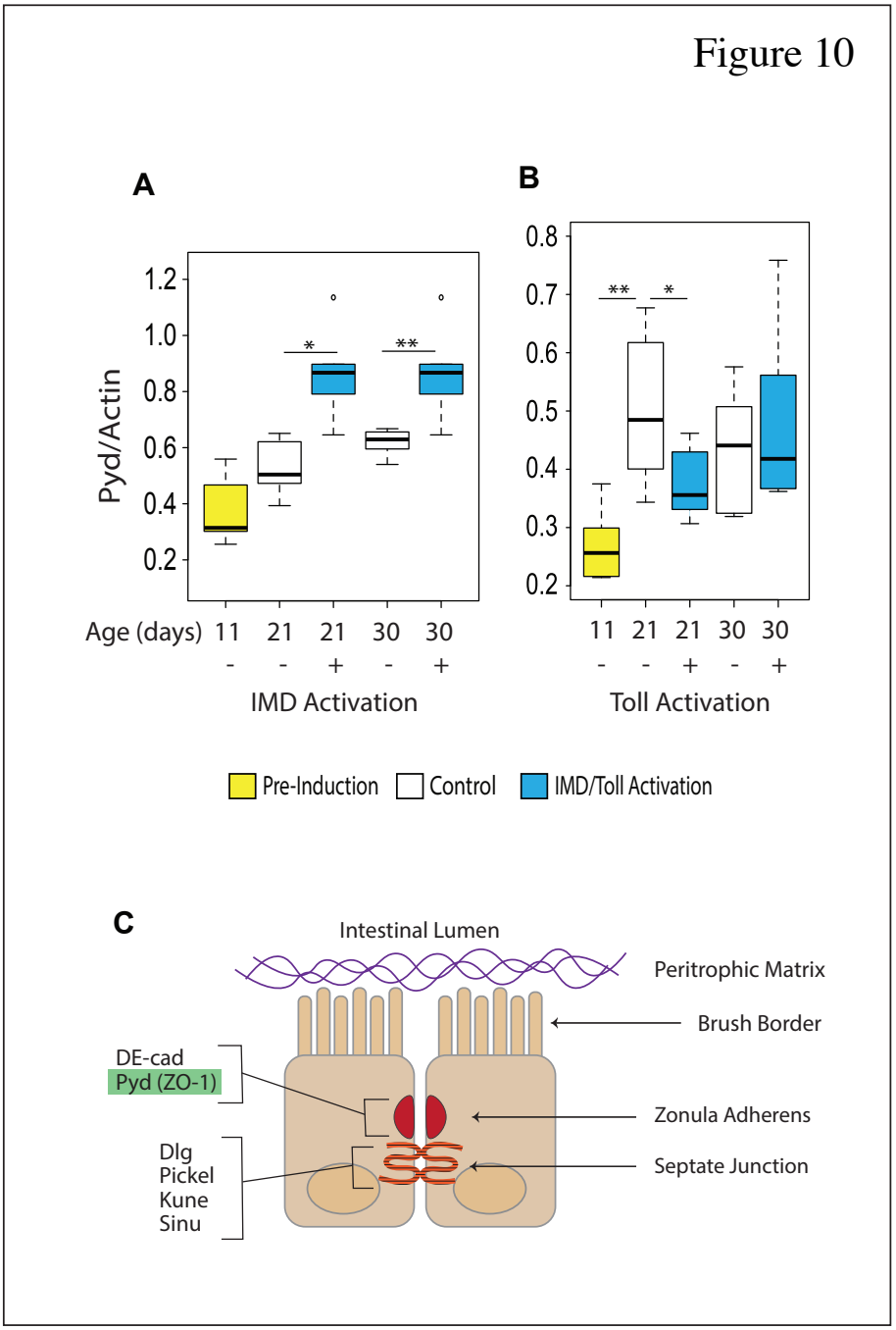

Figure 3.10: Immune activation drives misexpression of adherens junction gene Pyd

Quantification of Polychaetoid (Pyd) mRNA levels. Gene expression assayed by RT-qPCR from dissected intestines; non-Smurf female flies immune activated from day 10 of adulthood and uninduced controls. *5966GS > UAS-PGRP Lc* (A) and *UAS-Toll10b* (B). n = 6 replicates of five intestines. p-value <0.05 = *, <0.01 = **, in Wilcoxon Test, only significant changes shown. Cartoon depicting epithelial cell organization and respective localization of junction-associated protein Pyd (C).

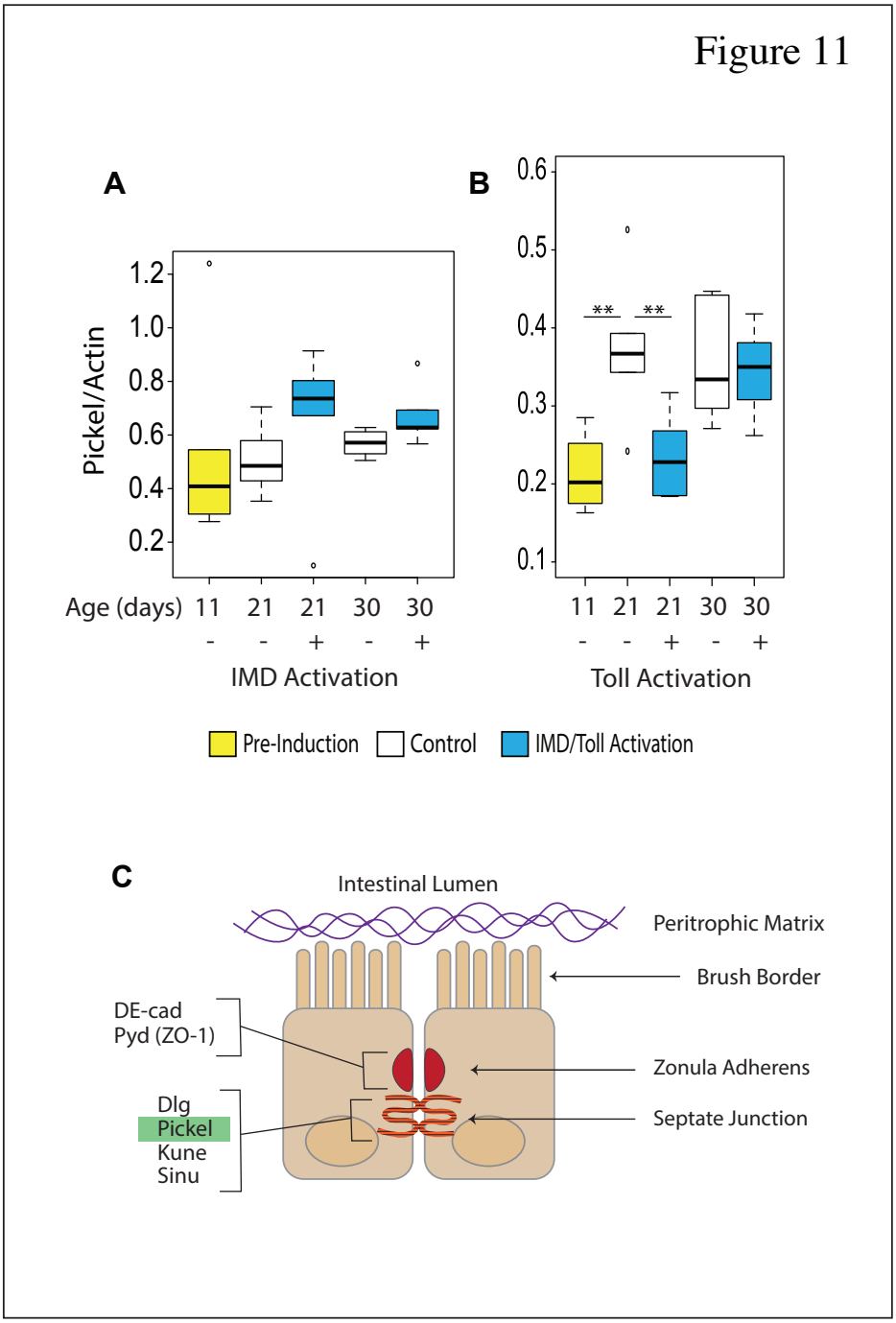

Figure 3.11: Immune activation drives misexpression of septate junction gene Pickel

Quantification of Pickel mRNA levels. Gene expression assayed by RT-qPCR from dissected intestines; axenic, non-Smurf female flies immune activated from day 10 of adulthood and uninduced controls. *5966GS > UAS-PGRP LCa* (A) and *UAS-Toll10b* (B). n = 6 replicates of five intestines. p-value <0.01 = **, in Wilcoxon Test, only significant changes shown. Cartoon depicting epithelial cell organization and respective localization of junction-associated protein Pickel (C).

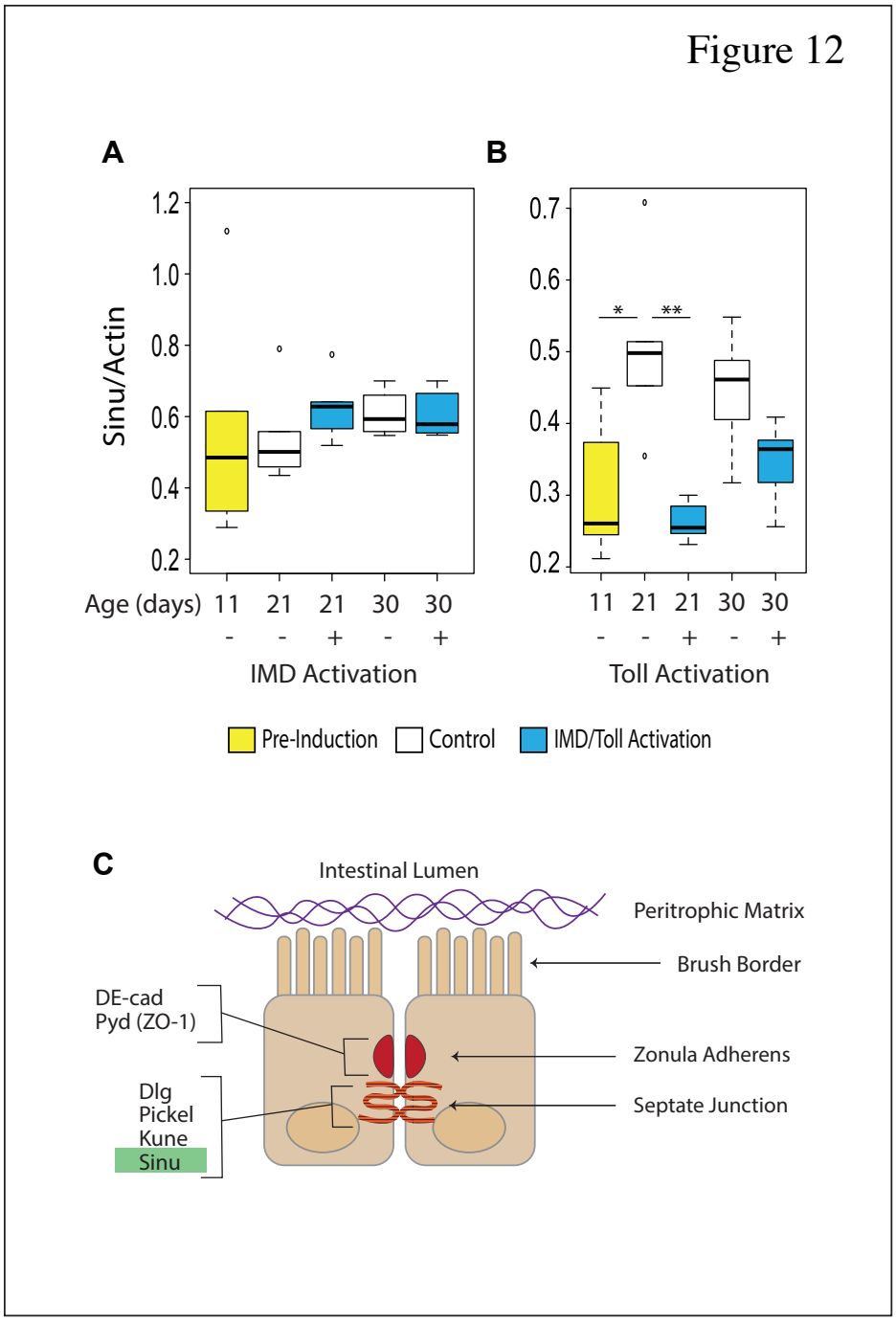

Figure 3.12: Immune activation drives misexpression of septate junction gene Sinu

Quantification of Sinuous (Sinu) mRNA levels. Gene expression assayed by RT-qPCR from dissected intestines; non-Smurf female flies immune activated from day 10 of adulthood and uninduced controls. *5966GS > UAS-PGRP LCa* (A) and *UAS-Toll10b* (B). n = 6 replicates of five intestines. p-value <0.05 = *, <0.01 = **, in Wilcoxon Test, only significant changes shown. Cartoon depicting epithelial cell organization and respective localization of junction-associated protein Sinu (C).

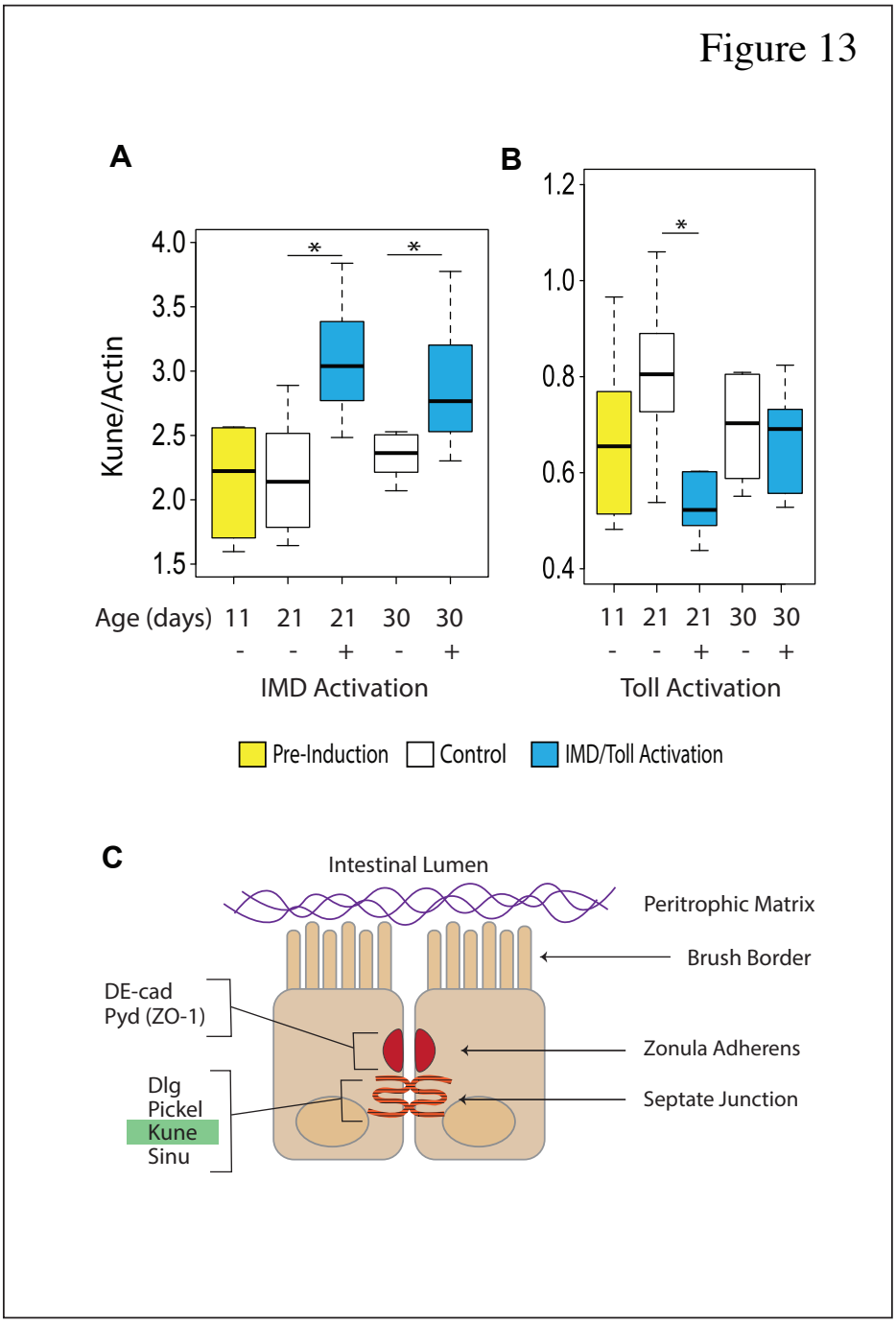

Figure 3.13: Immune activation drives misexpression of septate junction gene Kune

Quantification of Kune-Kune (Kune) mRNA levels. Gene expression assayed by RT-qPCR from dissected intestines; non-Smurf female flies immune activated from day 10 of adulthood and uninduced controls. *5966GS > UAS-PGRP LCa* (A) and *UAS-Toll10b* (B). n = 6 replicates of five intestines. p-value <0.05 = *, in Wilcoxon Test, only significant changes shown. Cartoon depicting epithelial cell organization and respective localization of junction-associated protein Kune (C).

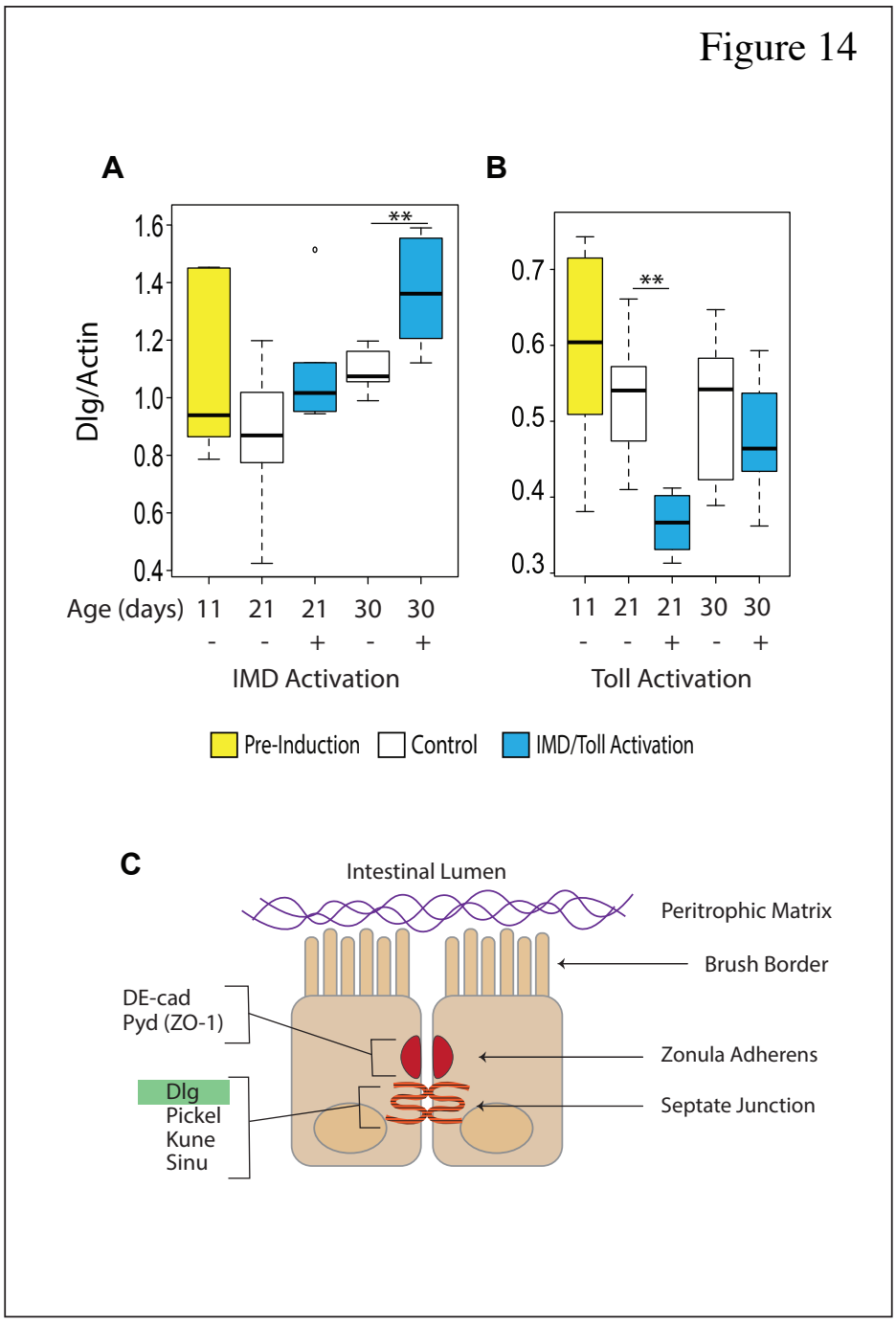

Figure 3.14: Immune activation drives misexpression of septate junction gene Dlg

Quantification of Discs Large-1 (Dlg) mRNA levels. Gene expression assayed by RT-qPCR from dissected intestines; non-Smurf female flies immune activated from day 10 of adulthood and uninduced controls. *5966GS > UAS-PGRP LCa* (A) and *UAS-Toll10b* (B). n = 6 replicates of five intestines. p-value <0.01 = **, in Wilcoxon Test, only significant changes shown. Cartoon depicting epithelial cell organization and respective localization of junction-associated protein Dlg (C).

Figure 15

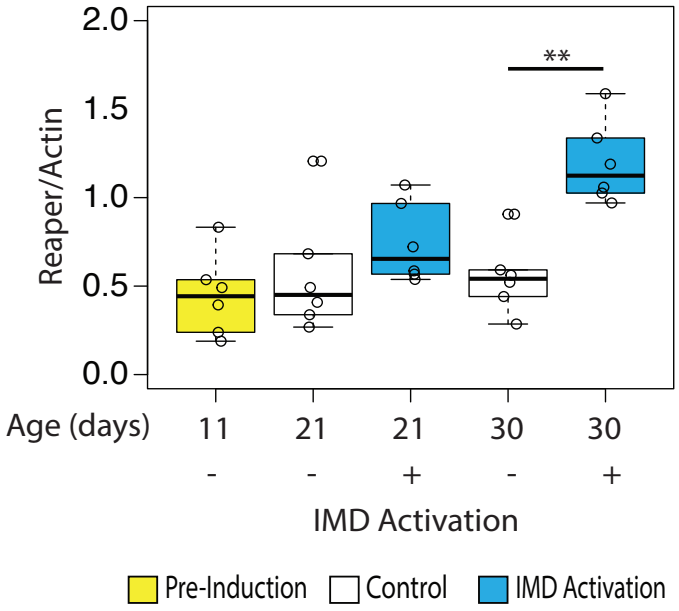

Figure 3.15: Immune activation drives misexpression of apoptosis-associated gene Reaper

Quantification of Reaper (rpr) mRNA levels. Gene expression assayed by RT-qPCR from dissected intestines; *5966GS > UAS-PGRP LCa* non-Smurf female flies immune activated from day 10 of adulthood and uninduced controls. n = 6 replicates of five intestines. p-value <0.01 = **, in Wilcoxon Test, only significant changes shown.

3.4.3.2 Immune activation drives misexpression of unpaired-3 gene

Unpaired-3 (upd3) is a cytokine ligand responsible for activating the Janus Kinase/Signal Transducer and Activator of Transcription (Jak/STAT) pathway in progenitor cells to induce proliferation (Jiang et al., 2009). Specifically, *upd3* is released by damaged or shedding enterocyte, or absorptive cells, and binds to the receptor *domeless* found on progenitor cells. *Upd3* also provides an indirect readout of the stress-response pathway, JNK (Figure 3.16 C). *Upd3* expression is significantly upregulated by IMD and Toll activation (Figure 3.16 A-B). Like the general pattern of junction expression, IMD-induced changes occur in late life (Figure 3.16 A).

3.4.3.3 Effects of immune activation on epithelial cell number and tissue composition

Notch is a transmembrane receptor associated with enteroblasts (EBs), or progenitor cells. Delta, membrane-tethered ligand for Notch, is used as a marker for intestinal stem cells. Together, delta and notch primarily coordinate the differentiation of enterocytes (Figure 3.17 C, Figure 3.18 C). Notch expression is unchanged by either IMD or Toll activation (Figure 3.17 A-B). There are, however, age-associated increases in notch expression in control and immune activated cohorts. Delta expression is unchanged by IMD activation, and significantly upregulated by Toll activation at mid-life (Figure 3.18 A-B). There are also age-associated increases in delta expression in Toll activated and uninduced control flies (Figure 3.18 B). To further determine the effects of IMD-induced epithelial changes, whole guts were assayed for changes in mitotic indices. Tissues were stained against mitotic marker phosphorylated histone-3 (PH3) to quantify intestinal stem cell proliferation (methods detailed in Section 2.8). IMD activation decreases the number of PH3+ cells in old Smurf flies (Figure 3.19). Apart from old Smurf flies, IMD activation

does not induce significant changes in mitotic events (Figure 3.19). This corresponds with unchanged delta expression levels in IMD activated flies (Figure 3.18 A).

To determine if immune-induced epithelial changes were driving progenitor differentiation, hormone-releasing cells or enteroendocrine cells (EEs) were quantified. Prospero is a transcription factor which marks EEs and was used as a proxy for quantifying shifts in differentiation events. The same guts dissected for PH3 counts were also co-stained against prospero and DAPI; posterior midguts were then imaged using confocal microscopy (methods detailed in Section 2.8). Mid-life IMD activated Smurf flies show a non-significant increase in prospero-positive (pros+) cells (Figure 3.20 G-H, Figure 3.21 A). IMD activation significantly increases the ratio of pros+ cells in late life (Figure 3.20 J-K, Figure 3.21 A), while IMD activated Smurfs show a significant decrease in pros+ cell ratio in late life (Figure 3.20 L, Figure 3.21 A). Immune induction increases differentiated cell ratios in old and barrier compromised flies. IMD activation significantly increases total cell number in early and midlife non-Smurf flies (Figure 3.20 B-C, G-H, Figure 3.21 B). Late life immune-induced Smurf flies also show a significant increase in total cell number (Figure 3.20 L, Figure 3.21 B). While number of proliferation events seem unchanged in IMD activated flies, total cell number increases.

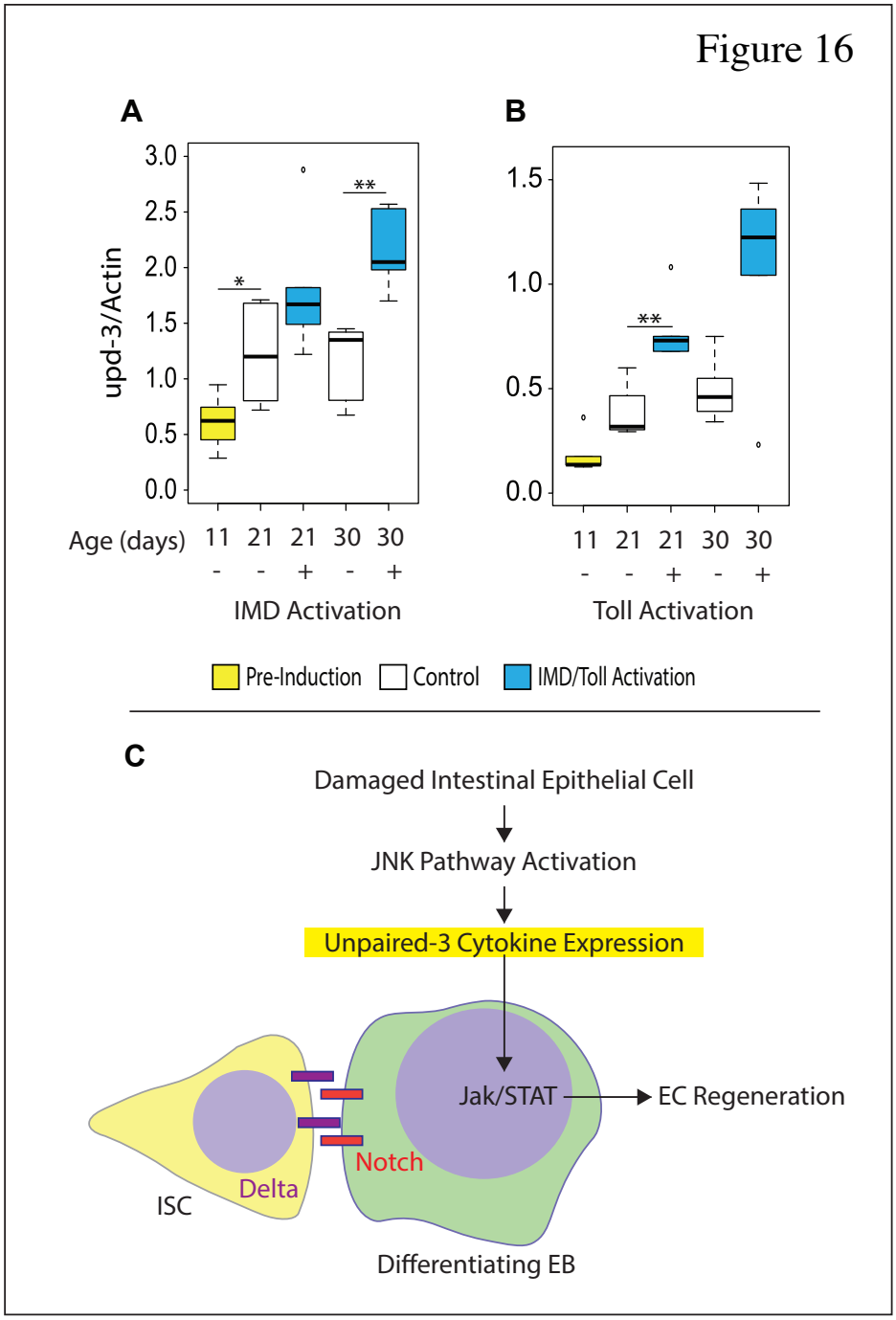

Figure 3.16: Immune activation drives misexpression of unpaired-3 gene

Quantification of unpaired-3 (upd3) mRNA levels. Gene expression assayed by RT-qPCR from dissected intestines; non-Smurf female flies immune activated from day 10 of adulthood and uninduced controls. *5966GS > UAS-PGRP LCa* (A) and *UAS-Toll10b* (B). n = 6 replicates of five intestines. p-value <0.05 = *, <0.01 = **, in Wilcoxon Test, only significant changes shown. Model of steps in enterocyte regeneration: upd3 activates the Jak/STAT pathway in progenitor cells inducing proliferation (C).

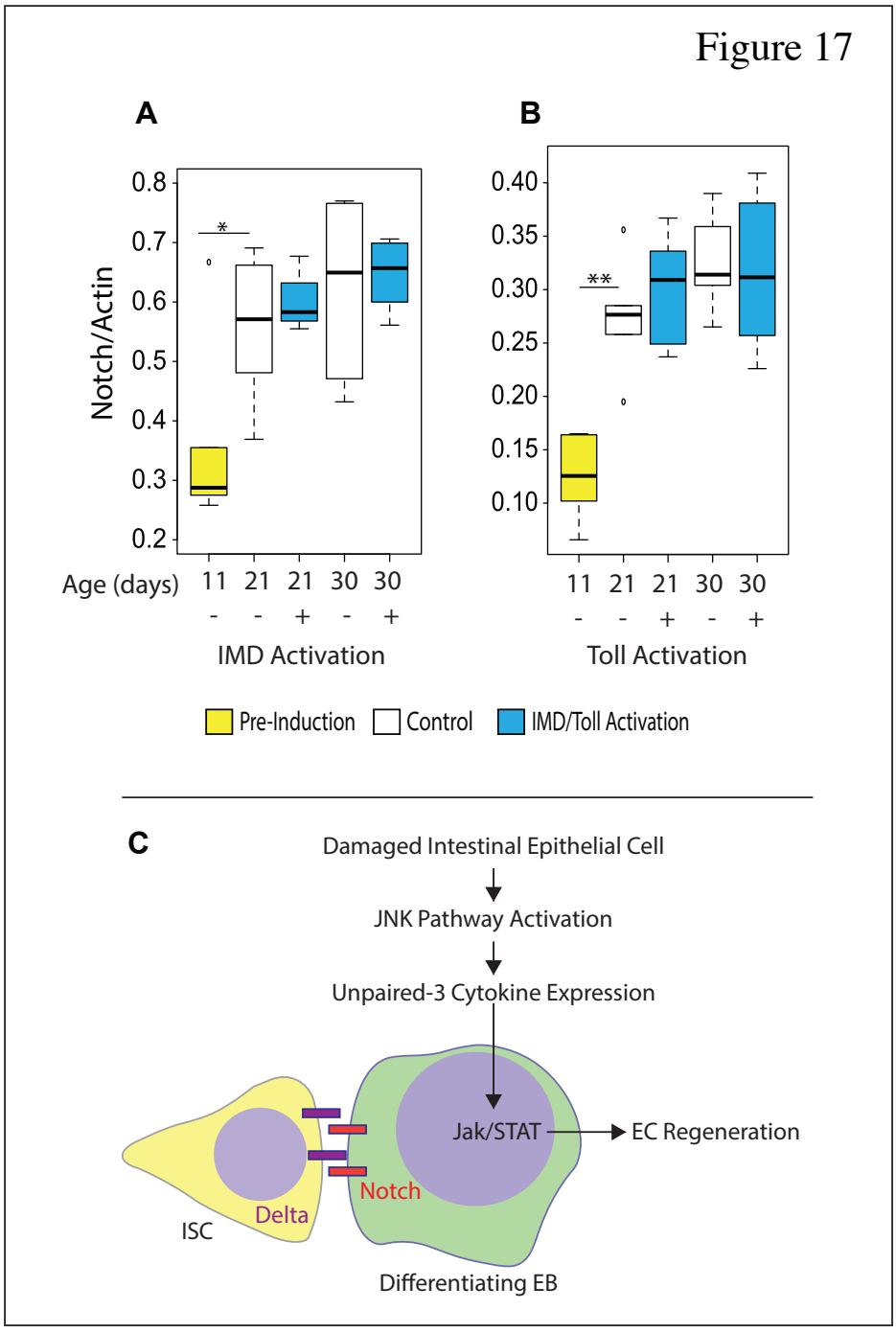

Figure 3.17: Effects of immune activation on progenitor cell marker Notch

Quantification of Notch mRNA levels. Gene expression assayed by RT-qPCR from dissected intestines; non-Smurf female flies immune activated from day 10 of adulthood and uninduced controls. *5966GS > UAS-PGRP LCa* (A) and *UAS-Toll10b* (B). n = 6 replicates of five intestines. p-value <0.05 = *, <0.01 = **, in Wilcoxon Test, only significant changes shown. Model of steps in enterocyte regeneration: Transmembrane receptor Notch is activated by membrane-tethered ligand, Delta (C).

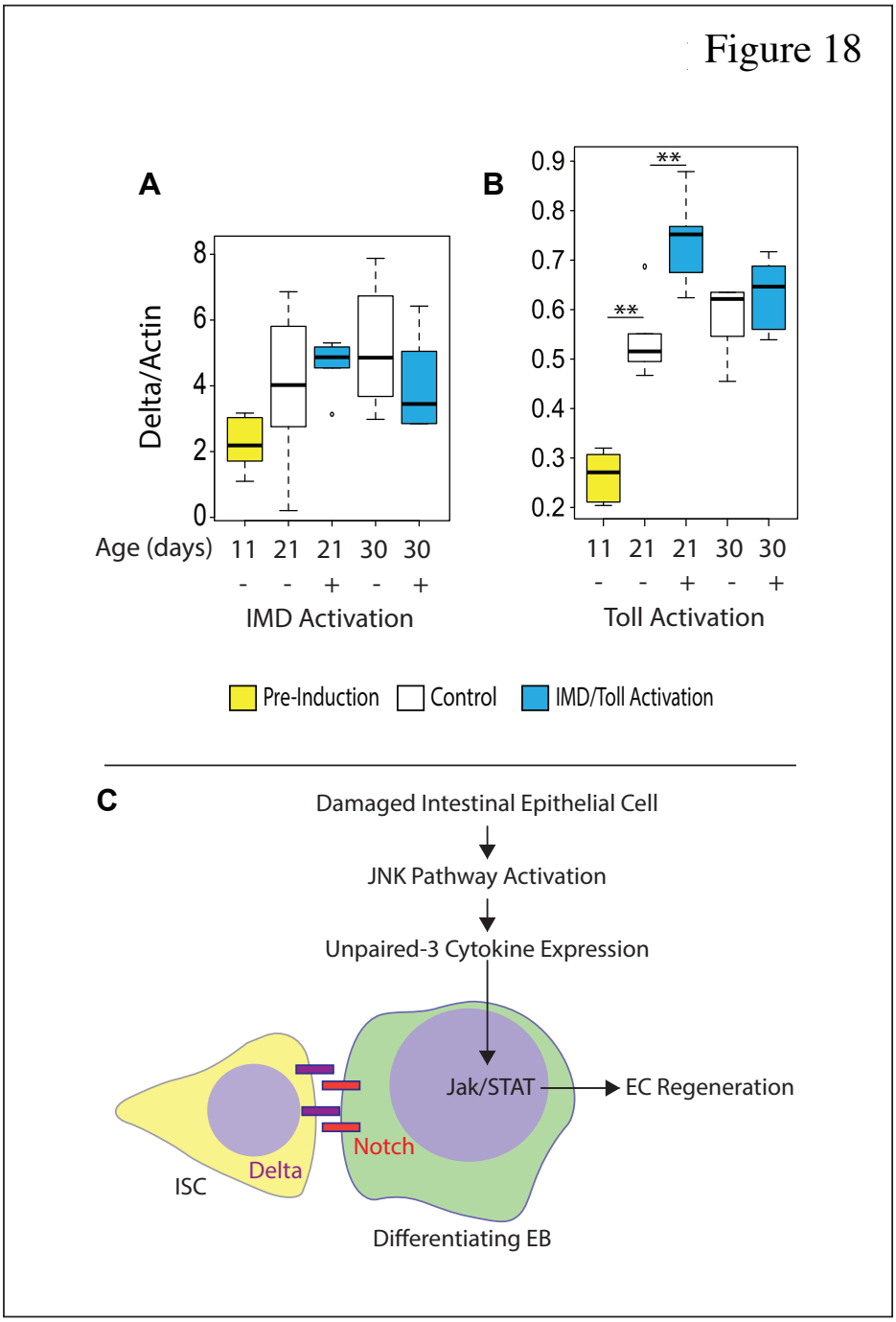

Figure 3.18: Effects of immune activation on intestinal cell marker Delta

Quantification of Delta mRNA levels. Gene expression assayed by RT-qPCR from dissected intestines; non-Smurf female flies immune activated from day 10 of adulthood and uninduced controls. *5966GS > UAS-PGRP LCa* (A) and *UAS-Toll10b* (B). n = 6 replicates of five intestines. p-value <0.01 = **, in Wilcoxon Test, only significant changes shown. Model of steps in enterocyte (EC) regeneration: Membrane-tethered ligand, Delta, activates progenitor cell (EB) differentiation via Notch signaling (C).

Figure 19

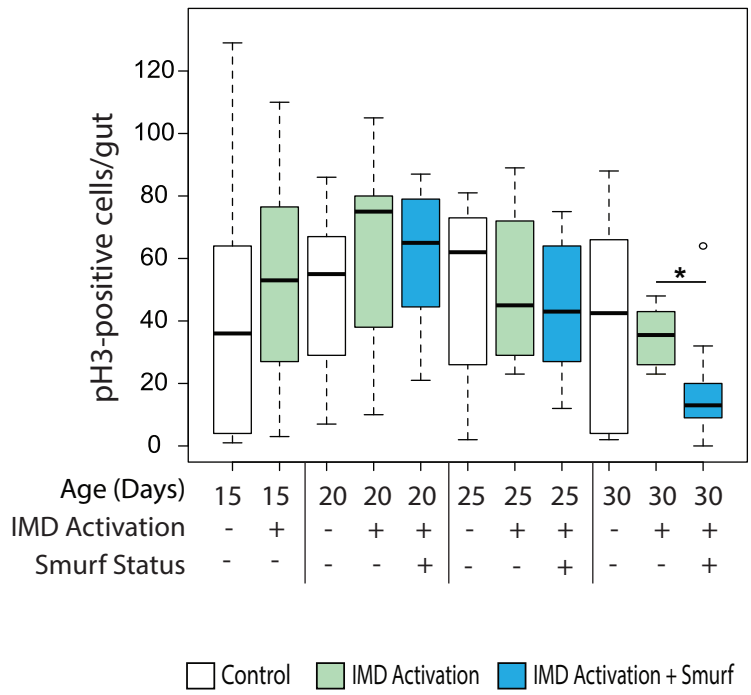

Figure 3.19: IMD activation impacts cell division in old Smurf flies

Quantification of changes in mitotic indices. Immunofluorescence images of whole dissected intestines stained against phosphor-histone H3 (pH3) manually quantified by cell counter. pH3+ cell number of the entire midgut from immune activated and control *5966GS > UAS-PGRP-LCa* non-Smurf and Smurf female flies. Immune induced from day 10 of adulthood. n ≥ 7 intestines for each condition at each time point. p-value <0.05 = * in Wilcoxon Test, only significant changes shown.

Figure 20

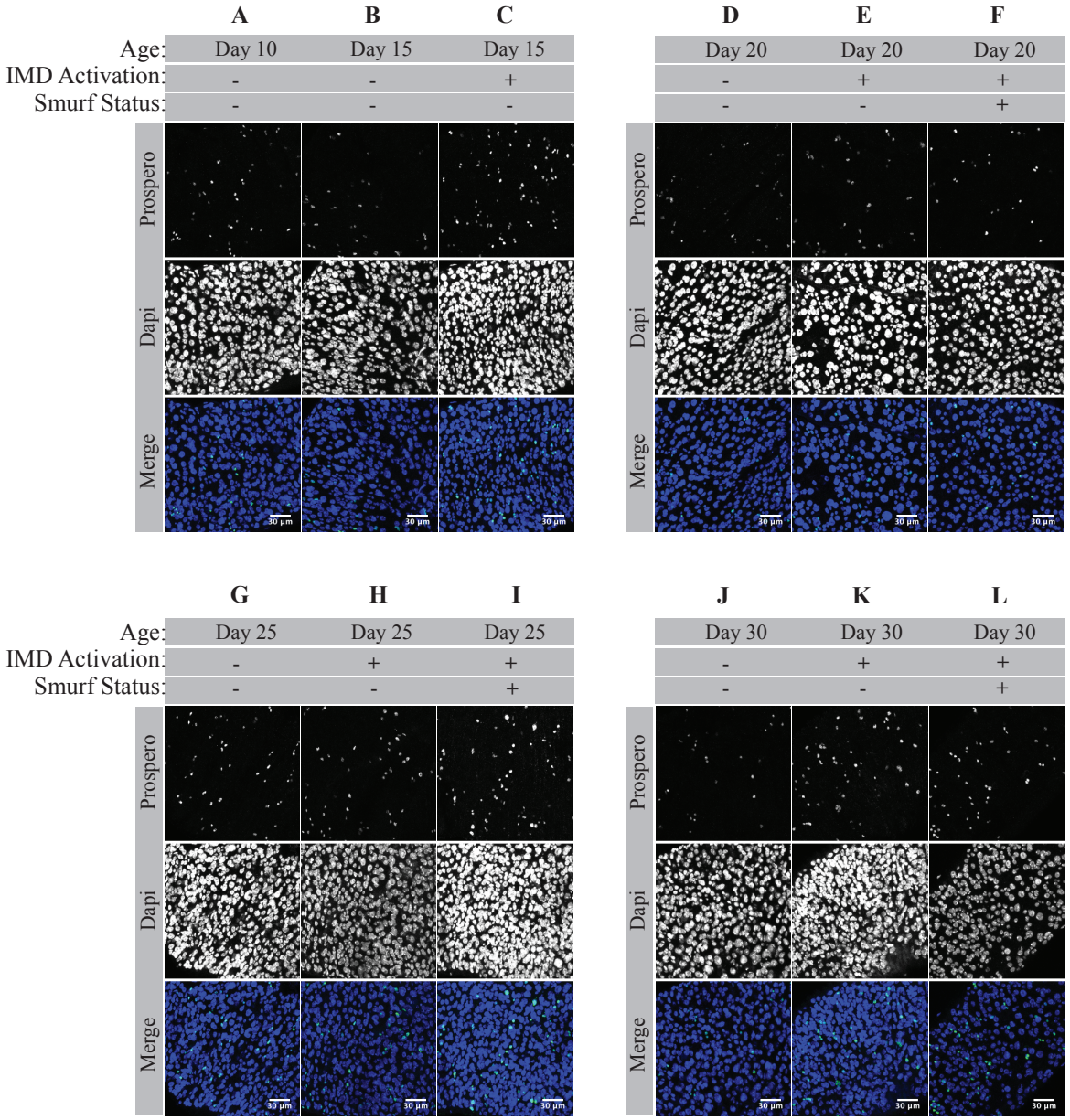

Figure 3.20: Confocal microscopy of changes in enteroendocrine maker prospero

Representative projected z-stack images of posterior midgut in immune activated and control non-Smurf and Smurf female flies. *5966GS > UAS-PGRP-LCa* (A-L) immune induced from day 10 of adulthood. n ≥ 7 intestines for each condition at each time point. For merge images: blue = DAPI; green = EE marker prospero. Scale bar = 30µm.

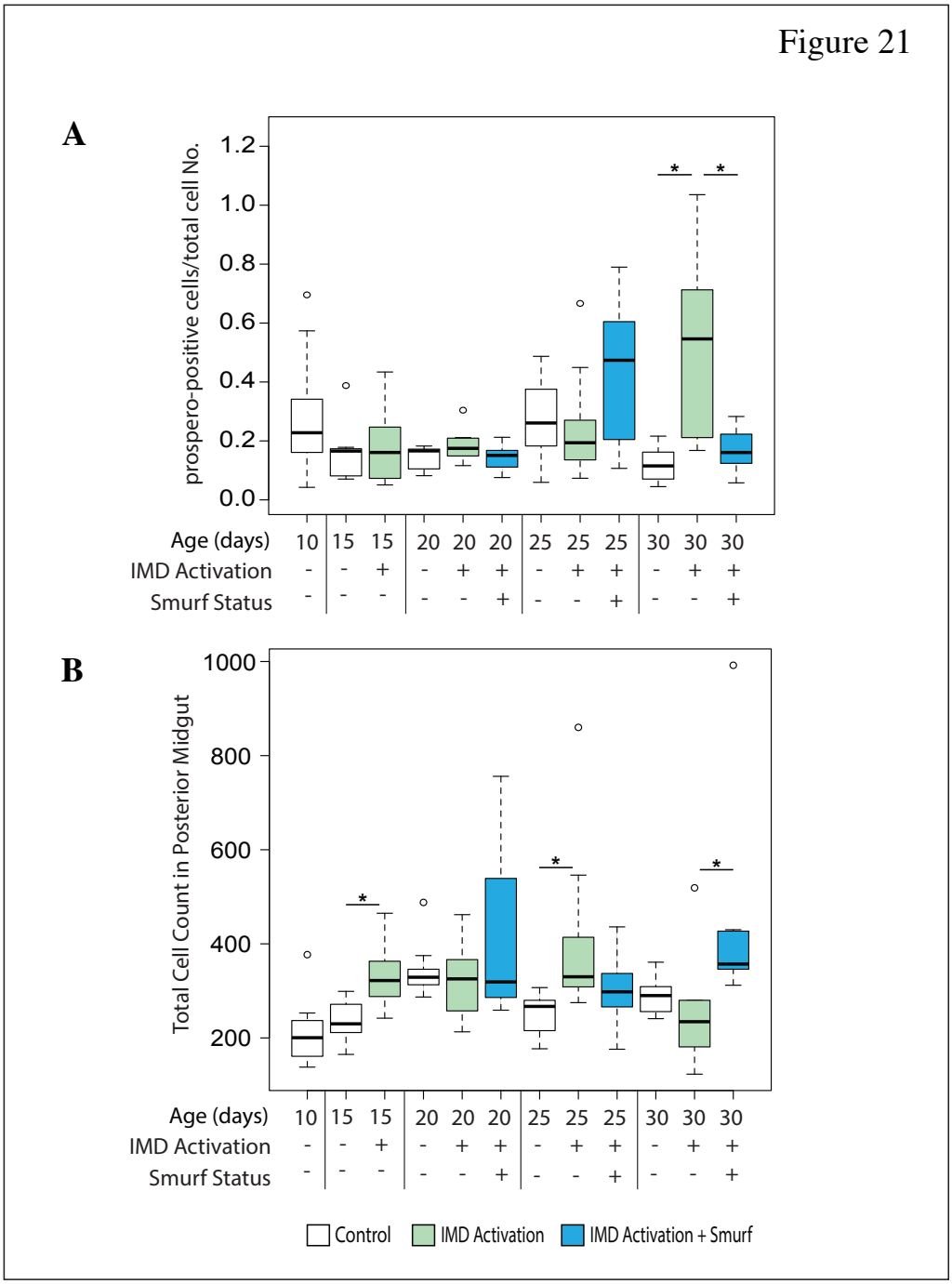

Figure 3.21: IMD activation drives dysplasia and impacts epithelial cell number

Quantification of immunofluorescence images stained against EE marker prospero (A). Quantification of total number of cells found in posterior midgut (B). Analysis completed from representative projected z-stack images of posterior midgut in immune activated and control non-Smurf and Smurf female flies. *5966GS > UAS-PGRP-LCa* immune induced from day 10 of adulthood. n ≥ 7 intestines for each condition at each time point. p-value <0.05 = * in Wilcoxon Test, only significant changes shown.

3.5 Discussion

3.5.1 Overview

Previous work from my M.Sc. indicates that immune activation in young flies drives early-onset mortality as well as accelerating loss of intestinal barrier function. Inducing immune activity in flies of chronologically young age also drives bacterial dysbiosis. Thus, there are clear physiological changes that occur not just with age, but also as a product of dysregulated immune responses. Doctoral work presented here gives further insight into the complex nature of microbiota and immune response dynamics. Thesis findings suggest that immune-induced barrier dysfunction leads to dysbiosis, regardless of microbial species associated with the fly. Data from this chapter offers two major points for discussion (1) the impact of forced immune induction on host microbiota (2) the impact of immune activation and resulting dysbiosis on the gut epithelium.

3.5.2 Impacts of constitutive immune activation on host microbiota

3.5.2.1 Immune activation is sufficient to induce microbial changes in the host

Sequencing data from this chapter highlight two bacterial species whose levels significantly increase following IMD activation. These species have been shown to facilitate protective processes in their respective hosts. *Commensalibacter intestini* is an important symbiotic bacterium in *Drosophila* responsible for maintaining low levels of pathogenic bacteria (Kim et al., 2012). *Lactobacillus antri* has been found in the gastric mucosa of healthy humans (Roos et al., 2005). Importantly, the exact strains utilized for these experiments were from fly populations originally housed in the Walker Lab, at the University of California, Los Angeles. While the Walker Lab gifted the same transgenic fly lines to the Clark Lab at Durham University, acute changes in microbial population were inevitable (Reedy et al., 2019, Kamareddine et al., 2020). Due to stark changes in

temperature during transit, amongst other external factors, the growth and abundance of certain bacteria were likely impacted. Perhaps those changes account for the increased bacterial loads were not observed in pre-Smurf flies during experimental repeats at Durham University. This is one piece of evidence supporting the idea that immune activation drives dysbiosis of specific bacterial species in pre-Smurf flies, and not in a general way.

Previously published works have consistently shown that chronic immune activation results in dysbiosis, and consequently fly death. For example, Ryu et al. (2008) showed that deletion of the *Caudal* gene results in overexpression of *Relish* transcript leading to bacterial overgrowth and a significant reduction in fly lifespan. Guo and colleagues have shown that PGRP-SC mutants, which would prevent degradation of bacterial DAP (diaminopimelic acid-type peptidoglycan), result in changes to gut epithelia organization and dysbiosis (Guo et al., 2014). Other published works have also reported that PGRP-SD, a signal enhancer for PGRP-LC, mutants result in *L. plantarum* overgrowth. Here, commensal overgrowth results in lactic acid buildup whereby intestinal acidification promotes ROS production, epithelial dysplasia, and shortened lifespan (Iatsenko et al., 2016, Iatsenko et al., 2018). Contrary to other work, results presented in this chapter are more nuanced. Here data suggest that immune activation drives loss of barrier function, and that epithelial disruption causes bacterial dysbiosis. In other words, immune activation alone can only induce dysbiosis in pre-Smurfs under certain conditions, but always induces dysbiosis post-Smurf, despite composition of commensals. This is a new and important finding that has not yet been published or discussed in the literature.

With these new results in mind, an alternative interpretation for previously published data emerges. Previous studies did not differentiate between Smurf and non-Smurf flies. Since there is a lack of sample segregation based on this critical phenotype, it

is possible that what the authors are showing is dysbiosis brought about by immune-induced barrier dysfunction. This leads to the hypothesis that there are observable differences between immune activated Smurf versus non-Smurf flies. Further, are there differences between pre- and post-immune-induced Smurfs that could help identify acute changes associated with dysbiosis. To discern how much is actual Smurf dysbiosis versus immune dysbiosis, the following experiments can be done using a timed Smurf assay (as previously published in Clark et al., 2015). Whereby flies of genetic background *5966GS>UAS-PGRP LCa* are collected at midlife, put on blue food for 24 hours, and collected alongside their non-Smurf (or pre-Smurf) counterparts. Flies in either cohort would then be fed control media or RU media, inducing IMD activation, for another 24 hours. Bacterial samples would be collected at the 24-hour mark. Genomic DNA would then be extracted and analyzed with *16S* primers via qPCR in the first instance. By catching Smurf flies that have only just lost barrier function, there would be a window into the effects of further immune activation on host dysbiosis. And the relative impacts that barrier loss and immune activation have independently and together. Ideally, the experiment that ultimately needs to be done involves isolation of the exact bacterial strains that mediate dysbiosis under constitutive immune activation. Culturing flies with these specific bacteria would allow for targeted assays where specific bacterial strains could be reinserted into the fly and changes to the host or other bacterial populations could be observed.

3.5.2.2 External factors associated with Drosophila model may impact host microbiota

Final points of consideration involve the influence of the fly's genetic makeup as well as sexual dimorphisms, or in this case potential biases from studying hypotheses in a female background only.

Generational bacterial composition and abundance have been shown to fluctuate depending on transgenic background (Early et al., 2017). Thesis findings presented here suggest that individual immune pathways may be impacting epithelia differently, and consequently certain bacterial populations. Toll activation data suggests an important pre-Smurf increase in bacterial load and composition. To discern if differences in *PGRP LCa* verses *Toll* genetic background could be responsible for immune-induced increases in bacterial load and/or shifts in microbiota composition, the following experiments can be done (1) create gnotobiotic flies with the same concentration of respective commensals (2) follow the evolution of respective bacterial populations with age.

Variations in immunity are also inherent between male and female flies. Findings in this thesis were produced by studying age-related changes exclusively in female flies. Duneau and colleagues have shown that in systemic bacterial infection Toll activation mediates sexual dimorphism (Duneau et al., 2017). Belmonte et al. consolidate findings across publications which suggest that female flies also exhibit increased gut permeability and lower bacterial load with age – when compared to male counterparts (Belmonte et al., 2019). Since female flies show a weaker Toll response with age, there is the potential that inducing constitutive Toll activity manufactures increased bacterial load pre-Smurf. By further understanding immune pathways direct link to barrier dysfunction could create opportunities for interventions that maintain intestinal homeostasis longer.

3.5.2.3 Immune activation may increase pathogenicity of commensal microbes

Pathogenesis in the fly is a well-studied phenomenon, whereby bacterial pathogens invade the host hemolymph and trigger a cascade of immune responses (Buchon et al., 2009b). More broadly, published works have also shown that overgrowth of commensal species can induce pathology, despite commensals not being invasive pathogens themselves

(reviewed in Younes et al., 2020). Interestingly, unpublished data (generated by Ellie Hughes while a student in the Clark Lab) shows that microinjection of *Lactobacillus plantarum* into adult *Canton-S* female fly hemolymph results in early onset mortality. Unpublished data show that *L. plantarum* injections increased transcript levels of antimicrobial peptides *diptericin* and *drosomycin* twenty-four hours post injection when compared to PBS injected controls. Further, these results show that bacterial load significantly increases post injection with *L. plantarum* and continues to increase in old flies, while stabilizing within a day in young flies. Taken together this unpublished data suggests that the introduction of a bacterial symbiont into circulation is sufficient to induce pathology-like symptoms in the adult fly.

Other published works provide an alternative hypothesis for how commensal species contribute to host pathology. Previously published studies have shown that commensal overgrowth increases production of *L. planta*rum derived lactic acid and bacteria-derived uracil (Lee et al., 2013b, Iatsenko et al., 2018, Kim, 2020). These bacterial byproducts have been shown to cause intestinal decline through the overproduction of reactive oxygen species (ROS) via NADPH oxidases, *DUOX* and *NOX*. An important distinction here is that *DUOX*-dependent ROS production is a pathogen-specific event, where peptidoglycan is unable to activate ROS activity (Lee et al., 2013b, Kim, 2020). Contrastingly, *NOX*-dependent ROS production is a symbiont-specific event (Iatsenko et al., 2018). Data presented in this chapter show that immune-induced barrier dysfunction drives dysbiosis, regardless of microbial composition. To examine if different states of intestinal barrier function (i.e., pre-Smurf versus Smurf) impact basal states of ROS generation, the following experiments can be done (1) profiling bacterial byproducts in immune-induced pre-Smurf and Smurf flies, specifically looking at lactic acid concentration following immune activation (2) RT-qPCR on *DUOX* to validate *PGRP-LCa*

overexpression is not altering *DUOX* transcript levels (3) measure DUOX-dependent production of reactive oxygen species - HOCl (hypochlorous acid) across conditions by staining dissected guts with HOCl-specific rhodamine-based R19-S dye (originally described in Chen et al., 2011).

3.5.2.4 Immune activation may impact regionalization of intestinal microbiota

Taking under consideration the changes in intestinal pH following immune activation, an alternative interpretation to chapter data arises. Instead of direct or indirect commensal induced pathology, this hypothesis postulates how changes to gut regionalization impact microbial distribution along the intestine. In other words, commensal species might also induce pathology by showing overgrowth in certain regions of the fly gut. For example, the Jasper Group has shown that gut compartmentalization and bacterial concentration are key factors in maintaining host-microbe balance (Guo et al., 2014, Li et al., 2016). Thus, the number of bacteria, type of bacteria, and age of the fly are critical features to consider when labeling bacterial populations and/or species as beneficial versus "pathogenic".

A recent pilot study provides methods to simultaneously visualize the localization of multiple bacterial species in the gut using fluorescence *in situ* hybridization (FISH) (Akhtar et al., 2021). Here, the authors designed fluorescent probes against specific bacterial cohorts and used a confocal microscopy approach to visualize bacterial populations. Regarding doctoral work, this tool provides an opportunity for protocol optimization, whereby the impacts of chronic immune activation on pre-Smurf and Smurf bacteria can be quantified based on intestinal region. This assay also presents an interesting follow up question to consider – is the overgrowth observed using a constitutive immune intervention due to an accumulation of dead bacteria? To answer this question, dead verses live bacteria can be labelled based on the membrane integrity of the bacterial cell. Well

established assay kits use a dual staining system, where dead or dying cells stain red with propidium iodide and cells with an intact membrane stain green with SYTO9 (Broderick et al., 2014). Changes in bacterial regionalization along the gut could then be quantified by fluorescent microscopy, and by flow cytometry to quantify abundance of dead versus live bacteria. Of note, *PGRP LC* isomers have been shown to recognize live verses dead bacteria, thus functioning as part of IMD pathway regulation and gut homeostasis (Neyen et al., 2016). For this reason, transcript levels of *PGRP LC* isoforms could be assayed for any changes in level driven by immune induction as compared to normal aging.

3.5.3 The impact of immune activation on gut epithelial health

3.5.3.1 Are gut epithelial cells less sticky in immune-induced flies?

M.Sc. work from the Walker Lab highlighted that immune activation increased Smurf proportions significantly (Alcaraz, 2016). Since loss of barrier function was so heavily influenced with a constitutive immune intervention, the working hypothesis was that immune activation must be decreasing junction expression, as had been previously noted in Smurf flies (Clark et al., 2015). Further, both Salazar et al. and Resnik-Docampo et al. do not see changes in transcript junction level in non-Smurf flies with age. Instead, these the authors show that mis-localization of septate junction in the cell cytoplasm increases with age in non-Smurfs flies (Resnik-Docampo et al., 2016, Salazar et al., 2018). Chapter results, however, show that immune activation increases expression of junction transcripts in pre-Smurf flies – under certain conditions. This suggests the existence of mechanistic differences in how junction gene expression is mediated between pre- and post-Smurf flies. Interestingly, work from Salazar and colleagues show that knockdown of one junction component, *snakeskin*, is sufficient to drive barrier loss – without initiating immune activation or dysbiosis (Salazar et al., 2018). Given chapter three findings, and the

published findings of other the authors, a follow-up hypothesis was that chronic immune activation in early life gives insight into changes occurring pre-Smurf at old age. To discern the validity of this theory, there would need to be biologically age-matched control samples (rather than the chronologically age-matched used here) as a comparison in repeat experiments.

In general, data presented in this chapter show that IMD activation drives increased junction transcript expression, whereas Toll activation drives decreased expression. Perhaps this indicates that the Toll pathway is more tightly linked to mechanisms involved in negative regulation of junction gene transcription. The differences observed between IMD and Toll activation may be due in part to the known regionalization of IMD expression along the gut (Buchon et al., 2014). Under normal circumstances the expression of IMD and Toll pathway reporter genes varies along the length of the gut – with higher/lower activity in different regions (Buchon et al., 2014). Under homeostatic conditions *PGRP-LC* transcript is expressed equally amongst progenitors and enterocytes, regional expression is also equal (Dutta et al., 2015). However, *diptericin* expression is greatest in R1 ECs, while *drosomycin* expression is greatest in R1 ISCs and EEs (Dutta et al., 2015). This implies differing areas of function between the two pathways and may be reflected in the differences observed with respective whole gut activation.

Future experiments to discern immune pathway contributions could involve an immunofluorescence approach, by taking dissected intestines of IMD and Toll genotypes and staining against various junction associated proteins. Confocal imaging could then be used to quantify the spatial distribution of junction proteins. A second theory that might explain the inverse nature of these changes includes changes in microbial composition. In other words, different bacteria drive differential pathway activation (as mentioned above, regarding genetic regulation of bacterial colonization). Finally, synergies which are

inherent between neighboring immune pathways, may lead to differences in overall junction gene expression. For example, the crosstalk that exists between IMD and JNK pathways could potentially explain why IMD changes happen later in life as there would be an indirect stress related response carried out by JNK but initiated by IMD.

While there is much to extract from these findings, there are limitations to the interpretations that can be made. Put simply, mRNA does not equal protein (Maier et al., 2009, Vogel and Marcotte, 2012). While these changes are interesting and a foundational step in understanding the relative roles of immunity versus bacteria in intestinal decline, further imaging work is needed to consider how changes in junction transcripts correlates to junction localization and organization. The take home message, however, remains immune activation leads to misexpression of junction genes. Of note, there are clear differences in mechanism of action and downstream effects between immune pathways – how this correlates with Smurf timing in different genetic backgrounds is still to be determined.

3.5.3.2 JNK stress-response pathway may mediate IMD driven gut decline

When new epithelial cells regularly replace the old, the organism can avoid dysplasia, or the over proliferation of cells leading to abnormally large organs/tissues (Liang et al., 2017, Gervais and Bardin, 2017). The accumulation of intestinal epithelial cells is an accepted and consistent phenotype observed in the aging fly (Biteau et al., 2008). Chapter data suggest that cell proliferation and differentiation may be mediated by IMD-induced JNK activation. IMD has an intermediate link to JNK via Tak1 (Silverman et al., 2003). Data presented here shows IMD activation drives an increase in expression of cell death-inducing gene, *reaper*, in enterocyte cells. Previously published work has shown that apoptosis induction can be triggered under nominal conditions, including acute exposure to

opportunistic bacteria (Loudhaief et al., 2017). Triggers can be environmental or genetic, according to the authors. While this thesis work suggests an increase in apoptotic activity, *reaper* transcript levels are only an indirect readout of JNK activity. To answer if IMD induces JNK activation, an imaging approach could be used to measure JNK (also known as *basket*) via visualization of *basket*-lacZ or JNK target gene *puckered*-lacZ activity, in the first instance.

Increases in *reaper* expression during IMD activation might be mediating rapid differentiation events during EC regeneration, as has been seen with increased with *upd3* (Zhai et al., 2017). Moreover, upd3 is also a readout of stress signal inducing JNK. Work done in "undead", or "almost dead" enterocytes indicates that enterocytes enter a transient state of death prior to shedding from the epithelial layer (Martin et al., 2018, Amcheslavsky et al., 2020). These compensatory apoptosis-induced proliferation (AiP) enterocytes use ROS as an intermediate between immune cells and ISCs, triggering JNK activation in immune cells and further JNK activation in AiP cells which triggers EC release of upd3 and ISC proliferation (Amcheslavsky et al., 2020). To test this, dissected guts could be stained against *Sox21a* (transcription factor known to regulate EB differentiation) and *armadillo* (β-catenin adherens junction protein). Following on from that, to test if ISC proliferation is being driven by AiP ECs, guts could be stained for *Dronc* (a caspase-like enzyme that promotes apoptosis) and quantify changes in *Dronc*+ cells between conditions.

Alternative hypotheses include (1) the potential for an excess buildup of ECs due to the absence of cell death (2) variability in the number of dead ECs increasing and then decreasing with ISC proliferation, or are dead ECs not being cleared and adding to a multilayer epithelium. To test whether gut epithelial cells are being replenished efficiently under immune activation, the following experiment could be done, staining of apoptotic

ECs in dissected guts across conditions using anti-activated-Caspase. Alternatively, published works have also shown that adherens associated protein *DE-Cad* plays an important role in homeostatic cell-turnover (Liang et al., 2017). Liang and colleagues have shown that enterocyte apoptosis controls ISC proliferation via loss of *E-Cad* and downstream induction of *rhomboid* (*rho*) – a marker of physiological apoptosis in enterocytes and EGF ligand activator. These chapter data suggest that in pre-Smurf flies, *DE-Cad* is kept at a basal level upon immune activation, almost as though it is acting as a buffer between immune activity and ISC proliferation – potentially mitigating immune dysregulation and age-associated hyperplasia.

3.5.3.3 Can IMD or Toll activation directly impact intestinal stem cell proliferation?

Petkau and colleagues have recently shown that constitutive IMD activation in progenitor cells induces hyperplasia and dysplasia in the adult fly gut (Petkau et al., 2017). However, there is still no direct causal link between IMD/Toll activation and cell turnover. If immune activation directly contributes to ISC hyper-proliferation, then it may be that there is also an increase in junction transcript expression from newly differentiated ECs. Further consequences of rapid cell turnover may then include insufficient temporal and/or spatial control for full junction formation in mature ECs – potentially leading to disorganized multi-layer gut epithelia. Since all gut cell types show similar junction expression patterns (Dutta et al., 2015), intestinal cell types from immune activated flies could be separated by FACS in the first instance. Specific cell-type populations could then be assayed via RNA-seq for junction gene expression levels. Additional experiments to help discern direct effects of IMD/Toll activation on progenitor and enterocyte cells could include the following (1) use of progenitor cell-specific driver *5961-GeneSwitch* crossed to a dominant

negative form of *unpaired* receptor *Dome* – thus stalling ISC proliferation and studying effects of immune activation alone on ECs (2) use of enterocyte cell-specific driver *5966-GeneSwitch* crossed to *UAS-upd3 RNAi* – thus stalling enterocyte stress signals known to activate ISC proliferation and assaying impacts of immune activation on progenitor cells alone.

3.5.3.4 Jak/STAT mediated impacts of immune activation on ISC proliferation

Jak/STAT activity facilitates the maintenance of gut homeostasis via regulation of ISC proliferation. This is important because upd3 is a ligand required for Jak-STAT induction (Jiang et al., 2009). My data show that immune activation drives overexpression of *unpaired-3* (*upd3*) transcript levels. Both IMD and Toll activation seemingly exacerbate the increase in *upd3* transcript expression already seen with age. It makes sense for an increase in immune activation to trigger expression of *upd3* – however, for reasons previously discussed i.e., mRNA does not equal protein, more is needed to discern how *upd3* expression is being induced. Perhaps transcript expression is being impacted, either directly or indirectly, by immune-mediated epithelial cell damage? To test this hypothesis downstream effectors of *upd3* would need to be quantified. Further experiments would need to assess if *upd3* is being released by a JNK-mediated mechanisms i.e., is immune activation stressing ECs and stimulating Jak/STAT activity? An important point pertaining to this doctoral work involves the complexity of overlapping intestinal pathologies, whose sequence and causal relationships are not yet fully understood. Of note, it is currently well established that microbial imbalance drives overactive immune responses, in turn inducing an increase in ISC turnover (reviewed in Lesperance and Broderick, 2020). Work presented here focuses on how bacteria influence ISC proliferation through damage induced via immune dysregulation.

Data presented in this chapter show no significant changes in mitotic indices with age or upon IMD activation. This proliferation data correlates with *delta* transcript levels in IMD activated flies, where *delta* expression remains unchanged with age or upon immune activation. Since ISCs are the only proliferative cells in the gut (Ohlstein and Spradling, 2006); presented data suggest that IMD-induced epithelial changes may not be driven by direct ISC proliferation. Of note, these results are contradictory to well established findings in the field of *Drosophila* stem cell aging. Previously published studies have shown that that ISC proliferation increases significantly with age; in addition, progenitor differentiation is impacted as shown by an increase in pre-ECs (Biteau et al., 2008, Buchon et al., 2009b, Jiang et al., 2009). Further, Guo and colleagues have shown that preventing dysbiosis in the adult fly prevents ISC over- proliferation (Guo et al., 2014). Since chapter three imaging and mRNA data were collected from immune activated pre-Smurfs, this may explain why differences in mitotic indices are not observed between conditions. These data also show the most significant decline in proliferation at 30 days old, following barrier dysfunction. In other words, old Smurf flies showed the lowest mitotic numbers. This finding aligns with previously published literature pertaining to ISC exhaustion at late age. The long-term efficacy of ISCs is reliant on regulated periods of quiescence, as hyperproliferation leads to exhaustion and premature aging (Rera et al., 2011). It follows that late life Smurf guts are exhibiting stem cell exhaustion. To test this theory, expression of ISC nuclear protein *piwi* can be quantified using a RT-qPCR technique in the first instance. *Piwi* facilitates maintenance of heterochromatin and by extension homeostasis of ISC divisions. Recently published work has shown that overexpression of *piwi* in old progenitor cells is sufficient to decrease age associated ISC hyperproliferation (Sousa-Victor et al., 2017). Additional follow-up hypotheses regarding this constitutive immune intervention include: (1) If *piwi* is overexpressed in immune-

induced Smurf flies, are increases in ISC proliferation observed? (2) Is *piwi* expression dependent on bacterial subtypes? (3) Does *piwi* expression change in relation to bacterial composition and/or load?

3.5.3.5 Jak/STAT mediated impacts of immune activation on EB differentiation

Another hallmark of the aging gut includes the mis-differentiation of progenitor cells (Ngo et al., 2020, Martin et al., 2018, Biteau et al., 2010, Biteau et al., 2008). Previously published works have identified two distinct subsets of EBs. While there are discrete pools of EE progenitors, there are varied explanations as to how epithelia shift between EE versus EC destined progenitor cell fates (Gervais and Bardin, 2017). Thesis data show that IMD activation does not change expression of EB target gene, *notch*. However, there are significant age-related increases in *notch* transcript expression. Levels of *notch* signaling have been shown to directly correlate with EB differentiation (Micchelli and Perrimon, 2006). Further, data presented in this chapter show a significant increase in total cell number at early and midlife and an increase in EE cell number at late life (Figure 3.21 B). Interestingly, immune-induced Smurf flies show an increase in total cell number at late life. Cell-lineage tracing may be helpful in identifying the fate of intestinal progenitor cells between immune activated pre-Smurf and immune activated Smurf flies. Because chapter data show low levels of proliferation, fewer EE cells and an increase in total cell number in immune-induced Smurfs, it was hypothesized that dysbiosis contributes to epithelial decline by forcing differentiation toward pre-ECs. This may then result in overnumbered pre-ECs, driving intestinal barrier dysfunction.

Broderick and colleagues have shown that bacteria heavily regulate differentiation of EE cells, as fewer EEs were quantified in conventional flies compared to axenic (Broderick et al., 2014). Other published work has shown that *Lactobacillus brevis* mono-

association decreases the number of EBs in progenitor pools (Ferguson et al., 2020). The authors further show that knockdown of *notch* signaling increases bacterial load in *Lactobacillus* mono-associated flies (Ferguson et al., 2020). Since EEs sense and respond to microbial metabolites in the gut, it may be that dysbiosis drives further differentiation of EE cells. Thus, indicating that *notch* signaling is required for host-microbiota symbiosis. Given this published data, it follows that immune activation may skew the commitment of progenitor cells toward EEs or ECs depending on the bacterial population that is present. To test for the accumulation of secretory EE cells, or pre-EEs, immunofluorescence using EB marker *Su[H]* (*Notch*-suppressor of *Hairless*) could be used across immune activated conditions. Results from follow-up experiments may further suggest a pre-Smurf timeline as being important in cell-lineage commitment, with immune activation acting as a catalyst toward barrier dysfunction and dysbiosis.

3.5.4 Summary

Intestinal decline may not be bacteria driven, there is evidence which suggests that immune activation on its own is sufficient to decrease intestinal homeostasis (Guo et al., 2014). Since presented data show immune activation can sufficiently imitate age-associated decline, it is important to understand which aspects are purely bacteria driven verses immune activation driven. It thus made sense to next look at how immune activation would impact intestinal decline in the absence of bacteria. This hypothesis is addressed in Chapter 4.

Chapter 4: Inflammation drives age-related physiological decline in the absence of bacteria

4.1 Introduction

Current literature regarding the effects of bacteria, or lack thereof, on intestinal physiology and aging show conflicting results regarding the associated benefits with germ-free conditions. Brummel et al. results suggested that keeping flies germ-free during development and adulthood decreased mortality (Brummel et al., 2004). Ren et al. completed a series of experiments that resulted in axenic flies having no lifespan trade-off compared to controls (Ren et al., 2007). Still, other hallmark findings have shown that feeding antibiotics after flies have lost barrier function significantly decreases expression of antimicrobial peptides and extends lifespan (Clark et al., 2015). The authors report that this extension in lifespan is due to the elimination of bacterial dysbiosis and the associated physiological decline associated with it. These antibiotic-fed flies, however, do not regain intestinal barrier function. Recently published data also corroborate extended survival in germ-free flies (Lee et al., 2019).

Salazar and colleagues report that axenic flies do not show lifespan extension when a core septate junction component, *snakeskin (ssk)* is overexpressed. The authors contextualize this finding by showing that lifespan extension only occurs in conventional flies, overexpressing *ssk* (Salazar et al., 2018). Thus, indicating that the maintenance of barrier function is only beneficial in the presence of bacteria and that once barrier function is lost – resulting in bacteria driven health decline. Further interpretation of work by Salazar et al. suggests that transient *ssk* knockdown *(ssk-RNAi)* from day three to nine of adulthood impacts bacterial load immediately, as an increase in bacterial load is immediate and correlated with a simultaneous decrease in immune gene expression. Recovered *ssk-RNAi* flies (only having undergone transient transgene expression) seemingly reversed

bacterial load to basal levels (Salazar et al., 2018). The authors also show that transient induction of *ssk-RNAi* from day three to fourteen of adulthood increases immune gene expression compared to uninduced control flies, contrary to transient induction from day three to nine of adulthood – of note, Salazar et al. do not show corresponding bacterial load data. The remaining question is whether the bacteria associated decline after junction knockdown occurs because the bacteria drive immune activation and immune activation drives health decline, or are bacteria mediating health decline by some other means? This chapter attempts to answer these questions.

4.1.1 Aims and objectives

The aim of this chapter is to discern causality by establishing the individual roles bacteria and immunity activation play in intestinal decline. By omitting bacteria, which is known to play a large part in age-related decline, more can be learned about how immune activation contributes to age-associated intestinal decline. This chapter will further expand on Chapter 3 data and will highlight the individual role of innate immune pathways IMD and Toll on intestinal integrity.

Objectives for this chapter: In order to discern the individual role immunity plays in age-related intestinal decline, I will compare the impacts of immune activation to normal age-associated decline in a completely germ-free background.

I will assess the effects of immune activation on:

- Mortality
- Intestinal barrier function
- Overall intestinal physiology and digestive transit
- Intestinal enterocyte and progenitor cell epithelial markers, prior to the loss of barrier function defined by the Smurf phenotype

4.2 Immune activation alone drives physiological decline

4.2.1 Activation of immune pathways leads to increased mortality

Survival was tracked over time in control and immune activated axenic flies (methods detailed in section 2.1.5). Age-onset mortality was markedly increased in axenic immune activated flies, when compared to age-matched controls. Activation of the IMD Pathway significantly decreased median survival (42 days compared to 81 days in controls) (Figure 4.1 A). Overall, activation of the IMD pathway was correlated with a 21-day decrease in maximum lifespan (70 days compared to 91 days in control flies), a 23.1% decrease. Similarly, activation of the Toll pathway led to an increase in axenic fly mortality. Median survival significantly decreased from 70 days in control flies to 43 days in Toll activated flies (Figure 4.1 B). Overall, activation of the Toll pathway was correlated with a 17 day decrease in lifespan (68 days compared to 85 days in control flies), a 20% decrease. Taken together, these data suggest that intestinal immune activation drives decline in an age-dependent manner and is sufficient to increase mortality in the absence of microbes.

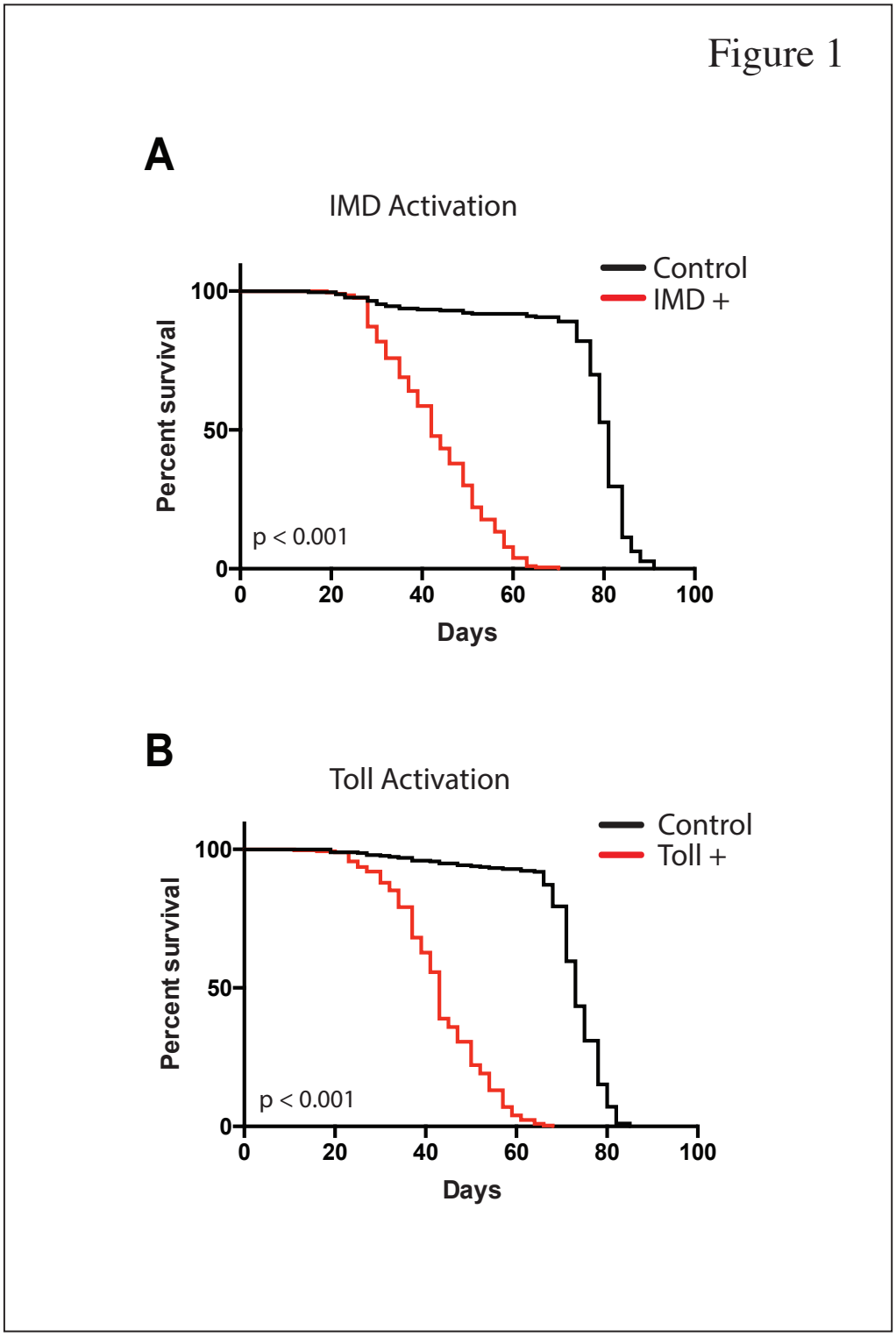

Figure 4.1: Immune activation is sufficient to increase mortality

Survival curves for *5966GS > UAS-PGRP-LCa* (A) and *UAS-Toll10b* (B), axenic female flies, immune activated from day 10 of adulthood and uninduced controls. n = >200 flies/condition. p-values < 0.001 in log rank test.

4.2.2 Activation of immune pathways alone leads to increased barrier dysfunction

The Smurf assay was used as a means of quantifying the change in number of flies which have lost barrier function (assay detailed in section 2.3). Immune activated axenic flies showed a six-fold increase in the proportion of Smurfs in the aged fly population. By 45 days old, IMD activated flies are 66% Smurf, compared to <1% of age-matched controls (Figure 4.2 A-B). Similarly, at 45 days of age 96% of the Toll activated population was Smurf compared to only <1% in age-matched uninduced controls (Figure 4.2 A, C). Disproportionate increases in Smurf number are closely correlated with significant rates of mortality observed at 45 days old, in IMD and Toll activated axenic flies. Both IMD and Toll activation significantly shorten lifespan and substantially increase the proportion of Smurfs in the aged fly population.

4.2.3 Immune activation is sufficient to impact digestive transit

Fecal deposit results were characterized by total number, mean hue, individual mean area, and mean lightness. Representative images of fecal plates illustrate the diversity of fecal excretion between axenic conditions (Figure 4.3 A-D). Changes in acid-base balance are quantified by hue of the fecal deposit. Numbers higher on the hue scale correlate with an increase in pH, those lower on the scale correlate with a decrease in pH. IMD activation significantly increases fecal deposit hue, or color, indicating greater alkalinity in the gut (Figure 4.4 A). Toll activation does not significantly change intestinal pH, however there is a significant age-associated increase in alkalinity (Figure 4.4 B). The intensity of fecal deposit color provides a readout of fluid excretion and water balance (Wayland et al., 2014). Color intensity and fecal concentration are positively correlated. Fecal concentration is measured on a scale from zero to one, with zero representing the most concentrated fecal deposit. IMD and Toll activation both significantly decrease the

concentration of fecal deposits, indicating more dilute fecal deposits (Figure 4.4 C-D). These findings suggest that immune activation is sufficient to impair water reabsorption in germfree flies. The average size of individual fecal deposits significantly decreased in both IMD, and Toll activated flies (Figure 4.5 A-B). The number of fecal excretions per fly remained unchanged in IMD activated flies (Figure 4.5 C). By contrast, Toll activation significantly increases the number of fecal excretions per fly (Figure 4.5 D). IMD and Toll activation both impact digestive transit, however significant changes observed in fecal number and deposit concentration showed opposing trends between pathways.

Age-related changes are observed mostly when comparing 10-day-old versus 30-day-old control flies of Toll background. With age, flies of Toll genetic background experience excreta that were more concentrated, more alkaline (Figure 4.4 B, D), and larger (Figure 4.5 B) in nature. Indicating perhaps more water reabsorption inherent to flies of Toll genetic background. By contrast, flies of IMD genetic background only show age-related changes between 10-days-old and 30-days-old in fecal pH (Figure 4.4 A). Whereby flies experience a decrease in hue, or an increase in excreta acidity inherent to IMD genetic background.

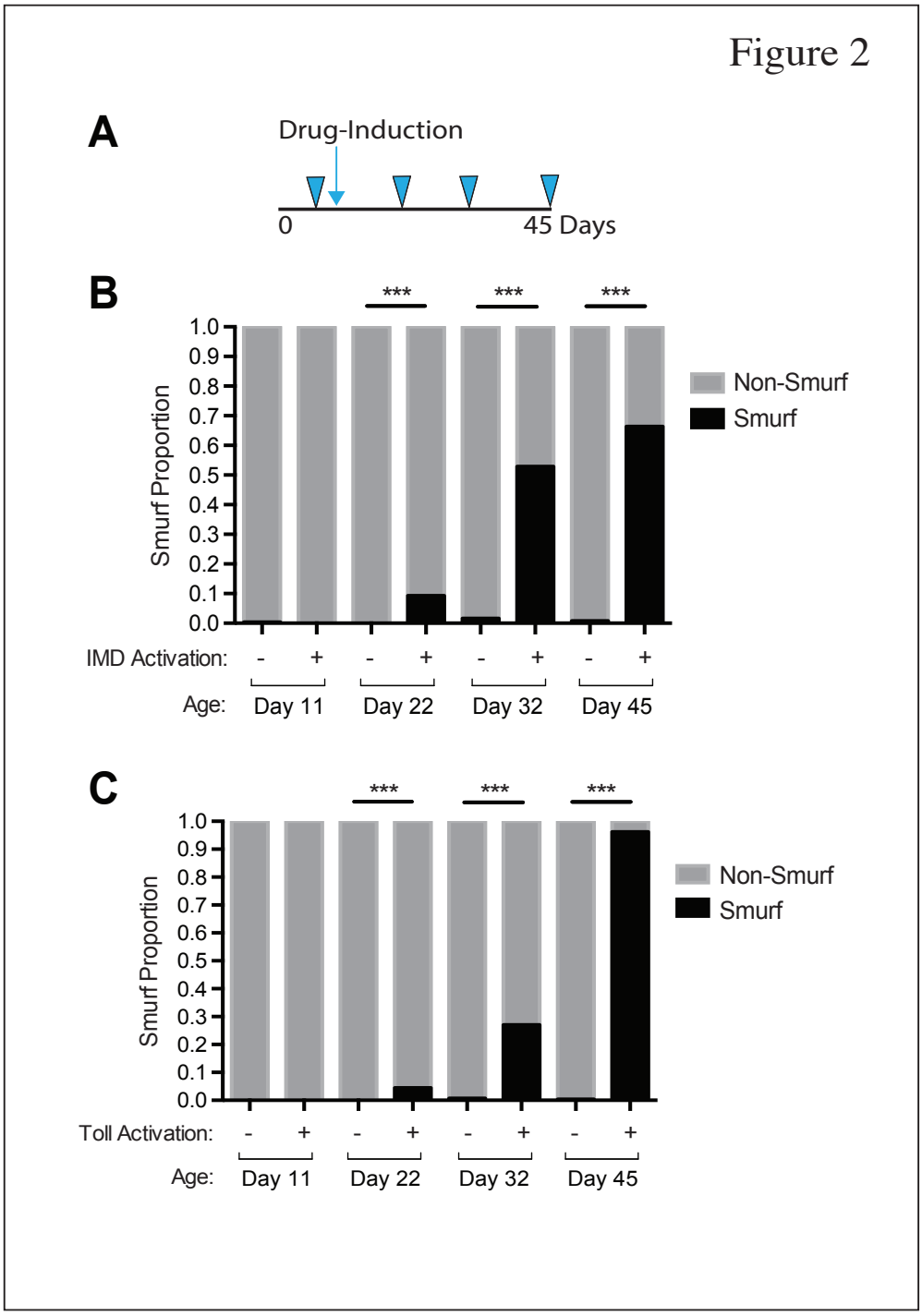

Figure 4.2: Immune activation is sufficient to drive loss of intestinal barrier function

Smurf proportions. Timeline: Immune activation was induced at day 10, Smurf status was analyzed at regular intervals throughout the lifespan at day 11, 22, 32, and 45 (triangles) (A). Stacked bar graphs show *5966GS > UAS-PGRP-LCa* (B) and *UAS-Toll10b* (C), axenic female flies, immune activated from day 10 of adulthood and uninduced controls. n = >200 flies/condition. p-value <0.001 = *** in Binomial Test, only significant changes shown.

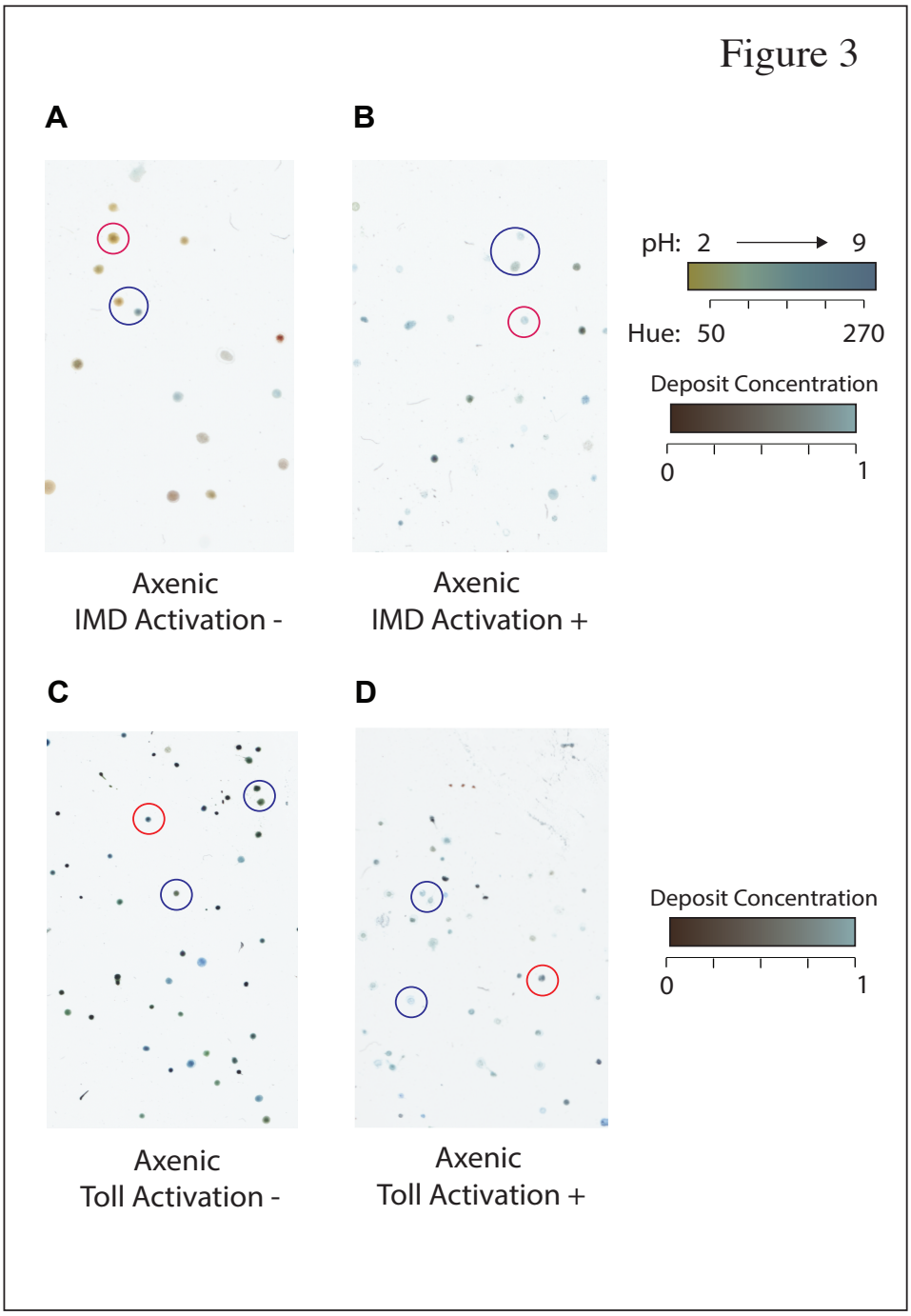

Figure 4.3: Representative images of fecal assay in axenic flies

Representative images highlight fecal output from axenic *5966GS > UAS-PGRP Lc* immune activated (A) and uninduced controls (B); *5966GS > UAS-Toll10b* immune activated (C) and uninduced controls (D). Droppings excreted from female non-Smurf flies at 30 days of age over 24 hrs. Circles indicate qualitative immune-associated changes in digestive transit - red circles indicate typical average color changes; black circles indicate typical average changes in deposit concentration. Scale bars indicate how deposit color (hue) and concentration are quantified.

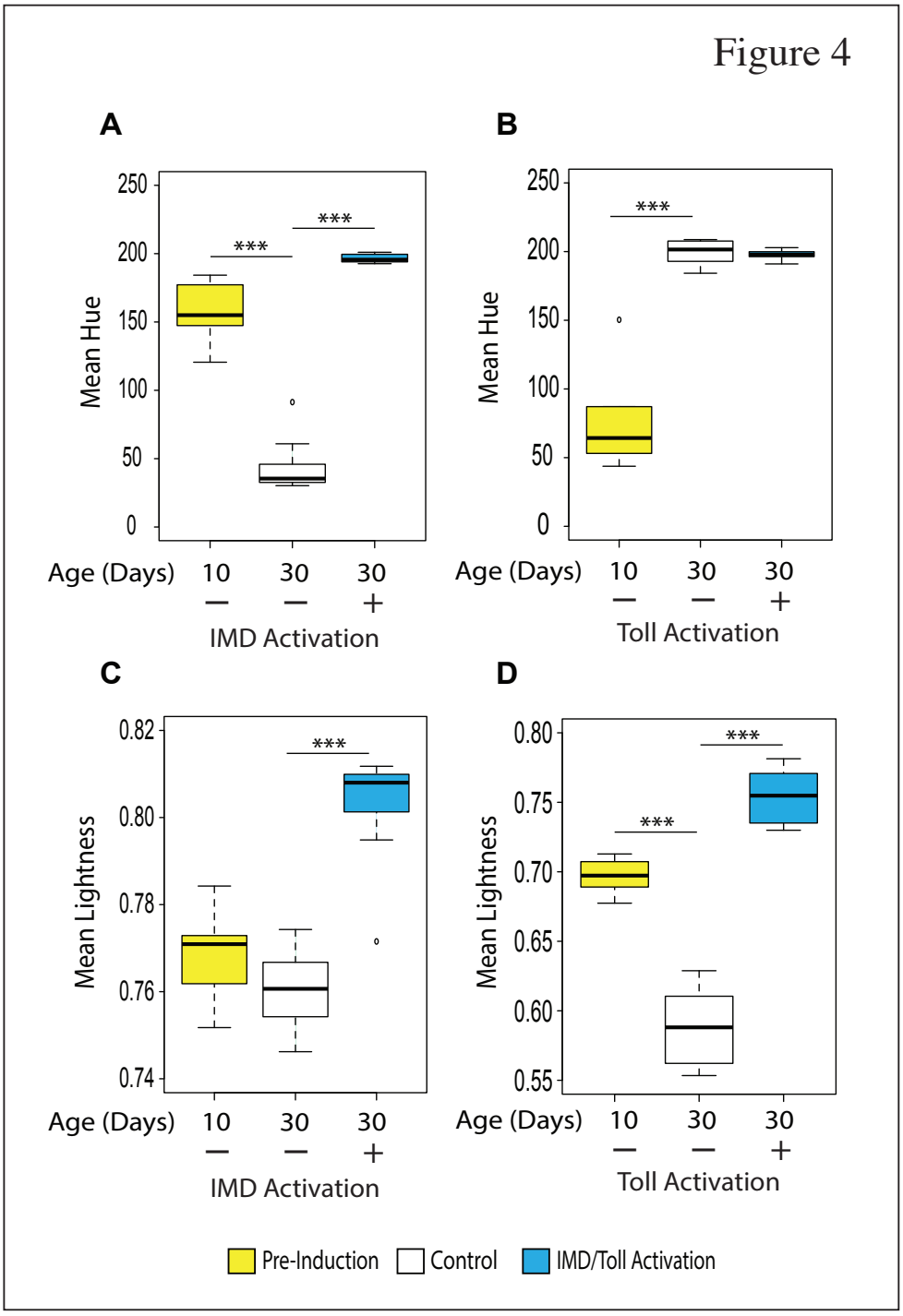

Figure 4.4: Immune activation is sufficient to impair measures of intestinal physiology

Quantification of changes in intestinal pH and fecal concentration in axenic *5966GS > UAS-PGRP Lc* (A, C) and *5966GS > UAS-Toll10b* (B, D). n = 10 replicate groups of 10 female non-Smurf flies. Boxplots display the first and third quartile, with the horizontal bar at the median. p-value <0.001 = *** in Mann-Whitney U Test, only significant changes shown. Hue = biological correlate of pH, lightness = dye concentration/diuresis.

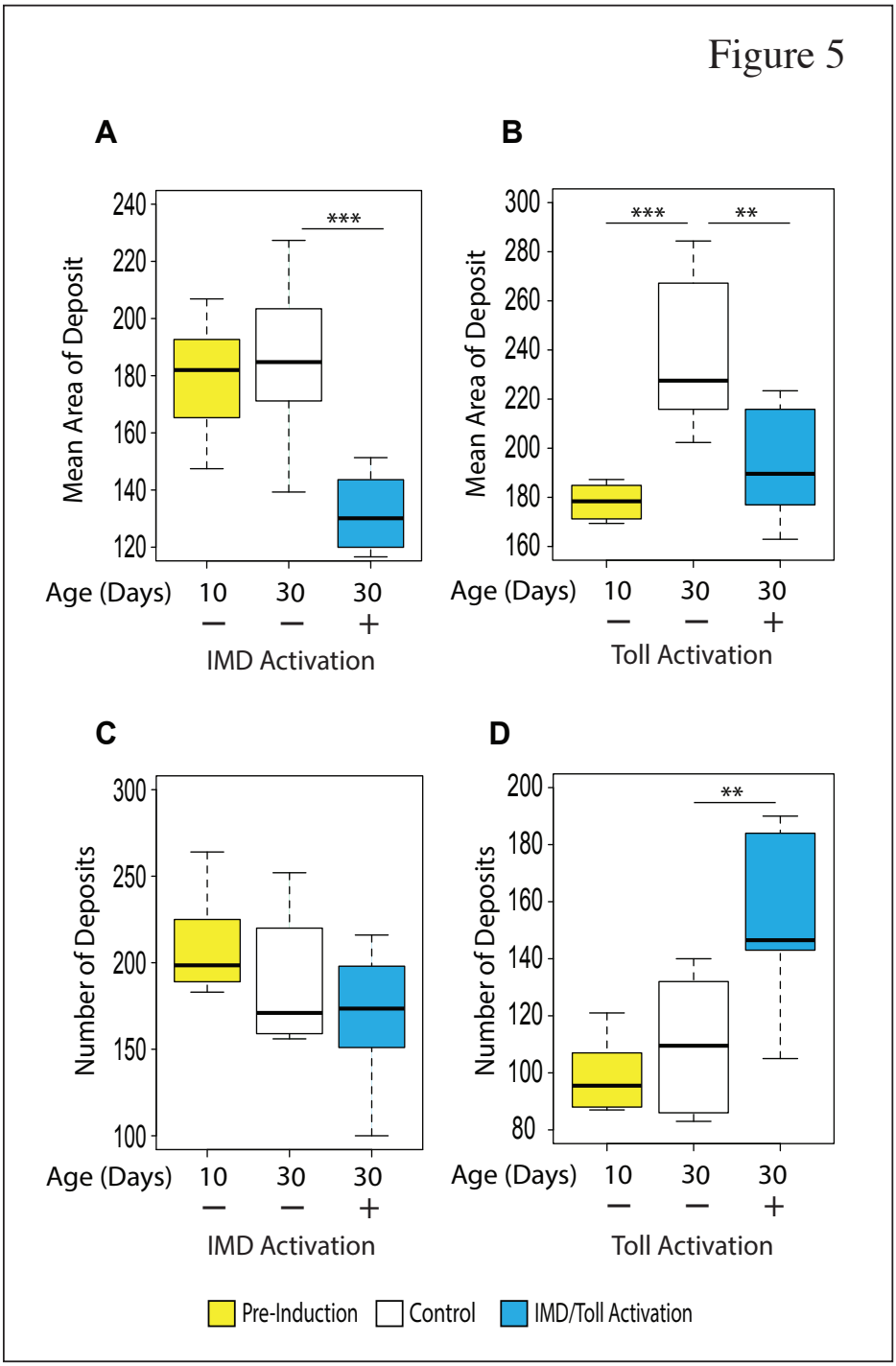

Figure 4.5: Immune activation is sufficient to impair digestive transit

Quantification of changes in individual fecal deposit area and number of deposits in axenic *5966GS > UAS-PGRP Lc* (A, C) and *5966GS > UAS-Toll10b* (B, D). n = 10 replicate groups of 10 female non-Smurf flies. Boxplots display the first and third quartile, with the horizontal bar at the median. p-value <0.01 = **, <0.001 = *** in Mann-Whitney U Test, only significant changes shown.

4.3 Immune activation alone drives loss of epithelial integrity

4.3.1 Immune activation drives misexpression of adherens junction genes

To further characterize the impact of immune activation on age-associated intestinal decline, expression of an array of intestinal epithelial markers were quantified. Similar to my work from Chapter 3, these markers include junctional proteins and stress response pathway ligands – both of which form a network to maintain intestinal homeostasis.

Expression was quantified by RT-qPCR from dissected intestines throughout fly lifespan. Importantly, these intestines were dissected from non-Smurf flies, or flies that still retained barrier function on the day of dissection. The scoring and segregation of flies maintaining barrier function allowed for data analysis and interpretation based on immune-induced effects in the absence of barrier loss. Thus, showing effects of immune activation pre-Smurf on intestinal epithelia. My data show that immune activation drives misexpression of adherens junction genes. *Drosophila E-Cadheren* (*DE-Cad)* transcript levels significantly increase in IMD and Toll activated flies (Figure 4.6 A-B). However, IMD activation only significantly increased expression of *DE-Cad* in late life (Figure 4.6 A); while Toll activation seemingly increases *DE-Cad* transcript levels throughout the lifespan (Figure 4.6 B). IMD activation significantly increase *polychaetoid (pyd)* expression at late life (Figure 4.7 A). While *pyd* expression remains unchanged upon Toll activation, there does seem to be a nonsignificant age-related increase in *pyd* transcript levels (Figure 4.7 B). Of note, this data is complex and includes varied changes in transcript levels across conditions and with age – further interpretation and discussion will follow at the end of this chapter.

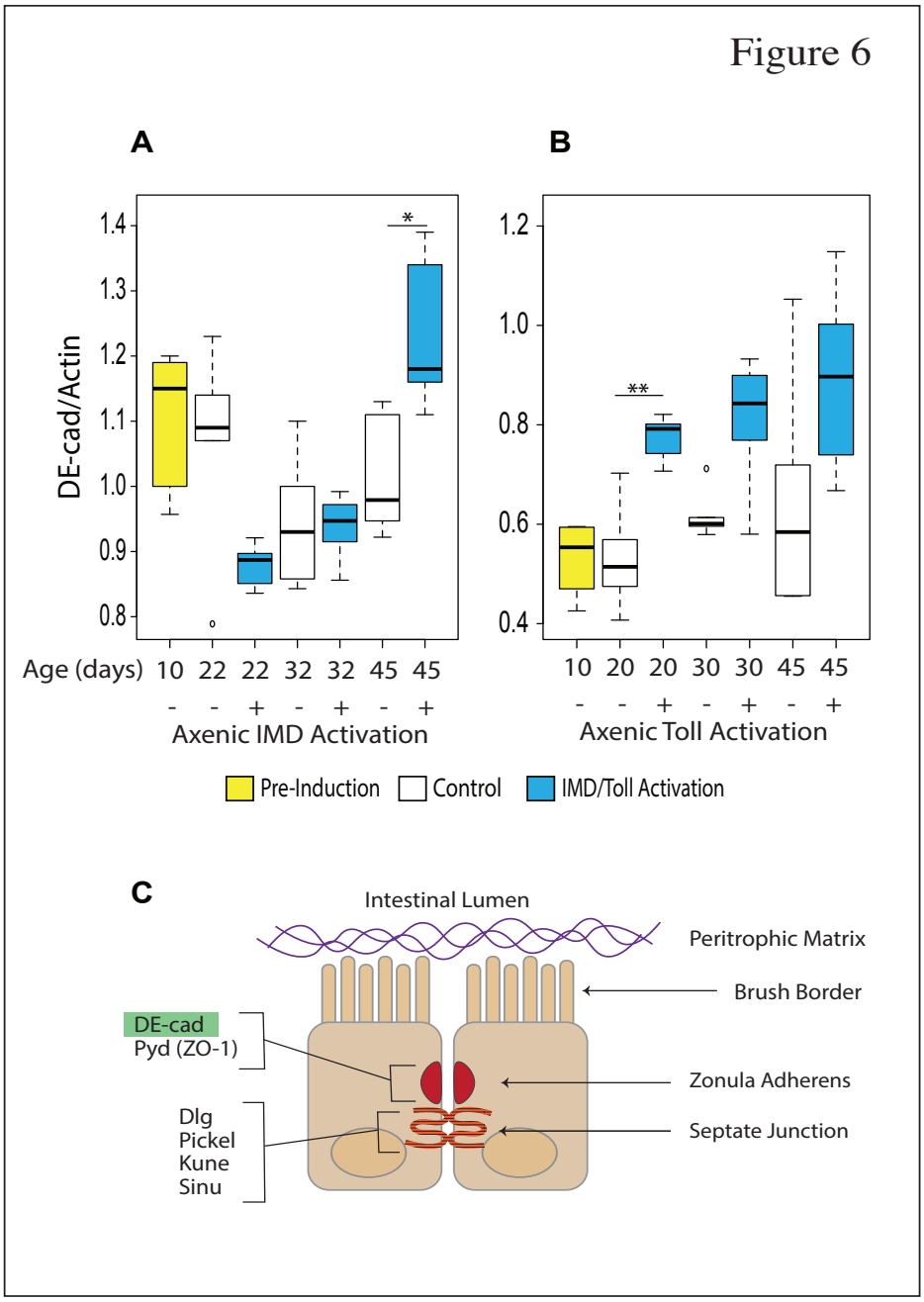

Figure 4.6: Immune activation drives misexpression of adherens junction gene DE-cad

Quantification of *Drosophila* E-Cadherin (DE-cad) mRNA levels. Gene expression assayed by RT-qPCR from dissected intestines; axenic, non-Smurf female flies immune activated from day 10 of adulthood and uninduced controls. *5966GS > UAS-PGRP Lc* (A) and *5966GS > UAS-Toll10b* (B). n = 6 replicates of five intestines. p-value <0.05 = *, <0.01 = ** in Wilcoxon Test, pairwise comparisons, only significant changes shown. Schematic depicting epithelial cell organization and respective localization of junction-associated protein DE-cad (C).

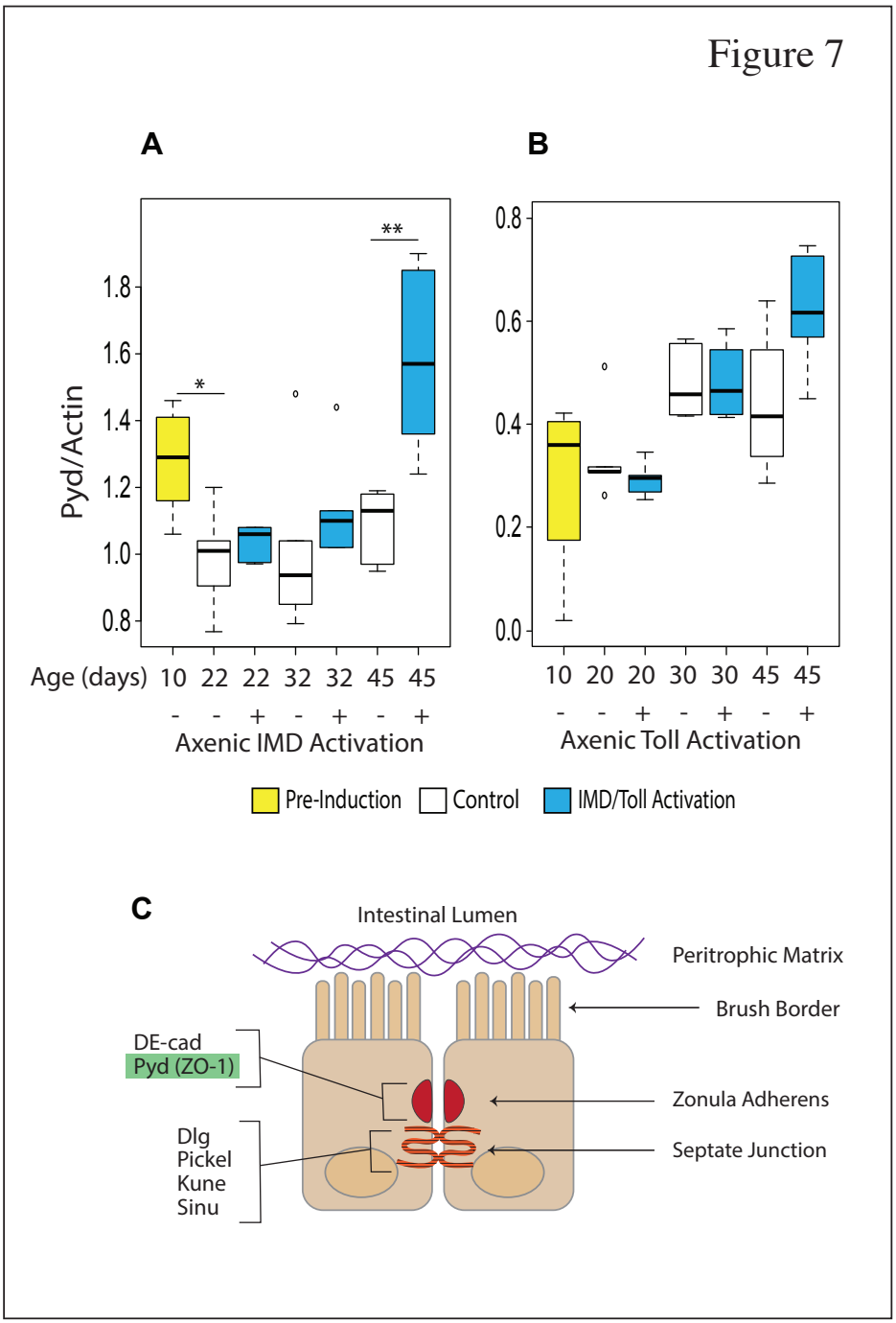

Figure 4.7: Immune activation drives misexpression of adherens junction gene Pyd

Quantification of Polychaetoid (Pyd) mRNA levels. Gene expression assayed by RT-qPCR from dissected intestines; axenic, non-Smurf female flies immune activated from day 10 of adulthood and uninduced controls. *5966GS > UAS-PGRP Lc* (A) and *5966GS > UAS-Toll10b* (B). n = 6 replicates of five intestines. p-value <0.05 = *, <0.01 = ** in Wilcoxon Test, pairwise comparisons, only significant changes shown. Schematic depicting epithelial cell organization and respective localization of junction-associated protein Pyd (C).

4.3.2 Immune activation drives misexpression of septate junction genes

Pickel expression is significantly upregulated by IMD activation, but not changed significantly by Toll activation (Figure 4.8 A-B). *Sinuous* expression is significantly upregulated by IMD in late life, and significantly downregulated by Toll in early life (Figure 4.9 A-B). *Kune-kune* expression is significantly upregulated in late life by IMD activation and remains unchanged by Toll activation (Figure 4.10 A-B). *Discs Large-1* expression is significantly upregulated in late life by IMD activation and significantly downregulated in midlife by Toll activation (Figure 4.11 A-B). Taken together these data suggest that while immune activation significantly impacts junction gene expression, immune pathways regulate those changes differently.

4.3.3 Immune activation may drive dysplasia via Jak/STAT pathway

4.3.3.1 Immune activation drives misexpression of unpaired-3 gene

Upd3 expression is significantly upregulated in late life by IMD activation and significantly upregulated at early, mid- and late life by Toll activation (Figure 4.12 A-B). This data suggests activation of stress-related pathways, as a result of immune pathway activation at the gut. Increased Upd3 expression, driven by immune activation, may in turn be driving increased proliferation and differentiation of progenitor cells.

4.3.3.2 Effects of immune activation on progenitor cell markers

Notch expression is significantly upregulated in late life by IMD activation, and significantly upregulated in midlife by Toll activation (Figure 4.13 A-B). There is also a non-significant increase in late life *notch* expression by Toll (Figure 4.13 B). *Delta* expression is not significantly changed by IMD activation (Figure 4.14 A). By contrast, Toll activation significantly increases *delta* transcript levels during early and mid-life

(Figure 4.14 B). Taken together, these data suggest that *notch* signaling may be impacted by immune upregulation in a bacteria-independent manner.

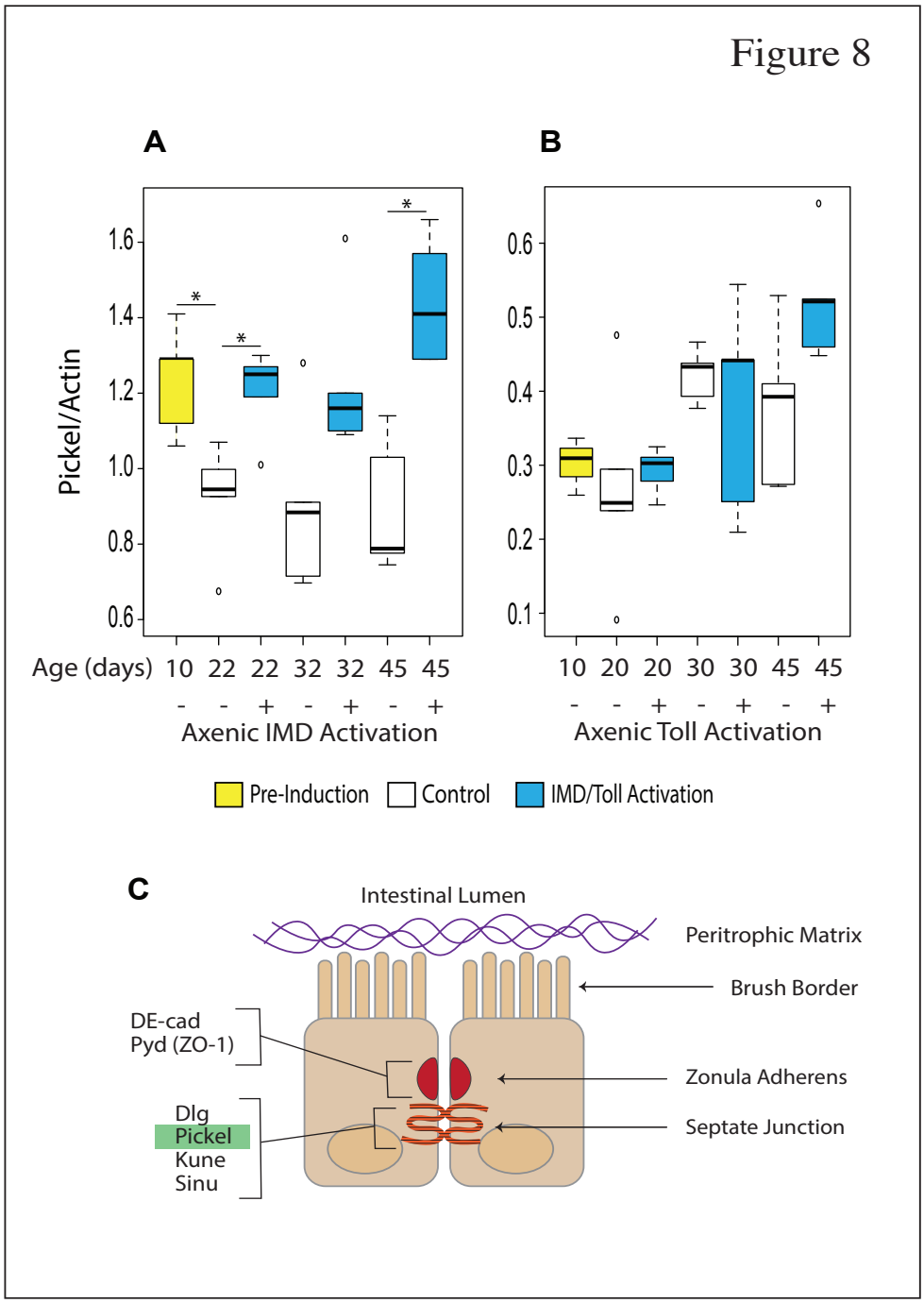

Figure 4.8: Immune activation drives misexpression of septate junction gene Pickel

Quantification of Pickel mRNA levels. Gene expression assayed by RT-qPCR from dissected intestines; axenic, non-Smurf female flies immune activated from day 10 of adulthood and uninduced controls. *5966GS > UAS-PGRP Lc* (A) and *5966GS > UAS-Toll10b* (B). n = 6 replicates of five intestines. p-value <0.05 = *, in Wilcoxon Test, pairwise comparisons, only significant changes shown. Schematic depicting epithelial cell organization and respective localization of junction-associated protein Pickel (C).

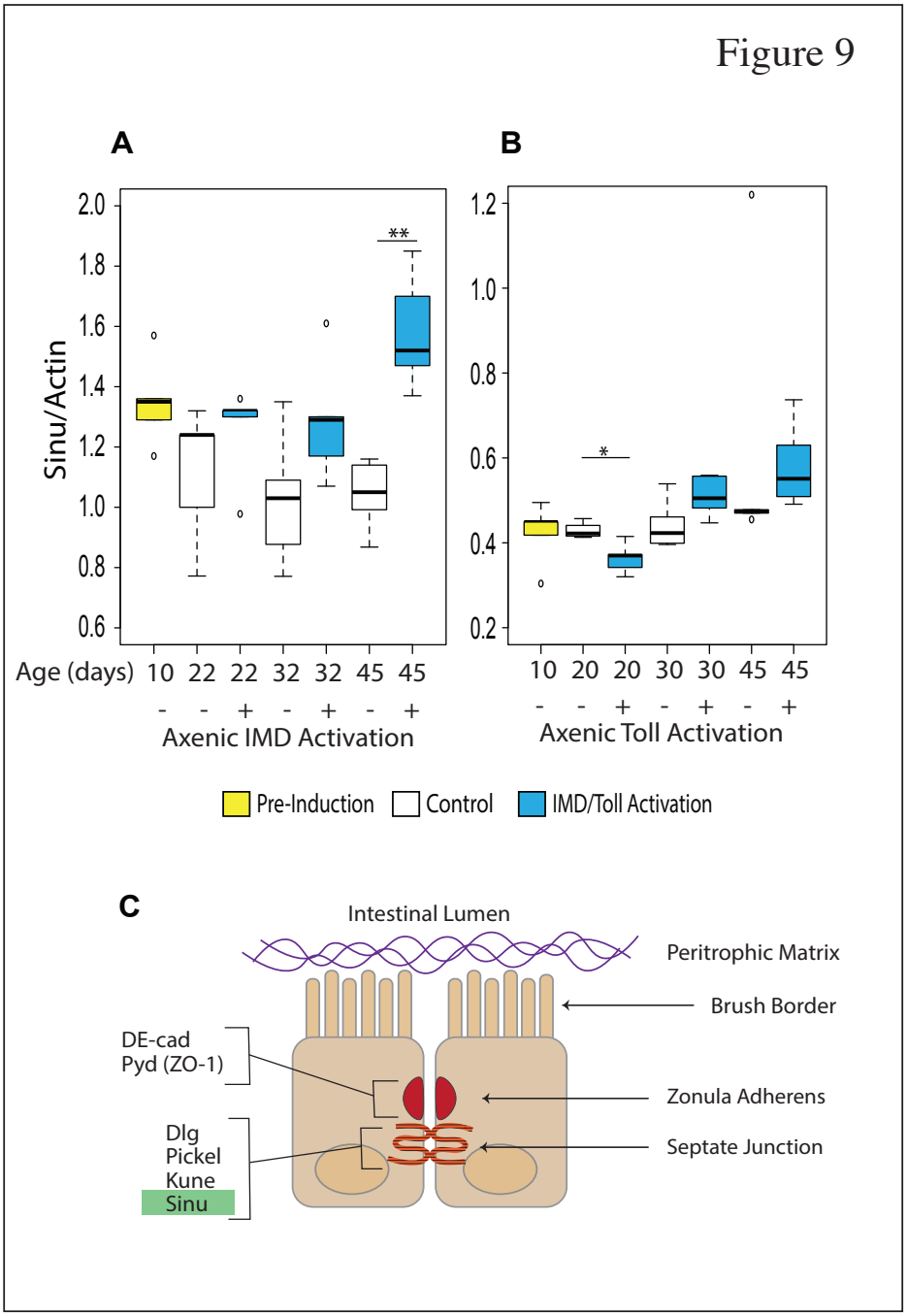

Figure 4.9: Immune activation drives misexpression of septate junction gene Sinu

Quantification of Sinuous (Sinu) mRNA levels. Gene expression assayed by RT-qPCR from dissected intestines; axenic, non-Smurf female flies immune activated from day 10 of adulthood and uninduced controls. *5966GS > UAS-PGRP Lc* (A) and *5966GS > UAS-Toll10b* (B). n = 6 replicates of five intestines. p-value <0.05 = *, <0.01 = ** in Wilcoxon Test, pairwise comparisons, only significant changes shown. Schematic depicting epithelial cell organization and respective localization of junction-associated protein Sinu (C).

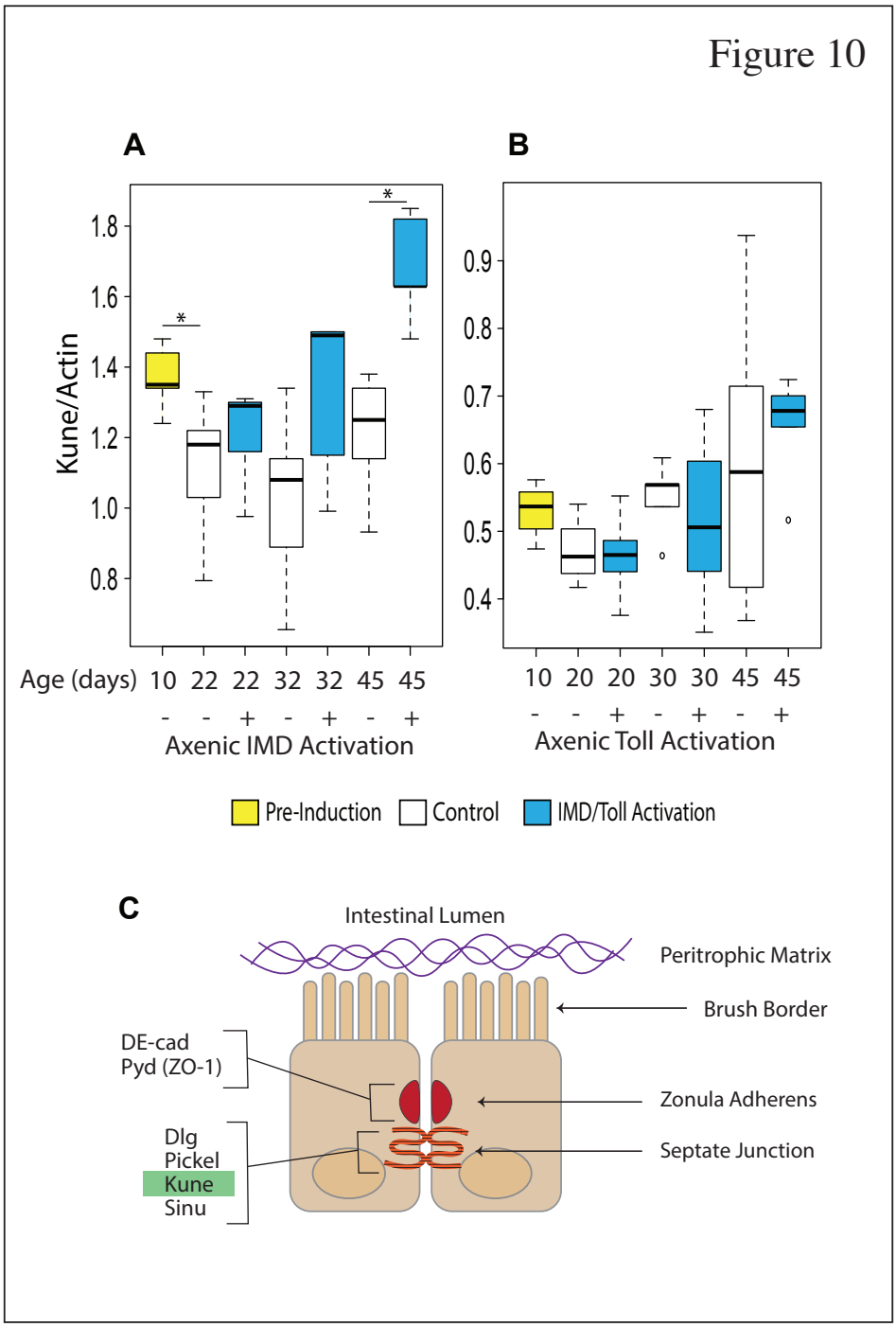

Figure 4.10: Immune activation drives misexpression of septate junction gene Kune

Quantification of Kune-Kune (Kune) mRNA levels. Gene expression assayed by RT-qPCR from dissected intestines; axenic, non-Smurf female flies immune activated from day 10 of adulthood and uninduced controls. 5966GS > UAS-PGRP Lc (A) and 5966GS > UAS-Toll10b (B). n = 6 replicates of five intestines. p-value <0.05 = * in Wilcoxon Test, pairwise comparisons, only significant changes shown. Schematic depicting epithelial cell organization and respective localization of junction-associated protein Kune (C).

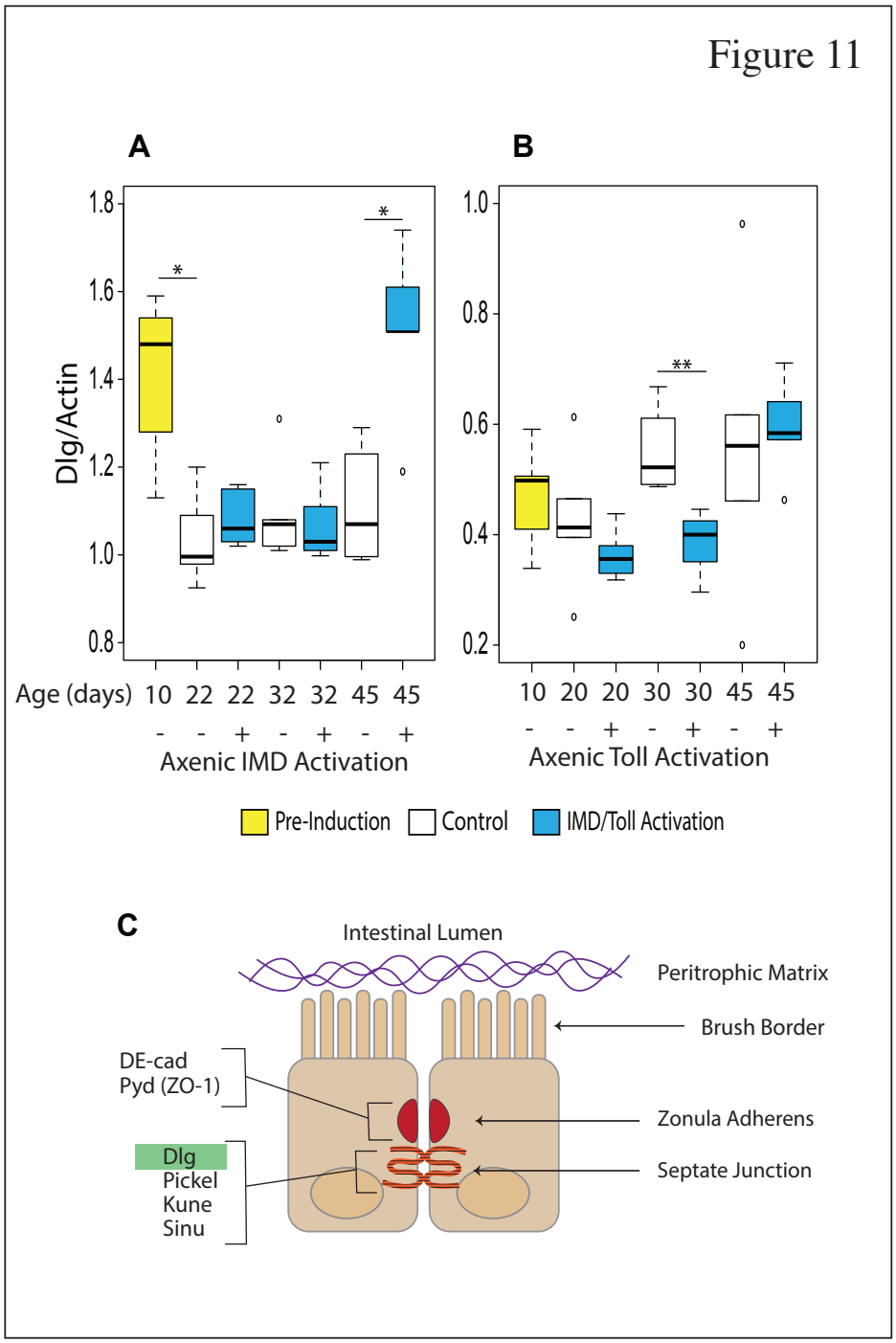

Figure 4.11: Immune activation drives misexpression of septate junction gene Dlg

Quantification of Discs Large-1 (Dlg) mRNA levels. Gene expression assayed by RT-qPCR from dissected intestines; axenic, non-Smurf female flies immune activated from day 10 of adulthood and uninduced controls. 5966GS > UAS-PGRP Lc (A) and 5966GS > UAS-Toll10b (B). n = 6 replicates of five intestines. p-value <0.05 = *, <0.01 = ** in Wilcoxon Test, pairwise comparisons, only significant changes shown. Schematic depicting epithelial cell organization and respective localization of junction-associated protein Dlg (C).

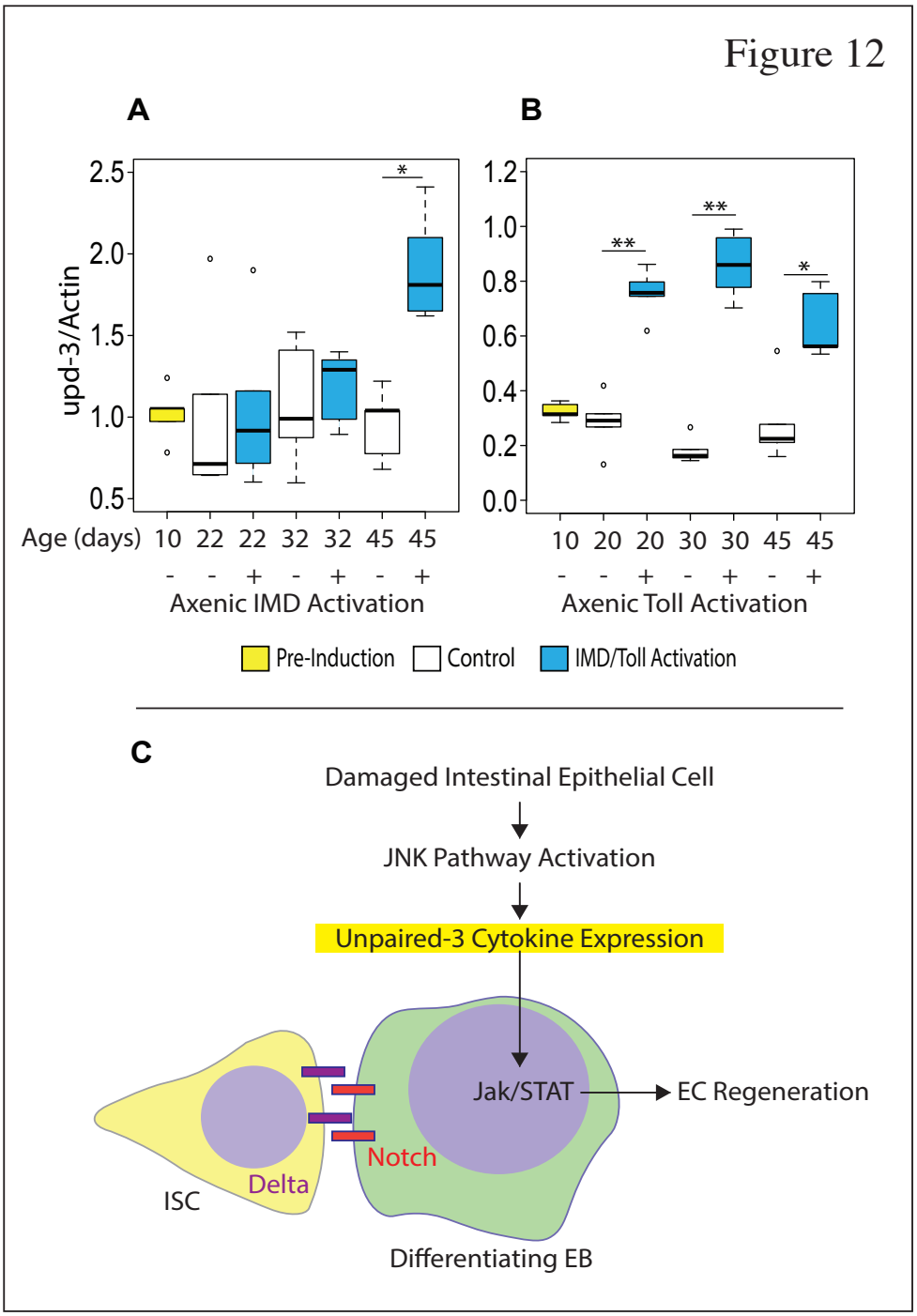

Figure 4.12: Immune activation drives misexpression of unpaired-3 gene

Quantification of unpaired-3 (upd3) mRNA levels. Gene expression assayed by RT-qPCR from dissected intestines; axenic, non-Smurf female flies immune activated from day 10 of adulthood and uninduced controls. 5966GS > UAS-PGRP Lc (A) and 5966GS > UAS-Toll10b (B). n = 6 replicates of five intestines. p-value <0.05 = *, <0.01 = ** in Wilcoxon Test, pairwise comparisons, only significant changes shown. Model of steps in enterocyte regeneration: upd3 activates the Jak/STAT pathway in progenitor cells inducing proliferation (C).

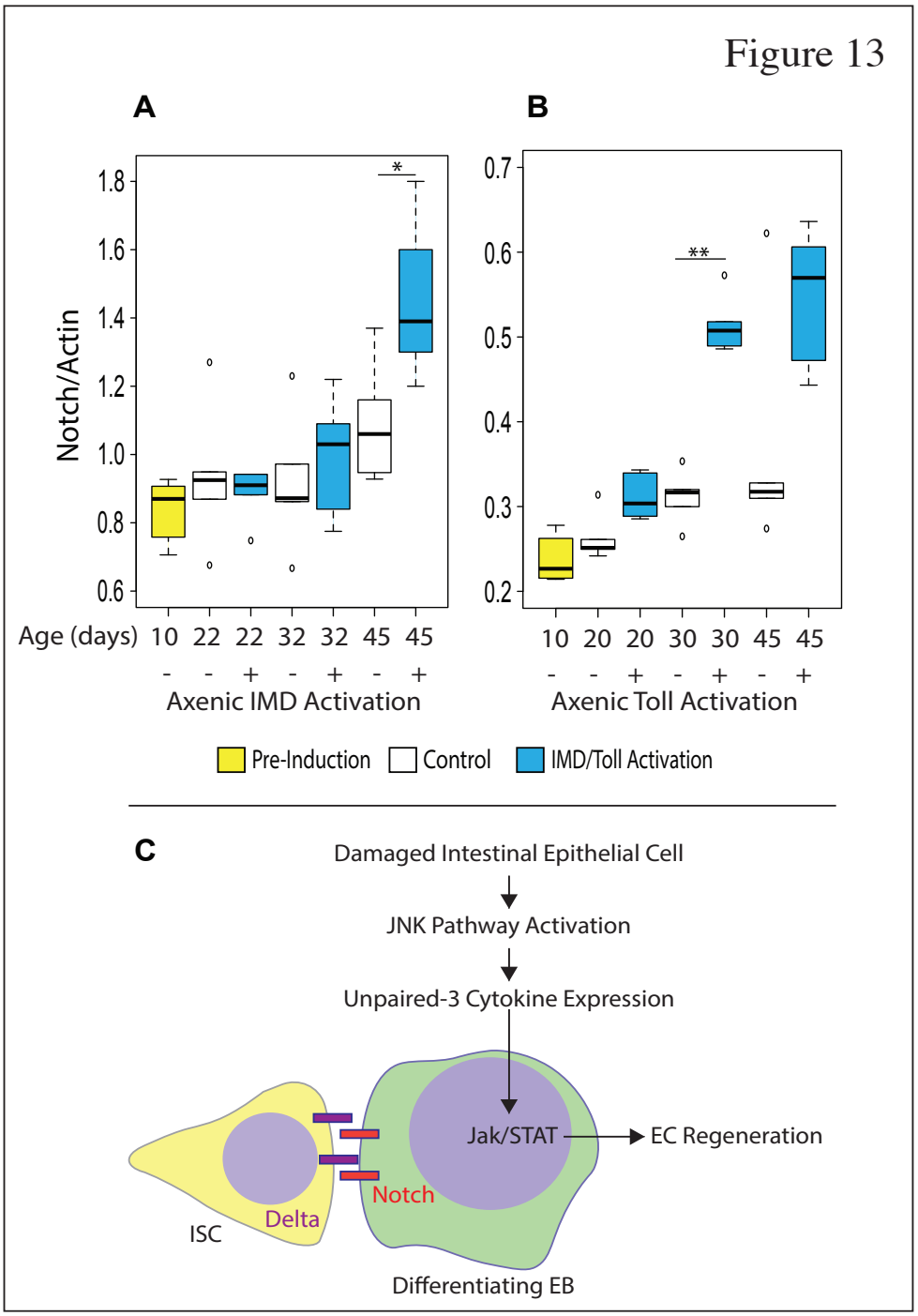

Figure 4.13: Effects of immune activation on progenitor cell marker Notch

Quantification of Notch mRNA levels. Gene expression assayed by RT-qPCR from dissected intestines; axenic, non-Smurf female flies immune activated from day 10 of adulthood and uninduced controls. 5966GS > UAS-PGRP Lc (A) and 5966GS > UAS-Toll10b (B). n = 6 replicates of five intestines. p-value <0.05 = *, <0.01 = ** in Wilcoxon Test, pairwise comparisons, only significant changes shown. Model of steps in enterocyte regeneration: Transmembrane receptor Notch is activated by membrane-tethered ligand, Delta (C).

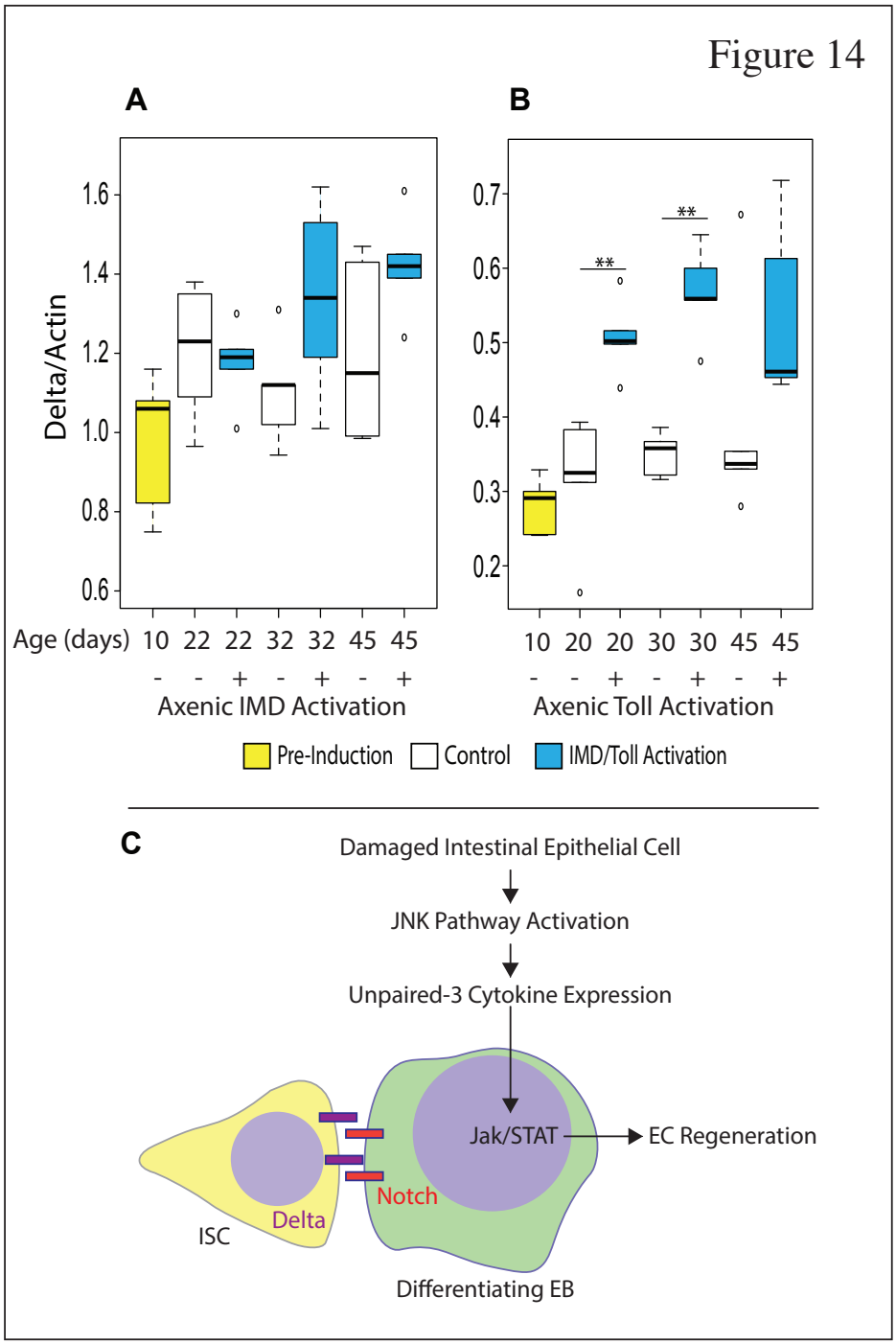

Figure 4.14: Effects of immune activation on intestinal cell marker Delta

Quantification of Delta mRNA levels. Gene expression assayed by RT-qPCR from dissected intestines; axenic, non-Smurf female flies immune activated from day 10 of adulthood and uninduced controls. 5966GS > UAS-PGRP Lc (A) and 5966GS > UAS-Toll10b (B). n = 6 replicates of five intestines. p-value <0.01 = ** in Wilcoxon Test, pairwise comparisons, only significant changes shown. Model of steps in enterocyte (EC) regeneration: Membrane-tethered ligand, Delta, activates progenitor cell (EB) differentiation via Notch signaling (C).

4.4 Discussion

4.4.1 Overview

Data from this chapter show that immune activation alone is indeed sufficient to drive intestinal decline. These findings offer two major points for discussion (1) what are immune-induced flies dying of, if not microbial imbalance? (2) what is the relevance of immune-induced decline to conventional aging?

4.4.2 Immune activation mimics age-related intestinal barrier dysfunction

Immune activation alone is sufficient to reduce lifespan in the absence of bacteria (Figure 4.1). The scale of the effect is equivalent whether axenic or conventional; whereby differences in maximum lifespan between immune activated and control flies is about 20 days regardless of bacterial presence (Alcaraz, 2016 and Figure 4.1). These findings suggest that an increase in mortality is not driven via a bacteria-based mechanism. However, immune-induced axenic flies live longer, thus showing the role of bacteria in aging as found previously (Brummel et al., 2004, Rera et al., 2012, Guo et al., 2014, Clark et al., 2015, Resnik-Docampo et al., 2018). Increasing negative regulation of the IMD pathway also results in a small but significant lifespan extension in axenic flies, compared to a larger lifespan extension in conventional counterparts (Guo et al., 2014). Guo et al. results suggest a potential buffering effect which happens only in the presence of bacteria, whereby the presence of bacteria is beneficial and necessary for immune-regulated lifespan extension. Similar to what is seen by Salazar et al. with *ssk* overexpression (Salazar et al., 2018).

While this thesis data show that significant immune pathway activation decreases lifespan, other works suggest that upregulation of specific antimicrobial peptides (AMPs)

is sufficient to rescue and extend lifespan. Loch et al. show how overexpression of individual antimicrobial peptides (AMPs) in a germ-free adult fly intestine results in lifespan extension (Loch et al., 2017). Interestingly, ubiquitous overexpression of AMPs also results in a small but significant lifespan extension, suggesting that both global and localized AMP overexpression can have positive effects on lifespan (Loch et al., 2017). For this reason, the follow-up hypothesis became that intestinal barrier function was being directly impacted by immune activation in a bacteria-independent manner. Indeed, immune activation alone is sufficient to drive and accelerate loss of barrier function (Figure 4.2). Interestingly, axenic immune activated flies experience larger increases in Smurf number with age than their conventional counterparts (Alcaraz, 2016 and Figure 4.2). Thesis data are consistent with the idea that bacterial presence can help the host resist harmful or detrimental changes to intestinal homeostasis. This could be considered a buffering effect, whereby bacteria are helping to mitigate immune responses targeted at epithelial cells – resulting in "fewer" conventional Smurfs as compared to axenic Smurfs. Although the number of axenic flies losing barrier function supersedes age-matched conventional fly cohorts, axenic flies still live longer than age-matched conventional flies. This suggests that barrier loss alone, while detrimental to the fly, is less important in the absence of bacteria. Based on results from immune activated conventional flies, the next hypothesis became that epithelial junction expression along the gut may be just as impacted by immune activation alone.

Recently published works have indicated independent roles for junction components in intestinal homeostasis and, by extension, lifespan (Salazar et al., 2018, Izumi et al., 2019, Izumi et al., 2020). Returning to work completed by Salazar and colleagues, *ssk* knockdown still drives barrier dysfunction and death of the fly even in fully axenic conditions. There are also changes to the morphology of the gut and increased *upd3*

expression, even in axenic flies. This shows that septate junction components alone can modify certain aspects of age-related decline. Still, lifespan extension is only seen when *ssk* is overexpressed in intestinal EBs and mature ECs (Salazar et al., 2018). Per quantified electron microscopy images of epithelial cell cross-sections, Salazar et al. show that *ssk* overexpression results in "tighter" epithelial cell contact. In the presence of bacteria, reversed barrier dysfunction would be undoubtedly helpful as it could keep bacteria from escaping the gut into fly circulation and mounting a whole-fly immune response. For this reason, it makes sense that lifespan extension is not observed in axenic *ssk* overexpressed flies – as it is bacteria plus a leaky gut phenotype that mediate intestinal damage. For these reasons, the next hypothesis was that intestinal decline is heavily impacted by immune dysregulation.

Junction-related mechanisms may provide further insight into how immune pathway activation compromises barrier function without bacteria. Since all septate junction components are hugely interdependent, mutations in any of these genes can lead to mis-localization of junction proteins (reviewed in Jonusaite et al., 2016). Future experiments could thus involve omitting downstream effectors from the IMD/Toll pathway, specifically in ECs, and screening for changes in expression patterns of known junction components. Looking at transcription patterns in the first instance would allow for more targeted imaging down the line. Imaging would provide further information about actual junction protein localization.

4.4.3 Immune activation induces dysentery-like phenotypes in adult fly excreta

The changes observed in intestinal physiology as measured by the T.U.R.D assay varies with condition, axenic versus conventional, and treatment, immune activated or not. In other words, a straight pairwise comparison is not available as there are no consistent

patterns that arise between different experimental cohorts. Although there are minor differences between immune pathway results and how they impact intestinal physiology, the take home message remains – microbes are not necessary to observe changes in physiology.

The developers of the T.U.R.D assay validated and confirmed that area of fecal deposits is biologically correlated to size (Cognigni et al., 2011, Wayland et al., 2014). The number of quantified fecal deposits informs on the rate of digestive transit and how it might be impaired i.e., longer transit time would result in fewer deposits, while faster transit time would result in more deposits – assuming equal intake. Recent findings show that knocking down antidiuretic hormone *ion transport protein* (IPT) in the adult fly results in increased rate of excretion in conventional adult flies (Gáliková et al., 2018). The authors demonstrate the importance of osmotic regulation as well as offer further validation of the T.U.R.D assay.

Thesis findings show that immune activation in the absence of bacteria is sufficient to change the amount and size of fecal deposits (Figure 4.5). Immune activated axenic fly excreta are smaller and greater in number, compared to conventional immune activated flies (Alcaraz, 2016 and Figure 4.5). Comparison of axenic and conventional data suggest that bacterial presence leads to a constipation-like phenotype. Whereby, bacteria-mediated metabolism slows digestive transit leading to the accumulation of waste products (Wayland et al., 2014). However, Wayland et al. confirm that bacterial composition alone does not significantly alter intestinal physiology. The authors tested and compared fecal deposits from axenic, commensal-reassociated, conventional flies, as well as flies induced with a non-lethal pathogenic infection – between all condition and treatments there was little to no change in fecal deposit output (Wayland et al., 2014). This is not to suggest that bacteria are not important regulators of intestinal physiology, but rather that there are

indirect bacterial consequences occurring at an epithelial cell level along the gut lumen. Moreover, the combination of bacterial presence with any known age-related pathology i.e., immune dysfunction, is necessary to see significant changes in intestinal physiology.

4.4.3.1 Are axenic immune activated flies dehydrated?

Water absorption was also investigated in axenic immune activated flies. Dye color intensity has been verified in T.U.R.D as the biological correlate of water balance and fluid excretion (Cognigni et al., 2011, Wayland et al., 2014). Maintenance of water absorption/excretion ensures that osmotic balance is maintained in the fly, preventing dehydration and/or osmotic stress (Demerec, 1994b). Thesis data show that immune activation alone is sufficient to increase deposit lightness, such that fecal deposits appear more dilute (Figure 4.4 C-D). Immune activation in axenic and conventional flies results in excrement that is lighter, or less intense in color, suggesting that an increase in water excretion is not driven by a bacteria-mediated mechanism. Perhaps immune activation is perturbing water reabsorption, desiccating the fly prematurely. This hypothesis could be tested using a water content assay modified from Gáliková et al. The authors used a microbalance to weigh fresh flies, then transferred flies to 65ºC, after 48 hours flies were reweighed (Gáliková et al., 2018). Water content was calculated as fresh weight minus dry weight as a proportion of fresh weight (Gáliková et al., 2018). For the purposes of work presented in this thesis, further categorization between immune-induced Smurf and non-Smurf would help discern the impacts of barrier dysfunction on water loss. Alternatively, gut contents could be quantified by measuring dye intensity on a spectrophotometer (Cognigni et al., 2011). These assays would allow for the discernment of flies experiencing osmotic stress due to immune-induced dehydration. If so, this would further suggest that

immune activation alone was able to drive changes at the level of the malpighian tubules and hindgut – areas which are the primary sites of osmotic control in the fly.

4.4.3.2 Implications of immune activation on intestinal regionalization

A key component of intestinal heath is regionalization of pH along the gut (Miguel-Aliaga et al., 2018). More specifically, the stomach-like parietal cells of the fly, hereafter referred to as the copper cell region (CCR), is the most acidic location of the fly intestine (Strand and Micchelli, 2011, Strand and Micchelli, 2013, Li et al., 2016, Mehrotra et al., 2020). CCR maintenance is required for intestinal and bacterial homeostasis (Li et al., 2016). Here, changes in pH were further explored to assess if immune activation could change the pH of luminal contents. The hue (or color of fecal deposits) is the biological correlate of acid-base balance in the gut, as previously verified by T.U.R.D developers (Cognigni et al., 2011, Wayland et al., 2014).

Thesis data show that immune activation alone is sufficient to increase intestinal pH (Figure 4.4 A-B). Immune activation in axenic and conventional flies results in excrement that is more alkaline, suggesting that an increase in pH is not driven by a bacteria-mediated mechanism (Alcaraz, 2016 and Figure 4.4 A-B). Previously published work has shown that loss of acidity with age further facilitates bacterial dysbiosis in the gut (Li et al., 2013, Li et al., 2016). Whereby, retained function of the CCR facilitates beneficial compartmentalization along the gut resulting in retained epithelial and digestive regulation with age. Perhaps it is basal acidity in control flies at midlife that consequently extends CCR function with age? The next hypothesis became that control flies may live longer because of preserved CCR function with age, while immune activation, regardless of bacterial presence, may result in reduced CCR function.

An alternative hypothesis involves IMD activation inducing neighboring immune and stress-response pathways. For example, increased Jak/STAT activation has been shown to contribute significantly to ectopic expression of enterocyte marker Pdm1 in the CCR – indicating a loss of copper cell number and by extension CCR function (Li et al., 2016). Future experiments that could help discern if immune activation is indeed perturbing copper cell division and CCR function includes (1) expression of copper cell associated transcription factor *cut* could be quantified by RT-qPCR to quickly assess whether there are changes in the middle midgut of immune-induced flies (2) if there are pronounced changes, then more elegant staining of guts across conditions using *anti-cut+* could be used to discern how acid-producing copper cells themselves are changing in number across conditions and treatments (Dubreuil, 2004, Strand and Micchelli, 2011, Li et al., 2013, Li et al., 2016, Mehrotra et al., 2020). Results from this first set of imaging experiments would give greater insight to how immune activation alone changes gut regionalization.

4.4.4 Potential effects of immune activation on nutrient absorption

Thesis data highlight the potential dysregulation of intestinal physiology driven by bacteria but mediated through immune activation. Previous work indicates the importance of the IMD pathway in enterocyte lipid metabolism (Kamareddine et al., 2018). The authors note a significant increase in lipid accumulation in axenic flies and a decrease in enteroendocrine (EE) cell hormone – *tachykinin (Tk)*. Axenic flies accumulate lipid because acetate from bacteria is needed to activate *PGRP LC* and downstream transcription factor *relish* in EE cells that release *Tk* (Kamareddine et al., 2018). To test if immune activation is indeed mediating metabolic dysregulation, the following experiments could be done (1) fat stores between experimental conditions could be compared (2) if

changes were observed staining against *Tk (Ohlstein and Spradling, 2006)* and BODIPY (stain for neutral lipids) could be done in immune activated axenic guts.

4.4.5 Immune activation may alter progenitor signaling through junction misexpression

Thesis findings confirm that immune induction alone is a strong driver of intestinal barrier dysfunction. Since the leaky gut phenotype is so prevalent in immune activated axenic flies, the working hypothesis became that there would be an impact in gut epithelial junction gene expression. Currently published works do not address the impact of constitutive immune activation on junction transcript/protein changes associated with physiological aging; nor do they assess the effects that infection or immune activation would have on proliferative mechanisms. It is, however, well understood that loss of turnover control in the adult gut can be driven by epithelial cell damage (Amcheslavsky et al., 2009). Further, it has been shown that inducing infection in adult flies changes localization of *DE-Cad* cellular partner *Armadillo* (*Arm*) in mature ECs from the outer membrane to the cytosol (Maeda et al., 2008, Buchon et al., 2010). For this reason, it was hypothesized that immune-induced barrier dysfunction may be directly activating cell-turnover mechanisms in intestinal cell cohorts. Thesis data show that immune activation in axenic flies is sufficient to significantly change expression patterns of epithelial junction markers. However, the directionality of these changes varies with genotype, condition, treatment, and age – indicating the complex relationship between and within immune pathways in intestinal epithelia.

4.4.5.1 Implications of immune activation on enterocyte signaling

Immune activation in axenic flies results in increased septate junction gene expression under IMD-induction and decreased/no change in septate junction gene expression under

Toll-induction (Figures 4.8-4.11). By contrast changes in septate junction gene expression in conventional flies, is unchanged/increases with IMD-induction and decreases with Toll-induction (Figures 3.18-3.21). Specifically, septate junction components *discs large (Dlg)* and *kune-kune* (*Kune*) seem to have expression levels regulated in a bacteria-independent manner during IMD activation; while *discs large* and *sinuous* (*Sinu*) seem to have expression patterns mediated by a bacteria-independent mechanism during Toll activation. While there are differences between how immune pathways mediate gene expression – this discussion subsection will largely focus on interpretations pertaining to why immune activation may be mediating changes, what is already known about septate junction changes in an axenic background, and how to test potential hypotheses.

Firstly, why is immune activation changing junction transcript expression? One hypothesis is that immune activation disproportionately affects the ratio of young (pre-) ECs to old (mature) ECs. This hypothesis assumes that an increase in young ECs would correlate with an increase in junction gene expression; as these cells begin to mature and integrate into the epithelial monolayer assemblage of junction scaffolding is required. Recently published work showed that *tetraspanin 2A* (Tsp2A) – a septate-specific protein found in the fly midgut – is recruited to the septate junction during differentiation after wound damage (Xu et al., 2019). The authors also showed that once ECs have reached maturation and damage repaired, Tsp2A is simultaneously endocytosed via Rab11 and signals to stop ISC proliferation. Thus, if an EC does not reach maturation, then presumably Tsp2A cannot be endocytosed to stop ISC proliferation. This perhaps then leads to gut epithelial multilayering. To test if this mechanism is regulated in part by immune activation the following experiments can be done (1) immune-activated axenic and conventional fly guts can be stained against Tsp2A and Rab11 (2) if immune-activated axenic guts show increased fluorescence levels in ECs, then RT-qPCR on *delta* levels can

follow as a proxy for ISC proliferation. In the first instance, these experiments will help discern if immune activation is indeed affecting septate junction organization via Tsp2A and facilitating a feedforward model of ISC proliferation.

If there is indeed a difference in the ratio of pre- to mature ECs, this could be further affected by an immune-induced increase in *DE-Cad* expression. Consistent with this idea, Maeda and colleagues have shown that there are quantifiable differences in *armadillo* between progenitor cells, pre-ECs, and mature ECs (Maeda et al., 2008). Since Xu and colleagues showed that young ECs and old ECs have different expression profiles, *DE-Cad* levels could also be different. Further, changes in *DE-Cad* expression could reflect an increase in ISC proliferation because every new EC is exhibiting 'basal levels' of *DE-Cad* expression prior to maturation. Increased *DE-Cad* from young ECs may be causing dysregulation of the normal coupling between EC loss and ISC divisions via epidermal growth factor (EGF) niche signaling. In other words, more *DE-Cad* expression could be causing increased ISC proliferation and because of active radii (active cell-signal zone with large numbers of neighboring ISCs) (Liang et al., 2017) ISCs continue to proliferate leading to hyperplasia. To test if constitutive immune activation affects progenitor cell differentiation, mosaic analysis with a repressible cell marker (MARCM) analysis could be used to identify individual mitoses and subsequent differentiation events in the axenic fly gut (Liang et al., 2017, Petkau et al., 2017, Germani et al., 2018).

Alternatively, there may be a compensatory mechanism regulated by immune activation resulting in junction overexpression. In other words, increased junction transcript overexpression may further constant-contact between cells by increasing cell-cell adhesion. According to previously published work, old axenic flies live longer and show increased expression of tricellular junction (TCJ) component *gliotactin*, compared to homogenate-fed controls (Resnik-Docampo et al., 2018). The authors suggest that axenic

flies live longer in part because they maintain barrier function in old age. Consistent with these findings, in conventional flies the absence of a scaffolding protein *Big Bang Gene* (*BBG*) leads to septate junctions becoming loose and disorganized – triggering immune activation and fly death (Bonnay et al., 2013). The authors show that axenic *BBG* mutants still induce strong AMP expression. Contrary to previous discussion involving *ssk-RNAi* (Salazar et al., 2018), Bonnay et al. suggests that disorganization of septate junctions is sufficient to induce immunity in a bacteria-independent manner. These contrasting results indicate the complex nature of intestinal epithelial decline and increased DE-Cad expression may reflect an attempt to strengthen the barrier to prevent/reverse immune-induced barrier loss.

4.4.5.2 Is Drosophila E-Cadheren mediating immune-induced epithelial decline?

Major adherens junction gene *DE-Cad* only changes expression under axenic immune activation (Figures 3.9 & 4.6). In axenic immune activation, *DE-Cad* levels increase with age. This suggests that a bacteria-mediated mechanism may be responsible for maintaining basal levels of *DE-Cad* in conventional flies. In other words, the presence of bacteria is repressing immune-induced *DE-Cad* expression. To test if immune-induced changes in *DE-Cad* expression are contributing to hyperplasia (1) since *rhomboid (rho)* is an EGF activator and marker for EC apoptosis (Liang et al., 2017, Ngo et al., 2020) – *rho* in ECs could be quantified via qPCR in the first instance (2) if indeed there is a decrease in *rho* expression, using transcriptional reporter *rho-lacZ* (Jiang et al., 2011) and immunostaining against *phospho-histone H3* (3) additional immunostaining of *dpErk (*dephosphorylated effector kinase) could quantify active Egfr signaling – which is predominantly associated with ISC division. Since activated *dpERK* acts as a signaling intermediate between EC-associated DE-Cad and ISCs, cell differentiation activity could be further quantified (Liang

et al., 2017). The results from these follow-up experiments would allow us to establish whether immune activation alone is sufficient to induce hyperplasia in pre-Smurf versus Smurf flies. Discerning how and why immune activation increases DE-Cad expression may be important in maintain intestinal homeostasis with age.

For context and comparison, *pyd* expression increases in both axenic and conventional IMD activated flies – indicating a bacteria independent mechanism responsible for IMD induced *pyd* junction expression. By contrast, axenic Toll activation results in unchanged levels of *pyd* junction expression; while conventional Toll activation results in decreased *pyd* expression (Figures 3.10 & 4.7). Taken together this data suggests that *pyd* junction transcripts are differentially regulated between immune pathways, with different immune pathways responding differently to the presence of bacteria – highlighting the complexity of immune-junction crosstalk.

4.4.5.3 Expression of stress-pathway ligand upd3 increases independent of bacteria

Immune activation in axenic flies is sufficient to significantly increase gene expression of cytokine *unpaired-3 (upd3)* (Figure 4.12). In conventional flies *upd3* expression is also increased under immune activation (Figure 3.16), suggesting that cytokine expression is mediated by a bacteria-independent mechanism. Of note, *upd3* induction mechanisms between conventional and axenic flies may not be the same. Increases in *upd3* expression during immune activation might be mediating rapid differentiation events during EC regeneration (Zhai et al., 2017). Consistent with the idea that immune activation may be directly stressing ECs and regulating cell turnover, it made sense to next look at expression levels of known progenitor markers, *delta* and *notch*. Thesis data show that both axenic and conventional immune activated flies share patterns of progenitor gene expression – suggesting that changes in expression are mediated by bacteria-independent mechanisms

(Figures 3.17-3.18, 4.13-4.14). Interestingly and more specifically, IMD activation does not change basal expression of *delta*, while Toll activation significantly increases *delta* expression at midlife – results between axenic and conventional flies are mirrored (Figures 3.18 & 4.14).

In contrast to *delta*, transcript levels of *notch* only increase in axenic immune activated flies (Figure 4.13). In conventional immune activated flies, *notch* transcript levels remain unchanged (Figure 3.17), suggesting a bacteria-dependent mechanism involved in regulation of *notch* expression. Similar to the immune-induced increase in *DE-Cad* expression in axenic flies (Figure 4.6), there may be a buffering effect by bacteria; whereby specific bacterial strains may be suppressing an immune-induced increase in *notch* signaling. Interestingly, previously published work has shown that overexpression of *DE-Cad* in progenitor cells leads to a delay in proper separation between ISCs and EB daughter cells (Maeda et al., 2008). Maeda and colleagues also show that impairments in EB migration additionally affected EC differentiation. For these reasons, it was hypothesized that bacteria are important facilitators of cell turnover regulation via *DE-Cad*/*notch* dynamics.

4.4.6 Differences in transcript expression between IMD and Toll pathway activation

Thesis data show distinct gene expression patterns between IMD-activated versus Toll-activated axenic flies. Interestingly, *DE-Cad* is the only gene expression pattern shared by both pathways across all conditions. This suggests that there may be some degree of redundancy between both NF-κB pathways i.e., both pathways may mediate *DE-Cad* expression in similar ways and thus preserve the coupling between *DE-Cad* expression in ECs and ISC proliferation. Regarding the other expression data shown in this chapter, the variable changes to gene expression between IMD and Toll might be explained by intrinsic

differences in pathway mechanisms. Alternatively, crosstalk inherent between IMD and JNK pathways, may lead to differences in overall junction gene expression – a potential reason for why IMD changes seem to happen later in life.

Under both conventional and axenic conditions Toll, but not IMD, activation increase *delta* expression throughout fly lifespan. Dutta and colleagues' extensive RNA-seq work in conventional flies has shown that upon infection with pathogenic bacteria, gut transcript levels of *diptericin (Dpt)* and *drosomycin (Drs)* increase significantly in ECs (Dutta et al., 2015). The authors also show that *Dpt* expression decreases in ISCs and increases in EBs, while *Dros* expression remains low in both ISCs and EBs. Using Dutta et al. findings as a proxy for impacts of immune activation on gut transcript expression, it is possible that IMD and Toll activation have direct effects on progenitor and enterocyte signaling. Further work focused on identifying downstream immune markers located in ISCs, EBs and ECs can potentially uncover epithelial cell mechanisms driven directly by immune genes.

4.4.7 Additive immune-induced & age-associated changes in intestinal decline

While the focus of this chapter is immune-independent effects on intestinal decline, thesis data also show interesting age-associated patterns that emerge between and within IMD and Toll activated flies. Looking at immune activated cohorts over time, gives further insight to the additive effects associated with constitutive immune activation on the aging organism – as well as how closely forced-immunity mimics normal age-related decline.

Most significant transcript level changes occur in axenic IMD activated flies at late life (Figures 4.6-4.11 A). During early and midlife there are generally no changes between axenic IMD induced and uninduced controls. Conventional IMD activated flies show fewer changes in gene transcript levels (Figures 3.9-3.14 A). Further, where conventional

IMD activation does increase transcript levels, these changes occur at mid- and late life (Figures 3.10 A, 3.13 A, 3.14 A). Thesis data suggests that bacteria might mediate junction transcript levels during midlife, while late life immune activation may be regulating expression through an alternative mechanism.

Axenic Toll activated flies show mostly increased transcript levels, from early through late life (Figures 4.6-4.11 B). By contrast, conventional Toll activated flies show most transcript level changes at midlife (Figures 3.9-3.14 B). Changes observed by conventional Toll activated flies at midlife are mostly decreases in transcript levels. Thesis data suggests that bacteria-dependent mechanisms help regulate transcript levels at certain periods throughout fly lifespan. Changes at midlife between axenic and conventional Toll activated flies suggests that bacteria are in part responsible for the observed decreases in septate junction transcript levels.

It is possible that differences observed with age between IMD and Toll genotypes i.e., between pre-induced and control cohorts how diversity based on genetic background. Consistent with this idea, Evangelou and colleagues have previously reported the importance of isogenic lines when studying age-related phenotypes (Evangelou et al., 2019). An option for ruling out genetic variability between backgrounds is to undergo a series of backcrosses for several generations, the outcome of which results in some donor parent i.e., w[1118] being incorporated back into the genome with the objective being that the genome between genetic lines become identical except for the insertion incorporated to formulate the transgene of interest. In this way lines are generated to be identical and otherwise genetic variability accounted for.

While Evangelou et al. observed differences in survival between backcrossed versus non-backcrossed lines the results were variable and line dependent. Importantly, the authors found that intestinal physiology readouts were often not impacted

by isogenic status. Thus, age-related differences observed between genetic lines insofar as T.U.R.D results are concerned may have more to do with immune expression and local pathway activity. Further, the use of mifepristone, or RU-486, used as a molecular inducer of transgene activity did not impact physiological readouts in conditions assayed (see Appendices 1-3). There are published works, however, which note the leakiness of certain transgenic driver lines (Poirier et al., 2008). In other words, even in the absence of RU-486, data has shown there is still upregulation of transgenes. This leaky expression can be observed outside of target tissues and is a major caveat of tools available to study age-related pathologies in the fly. This topic will be further discussed at length in Chapter 5.

4.4.8 Summary

Immune activation does not need a bacterial-intermediate to drive intestinal decline with age. Both IMD and Toll activation are sufficient to drive mortality and barrier dysfunction, albeit slightly slower than their conventional counterparts. Immune activation is also sufficient to change aspects of intestinal physiology, confirming immune-directed mechanisms. Findings from this chapter highlight an alternative hypothesis regarding age-induced versus immune-induced intestinal decline. Namely that there may not be immune activation differences at individual timepoints, but over time immune activation cumulatively results in changes i.e., the impact of immune activation and ageing are combinatorial. Of note, there are many contributing factors associated with this work, as such it is important to remember to look at one factor at a time. Findings from this chapter, however, highlight that impacts of immune activation are most significant on intestinal barrier function. By understanding these differences, however, we can better establish causative drivers of loss of barrier function with age.

Chapter 5: The relative roles of intestinal and systemic inflammation in driving intestinal decline and whole-organism aging

5.1 Introduction

To understand local impacts of gut-immunity, there must also be consideration of the pathophysiology associated with systemic immune activation. Previously published works have pointed to the relevance and importance of organ-to-organ communication as it regards the activation of systemic immunity (reviewed in Liu and Jin, 2017). Published studies have shown how gut expressed immune receptors impact AMP expression levels in the fat body (Bosco-Drayon et al., 2012). The authors suggest that the gut-to-fat body axis controls systemic AMP expression for greater defense against pathogens. Briefly, systemic immune responses in the fly are largely driven by the fat body – the fly's major immune organ and analogous to the mammalian liver and white adipose tissue (Demerec, 1994b, Leopold and Perrimon, 2007, Buchon et al., 2014). In the context of my thesis work, organ-to-organ communication is best defined as gut-focused. Whereby the central structure is the gut, to which all other structures connect and/or communicate. As such, the terminology of systemic versus local immune response can be further defined as gut-originating (local) e.g., oral infection versus whole fly-originating (systemic) e.g., cuticle wounding/hemolymph infection/environmental stress – occurring first in circulation/other tissues. For these reasons I need to establish if my intervention was directly inducing gut immunity only or if it was inducing a secondary immune response elsewhere.

Previously published works have relied on several gut-specific drivers, namely *5966-GeneSwitch*. Although not comprehensive, the following publications used *5966-GS* for studies in *Drosophila*:

- (Mathur et al., 2010) – show *5966-GS* expresses in adult fly posterior midgut EBs

- (Hur et al., 2013) – use *5966-GS* to study age-related intestinal decline in the adult fly
- (Guo et al., 2014) – use *5966-GS* to study intestinal immunity with age in the adult fly
- (Clark et al., 2015) – used *5966-GS* to drive barrier dysfunction and study dysbiosis
- (Koehler et al., 2017) – used *5966-GS* to drive *pirk-RNAi* in ECs to study epithelial decline with age in the adult fly midgut

My own validation, however, drives the specificity of *5966-GS* into question. Data from this chapter will show that there is currently no GeneSwtich line that only drives expression in the adult fly gut. For this reason, wider systemic inflammation could be causing the phenotypes observed in previous thesis datasets. This chapter also considers the biological relevance of organ-to-organ communication, where driving gut expression may still result in systemic immune activation – suggesting that it may not be feasible to study only a gut response in vivo. Of note, to further understand and establish a causative mechanism between immunity and gut decline, the timeline of immune induction needs to be understood.

5.1.1 Aims and objectives

The aims of this chapter are to:

- Validate/check if my intervention drove secondary activation elsewhere in the fly
- Identify a suitable gut specific driver
- Perform key assays with this driver to check if gut expression alone is sufficient to drive age related decline.

Objectives for this chapter: To screen a selection of previously published drug-inducible Gal-4$^{\textbf{GeneSwitch}}$ (GS) and traditional Gal-4 driver lines and identify a truly gut-specific

driver. Qualitative widefield microscopy and quantitative RT-qPCR were used to further characterize expression patterns for select drivers. For consistency with other works in this thesis, this chapter only uses reporter lines *UAS-GFP* and *UAS-PGRP LC*, activating the IMD pathway.

I will assess the expression patterns of previously published driver lines by:

- Screening *UAS-GFP* expression patterns from a range of candidate driver lines
- Analyzing expression levels of *dpt* from systemic versus intestinal immune activation using ubiquitous driver *daughterless-GS* and gut/salivary gland diver *TIGS-GS*
    - Contextualizing *5966-GS* gene expression as it compares to *da-GS* and *TIGS-GS* expression patterns
- Tracking lifespan and barrier dysfunction to assay systemic versus intestinal immune activation effects on age-associated intestinal decline

5.2 5966-GeneSwitch > UAS-PGRP LC drives transgene expression in multiple tissues

5.2.1 Characterizing the resulting immune activation in different tissues

I hypothesized that previously established gut-specific driver *5966-GS* might induce systemic effects indirectly. For this reason, *diptericin* expression was checked in four different fly components – the entire head, the dissected gut (including crop, malpighian tubules, and rectal papilla), abdominal carcass, and thoracic carcass. To check if differences in gene expression were dose dependent in drug-inducible *5966-GeneSwitch* lines – two independent RU-486 (RU) doses were used and quantified. In the thoracic carcass, *diptericin* expression is significantly and largely upregulated by RU-50; there is also a non-significant increase by RU-10 (Figure 5.1). In the abdominal carcass, there is a

non-significant increase in *diptericin* expression by RU-50 (Figure 5.1). In the head and gut, there is a small nonsignificant increase in *diptericin* expression by RU-10 and RU-50 (Figure 5.1). Broad *diptericin* expression could indicate indirect systemic activation, or that *5966-GS* is not gut-specific. Therefore, I next assayed *5966-GS* expression by following its induction of a fluorescent reporter.

5.2.2 Qualitative observations of 5966-GeneSwitch expression patterns

To further corroborate quantitative *dipt* expression results, qualitative images were taken under a widefield microscope where *5966-GS* was crossed to reporter line *UAS-GFP* and subsequent fluorescence was observed and noted. After 48 hours on RU-50, flies were dissected into respective tissues and imaged. Green fluorescent protein was detected throughout the gut (Figure 5.2 A-B), head and abdominal carcasses (Figure 5.2 C), possibly oenocytes (Figure 5.2 D), and salivary glands (Figure 5.2 E). My results suggest a more systemic expression pattern than a gut-specific effect with *5966-GS*.

Figure 1

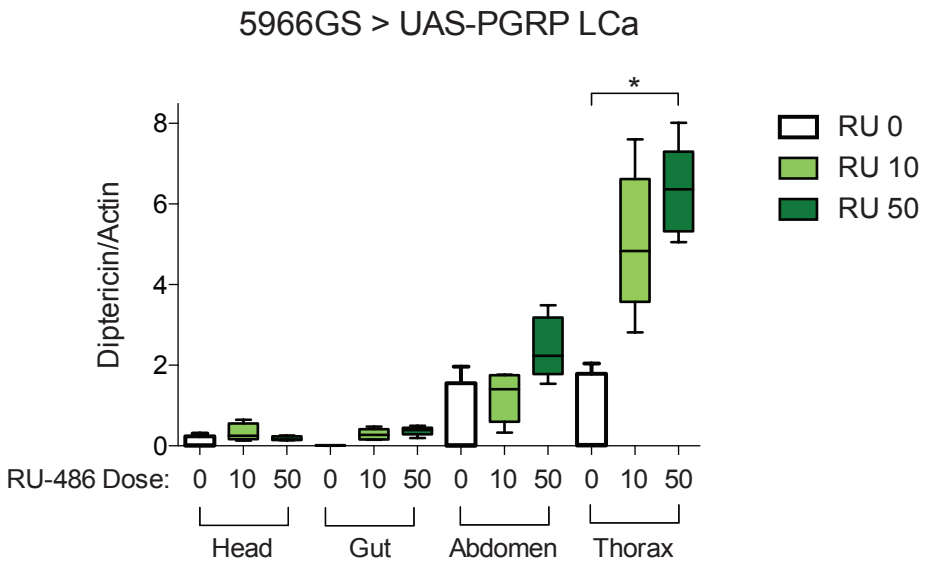

Figure 5.1: 5966-GeneSwitch induces gene expression in multiple tissues

Quantification of diptericin mRNA levels. Gene expression assayed by RT-qPCR from 12-day old, dissected intestines; *5966GS > UAS-PGRP LCa*, non-Smurf female flies, drug-induced from day 10 of adulthood for 48 hrs. and uninduced controls. n = 6 replicates of five intestines. p-value <0.05 = * in Wilcoxon Test, pairwise comparisons, only significant changes shown.

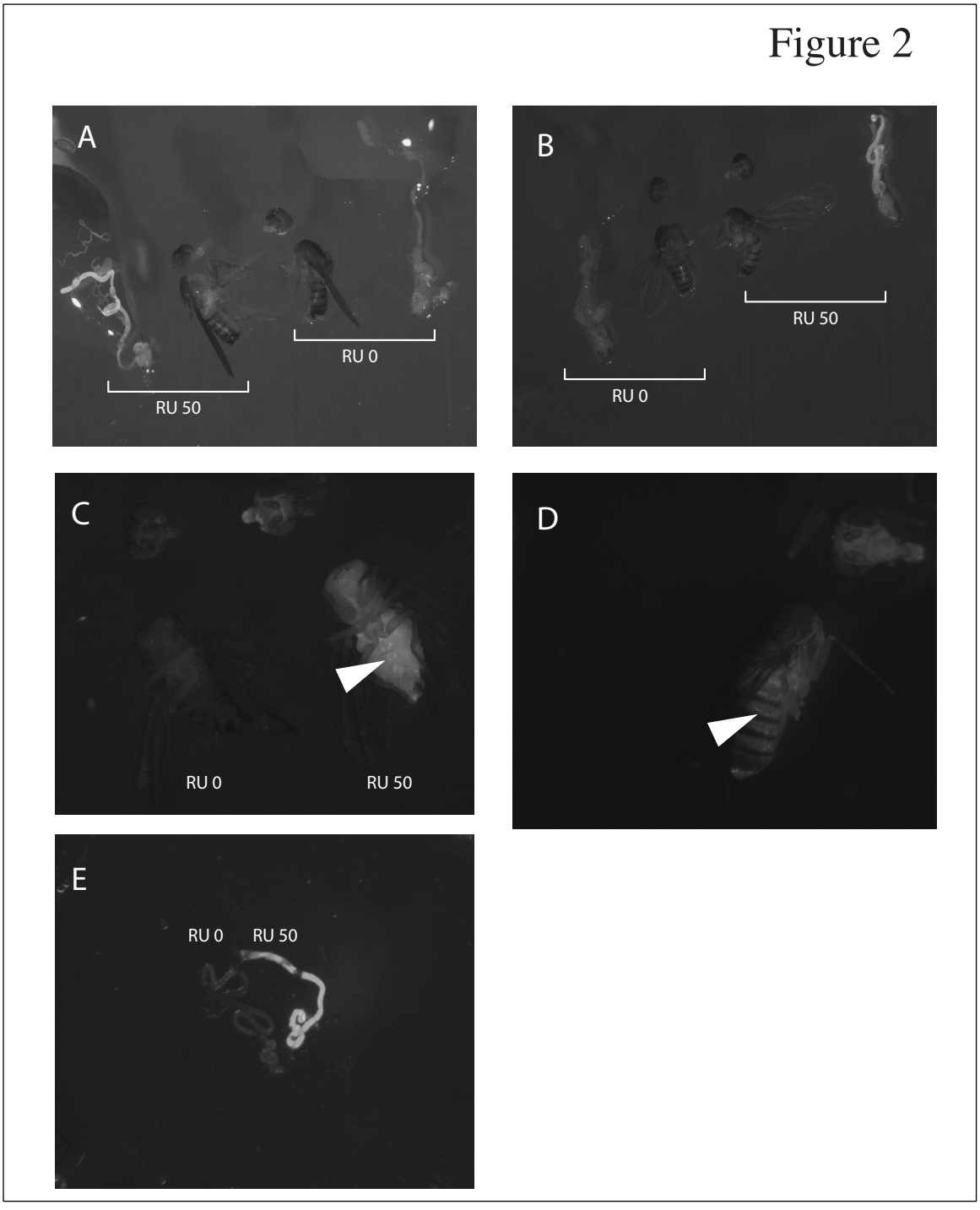

Figure 5.2: 5966-GeneSwitch drives broad tissue expression of GFP reporter

Representative example widefield images fluorescent images showing induction pattern of *5966GS > UAS-GFP*; GFP expression pattern was observed in 10-day old non-Smurf female flies, RU50-induced for 48hrs and uninduced controls. n = 5 replicates. Example 1 showing heads, carcasses, and dissected guts with crops per fly (A). Example 2 showing heads, carcasses, and dissected guts with crops per fly (B). Higher magnification example 3 showing heads and carcasses per fly; white arrow pointing to ventral clusters of GFP-positive cells on RU50 abdomen only (C). Lateral view of fly carcass; white arrow pointing to GFP-positive dorsal stripes – organized segmentally along fly abdomen, on RU50 abdomen only (D). Dissected salivary glands (E).

5.3 Selected GeneSwitch and Gal-4 Driver lines – Qualitative tissue expression

After establishing that *5966-GS* is not tissue specific in the adult female fly, I needed to identify whether any of the other published gut drivers were sufficiently specific to distinguish local versus systemic activation. Using the same qualitative approach as above, various GeneSwitch and normal Gal-4 driver lines were crossed to *UAS-GFP* to further characterize expression patterns in adult female fly tissue. GFP-positive tissues were qualitatively defined as bright, intermediately bright, or faint. To better characterize the effects of gut origin immunity, this screen included some gut drivers and others that were not – allowing for the independent manipulation of systemic and local immunity. By extension screening of driver lines will also establish the relative degrees of intestinal and systemic immunity on intestinal decline and whole organism aging. A range of fly aging literature was surveyed, the following publications were chosen for their use of listed candidate drivers:

a) (Poirier et al., 2008) – *TIGS-2, S32-GS, S106-GS, ELAV-GS, 10759-2-GS* used to study effects of aging on GeneSwitch expression patterns in the adult fly
b) (Copeland et al., 2009) – *daughterless-Gal4* used as part of whole-fly lifespan analysis
c) (Rera et al., 2011) – *S$_1$106, 5961-GS, ELAV-GS, TIGS-2, Tubulin-Gal4* used to study adult fly lifespan as it relates to intestinal integrity
d) (Clark et al., 2011, Woodcock et al., 2015) – *c564-Gal4* used to study immunity with age in the adult fly
e) (Ulgherait et al., 2014) – *ELAV-GS, TIGS-2* used to study age-related brain and gut decline in the adult fly
f) (Doupé et al., 2018) – *Myo1A-Gal4* used as part of stem and progenitor cell study in the adult fly midgut

g) (Salazar et al., 2018) – *5966-GS* used to study intestinal decline with age in the adult fly

5.3.1 GeneSwitch

GeneSwitch lines were broadly classified by previously published expression location – ubiquitous expression, fat body and digestive system expression, and gut expression (see Table 2 in Chapter 2 for respective references). Of the previously classified ubiquitous GeneSwitch (GS) driver lines –*daughterless-GS* drove expression of GFP in all tissues (Figure 5.3, Row 4); *actin5C-GS* and *actin-GS-255B* did not drive expression of GFP in all tissues (Figure 5.3, Row 2&3). Previously classified pan neuronal GeneSwitch driver *ELAV* indeed largely expressed GFP in the head (Figure 5.3, Row 1). Previously classified fat body GeneSwitch driver *S32* did not drive GFP expression in the fat body exclusively or at all (Figure 5.3, Row 5). Of the previously classified dual digestive system and fat body GeneSwitch driver lines – *S106-GS* expressed GFP along the gut, in other digestive tissues, fat body and head (Figure 5.3, Row 6); *10759-2-GS* expressed GFP along the anterior gut and a portion of the mouthpiece (Figure 5.3, Row 7). Of the previously classified gut-specific GeneSwitch driver lines – *4073-GS* expressed GFP in isolated gut regions only (Figure 5.3, Row 8); *5961-GS* expressed GFP along the anterior gut and salivary glands (Figure 5.3, Row 9); *5966-GS* expressed GFP along the entire gut, in other digestive tissues, abdominal carcass and head (Figure 5.3, Row 10); *TIGS* only expressed GFP along the entire gut and salivary glands (Figure 5.3, Row 11).

5.3.2 Gal-4

To create a comprehensive survey of driver expression pattern, traditional Gal-4 drivers were also characterized. Previously classified ubiquitous driver *tubulin-Gal4* expressed

GFP in all tissues (Figure 5.3, Row 12). Previously classified fat body specific driver *c564-Gal4* expressed GFP along the gut, other digestive tissues, fat body and head (Figure 5.3, Row 13). Previously classified gut specific driver *myo1A-Gal4* expressed in the midgut and salivary glands ((Figure 5.3, Row 14). Previously classified eye-specific driver line *GMR-Gal4* (Lee et al., 2004) expressed in the eyes, the midgut-hindgut junction, and salivary glands (Figure 5.3, Row 15).

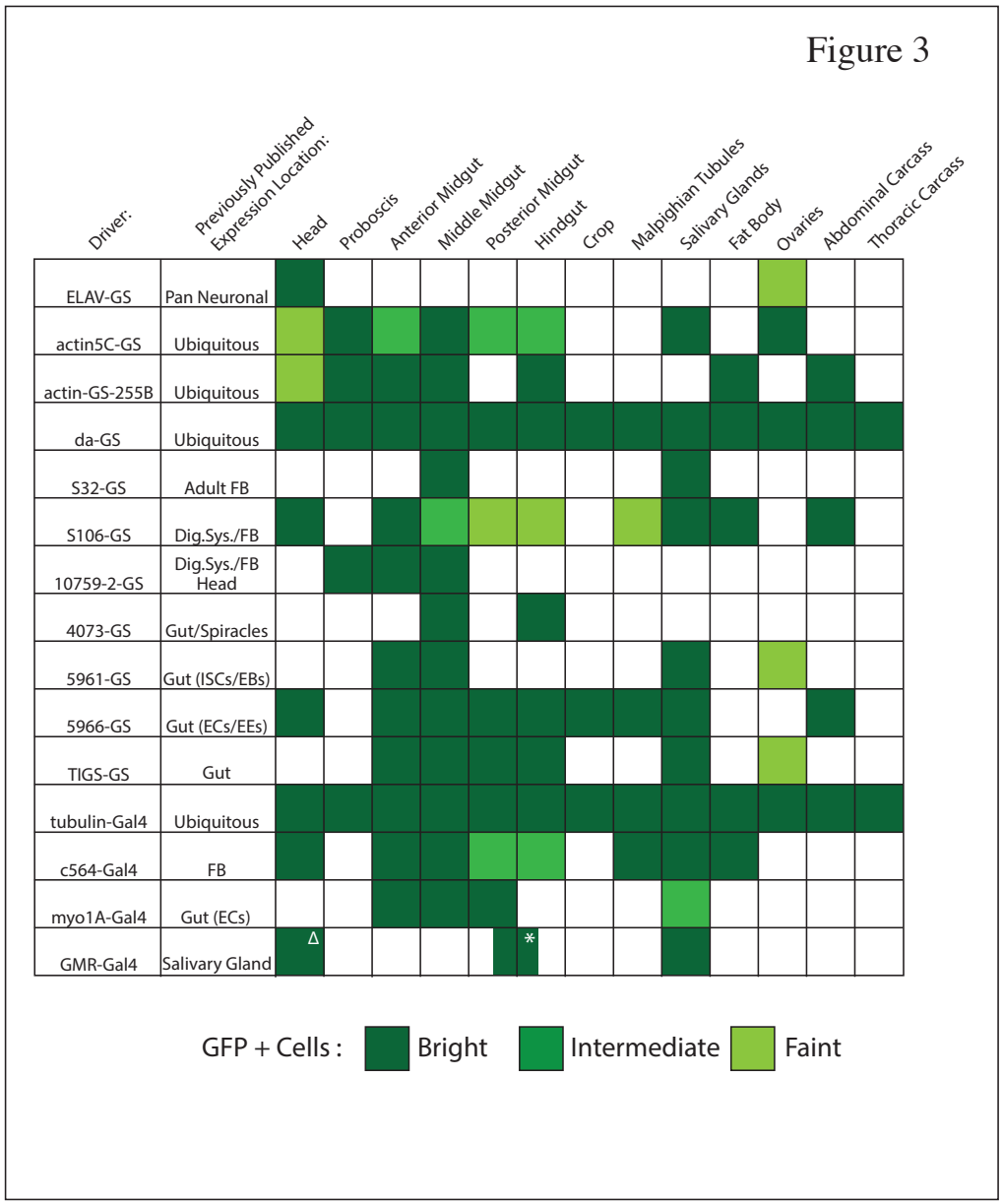

Figure 5.3: Screen of multiple GeneSwitch and Gal-4 driver induction patterns

Presence and level of GFP positivity by region assessed qualitatively by widefield fluorescent microscopy. Screen of previously published tissue-specific drivers (references found in Table 2-2). All drivers were crossed to *UAS-GFP*, induction patterns were then classified as bright, intermediately bright, or faint. Drug-inducible GeneSwitch (GS) fly cohorts were drug-induced by RU50 for 48 hrs. prior to imaging. Traditional GAL-4 lines were transferred from 25ºC to 29ºC 72 hrs. prior to imaging. n = 5 flies per genotype. White triangle symbol = GFP+ cells in eyes only; white asterisk symbol = GFP+ cells at midgut/hindgut junction only.

5.4 Tissue-specific contributions to aspects of age-related decline

Qualitative results from driver characterization indicates that most of the afore published tissue-specific drivers are not tissue specific. Findings already presented in this chapter indicate that *5966-GS* does not activate immunity solely in the gut, it may thus be an intermediary between systemic and intestinal immune activation. To better understand the data presented in previous chapters of this thesis, the expression pattern of *5966-GS* needed to be contextualized in a range between a ubiquitous driver line and the most gut-specific line available, *TIGS*. Equally, by further characterizing age-related phenotypes in *da-GS* and *TIGS* we would be able to discern if intestinal immune activation alone could drive some or all aspects of age-related decline and early death.

5.4.1 Lifespan and Smurf counts

To discern the effects of systemic versus intestinal immune activation, fly survival was tracked over time in *da-GS* and *TIGS-GS* immune activated flies. Age-onset mortality was markedly increased in immune activated flies, independent of tissue of origin. Systemic immune activation significantly decreased median survival (36 days compared to 63 days in controls) (Figure 5.4 A). Overall, systemic immune activation was correlated with a 28-day decrease in maximum lifespan (59 days compared to 87 days in control flies), a 32.2% decrease. Similarly, gut originating immune activation led to an increase in mortality. Median survival significantly decreased from 70 days in control flies to 44 days in immune activated flies (Figure 5.5 A). Overall, intestinal immune activation was correlated with a 16 day decrease in lifespan (64 days compared to 80 days in control flies), a 20% decrease.

The Smurf assay was used to quantifying the intestinal barrier loss with age in systemic versus intestinal immune activated flies. Systemic immune activated flies showed an eight-fold increase in the proportion of Smurfs in the aged fly population. By 29 days

old, systemic immune activated flies are 38.6% Smurf, compared to 3.4% of age-matched controls (Figure 5.4 B). Intestinal immune activation also showed an increase in the number of Smurf flies, although not staggeringly as with systemic activation, at 39 days of age 16.9% of the intestinal immune activated population was Smurf compared to only 6.8% in age-matched uninduced controls (Figure 5.5 B). Significant increases in Smurf number are closely correlated with increased rates of mortality observed at midlife, for both systemic and intestinal immune activated flies respectively.

5.4.2 Characterizing the resulting immune activation in different tissues

To further contextualize my previous thesis findings using 5966-GS and to determine if intestinal immune activation showed the same age-associated phenotypes, *diptericin* expression was checked in four different fly components – the entire head, the dissected gut (including crop, malpighian tubules and rectal papilla), abdominal and thoracic carcasses. To check if differences in *diptericin* expression were dose dependent in drug inducible GeneSwitch lines, two RU-486 doses were used and quantified.

5.4.2.1 Systemic immune activation using daughterless-GeneSwitch

In the thoracic carcass, *diptericin* expression is significantly and largely upregulated by RU-50; there is also a significant increase by RU-10 (Figure 5.6). In the abdominal carcass, there is a significant increase in diptericin expression by RU-50; there is also a small nonsignificant increase by RU-10 (Figure 5.6). In the gut, there is a nonsignificant increase in *diptericin* expression by RU-10 and RU-50 (Figure 5.6). In the head, diptericin expression is significantly increased by RU-50 (Figure 5.6). Qualitative widefield images of *da-GS>UAS-GFP* show expression patterns consistent with quantitative RT-qPCR results (Figure 5.8 A, A').

5.4.2.2 Intestinal immune activation using TIGS-GeneSwitch

In the thoracic carcass, *diptericin* expression is significantly and largely upregulated by RU-50 (Figure 5.7). In the gut, there is a significant increase in *diptericin* expression by RU-50 (Figure 5.7). In the head and abdominal carcass, *diptericin* expression is not changed by either RU dose (Figure 5.7). Qualitative images of *TIGS>UAS-GFP* show expression patterns consistent with quantitative RT-qPCR results (Figure 5.8 B). Together these data suggest that *TIGS* induces GFP expression directly, rather than inducing reporter expression indirectly via systemic induction.

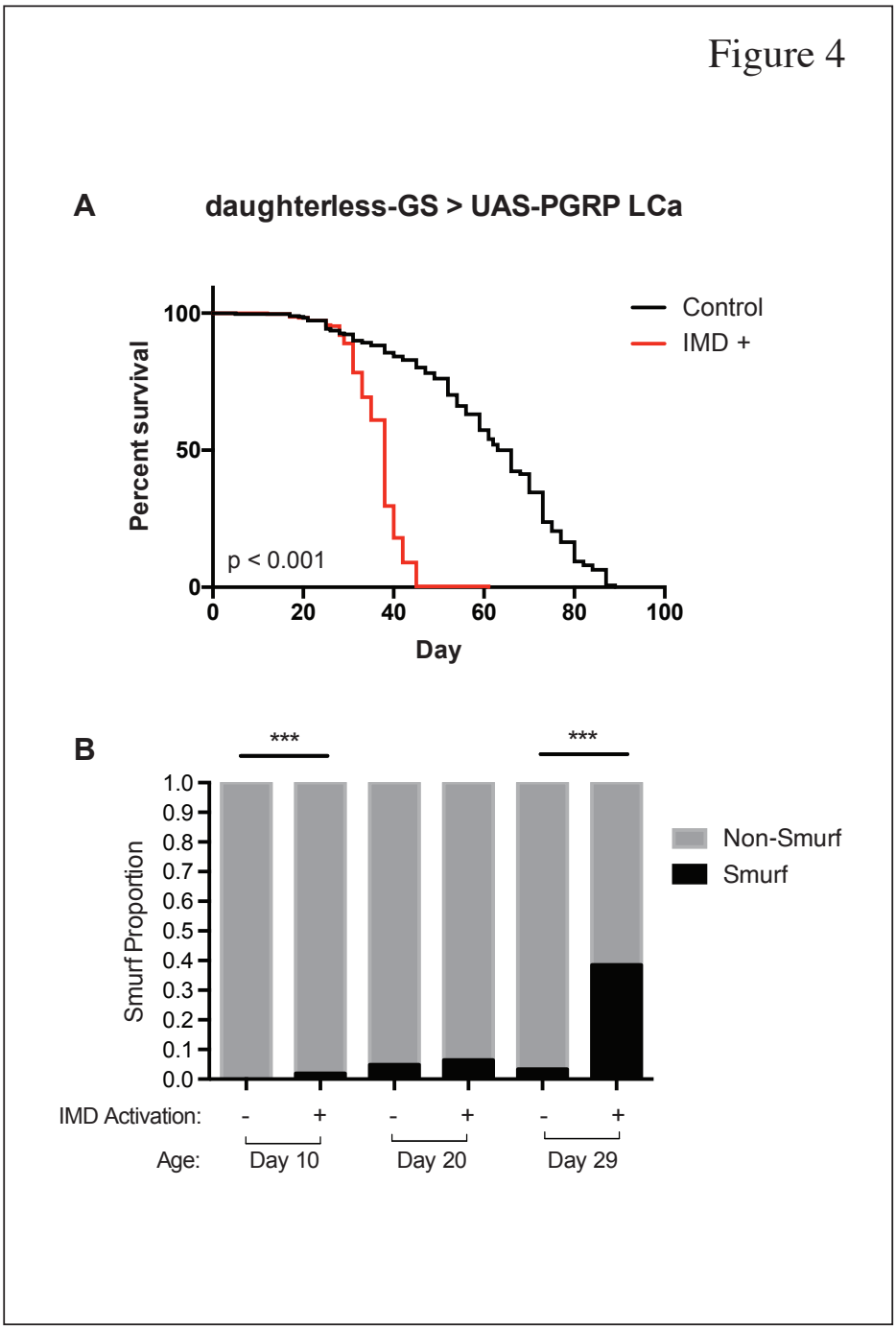

Figure 5.4: Systemic immune activation increases mortality and drives loss of barrier function

Survival curves for *daGS > UAS-PGRP-LCa* (A); female flies, immune activated from day 10 of adulthood and uninduced controls. n = >200 flies/condition. p-values < 0.001 in log rank test. Smurf proportions for *daGS > UAS-PGRP-LCa* (B); stacked bar graphs show female flies, immune activated from day 10 of adulthood and uninduced controls. n = >200 flies/condition. p-value <0.001 = *** in Binomial Test, only significant changes shown.

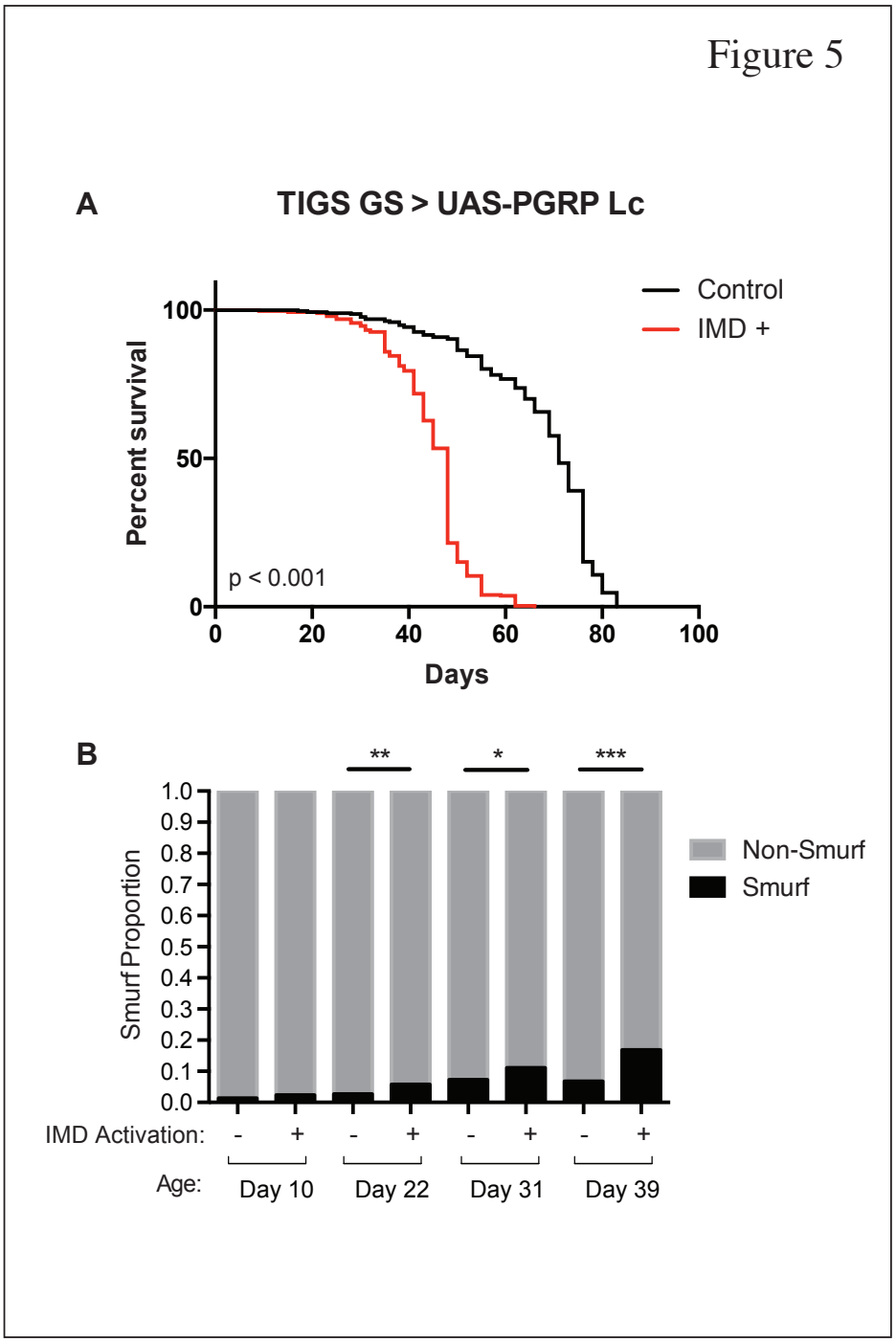

Figure 5.5: Intestinal immune activation is sufficient to increase mortality and drive loss of barrier function

Survival curves for *TIGS-GS > UAS-PGRP-LCa* (A); female flies, immune activated from day 10 of adulthood and uninduced controls. n = >200 flies/condition. p-values < 0.001 in log rank test. Smurf proportions for *TIGS-GS > UAS-PGRP-LCa* (B); stacked bar graphs show female flies, immune activated from day 10 of adulthood and uninduced controls. n = >200 flies/condition. p-value <0.05 = *, <0.01 = **, <0.001 = *** in Binomial Test, only significant changes shown.

Figure 6

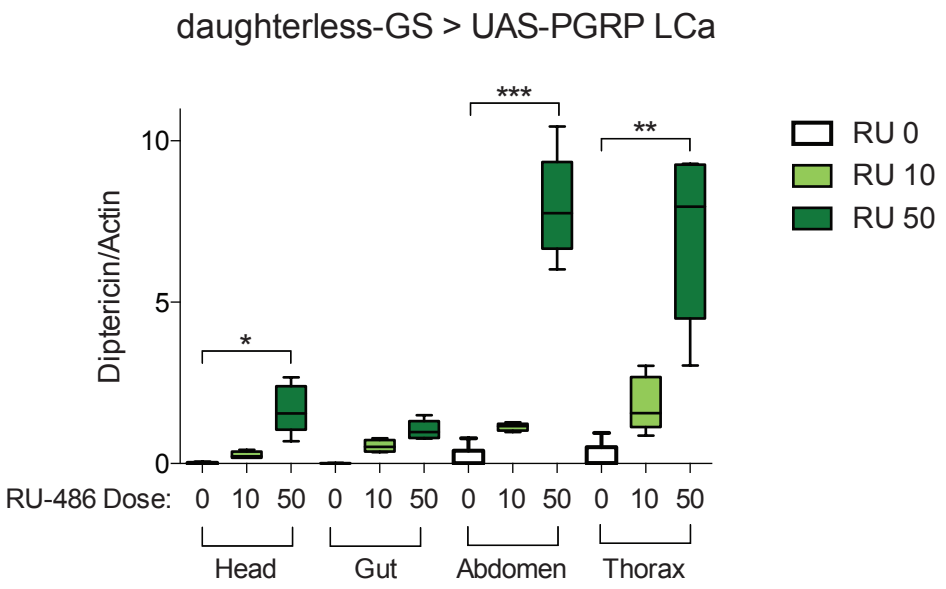

Figure 5.6: Daughterless-GeneSwitch induces gene expression in multiple tissues

Quantification of diptericin mRNA levels. Gene expression assayed by RT-qPCR from 12-day old, dissected intestines; *daGS > UAS-PGRP LCa*, non-Smurf female flies, drug-induced from day 10 of adulthood for 48 hrs. and uninduced controls. n = 6 replicates of five intestines. p-value <0.05 = *, <0.01 = **, <0.001 = *** in Wilcoxon Test, pairwise comparisons, only significant changes shown.

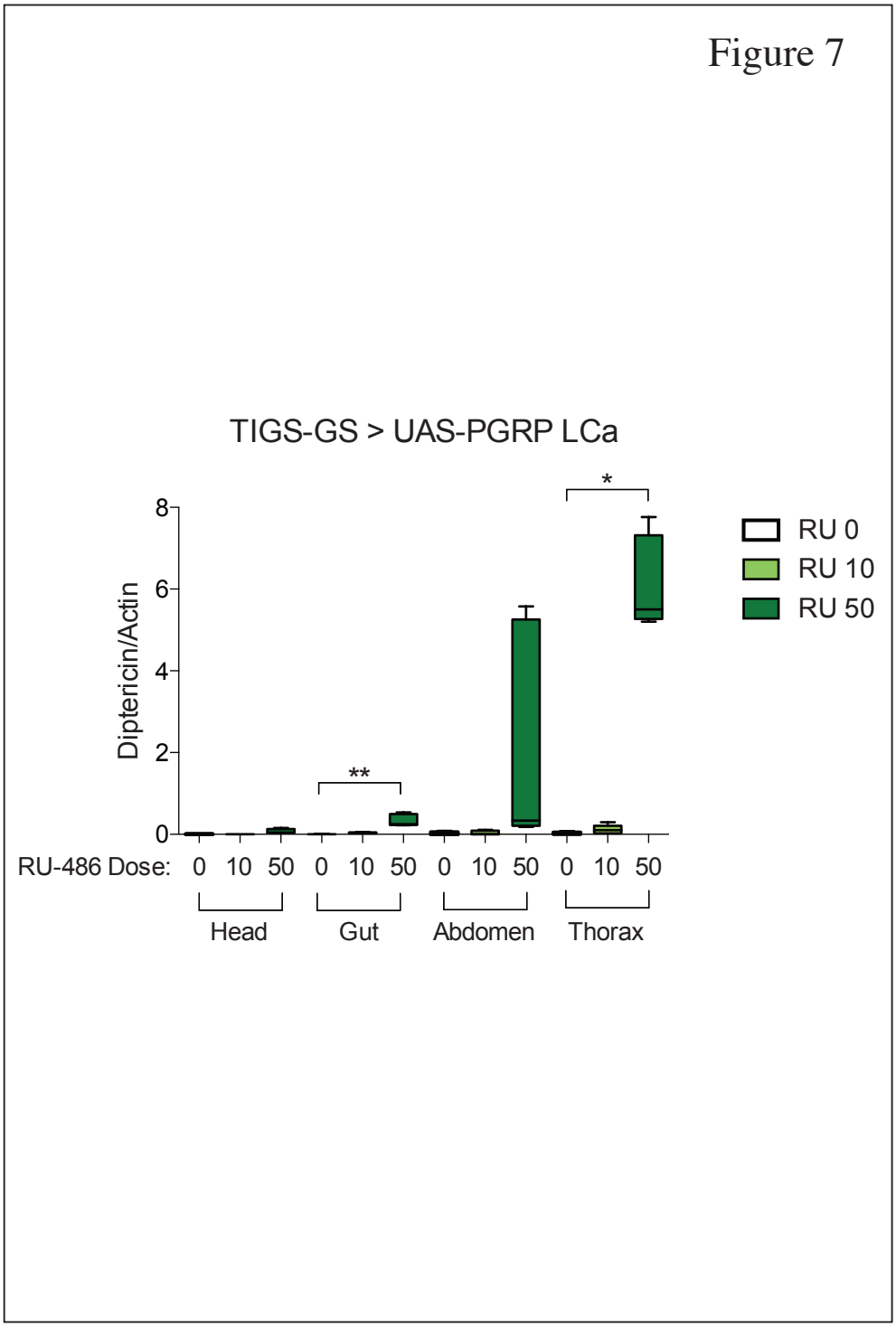

Figure 5.7: TIGS-GeneSwitch induces gene expression in multiple tissues

Quantification of diptericin mRNA levels. Gene expression assayed by RT-qPCR from 12-day old, dissected intestines; *TIGS-GS > UAS-PGRP LCa*, non-Smurf female flies, drug-induced from day 10 of adulthood for 48 hrs. and uninduced controls. n = 6 replicates of five intestines. p-value <0.05 = *, <0.01 = ** in Wilcoxon Test, pairwise comparisons, only significant changes shown.

Figure 8

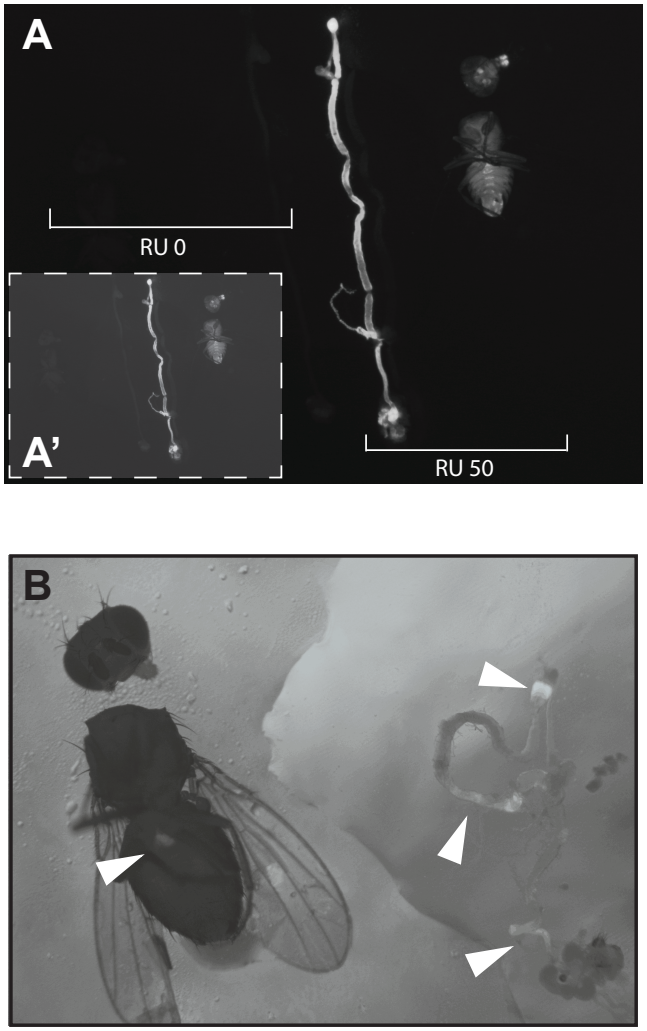

Figure 5.8: Representative images of daughterless and TIGS GeneSwitch induction patterns

Representative widefield image of *da-GS > UAS-GFP;* original image (A) modified brightness to enhance the outline of uninduced control (A'). *TIGS-GS > UAS-GFP* (B); white arrows indicate GFP+ cells. GFP expression pattern was observed in 10-day old non-Smurf female flies, RU50-induced for 48hrs and RU0-uninduced controls. n = 5 replicates. mMG = middle midgut, HG = hindgut. Images (A) and (B) appear different, as respective driver lines were imaged at different times with different widefield camera setting.

5.5 Discussion

5.5.1 Overview

My results show that *diptericin* transcript expression is broad and in more than just gut tissue, indicating misexpression of driver *5966-GS*. Induced fluorescent patterns further confirm that *5966-GS* indeed drives expression primarily and directly in the fly. My findings from this chapter highlight the importance in distinction between systemic and local immune activation. There is currently no GeneSwitch that is gut specific – however, gut immune activation using *TIGS* still shows similar age-related phenotypes compared to *5966-GS*. In other words, gut activation alone still shows similar intestinal decline phenotypes. The remainder of this discussion will interpret my findings in the context of previously literature.

5.5.2 The importance of tissue of origin

My findings corroborate previously published work by the Seroude Group, where the authors show misexpression of 'tissue-specific' driver lines (Poirier et al., 2008). Further, the authors caution that GeneSwitch expression is subject to change based on the age and sex of the fly – highlighting the restrictions placed on age-related studies until further drivers are isolated. Work completed by the Jasper Group also show that *5966-GS* is indeed expressed in other tissues – notably the salivary glands (supplementary findings Guo et al., 2014). But does tissue of origin really matter? Indeed it might because current understanding demonstrates several mechanisms by which immune activation in different tissues results in systemic inflammation, and these mechanisms are different dependent on tissue origin (Liu and Jin, 2017). While gut may lead to systemic, the mechanism for gut to body signals are different than body to gut. For example, in larvae, oral infection with pathogenic bacteria triggers diptericin expression, and it is diptericin that acts as a

signaling molecule to the fat body mounting systemic immune activation (Wu et al., 2012). In reverse, fat body to gut communication, so systemic originating "provides a potential link between fat body-expressed factors and intestinal actions" (Chen et al., 2014). Chen and colleagues note that age-associated loss of lamin-B from fat body cells affects IMD pathway activity in the gut resulting in hyperplasia.

In the context of this study, we are focusing on gut-originating immunity. This does not preclude the possibility of systemic immune responses being induced as a result, which is something we must consider in the interpretation of our results. Looking at directionality of immune activation during normal ageing, we assume that in normal aging gut immune activation is an early event, likely driven by environmental/microbiota changes. Therefore, to assess the downstream consequences of gut immune activation on the rest of the body we really need a way to induce gut-specific immune activation. To ensure gut-origin and recapitulation "normal" age-related inflammation and its downstream consequences.

5.5.3 Are we inducing secondary immune activation?

We don't see strong evidence that immune activation is being induced outside of the tissue in which each driver is expressed. This interpretation is based on the fact that diptericin and GFP expression appear largely the same. Abdominal expression levels driven by TIGS can be explained by the faint expression recorded in the ovaries. Variability in the RT-qPCR data can then be explained by the fact that sometimes the ovaries come out with the gut during dissection and are removed, and sometimes they stay with the abdominal carcass. Strong thoracic expression of all drivers can be explained by the high expression in the salivary glands. This suggests that secondary immune activation is unlikely to be causing the phenotypes recorded here.

5.5.4 Future solution for tissue-specific immune expression in adult Drosophila

While recent published works by Lim and colleagues present available gut-specific Gal-4 lines. Lim et al. complete a screen of Gal-4 drivers and image specific cell expression patterns for each line. This methods paper was written "to serve as a resource for studies involved in the genetic manipulation of cells along the gastrointestinal tract"(Lim et al., 2021). This is not enough for age-related studies in which phenotypes outside of the gut are also being measured.

The spatiotemporal expression pattern of a driver is defined by which cells and at what time reporter protein is produced. It's important to consider whether it's realistic to expect to find truly gut-specific gene expression. Experience would suggest that truly tissue specific drivers are very rare, and likely for good biological reasons. Why make a new gene when you can repurpose an old one and just express it differently? This suggests that trying to identify a properly gut-specific driver among the vast array of drivers out there would take a massive effort and may ultimately fail. Given most drivers appear to be expressed in multiple tissues, an alternative approach may be to combine tools to block expression in some tissues and allow expression only in the tissue of interest. There are a number of tools that allow suppression of Gal4 activity, for example Gal80. There are also several options for binary expression systems in the fly beyond the UAS/Gal4, for example the Q system. However, complex genetic crosses would be required to assemble these tools in a useable way. Currently available Gal80 lines are also limited, necessitating the generation of new lines that express Gal80 in the necessary combination of tissues. This could be achieved by replacing the Gal4 of lines known to express Gal4 in appropriate tissues with Gal80. In the context of ageing studies, there is also the caveat that each genetic intervention affects lifespan and so producing relevant control lines may be

problematic. Further to this, the question then becomes if indeed all this genetic work is achievable, would it be physiologically relevant?

In the absence of tissue specific tools, the approach developed here is to compare drivers with overlapping but increasingly restricted expression domains. This can be further developed in future work using the GMR-Geneswitch (Roman and Davis, 2002) crossed to *UAS-PGRP LC* to restrict expression even further and establish the impact of salivary gland expression. i.e., is salivary gland expression sufficient to drive the phenotypes observed? Taken together, this will help discern whether it is gut expression that is sufficient/necessary for the presentation of age-related decline phenotypes.

5.5.5 Summary

The closest driver to gut-induced immune activation (TIGS), presented in this chapter, reveals that gut activation alone still shows similar phenotypes to 5966GS. Confirming that gut-originating immune activation is indeed sufficient to drive early onset mortality and loss of barrier function.

Most recently, the Southall Lab developed auxin-inducible gene expression system (AGES) functions as an alternative to temperature shift Gal-4/Gal-80^{ts} and drug-inducible GeneSwitch systems (Mcclure et al., 2022). AGES relies on auxin-dependent degradation of ubiquitous Gal-80 and is compatible with the extensive catalog of Gal-4 drivers developed by the *Drosophila* community. McClure et al. have circumvented the potential leaky expression associated with GeneSwitch control cohorts, which show transgene expression in the absence of the drug RU-486. Adding auxin to fly food also mitigates impacts on fly survival, thus confirming the lack of toxicity associated with feeding auxin to flies (Mcclure et al., 2022). Based on the expression patterns surveyed in this thesis chapter, as well as the development of a new ubiquitous Gal-80 by the Southall Lab,

myo1A-Gal4 provides the most targeted intestinal expression pattern, specific the midgut alone. Using this new and innovative technique, overexpression of gut immunity may be more tightly controlled and impacts on whole organism decline better understood.

Chapter 6: Effects of age-associated intestinal decline on macrophage function

6.1 Introduction

In general, not much is known about macrophage cells in the adult fly. Most immune cell work in *Drosophila* has been completed during developmental stages, mostly due to ease of technique and well-established protocols. Of note, the field widely accepts that following the pupal stage, the adult fly maintains a set number of mature plasmatocytes (or endocytosing immune cells, also known as hemocytes) derived from embryonic and larval lymph gland hematopoiesis (Holz et al., 2003). Additionally, most literature argues that post-metamorphosis the adult fly is incapable of producing new immune cells – pointing to the lack of evidence surrounding a hematopoietic organ in the adult. Costa and colleagues findings suggest that immune cells were completely depleted after several hours of viral infection (Costa et al., 2009). This point, however, has been contested in recently published work which suggests that adult *Drosophila* indeed has hematopoietic capabilities (Ghosh et al., 2015). Plasmatocytes, hereafter referred to as macrophages, make up most of the circulating immune cell population in adult flies. There is very limited understanding about how adult macrophage cells change with age, and how they are impacted by intestinal barrier loss and immune dysfunction.

Previously published work in adult *Drosophila melanogaster* has shown that lack of immune cell protein *eater* (related to scavenger receptors) results in increased sensitivity to pathogenic bacteria (Matova and Anderson, 2006). Indicating that macrophage cells are an important part of adult fly defenses. Published works suggest that macrophage function changes with age. Horn et al. show that macrophage cells retain the ability to phagocytose with age, but the accumulation of phagocytic vesicles increases with age. Indicating that

while bacteria are taken up by immune cells, with age the ability to clear phagocytic vesicles declines leading to 'full' macrophage cells (Horn et al., 2014). Other previously published findings show that circulating macrophage number decreases with age in adult female flies only (Mackenzie et al., 2011). The total number of macrophages has also been shown to decrease with age, and adult fly lifespan decreases in the absence of phagocytic cells (Sanchez Bosch et al., 2019). An important consideration regarding these studies is that flies were mostly aged to midlife. Indicating changes between early and midlife. But there is a lot we can learn from assays throughout lifespan i.e., from early to late life. Of note, most age-related phenotypes begin to occur between mid- and late life. To truly understand how immune cells are changing with age – they must be assayed over the course of an entire lifespan.

Regarding interplay or crosstalk between immune cells and the intestine. Studies have mostly focused on the impacts of macrophage cells on intestinal epithelia signaling – with a concentration on how macrophages regulate ISC homeostasis. The Jasper Group has shown that macrophage cells recruited by gut-originating damage signals, release DPP (a bone morphogenic protein ligand). According to authors this triggers activation of transcription factor *SMOX* – promoting ISC proliferation (Ayyaz et al., 2015). Importantly, this innovative work has shown how hemocyte cells aggregate around the gut epithelia and suggest that macrophage cells interact with gut epithelia physically not just through molecular signaling (Ayyaz et al., 2015). The Lemaitre Group have also shown that septic-injury induces macrophage expression of *upd-3*. Authors suggest that *upd-3* expression by macrophage cells is regulated by the JNK pathway and results in increased stem cell proliferation in the gut (Chakrabarti et al., 2016). Previously published works, however, have largely ignored impacts of intestinal barrier dysfunction on macrophage longevity and function. Since macrophages are an integral part of the immune response, it is important to

understand if and how they are impacted by loss of intestinal barrier function. To my knowledge, this question has not been addressed in the presently published literature.

6.1.1 Aims and Objectives

The aim for this chapter is to further understand how extrinsic factors, such as loss of barrier function, are responsible for changes seen in age-associated macrophage decline. Objectives for this chapter:

- Characterize lifespan and timing of barrier dysfunction for available macrophage transgenic lines
- Using confocal microscopy, visualize in vivo sessile macrophage cells along the dorsal fly cuticle and use cell counts as proxies for changes in macrophage number
- Where possible, extract macrophage cells from the whole fly and tally differences in number between non-Smurf and Smurf flies
- Study changes in macrophage phagocytic function through in vivo live-imaging protocols, optimized for studying adult fly macrophages with age

6.2 Loss of gut integrity leads to changes in sessile macrophage number

6.2.1 Live imaging of macrophage cells in adult Drosophila

In keeping with in vivo assays i.e., the Smurf assay, a live imaging approach was taken to study macrophage cells in the aging fly. By keeping flies alive, dynamic changes in sessile (or tissue associated cells, not in circulation) macrophage cells could be quantified. Importantly, this method could be used in conjunction with blue dye feeding to study how barrier dysfunction might be impacting macrophage number – regardless of chronological age. Four transgenic lines were characterized for age-related phenotypes that are widely

used and accepted in the field. In these lines, inserted genomic elements allowed for endogenously marked macrophage cells that were imaged *in vivo* (Gyoergy et al., 2018). Specifically, *hemolectin*, *serpent*, and *croquemort* are used as markers for immune cells. *Hemolectin*, an ortholog of human *von Willebrand factor*, is used as a marker for phagocytic macrophage cells in the adult fly (Goto et al., 2001, Lesch et al., 2007). *Serpent* or *dGATAb*, orthologous to human transcription factor *GATA1/6*, was used as a second macrophage marker (Petersen et al., 1999, Agaisse et al., 2003). *Croquemort*, orthologous to human *SCARB1* (*scavenger receptor class B member 1*), located in the macrophage cell membrane, was the final marker used (Franc et al., 1996, Guillou et al., 2016). Initially, lifespan and loss of barrier function were characterized in these lines to create a baseline for longevity and age-associated decline, since not all transgenic fly lines behave the same. Changes in cell number were then quantified at appropriate time points, with a focus on tracking changes with normal aging and following barrier dysfunction.

6.2.2 Characterization of macrophage line Hemolectin-GFP

Survival was tracked over time in transgenic *hemolectin (Hml)-GFP* flies. Median survival was reached at 72 days. Maximum lifespan was reached at 84 days (Figure 6.1 A). Conventionally reared flies under this genetic background showed a comparable median lifespan to that of axenic control flies from previous experiments (Figure 4.1 A-B). For comparison, conventionally reared flies from previous M.Sc. experiments showed an average median lifespan of 60 days (Alcaraz, 2016). The Smurf assay was used to quantify changes in the number of flies experiencing barrier dysfunction with age. *Hml-GFP* flies showed few Smurfs in the aging population. At 68 days old, flies are only 8.7% Smurf, a significant increase from 1.3% Smurf at 47 days old (Figure 6.1 B).

6.2.2.1 Changes in Hml-GFP marked cells with age

Macrophage number was tracked beneath the dorsal cuticle with age by cells endogenous marked with *Hml-GFP*. Sessile macrophages associated with the abdomen and thorax show a significant increase at midlife (Figure 6.2 A-C, F-H, K). Sessile macrophage number gradually and significantly decreases between midlife and late life (Figure 6.2 B-D, G-I, K). Sessile macrophage cells associated with the dorsal abdomen remain unchanged following barrier dysfunction in late life (Figure 6.2 D-E, K). By contrast, thorax-associated sessile macrophage cells significantly increase in late life Smurf flies (Figure 6.2 I-J, K). Results indicate that *Hml-GFP* marked sessile cells change in quantity with age and following loss of intestinal barrier function along the thorax. Results suggest that *Hml-GFP* marked cells change in quantity with age and following loss of intestinal barrier function in the thorax. Changes observed in sessile cell number may also indicate changes in macrophage location i.e., more cells are localizing to the cuticle.

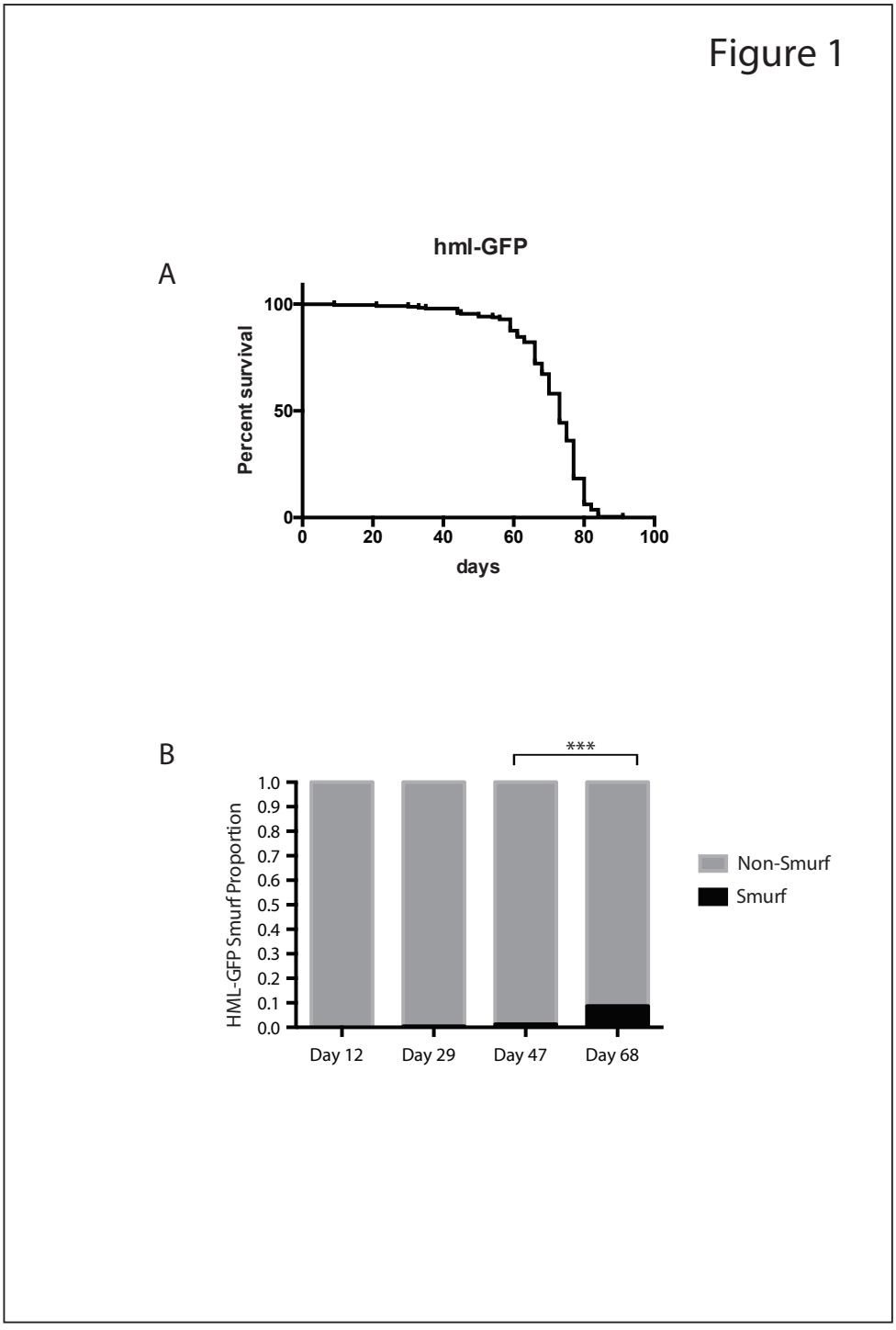

Figure 6.1: Characterization of aging phenotype in Hemolectin-GFP line

Survival curve for *w[1118]; HmlΔGal4,UAS-2xeGFP* (A). n = >200 female flies/condition. Smurf proportions for *w[1118]; HmlΔGal4,UAS-2xeGFP* (B). Stacked bar graphs show female flies assayed at day 12, 29, 47, and 68 of adulthood. n = >200 flies/condition. p-value <0.001 = *** in Binomial Test, only significant changes shown.

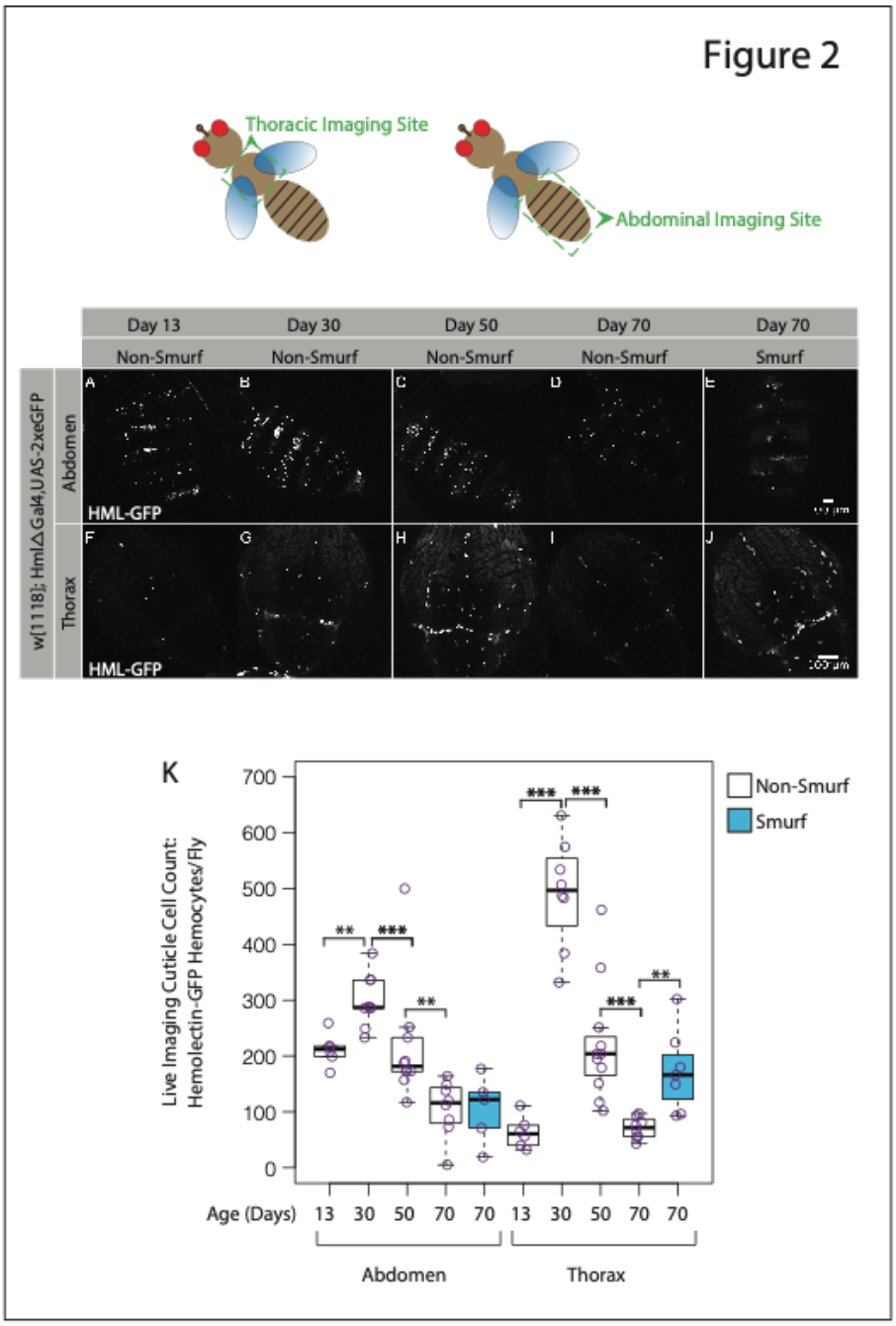

Figure 6.2: Hemolectin-GFP marks significant changes in macrophage number

Confocal images depict the abdomen (A-E) and thorax (F-J) of endogenously marked female flies at 13, 30, 50, and 70 days of adulthood. Representative max intensity projections (A-J) show sessile macrophages associated with the dorsal fly cuticle. Cuticle counts of macrophage cells are shown in the corresponding boxplot; overlayed purple scatter plots indicate individual replicates (K). n = 7-9 flies/condition. Flies were fed a nonabsorbable blue dye for 24 hours and scored as Smurf or Non-Smurf prior to imaging. p-value <0.01 = **, <0.001 = ***, in Wilcoxon Test, only significant changes shown. HML-GFP = *w[1118]; HmlΔGal4,UAS-2xeGFP*.

6.2.3 Characterization of macrophage line Hemolectin-dsRed

Survival was tracked over time in transgenic *hemolectin (Hml)-dsRed* flies. Median survival was reached at 61 days. Maximum lifespan was reached at 82 days (Figure 6.3 A). Conventional flies of this genetic background showed comparable median lifespan to that of other transgenic, conventional flies previously characterized (Alcaraz, 2016). The Smurf assay was used to quantify the change in number of flies which have lost barrier function. *Hml-dsRed* flies showed variable Smurf proportions in the aging fly population. At 40 days old, flies are only 7.3% Smurf, a significant decrease from 15.4% at 23 days old (Figure 6.3 B). However, even in late life, *Hml-dsRed* flies did not show a robust number of Smurf flies (data not shown).

6.2.3.1 Changes in Hml-dsRed marked cells with age

Macrophage number was tracked beneath the dorsal cuticle with age by cells endogenous marked with nuclear *Hml-dsRed*. Sessile macrophages associated at the dorsal abdomen and thorax show no significant age-related changes (Figure 6.4 A, C, E, G, I). Sessile macrophage cells at the abdominal cuticle remain unchanged following barrier dysfunction (Figure 6.4 B, D, I). By contrast, sessile macrophage cells at the thoracic cuticle significantly increase in Smurf flies (Figure 6.4 F, H-I). Results indicate that *Hml-dsRed* marked sessile cells change following intestinal barrier dysfunction at the thoracic cuticle, regardless of chronological age.

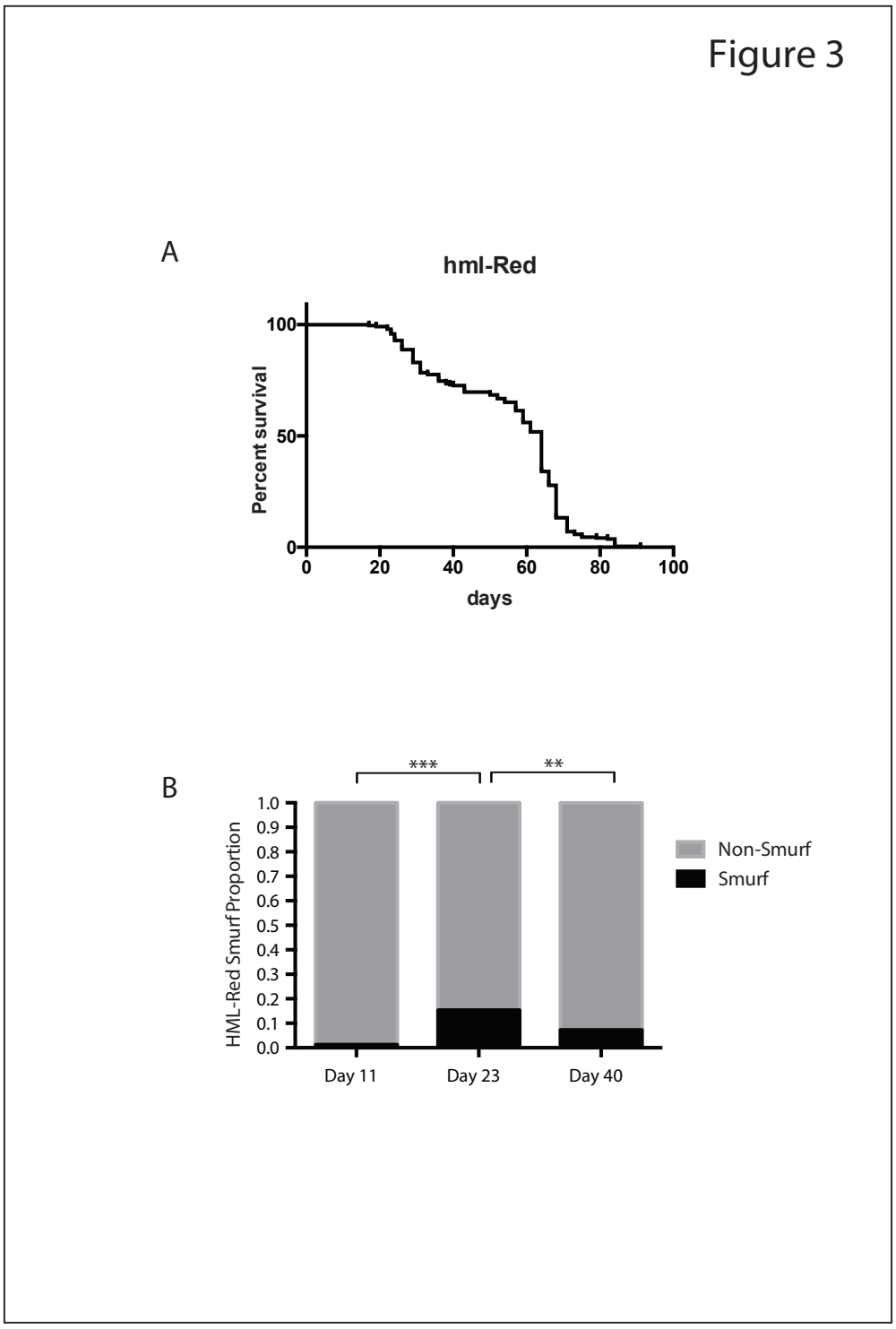

Figure 6.3: Characterization of aging phenotype Hemolectin-dsRed line

Survival curve for *w[1118]; HmlΔ-dsRed*/+ (A). n = >200 female flies/condition. Smurf proportions for *w[1118]; HmlΔ-dsRed*/+ (B). Stacked bar graphs show female flies assayed at day 11, 23, and 40 of adulthood. n = >200 flies/condition. p-value <0.01 = **, <0.001 = *** in Binomial Test.

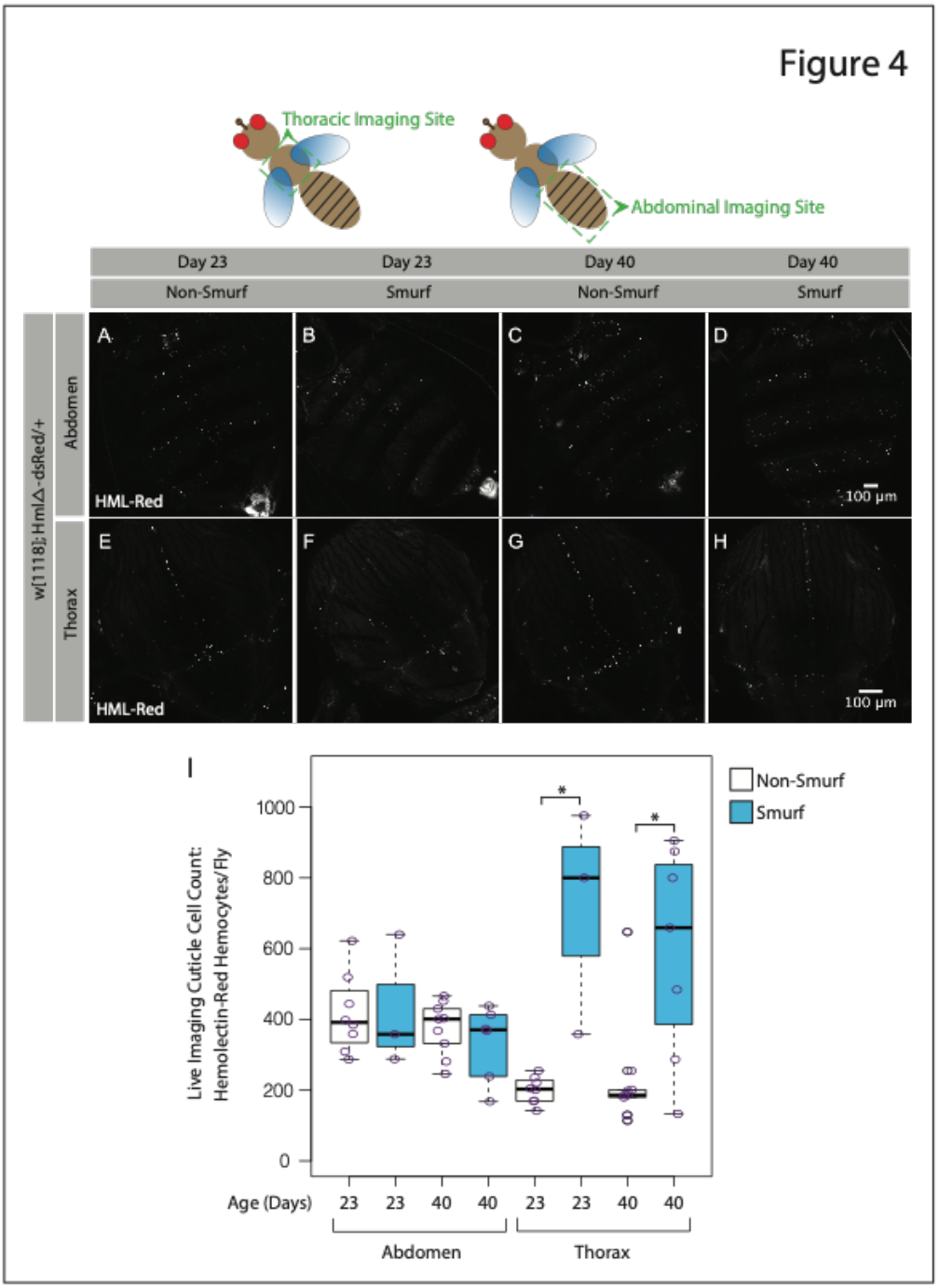

Figure 6.4: Hemolectin-dsRed marks significant changes in macrophage number

Confocal images depict the abdomen (A-D) and thorax (E-H) of endogenously marked female flies at 23 and 40 days of adulthood. Representative max intensity projections (A-H) show sessile macrophages associated with the dorsal fly cuticle. Cuticle counts of macrophage cells are shown in the corresponding boxplot; overlayed purple scatter plots indicate individual replicates (I). n = 7-9 flies/condition. Flies were fed a nonabsorbable blue dye for 24 hours and scored as Smurf or Non-Smurf prior to imaging. p-value <0.05 = *, in Wilcoxon Test, only significant changes shown. HML-Red = *w[1118]; HmlΔ-dsRed/+*.

6.2.4 Characterization of macrophage line Serpent-mCherry

Survival was tracked over time in transgenic *serpent (srp)-mCherry* flies. Median survival was reached at 48 days. Maximum lifespan was reached at 84 days (Figure 6.5 A). Conventional flies of this genetic background showed decreased median lifespan compared to that of other transgenic, conventional flies (Alcaraz, 2016). The Smurf assay was used to quantify the change in number of flies which have lost barrier function. *Srp-mCherry* flies showed a significant increase in Smurf proportion in the aging fly population. At 39 days old, flies are 19.2% Smurf, a significant increase from 1.4% at 11 days old (Figure 6.5 B).

6.2.4.1 Changes in srp-mCherry marked cells with age

Macrophage number was tracked beneath the dorsal cuticle with age by cells endogenous marked with *srp-mCherry*. Abdomen and thorax cuticle-associated macrophages show no significant age-related changes (Figure 6.6 A-B, D-E, G). Both abdomen and thorax associated macrophage cells significantly increase in number following barrier dysfunction (Figure 6.6 B-C, E-F, G). Further, there is a 2.5-fold increase in sessile macrophage number associated with the thoracic cuticle. Results indicate that the amount of *srp-mCherry* marked sessile cells changes following loss of intestinal barrier function.

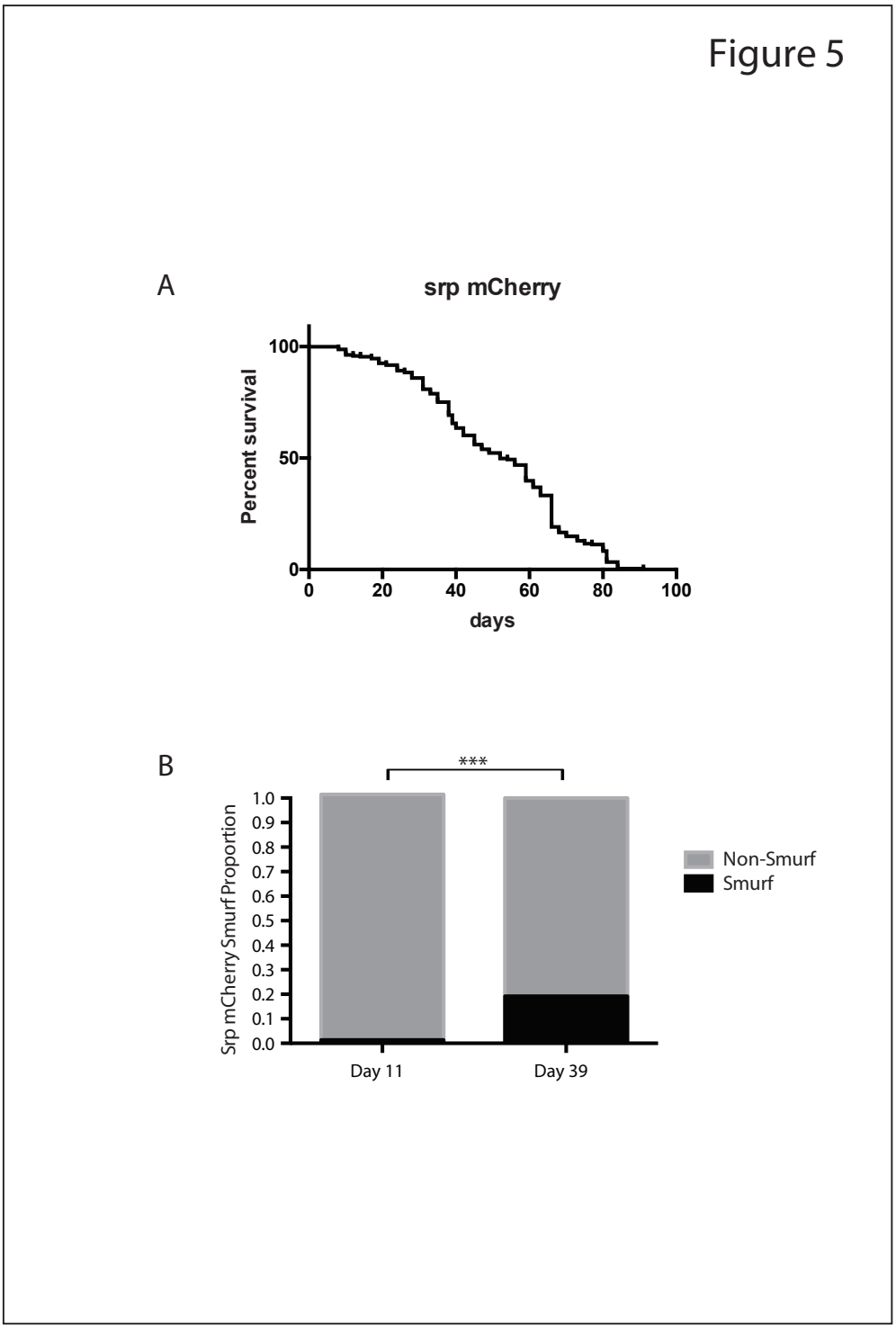

Figure 6.5: Characterization of aging phenotype Serpent-mCherry line

Survival curve for *w[1118];; srpHemo-3xmCherry*/+ (A). n = >200 female flies/condition. Smurf proportions for *w[1118];; srpHemo-3xmCherry*/+ (B). Stacked bar graphs show female flies assayed at day 11 and 39 of adulthood. n = >200 flies/condition. p-value <0.001 = *** in Binomial Test.

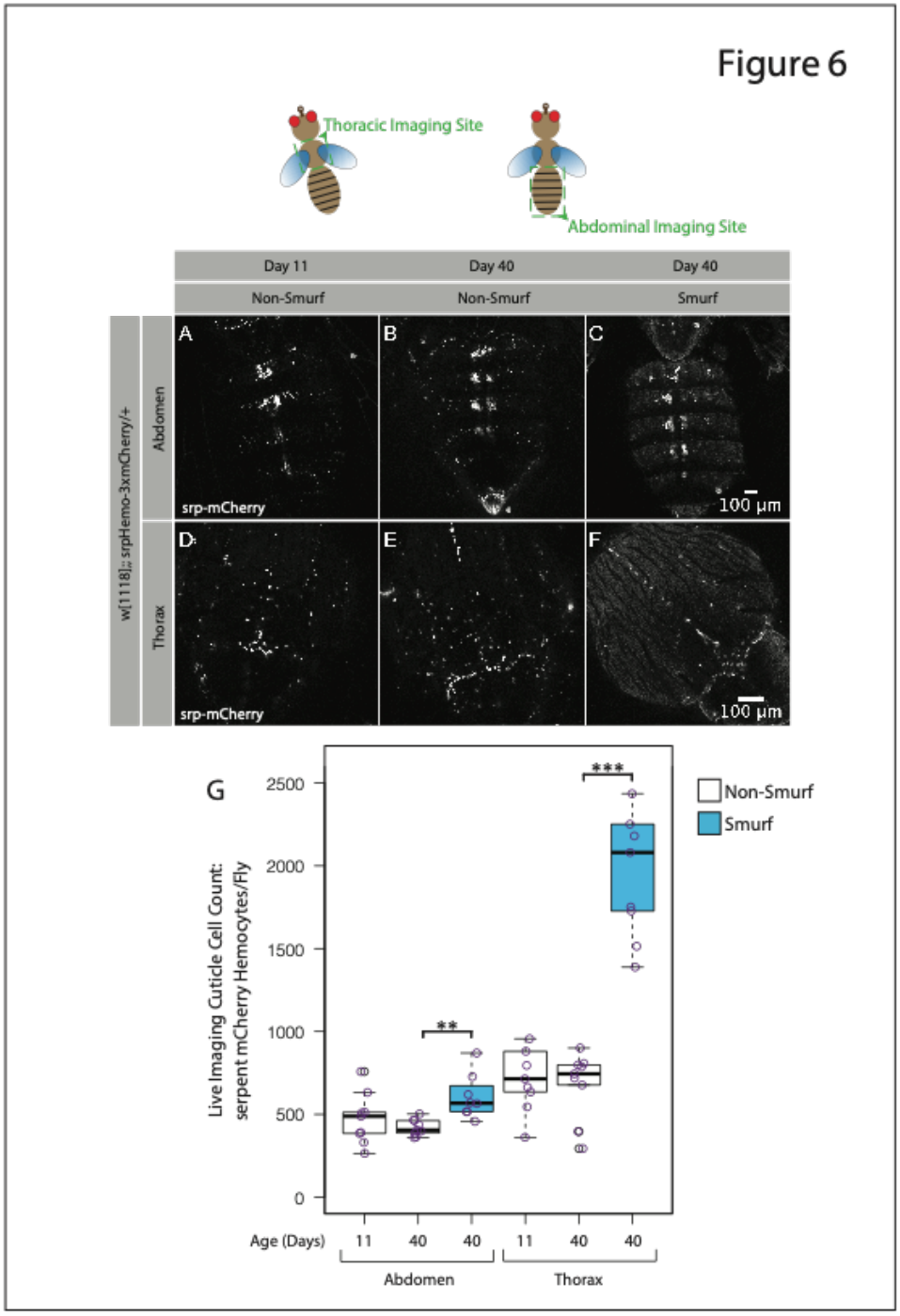

Figure 6.6: Serpent-mCherry marks significant changes in macrophage number

Confocal images depict the abdomen (A-C) and thorax (D-F) of endogenously marked female flies at 11 and 40 days of adulthood. Representative max intensity projections (A-F) show sessile macrophages associated with the dorsal fly cuticle. Cuticle counts of macrophage cells are shown in the corresponding boxplot; overlayed purple scatter plots indicate individual replicates (G). n = 7-9 flies/condition. Flies were fed a nonabsorbable blue dye for 24 hours and scored as Smurf or Non-Smurf prior to imaging. p-value <0.01 = **, <0.001 = ***, in Wilcoxon Test, only significant changes shown. srp-mCherry = *w[1118];; srpHemo-3xmCherry/+*.

6.2.5 Characterization of macrophage line Croquemort-GFP

Survival was tracked over time in transgenic *croquemort (crq)-GFP* flies. Median survival was reached at 64 days. Maximum lifespan was reached at 80 days (Figure 6.7 A). Conventional flies of this genetic background showed similar median lifespan to that of other transgenic, conventional flies (Alcaraz, 2016). The Smurf assay was used to quantify the change in number of flies which have lost barrier function. *Crq-GFP* flies showed a significant increase in Smurf proportion in the aging fly population. At 40 days old, flies are 9.5% Smurf, a significant increase from 0.9% at 11 days old (Figure 6.7 B).

6.2.5.1 Changes in crq-GFP marked cells with age

Macrophage number was tracked beneath the dorsal cuticle with age by cells endogenous marked with *crq-GFP*. Abdomen and thorax cuticle-associated macrophages show no significant age-related changes (Figure 6.8 A-B, D-E, G). Sessile macrophage number along the abdominal and thoracic cuticle remains unchanged following loss of barrier function (Figure 6.8 B-C, E-F, G). Results indicate that the amount of *crq-GFP* marked sessile cells remains unchanged with age and following intestinal barrier dysfunction.

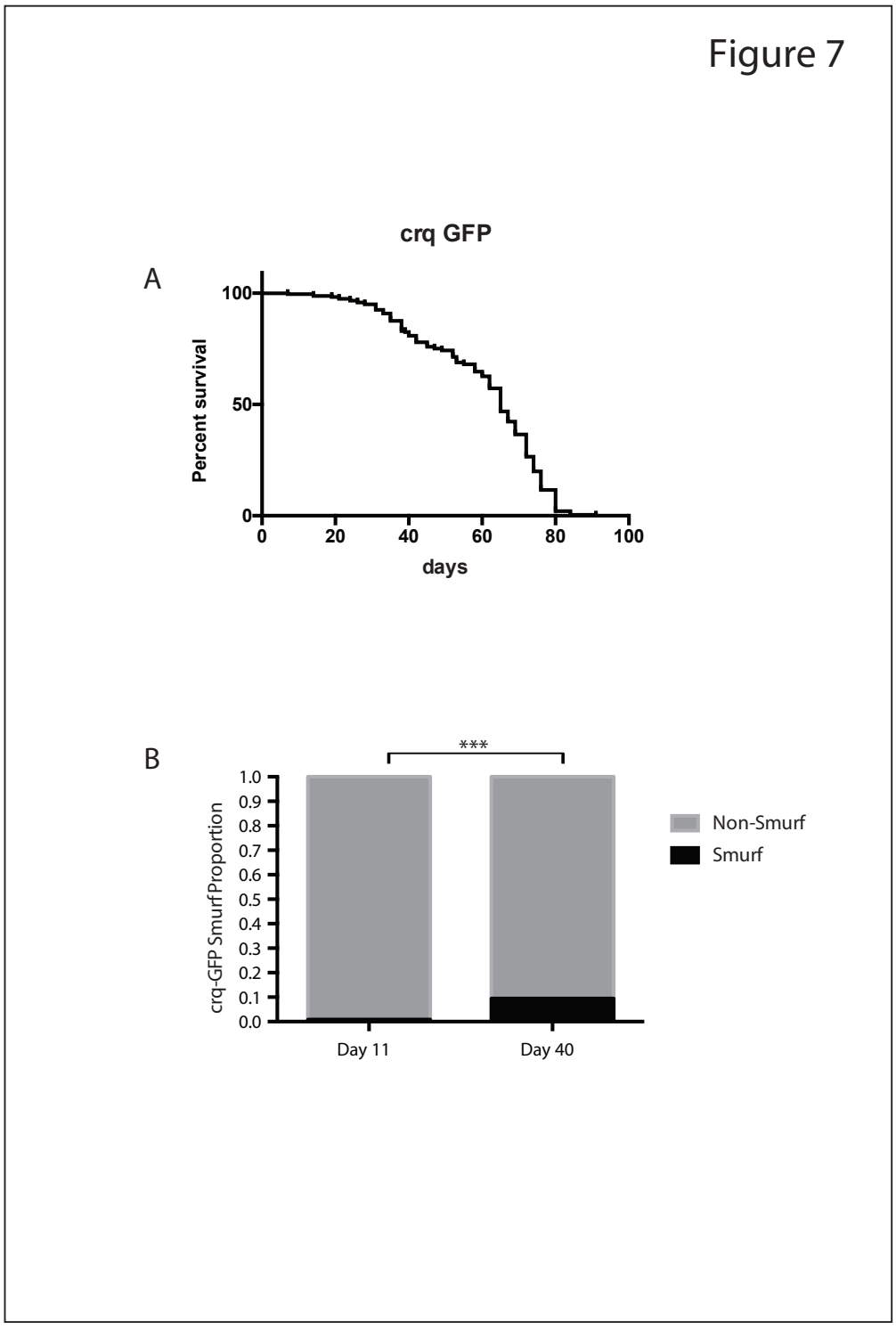

Figure 6.7: Characterization of aging phenotype in Croquemort-GFP line

Survival curve for *w[1118];UAS-2xeGFP/+; crq-Gal4/+* (A). n = >200 female flies/condition. Smurf proportions for *w[1118];UAS-2xeGFP/+; crq-Gal4/+* (B). Stacked bar graphs show female flies assayed at day 11 and 40 of adulthood. n = >200 flies/condition. p-value <0.001 = *** in Binomial Test.

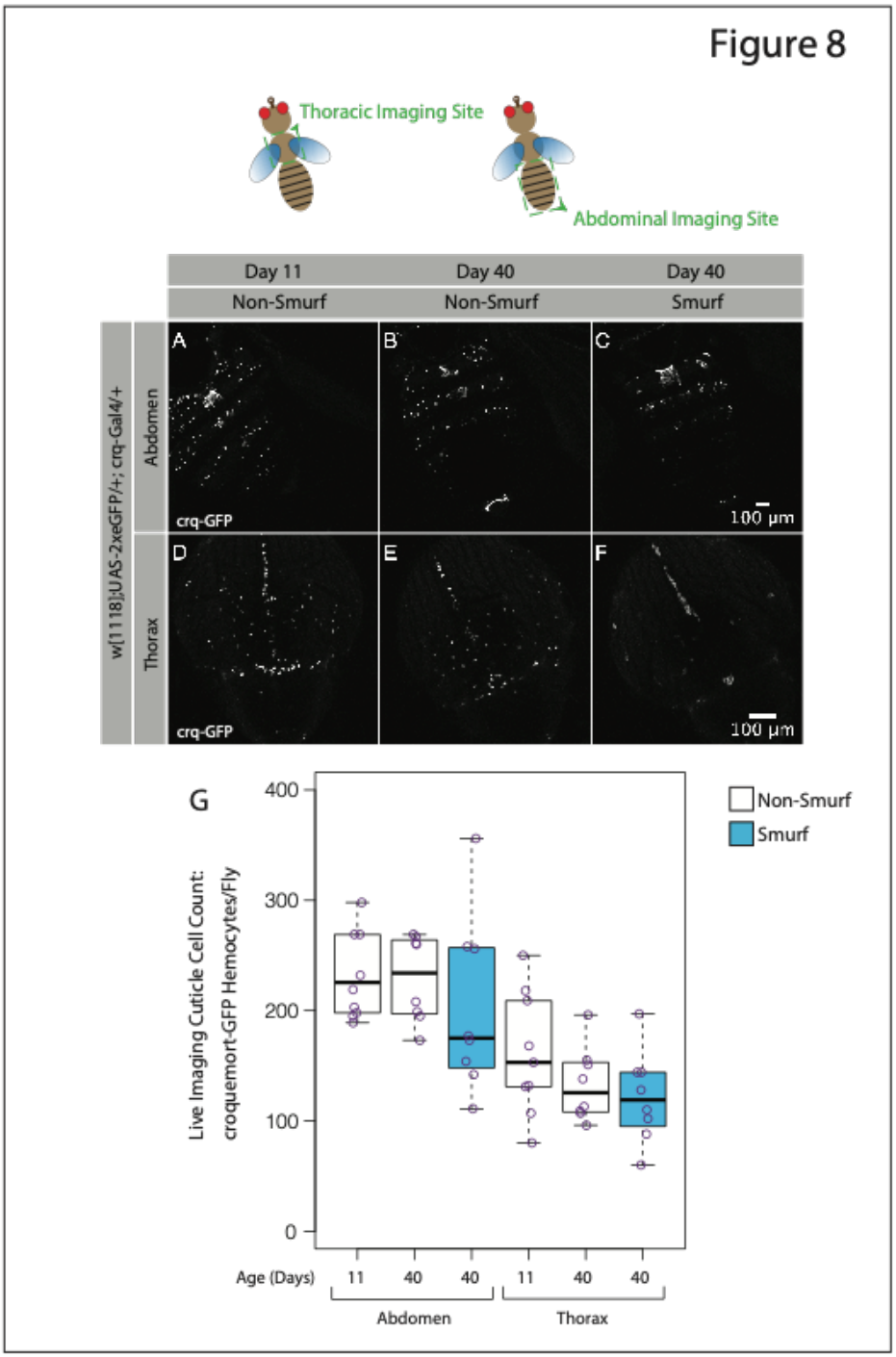

Figure 6.8: Croquemort-GFP marks non-significant changes in macrophage number

Confocal images depict the abdomen (A-C) and thorax (D-F) of endogenously marked female flies at 11 and 40 days of adulthood. Representative max intensity projections (A-F) show sessile macrophages associated with the dorsal fly cuticle. Cuticle counts of macrophage cells are shown in the corresponding boxplot; overlayed purple scatter plots indicate individual replicates (G). n = 7-9 flies/condition. Flies were fed a nonabsorbable blue dye for 24 hours and scored as Smurf or Non-Smurf prior to imaging. No significant changes, in Wilcoxon Test. Crq-GFP = *w[1118];UAS-2xeGFP/+; crq-Gal4/+*.

6.3 Immune-induced barrier dysfunction leads to changes in sessile macrophage number

Hemocyte transgenic line characterization in the adult fly show changes in macrophage number following barrier dysfunction. I next asked if forcing intestinal barrier dysfunction would still increase macrophage counts. From previous work, both published and from this thesis, it is well documented that the Smurf phenotype is associated with a dramatic increase in inflammation (Rera et al., 2012, Clark et al., 2015, Salazar et al., 2018). For this reason, it made sense to look at how constitutive immune activation i.e., driving inflammation in the gut and systemically, would impact barrier function and macrophage number consequently.

6.3.1 Gut immune activation leads to changes in sessile macrophage number

To further investigate the role of constitutive immune activation on macrophage cells, the *Drosophila* GeneSwitch (GS) System was again used (mechanism detailed in Section 2.2.1). In brief, this system allows for the drug-inducible control of gene expression within a target tissue(s). The following transgenic line was generated for use in this study: *TiGS-2-GS>UAS-PGRP LCa; Hml-GFP*. By utilizing a mostly gut-specific driver, the origin of immune deficiency (IMD) pathway activation was known and maintained throughout the adult fly lifespan. Macrophage cells were endogenously marked by *hemolectin (hml)-GFP* and live imaged along the dorsal fly cuticle at early, mid-, and late life. Of the four transgenic lines characterized in Section 6.2, *hml-GFP* was used due to chromosomal location and homogeneity of the transgene.

At midlife, immune activated abdominal sessile macrophage number significantly increases when compared to uninduced controls (Figure 6.9 A-B, G). Following barrier dysfunction at midlife, immune activated flies show a significant decrease in sessile

macrophage number (Figure 6.9 B-C, G). At late life, abdomen-associated sessile macrophage number remains unchanged with age and following loss of barrier function. Images also show increased macrophage localization to the gut in immune activated flies, more prominently in flies retaining barrier function but also seen following barrier dysfunction (Figure 6.9 B-C, E-F). Contrastingly, thorax-associated sessile macrophage number remains unchanged in immune activated flies at both mid- and late life (Figure 6.10 A-G). Loss of barrier function in immune activated flies also does not change sessile thoracic macrophage number (Figure 6.10 C, F-G). There is however an age-related significant increase in sessile thoracic macrophage number between mid- and late life (Figure 6.10 A-C, D-F, G). Localized constitutive immune activation impacts sessile macrophage number along the abdominal and thoracic cuticle differently.

6.3.2 Systemic immune activation leads to changes in sessile macrophage number regardless of chronological age

The origin and degree of immune activation were next tested to understand immune impact on sessile macrophage number following barrier dysfunction. The following transgenic line was generated for use in this study: *da-GS>UAS-PGRP Lc; Hml-GFP*. By utilizing pan GeneSwitch driver *daughterless (da)*, systemic IMD activation was achieved and maintained throughout the adult fly lifespan. Sessile macrophage cells were endogenously marked by *hemolectin (hml)-GFP* and live imaged along the dorsal fly cuticle at early, mid-, and late life. *Hml-GFP* was used again due to chromosomal location as well as to compare fluorophore intensity between systemic and gut immune activation.

Qualitative images from pre-immune activation flies, show baseline macrophage numbers at day ten of adulthood (Figure 6.11 A-B). Systemic immune activation induces a significant increase in sessile abdomen associated macrophage cells, compared to uninduced controls (Figure 6.11 C, E, G, I, Figure 6.12 A). Forced Smurfs (or flies with

immune-induced barrier dysfunction) show an increase in sessile macrophage number proportional to immune activated non-Smurf flies (Figure 6.11 C-J, Figure 6.12 A). Increases in abdomen-associated sessile macrophage number are seen at mid- and late life (Figure 6.12 A). Qualitative results show changes in fluorescence intensity along the thoracic cuticle of immune activated flies (Figure 6.11 K-R). Thoracic fluorescence intensity increases at midlife, with more puncta observed along the dorsal cuticle in immune activated flies (Figure 6.11 K-N). The greatest increase in fluorescence intensity is in late life immune activated flies (Figure 6.11 O-R). Whereby individual puncta are no longer visible, and the dorsal thoracic cuticle is entirely fluorescent (Figure 6.11 Q-R).

6.3.3 Potential effects of PGRP-LCa overexpression on hemolectin expression in the gut

The technique used here to induce immune activation may have a knock-on effect on the expression of other immune associated proteins. Here, a potential consequence of driving overexpression of *PGRP-LCa* may be an increase in *hemolectin* mRNA expression. To ensure that macrophage quantification at the dorsal fly cuticle was a result of immune-induced changes and not a result of *PGRP-LCa* overexpression, mRNA levels were assayed. RT-qPCR was run on samples made up of dissected guts from transgenic adult flies of genetic background *5966-GS > UAS-PGRP-LCa*. Indeed, results show that induction of *PGRP-LCa* does not significantly change expression patterns of *hemolectin* transcript in the gut – either with IMD activation or with age (Figure 6.12 B). Whether the IMD pathway regulates hemolectin expression in other tissues remains to be determined.

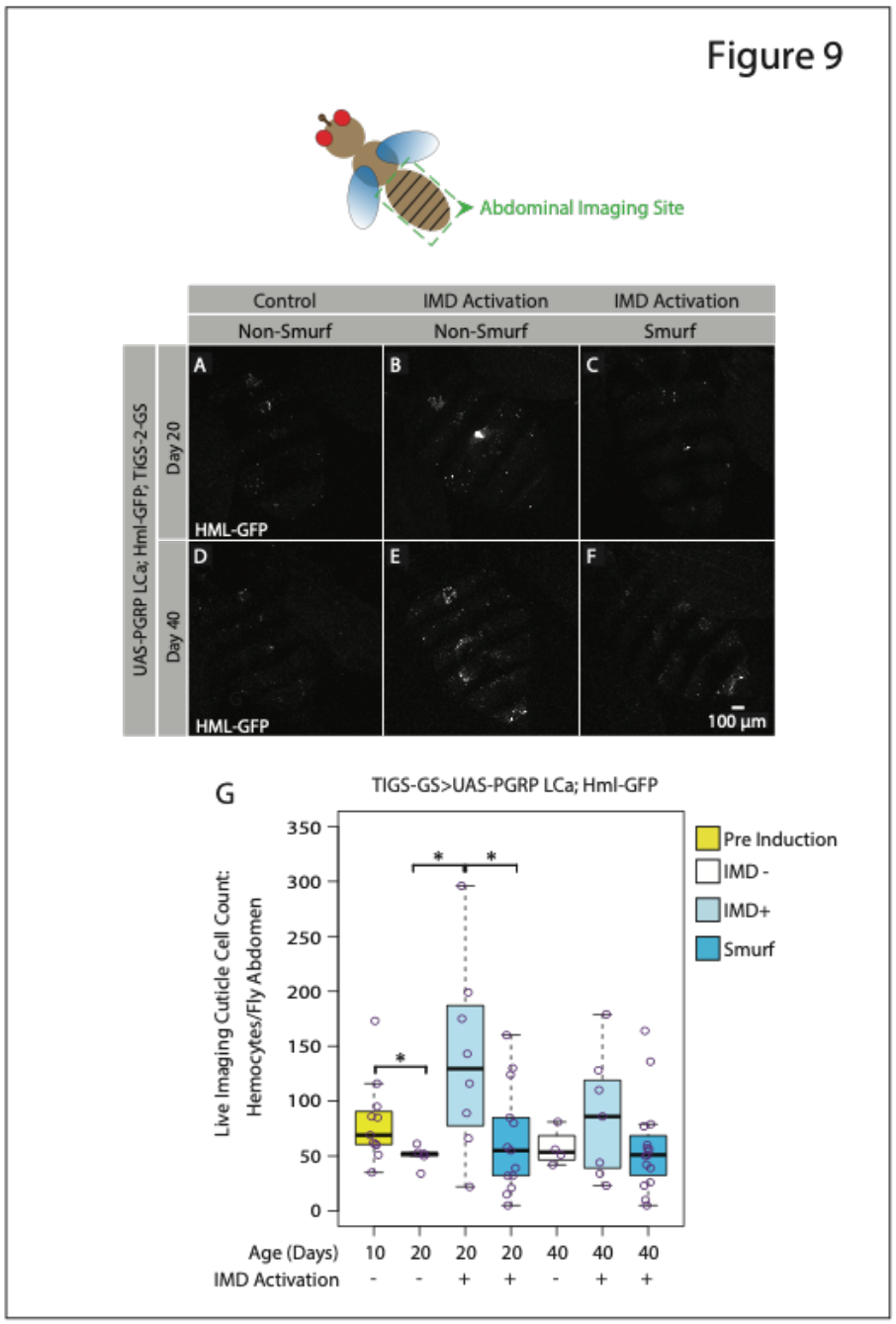

Figure 6.9: Gut immune activation leads to an increase in abdominal macrophage number regardless of chronological age

Confocal images depict the abdomen of endogenously marked female flies at 20 days (A-C) and 40 days (D-F) of adulthood. Representative max intensity projections (A-F) show sessile macrophages associated with the dorsal fly cuticle. Boxplot quantifies external macrophage counts at the abdomen in *TiGS-2-GeneSwitch>UAS-PGRP LCa; Hml-GFP* female flies immune activated from day 10 of adulthood and uninduced controls; overlayed purple scatter plots indicate individual replicates (G). n = 7-11 flies/condition. p-value < 0.05 = * in Wilcoxon Test, only significant changes shown. PGRP LCa = Peptidoglycan recognition protein Lc, IMD = Immune Deficiency Pathway.

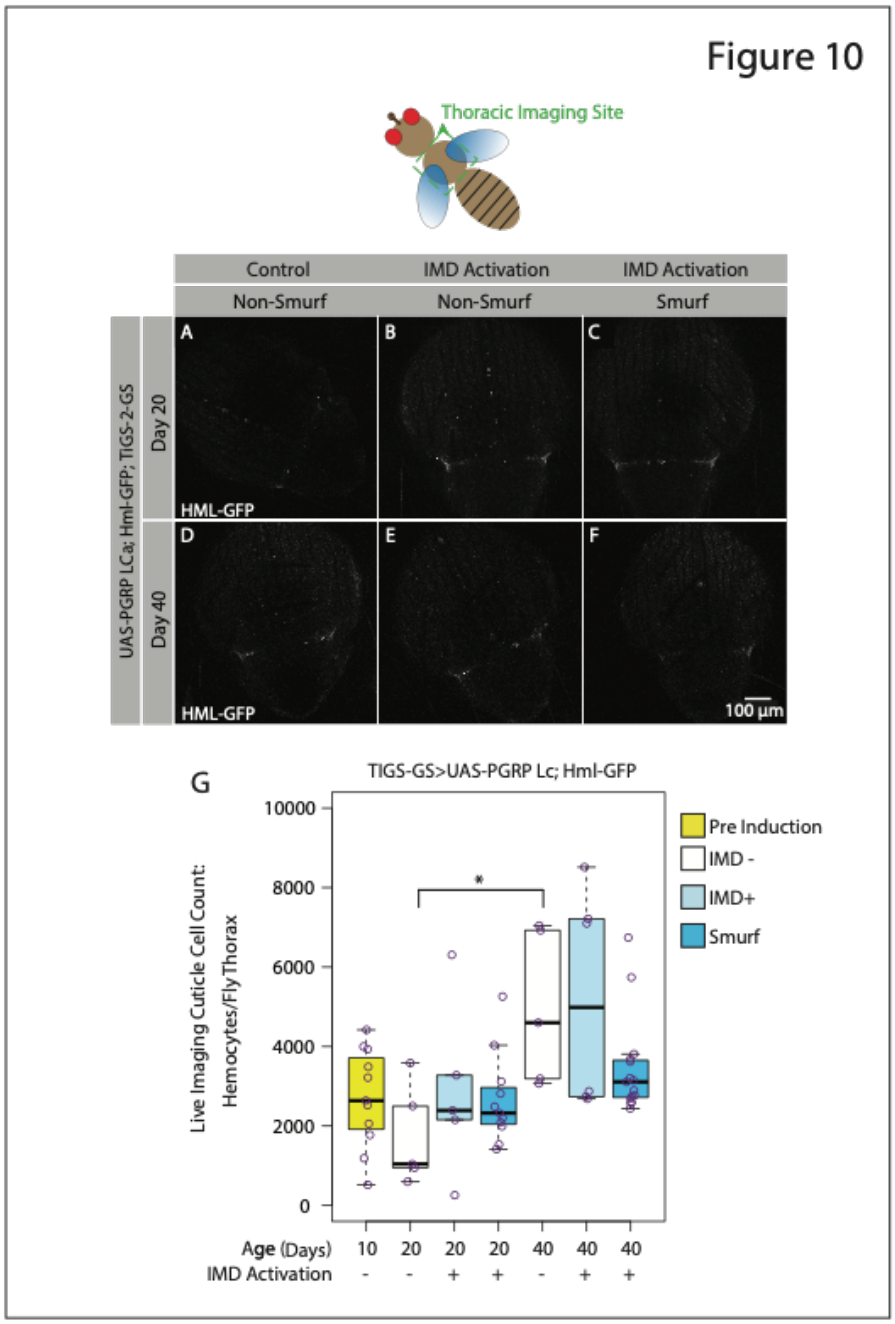

Figure 6.10: Thorax associated macrophage number remains unchanged with gut immune activation

Confocal images depict the thorax of endogenously marked female flies at 20 days (A-C) and 40 days (D-F) of adulthood. Representative max intensity projections (A-F) show sessile macrophages associated with the dorsal fly cuticle. Boxplot quantifies external macrophage counts at the thorax in *TiGS-2-GeneSwitch>UAS-PGRP LCa; Hml-GFP* female flies immune activated from day 10 of adulthood and uninduced controls; overlayed purple scatter plots indicate individual replicates (G). n = 7-11 flies/condition. p-value < 0.05 = * in Wilcoxon Test, only significant changes shown. PGRP LCa = Peptidoglycan recognition protein LCa, IMD = Immune Deficiency Pathway.

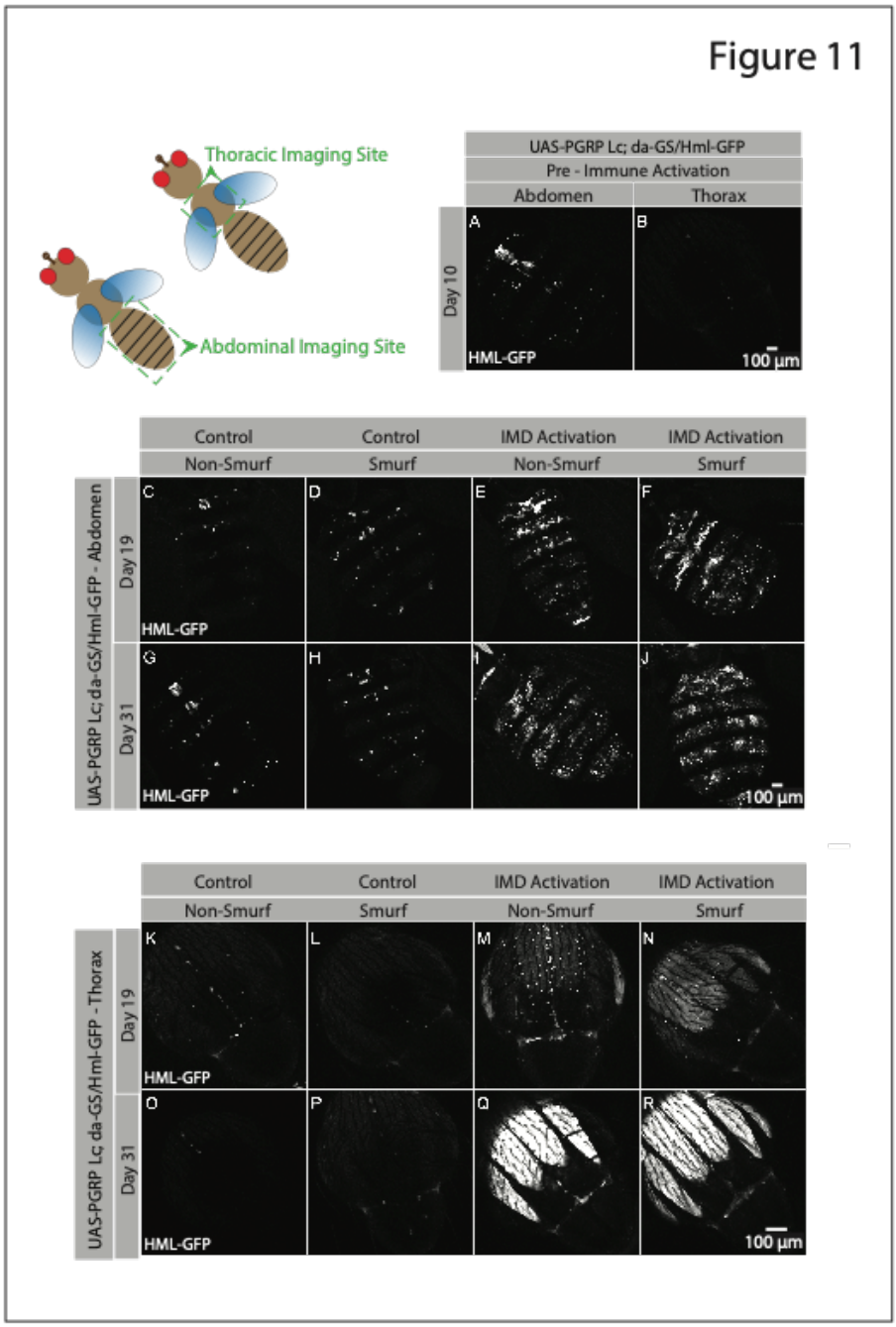

Figure 6.11: Representative images of confocal microscopy show impacts of systemic immune activation on macrophage quantity

Confocal images depict the abdomen (A, C-J) and thorax (B, K-R) of endogenously marked female flies at 10, 19, and 31 days of adulthood. Representative max intensity projections (A-R) show sessile macrophages associated with the dorsal fly cuticle in *daughterless-GeneSwitch>UAS-PGRP LCa; Hml-GFP* female flies immune activated from day 10 of adulthood and uninduced controls. Quantification shown in Figure 3.12. PGRP LCa = Peptidoglycan recognition protein LCa, da = daughterless, IMD = Immune Deficiency Pathway.

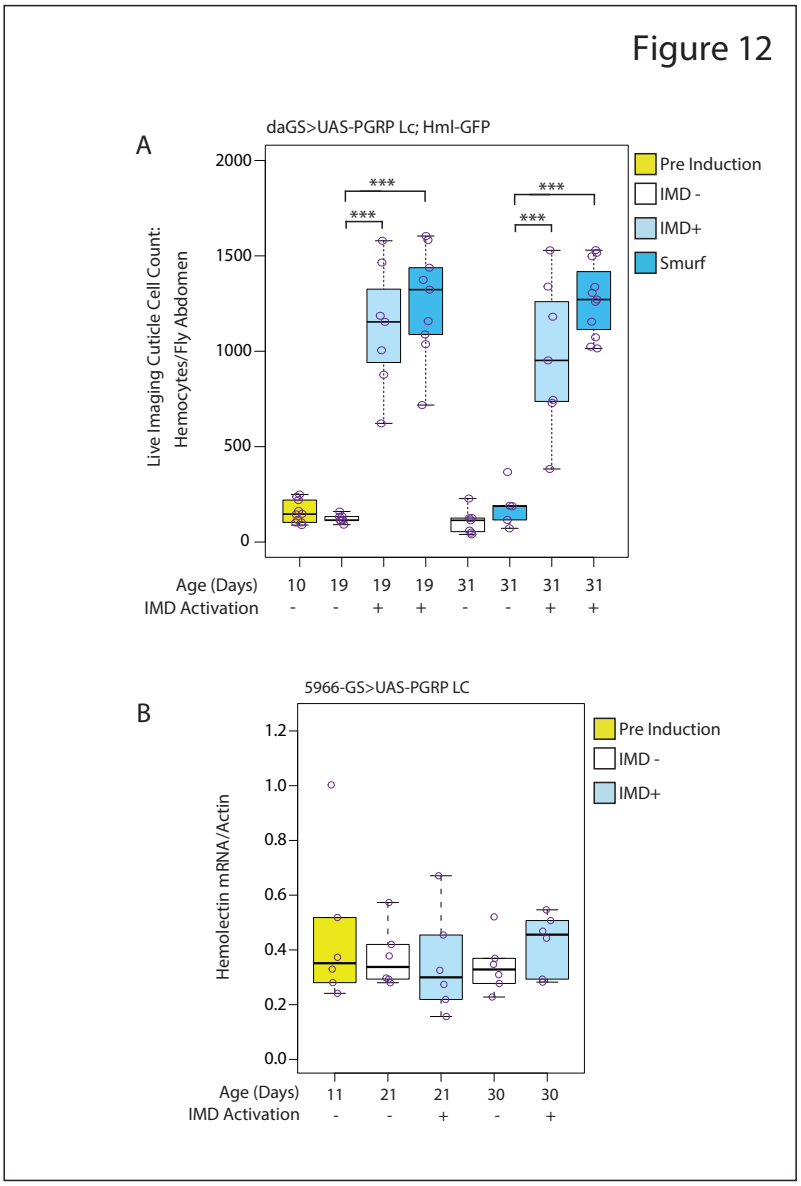

Figure 6.12: Systemic immune activation leads to an increase in abdominal macrophage number regardless of chronological age

Quantification of external macrophage counts at the abdomen in daughterless-GeneSwitch>UAS-PGRP LCa; Hml-GFP female flies, immune activated from day 10 of adulthood and uninduced controls (A). n = 7-11 flies/condition. Boxplot displays the first and third quartile, with the horizontal bar at the median; overlayed purple scatter plots indicate individual replicates. Insufficient replicates for quantification of thorax images. Quantification of Hemolectin (Hml) mRNA levels (B). Gene expression assayed by RT-qPCR from dissected intestines in 5966GS > UAS-PGRP LCa; non-Smurf female flies immune activated from day 10 of adulthood and uninduced controls. n = 6 replicates of five intestines. For (A) and (B), p-value < 0.001 = *** in Wilcoxon Test, only significant changes shown. Representative images shown in Figure 6.11. PGRP LCa = Peptidoglycan recognition protein Lc, da = daughterless, IMD = Immune Deficiency Pathway.

6.4 Bacteria-independent mechanism may mediate changes in macrophage number following barrier dysfunction

Macrophage cells are responsible, in part, for bacterial recognition and phagocytic removal (Franc et al., 1996). Dysbiosis is another distinct hallmark of the Smurf phenotype, bacterial imbalance is known to occur prior-to and after intestinal barrier loss (Clark et al., 2015). For these reasons, I next hypothesized that perhaps bacterial imbalance was facilitating changes observed in sessile macrophage number.

6.4.1 Antibiotic-fed flies show changes in sessile macrophage number

As a proxy for germ-free flies, initial work was conducted using antibiotic feeding. Briefly, flies were fed a standard diet with the addition of an antibiotic cocktail (tetracycline, rifamycin and ampicillin combined in ethanol solution), or an equivalent volume of ethanol only for untreated controls (methods detailed in Section 2.1.3.4). Macrophage cells were endogenously marked with either *hemolectin-dsRed* or *serpent-mCherry* and live imaged along the dorsal fly cuticle at early, mid-, and late life. *Hml-dsRed* and *srp-mCherry* were chosen as endogenous markers since data from initial characterizations showed similar fluorescent quantifications with age and barrier dysfunction in each line respectively.

6.4.1.1 Live imaging shows changes in hemolectin-dsRed marked sessile macrophage cells

Abdomen-associated sessile macrophage number remains unchanged with age in antibiotic fed flies (Figure 6.13 A-C, L). Like ethanol fed controls, antibiotic fed flies maintain similar sessile macrophage numbers at early, mid-, and late life (Figure 6.13 G-I, L). At midlife, antibiotic fed flies show a significant increase in abdomen-associated sessile macrophage number following barrier dysfunction (Figure 6.13 D-F, L). By contrast, control flies show nonsignificant changes in sessile macrophage number following barrier

dysfunction (Figure 6.13 J-L). Qualitative analysis of control images shows a slight increase in fluorescence intensity in Smurfs compared to non-Smurfs (Figure 6.13 G-K). Thorax-associated sessile macrophage number remains unchanged with age in antibiotic fed flies (Figure 6.14 A-C, L). Like ethanol fed controls, antibiotic fed flies maintain similar sessile macrophage numbers at early, mid-, and late life (Figure 6.14 G-I, L). At late life, antibiotic fed flies show a nonsignificant increase in sessile macrophage number following barrier dysfunction (Figure 6.14 C, F, L). Similarly, at midlife control flies show nonsignificant increases in sessile macrophage number following barrier dysfunction (Figure 6.14 J-L). Qualitative analysis of antibiotic fed, and control images shows an increase in fluorescence intensity in Smurf flies compared to non-Smurf flies (Figure 6.14 A-K). Results indicate an increase in sessile macrophage number following barrier dysfunction, independent of bacteria. For comparison, the initial characterization of sessile macrophages marked by *hml-dsRed* showed increased cell number in the thorax of Smurf flies (Figure 6.4), this result is unchanged by antibiotic treatment and controls are consistent although the threshold for statistical significance for these changes was not reached in this experiment.

6.4.1.2 Live imaging shows changes in serpent-mCherry marked sessile macrophage cells

Abdomen-associated sessile macrophage number shows a nonsignificant decrease with age in antibiotic fed flies (Figure 6.15 A-B, I). Following barrier dysfunction, antibiotic fed flies also show a nonsignificant decrease in sessile macrophage number (Figure 6.15 A-D, I). In ethanol fed control flies, sessile macrophage number remains unchanged with age (Figure 6.15 E-F, I). At late life, there is a significant decrease in sessile macrophage number following barrier dysfunction in control flies (Figure 6.15 F, H-I). Thorax-

associated sessile macrophage number shows a nonsignificant decrease with age in antibiotic fed flies (Figure 6.16 A-B, I). Following barrier dysfunction, sessile macrophage number remains unchanged in antibiotic fed flies (Figure 6.16 A-D, I). Sessile macrophage number significantly decreases with age in control flies (Figure 6.16 E-I). Results indicate *srp-mCherry* marked sessile macrophage cells may be more sensitive to age-associated changes. For comparison, the initial characterization of sessile macrophages marked by *srp-mCherry* showed increased cell number along the thoracic and abdominal cuticle of Smurf flies (Figure 6.6), so the data shown here are inconsistent with initial characterization data.

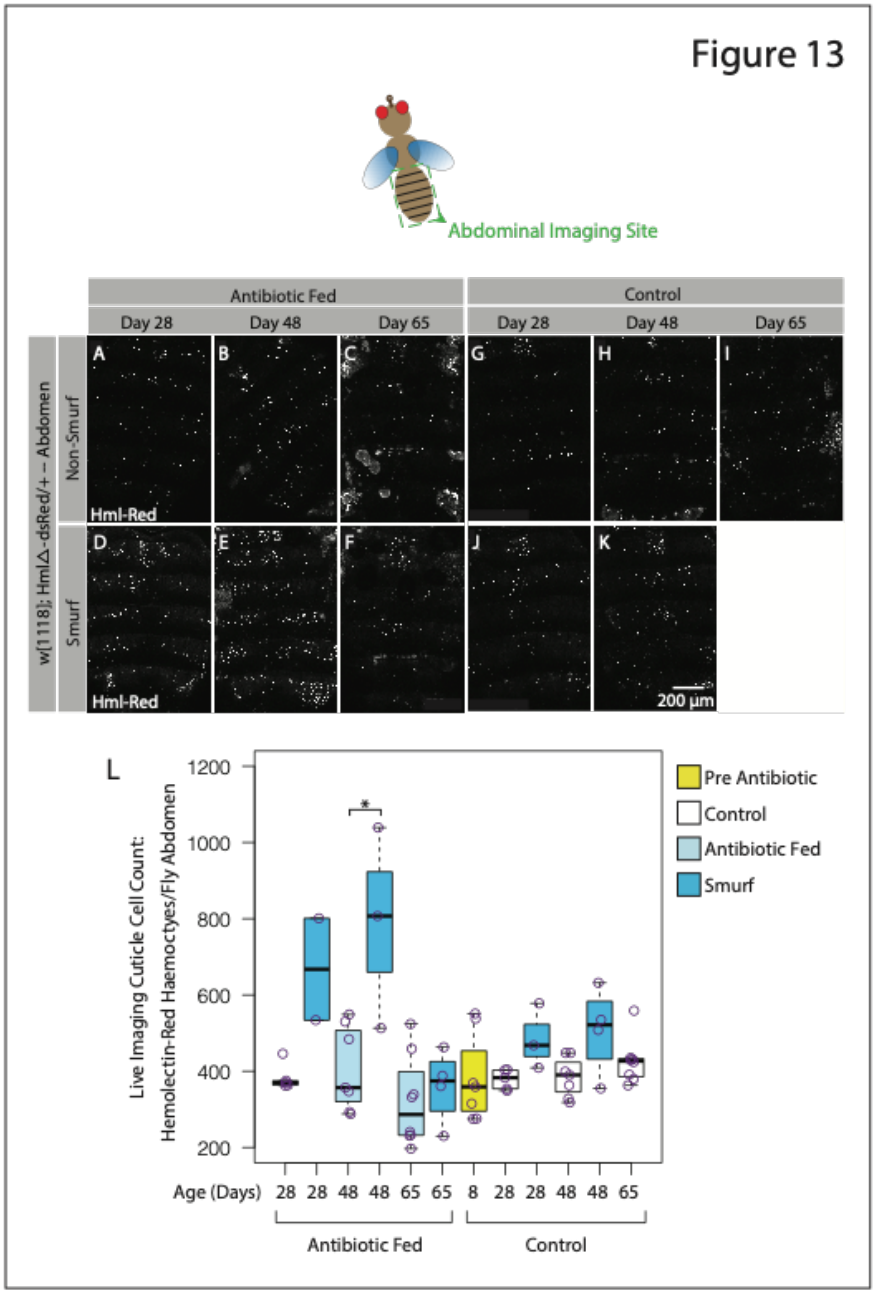

Figure 6.13: Abdominal macrophages marked by Hemolectin-dsRed increase following loss of barrier function even after antibiotic treatment

Confocal images depict the abdomen of endogenously marked female flies at 28, 48, and 65 days of adulthood. Representative max intensity projections (A-K) show sessile macrophages associated with the dorsal fly cuticle. Antibiotic cocktail diet fed from 10 days of adulthood (A-F) and ethanol-control diet (G-K). Cuticle counts of macrophage cells are shown in the corresponding boxplot; overlayed purple scatter plots indicate individual replicates (L). n = 7-9 flies/condition. Flies were fed a nonabsorbable blue dye for 24 hours and scored as Smurf or Non-Smurf prior to imaging. p-value <0.05 = *, in Wilcoxon Test, only significant changes shown. Hml-Red = *w[1118]; HmlΔ-dsRed/+*.

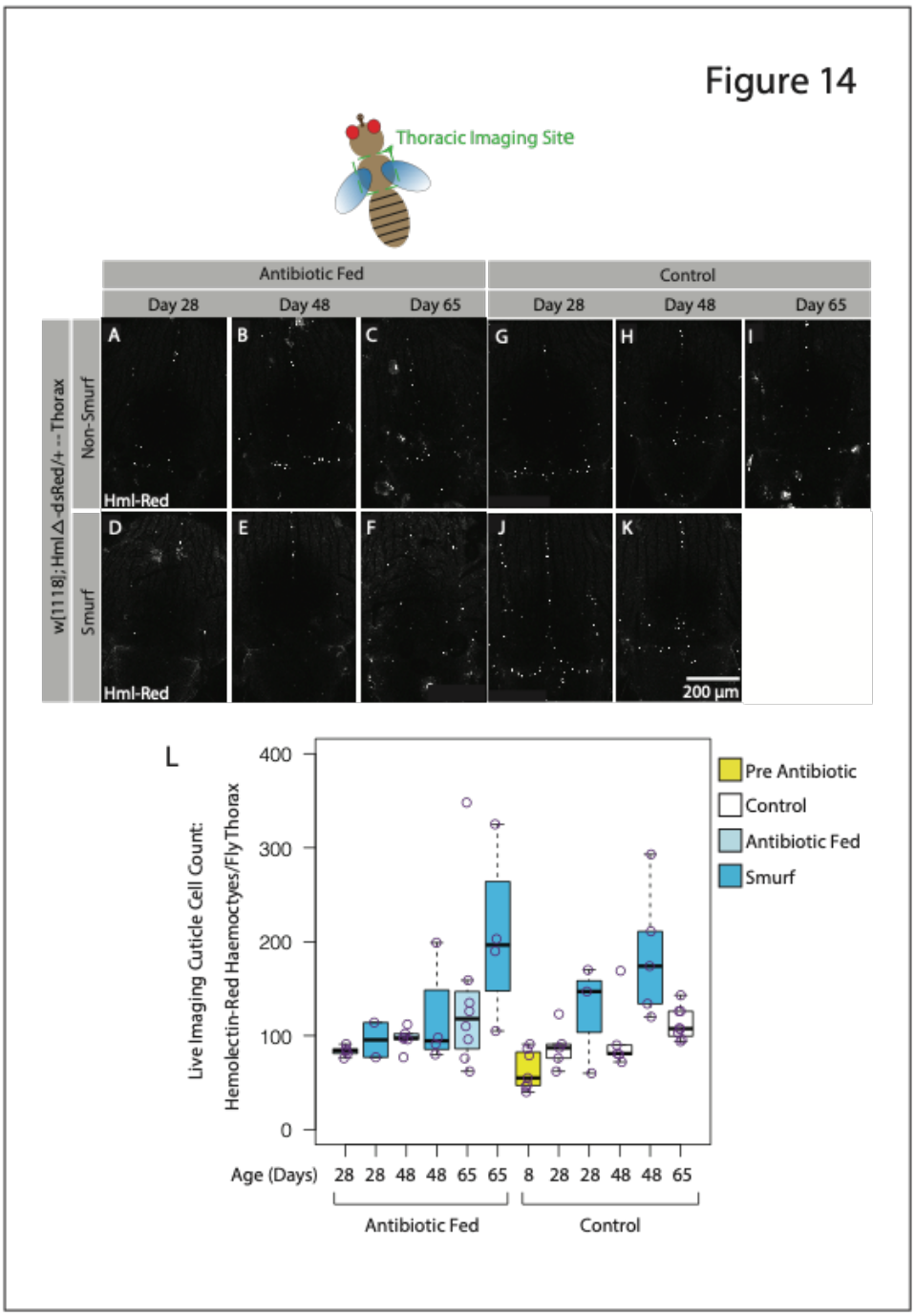

Figure 6.14: Thoracic macrophages marked by Hemolectin-dsRed change following loss of barrier function even after antibiotic treatment

Confocal images depict the thorax of endogenously marked female flies at 28, 48, and 65 days of adulthood. Representative max intensity projections (A-K) show sessile macrophages associated with the dorsal fly cuticle. Antibiotic cocktail diet fed from 10 days of adulthood (A-F) and ethanol-control diet (G-K). Cuticle counts of macrophage cells are shown in the corresponding boxplot; overlayed purple scatter plots indicate individual replicates (L). n = 7-9 flies/condition. Flies were fed a nonabsorbable blue dye for 24 hours and scored as Smurf or Non-Smurf prior to imaging. No significant changes, in Wilcoxon Test. Hml-Red = *w[1118]; HmlΔ-dsRed/+*.

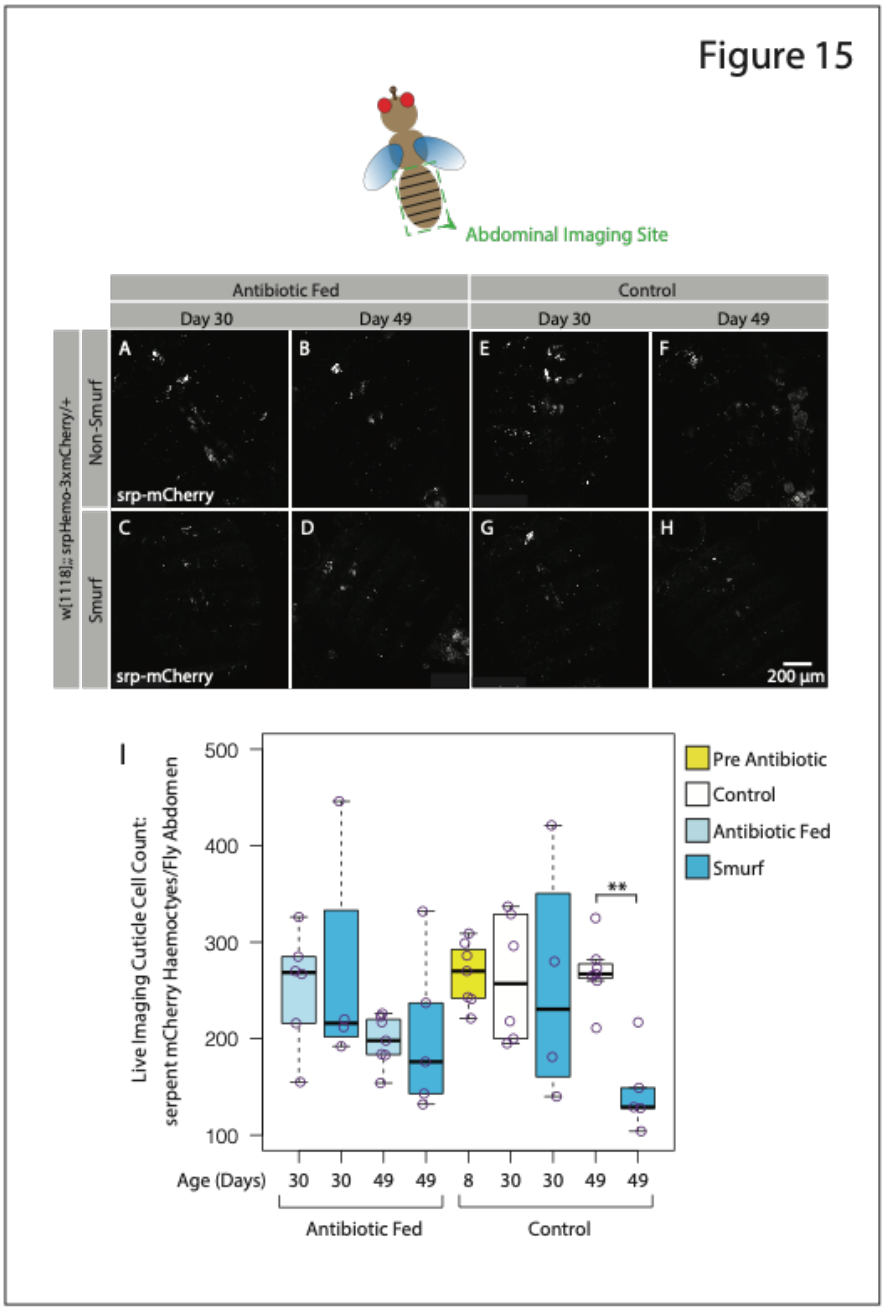

Figure 6.15: Abdominal macrophages marked by Serpent-mCherry remain unchanged following loss of barrier function after antibiotic treatment

Confocal images depict the abdomen of endogenously marked female flies at 30 and 49 days of adulthood. Representative max intensity projections (A-H) show sessile macrophages associated with the dorsal fly cuticle. Antibiotic cocktail diet fed from 10 days of adulthood (A-D) and ethanol-control diet (E-H). Cuticle counts of macrophage cells are shown in the corresponding boxplot; overlayed purple scatter plots indicate individual replicates (I). n = 7-9 flies/condition. Flies were fed a nonabsorbable blue dye for 24 hours and scored as Smurf or Non-Smurf prior to imaging. p-value <0.01 = **, in Wilcoxon Test, only significant changes shown. srp-mCherry = *w[1118];; srpHemo-3xmCherry/+*.

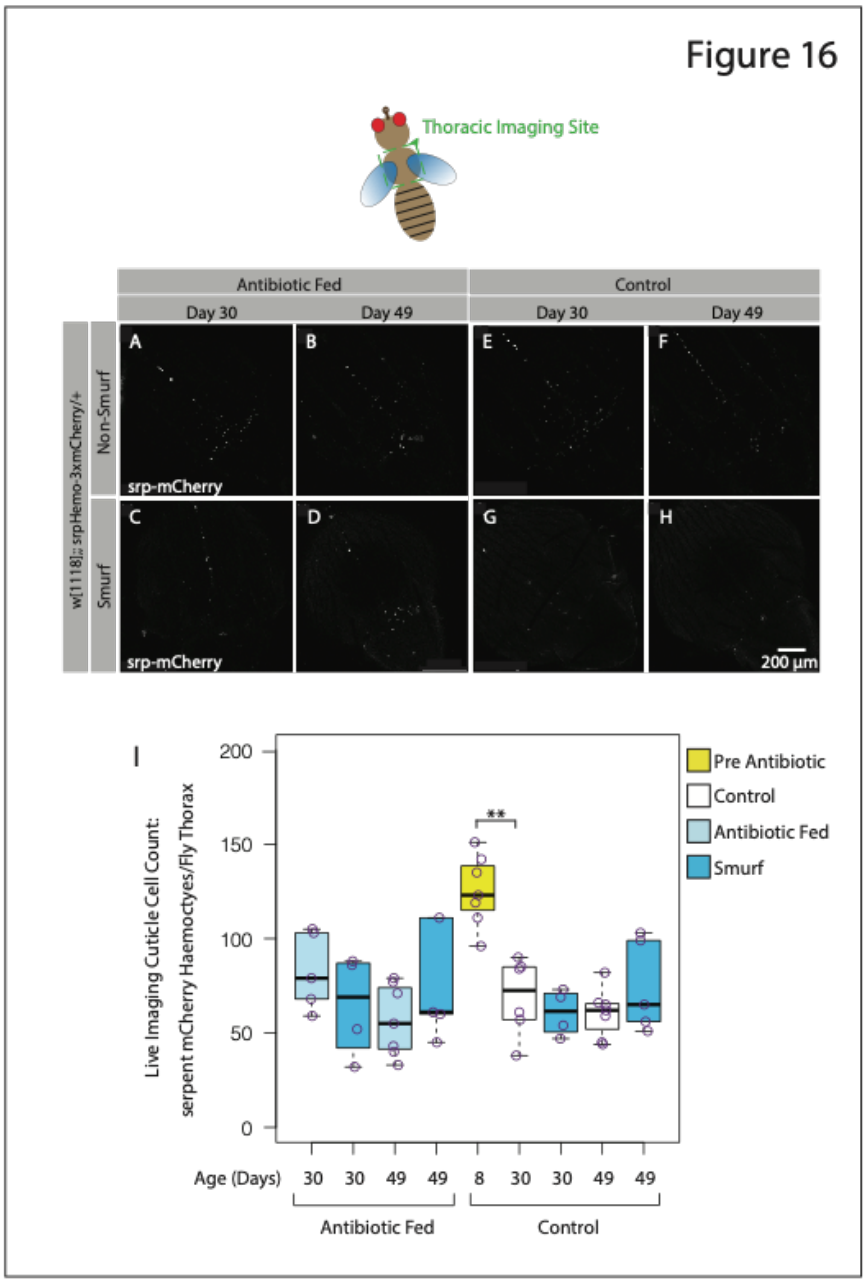

Figure 6.16: Thoracic macrophages marked by Serpent-mCherry remain unchanged following loss of barrier function after antibiotic treatment

Confocal images depict the thorax of endogenously marked female flies at 30 and 49 days of adulthood. Representative max intensity projections (A-H) show sessile macrophages associated with the dorsal fly cuticle. Antibiotic cocktail diet fed from 10 days of adulthood (A-D) and ethanol-control diet (E-H). Cuticle counts of macrophage cells are shown in the corresponding boxplot; overlayed purple scatter plots indicate individual replicates (I). n = 7-9 flies/condition. Flies were fed a nonabsorbable blue dye for 24 hours and scored as Smurf or Non-Smurf prior to imaging. p-value <0.01 = **, in Wilcoxon Test, only significant changes shown. srp-mCherry = *w[1118];; srpHemo-3xmCherry/+*.

6.4.2 Entirely germ-free or axenic flies show changes in macrophage number

Published literature provides two major conventions for generating germ-free flies, either to bleach embryos after laying and maintain development on sterile media, or to develop and maintain flies on antibiotic medium through adulthood (Lee et al., 2019). There are data regarding toxicity, or a decline in lifespan, with either convention. Lee and colleagues, show that antibiotic toxicity is hugely dependent on dosage (Lee et al., 2019). The transgenic lines used for macrophage assays in this chapter showed acute toxicity when fed antibiotics (data not shown). The antibiotic dosage used was equivalent to that used by previous groups (Ren et al., 2007). Here, each hemocyte fly strain used may be influencing host response to antibiotics as toxic (Han et al., 2017). For this reason, further bacterial influence on macrophage dysfunction was also studied in entirely germ-free, or axenic, flies. *Hml-dsRed* and *srp-mCherry* were again used as endogenous markers to confirm findings regarding the role of bacteria in macrophage dysfunction.

6.4.2.1 Live imaging shows changes in serpent-mCherry marked sessile macrophage cells

Abdomen-associated sessile macrophage number remains unchanged with age in axenic and conventional control flies (Figure 6.17 A-C, E-G, I). Following barrier dysfunction, abdominal sessile macrophage number remains unchanged in axenic flies, while control flies show a nonsignificant increase in sessile macrophage number (Figure 6.17 C-D, G-I), consistent with initial data (Figure 6.6). Thorax-associated sessile macrophage number remains unchanged with age in axenic flies (Figure 6.18 A-C, I). By contrast, thoracic sessile macrophage number significantly decreases with age in conventional flies (Figure 6.18 E-G, I). Following barrier dysfunction in axenic and conventional flies, sessile macrophage numbers show a nonsignificant increase (Figure 6.18 C-D, G- I), consistent

with initial data (Figure 6.6). These results indicate that sessile macrophage cells detected using endogenous marker *srp-mCherry* are impacted by both age and loss of barrier function.

6.4.2.2 Macrophage cells extracted from the whole adult fly show age-related changes

To further contextualize the preceding data involving live imaging at the dorsal fly cuticle, total macrophage number from inside the whole fly was quantified. By optimizing a protocol developed by Bosch and colleagues (Sanchez Bosch et al., 2019), sessile and circulating macrophages were successfully released from the whole adult fly (Figure 6.19 A). Dissected flies came from the same *srp-mCherry* population used for live imaging at the dorsal cuticle (Section 6.4.2.1).

In axenic flies, total macrophage number remained unchanged with age (Figure 6.19 B). By contrast, conventional flies showed a significant decrease in total macrophage number by midlife (Figure 6.19 B). In axenic flies, there is a nonsignificant decrease in total macrophage number following barrier dysfunction (Figure 6.19 B). By contrast, in conventional flies there is a significant decrease in total macrophage number following barrier dysfunction. This decrease in conventional Smurf flies occurs regardless of chronological age (Figure 6.19 B). Results indicate that total macrophage number decreases upon loss of barrier function in a bacteria independent manner. Further, this data suggests that age-related decreases in total macrophage number in non-Smurf flies is bacteria dependent.

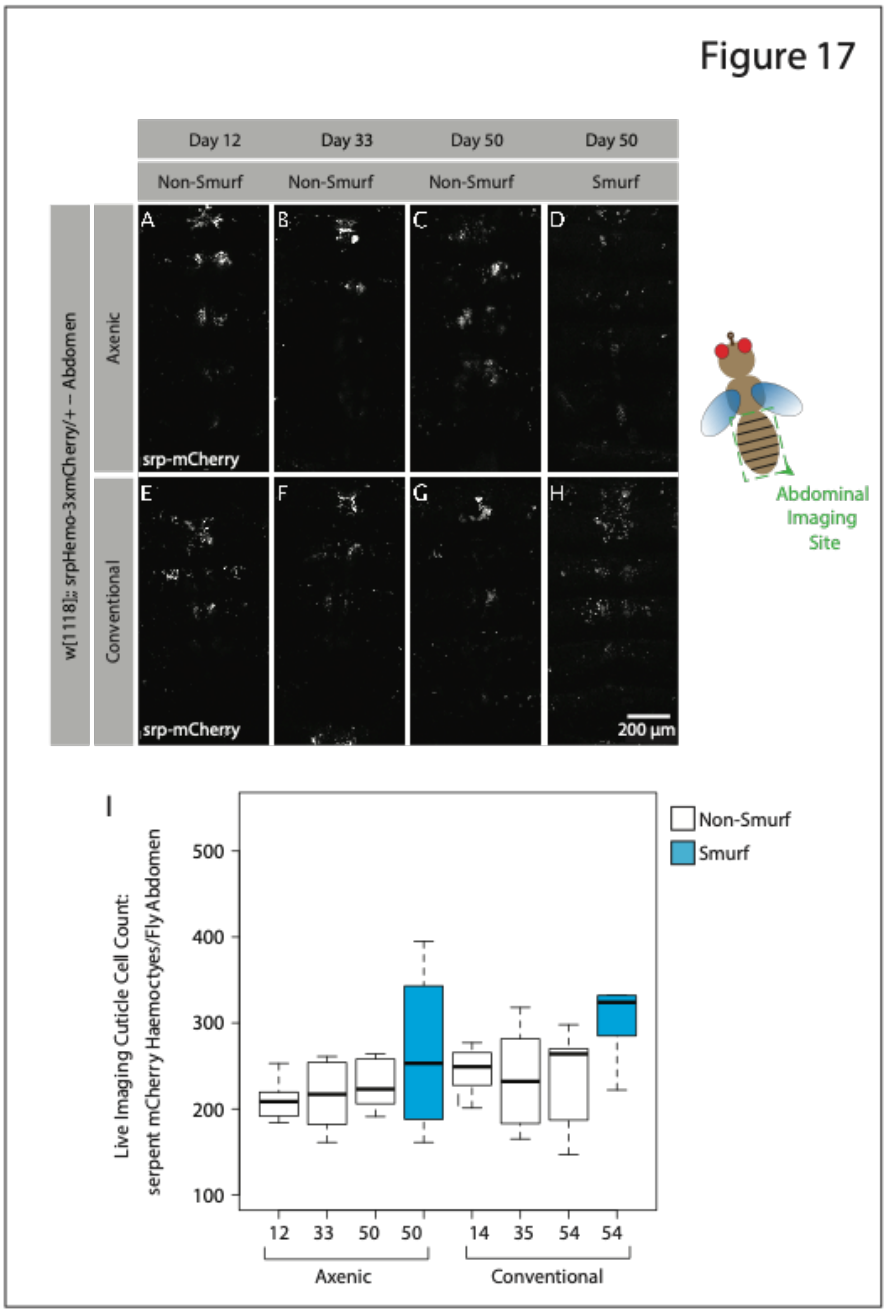

Figure 6.17: Abdominal macrophages marked by Serpent-mCherry remain unchanged following loss of barrier function in entirely germ-free flies

Confocal images depict the abdomen of endogenously marked female flies at 12, 30, and 50 days of adulthood. Representative max intensity projections (A-H) show sessile macrophages associated with the dorsal fly cuticle; axenic flies developed and maintained on sterile media throughout adulthood (A-D) and conventionally reared controls (E-H). Cuticle counts of macrophage cells are quantified in boxplot displaying the first and third quartile, with the horizontal bar at the median (I). n = 5-9 flies/condition. Flies were fed a nonabsorbable blue dye for 24 hours and scored as Smurf or Non-Smurf prior to imaging. No significant changes, in Wilcoxon Test. srp-mCherry = *w[1118];; srpHemo-3xmCherry/+*.

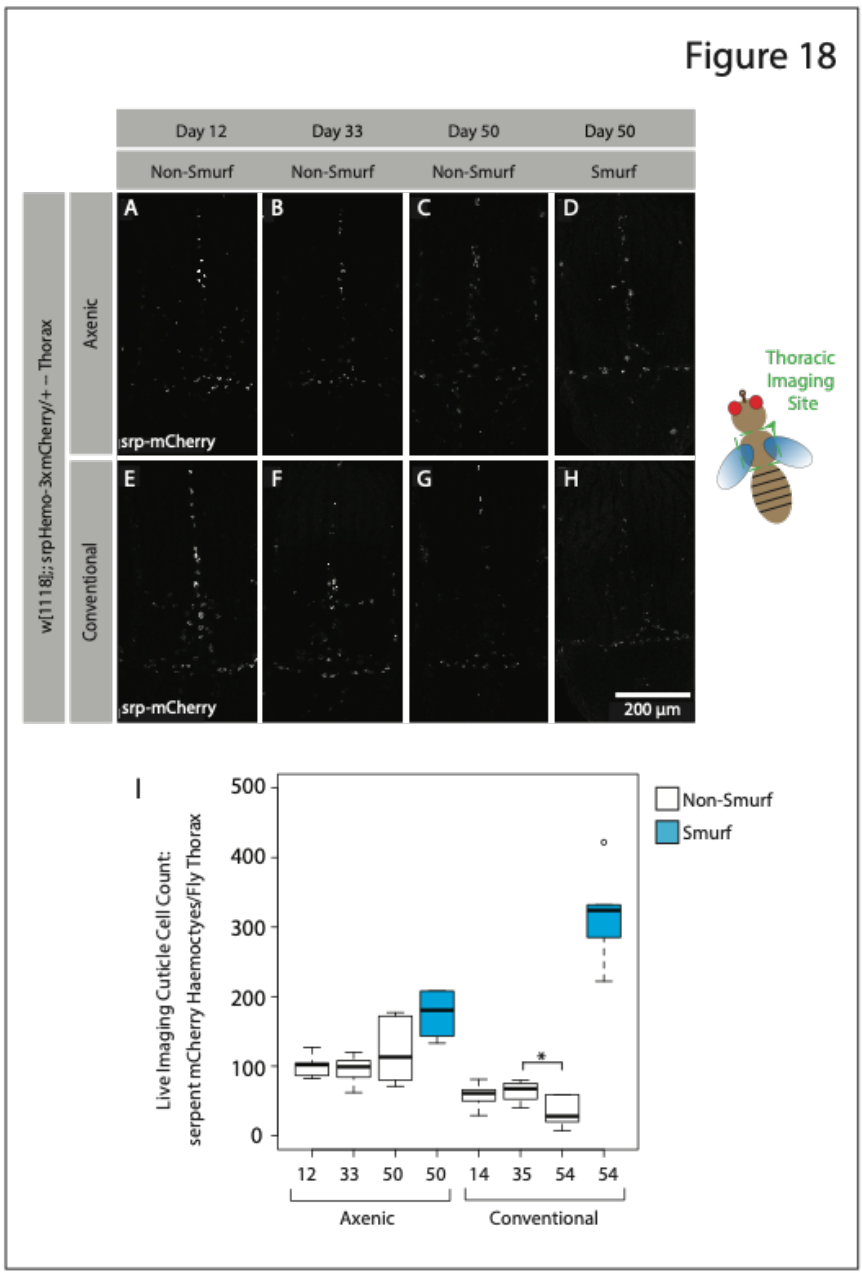

Figure 6.18: Thoracic macrophages marked by Serpent-mCherry remain unchanged following loss of barrier function in entirely germ-free flies

Confocal images depict the thorax of endogenously marked female flies at 12, 30, and 50 days of adulthood. Representative max intensity projections (A-H) show sessile macrophages associated with the dorsal fly cuticle; axenic flies developed and maintained on sterile media throughout adulthood (A-D) and conventionally reared controls (E-H). Cuticle counts of macrophage cells are quantified in boxplot displaying the first and third quartile, with the horizontal bar at the median (I). n = 5-9 flies/condition. Flies were fed a nonabsorbable blue dye for 24 hours and scored as Smurf or Non-Smurf prior to imaging. p-value <0.05 = *, in Wilcoxon Test, only significant changes shown. srp-mCherry = *w[1118];; srpHemo-3xmCherry/+*.

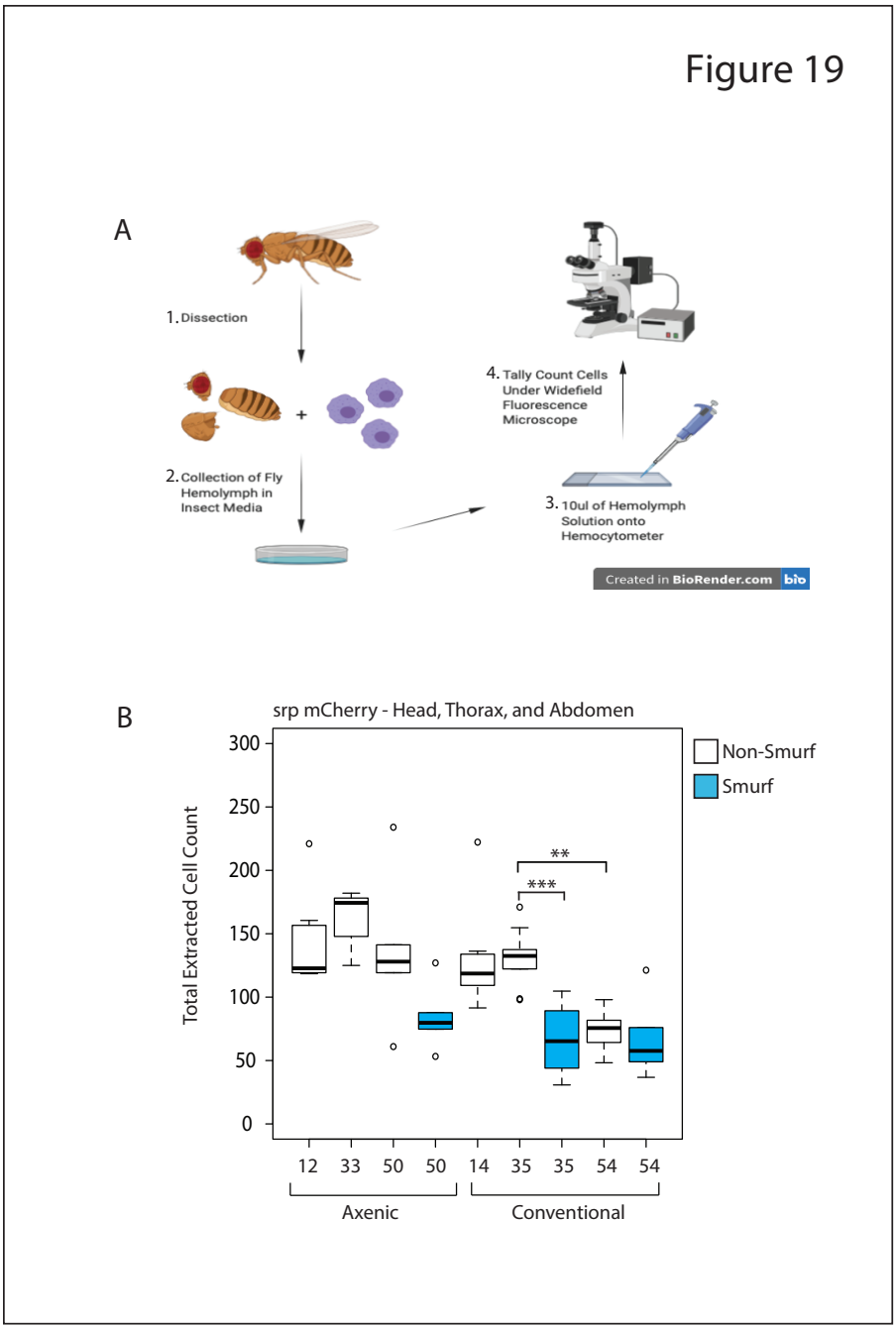

Figure 6.19: Serpent-mCherry marked macrophage number decreases in the whole fly following loss of barrier function

Quantifying total macrophage number in the whole fly. Protocol illustration: macrophage cells extracted and manually counted using hemocytometer and widefield fluorescence microscope (A). Boxplot shows total macrophage cells released from the entire fly per condition with age (B). n = 8-10 flies/condition. Flies were fed a nonabsorbable blue dye for 24 hours and scored as Smurf or Non-Smurf prior to imaging. p-value <0.01 = **, <0.001 = ***, in Wilcoxon Test, only significant changes shown. srp-mCherry = *w[1118];; srpHemo-3xmCherry*/+. Figure (A) generated using BioRender.com.

6.4.2.3 Live imaging shows changes in hemolectin-dsRed marked sessile macrophage cells

A second endogenous marker, *hml-dsRed* was used to confirm findings regarding the role of bacteria in macrophage dysfunction. For comparison, initial characterization of both lines showed increased macrophage number in the thorax in Smurf flies (Figure 6.4, Figure 6.6). Sessile macrophage number in axenic *srp-mcherry* flies remained unchanged in Smurf flies. In *hml-dsRed* flies, abdomen-associated sessile macrophage number significantly increases in axenic flies with age (Figure 6.20 A-C, I). By contrast, sessile macrophage number remains unchanged in conventional flies with age (Figure 6.20 E-G, I), consistent with initial data (Figure 6.4). Abdomen-associated sessile macrophage number significantly decreases following barrier dysfunction in axenic flies (Figure 6.20 C-D, I). By contrast, sessile cell number remains unchanged following barrier dysfunction in conventional flies (Figure 6.20 G-H, I), consistent with initial data (Figure 6.4). Thorax-associated sessile macrophage number significantly increases with age in both axenic and conventional flies (Figure 6.21 A-C, E-G, I), which was not recorded in initial data (Figure 6.4). Thoracic sessile macrophage number significantly increases following barrier dysfunction in axenic flies (Figure 6.21 C-D, I), as well as showing a nonsignificant increase following barrier dysfunction in conventional flies (Figure 6.21 G-I), largely consistent with initial data (Figure 6.4). Results indicate that sessile macrophage cells marked by *hml-dsRed* are impacted differently depending on cuticle region. Abdominal sessile macrophage numbers show changes in the absence of bacteria that are not seen during conventional aging; thoracic sessile macrophage numbers increase with age and barrier loss in a bacteria independent manner.

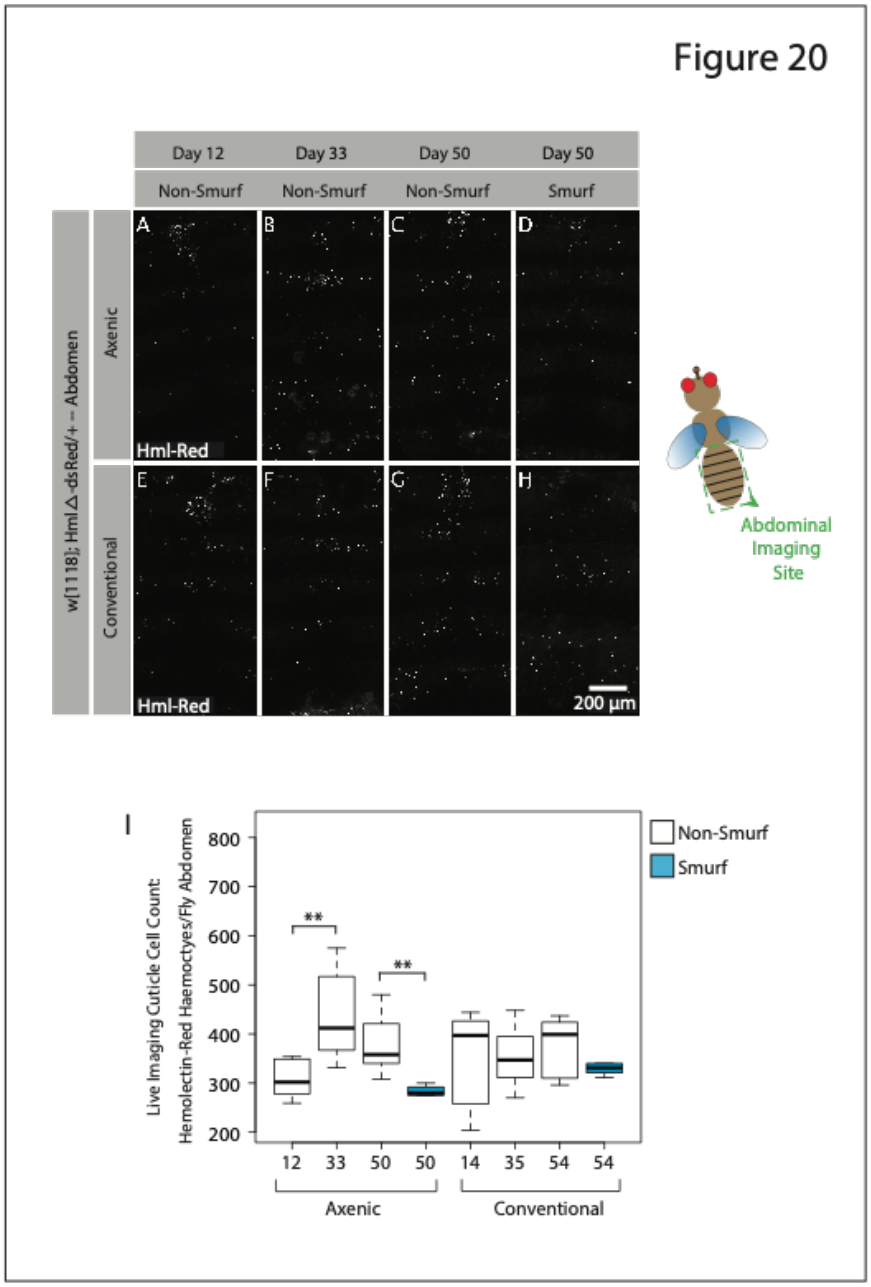

Figure 6.20: Abdominal macrophages marked by Hemolectin-dsRed decrease following loss of barrier function in entirely germ-free flies

Confocal images depict the abdomen of endogenously marked female flies at 12, 33, and 50 days of adulthood. Representative max intensity projections (A-H) show sessile macrophages associated with the dorsal fly cuticle; axenic flies developed and maintained on sterile media throughout adulthood (A-D) and conventionally reared controls (E-H). Cuticle counts of macrophage cells are quantified in boxplot displaying the first and third quartile, with the horizontal bar at the median (I). n = 5-9 flies/condition. Flies were fed a nonabsorbable blue dye for 24 hours and scored as Smurf or Non-Smurf prior to imaging. p-value <0.01 = **, in Wilcoxon Test, only significant changes shown. Hml-Red = *w[1118]; HmlΔ-dsRed/+*.

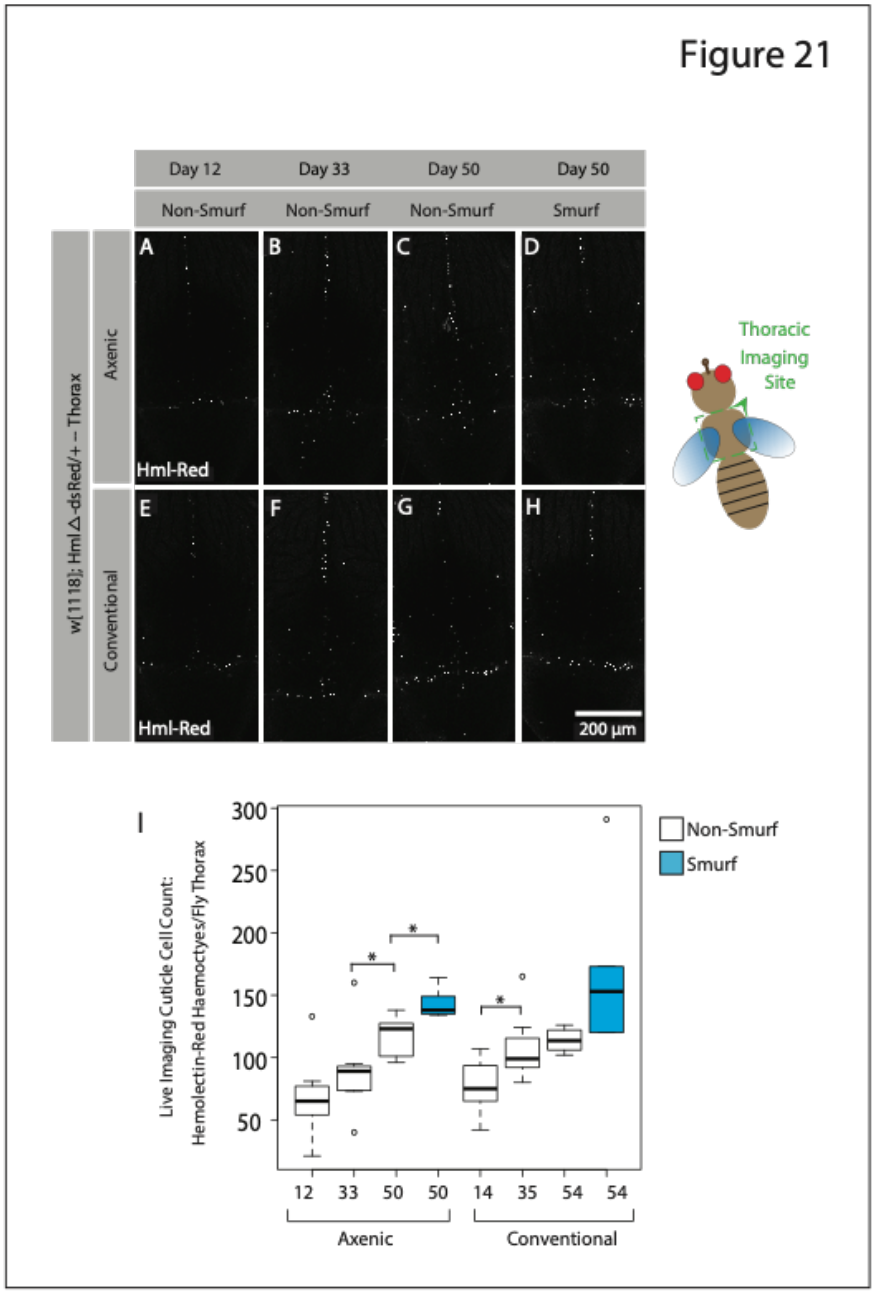

Figure 6.21: Thoracic macrophages marked by Hemolectin-dsRed increase following loss of barrier function in entirely germ-free flies

Confocal images depict the thorax of endogenously marked female flies at 12, 33, and 50 days of adulthood. Representative max intensity projections (A-H) show sessile macrophages associated with the dorsal fly cuticle; axenic flies developed and maintained on sterile media throughout adulthood (A-D) and conventionally reared controls (E-H). Cuticle counts of macrophage cells are quantified in boxplot displaying the first and third quartile, with the horizontal bar at the median (I). n = 5-9 flies/condition. Flies were fed a nonabsorbable blue dye for 24 hours and scored as Smurf or Non-Smurf prior to imaging. p-value <0.05 = *, in Wilcoxon Test, only significant changes shown. Hml-Red = *w[1118]; HmlΔ-dsRed/+*.

6.5 Could differences observed between hemocyte lines indicate differential marking of immune cells with age?

Changes in macrophage number across varying conditions and time points suggests that endogenous markers may be highlighting differential macrophage population with age. To test this hypothesis a transgenic line was created combining two endogenous macrophage markers, *serpent-mCherry* and *hemolectin-GFP*, into one genetic background: *w[1118]; HmlΔGal4,UAS-2xeGFP; srpHemo-3xmCherry/+*. Macrophage cells marked with either one or both markers were then quantified as previously described. Here, *hml-GFP* and *srp-mCherry* were used due complimentary fluorophore colors.

The number of cells marked *srp-mCherry* (*srp*) only, decrease with age (Figure 6.22 A-F). In other words, an age-associated decrease in *srp* only cells led to a significant increase in the relative proportion of cells showing both markers ("colocation events") in the aged fly (Figure 6.22 A"-F", Figure 6.23 A, C). Simultaneously, cells marked *hml-GFP* (*hml*) only, increase with age (Figure 6.22 A'-F'). In other words, colocalization events as a ratio of *hml* expressing only cells significantly decrease with age (Figure 6.22 A"-F", Figure 6.23 B, D). Results indicate a transition of *srp* only cells to *hml* only cells with age.

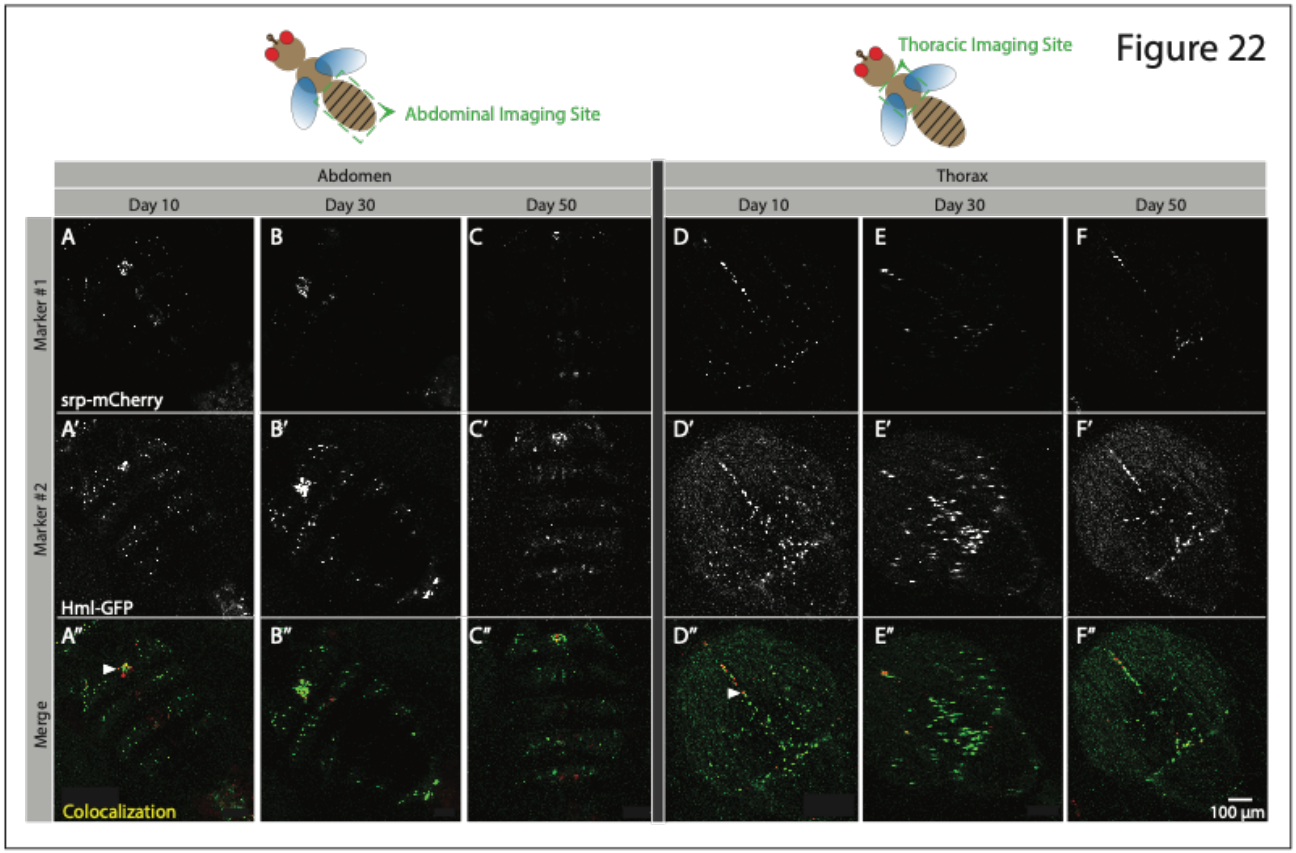

Figure 6.22: Confocal microscopy of macrophage subpopulations in the adult fly

Confocal images depict the abdomen of endogenously marked female flies at 12, 33, and 50 days of adulthood. Representative max intensity projections (A-F) show sessile macrophages associated with the dorsal fly cuticle; fly abdomen (A-C) and fly thorax (D-F). n = 5 flies/condition. Flies were fed a nonabsorbable blue dye for 24 hours and scored as Smurf or Non-Smurf prior to imaging. Contrast uniformly increased for clarity using the *Enhanced True Color Contrast* function (Fiji). White arrows in merged images point to colocalization events. Hml-GFP = w*[1118]; HmlΔGal4,UAS-2xeGFP*. srp-mCherry = *w[1118];; srpHemo-3xmCherry*/+.

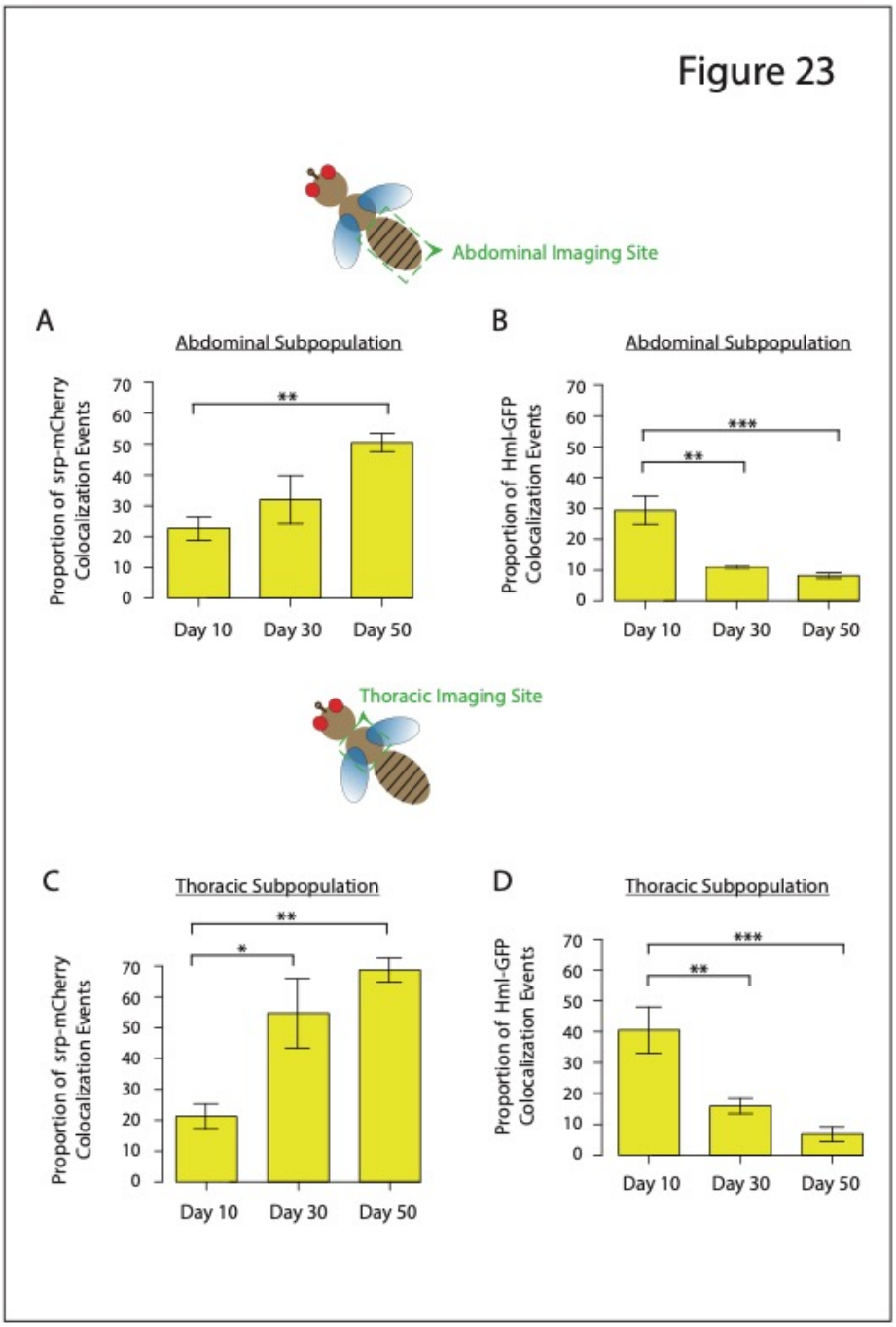

Figure 6.23: Distinct subpopulations of macrophages in the adult fly change in proportion with age

Quantification of live-imaging colocalization events per marker type in the fly abdomen (A-B) and thorax (C-D). y-axis equation = merge/marker #1 or marker #2 from representative images shown in Figure 6.22. Bar graphs show changes in endogenous marker ratio at 10, 30, and 50 days of adulthood. n = 5 flies per time point. p-value <0.05 = *, <0.01 = **, <0.001 = ***, in One-way ANOVA/Kruskal-Wallis Test, only significant changes shown. Error bars show mean and SEM.

6.6 Macrophage function changes with age and in the absence of bacteria

Previously published works indicated a loss of macrophage phagocytic function with age (Horn et al., 2014). To quantify the effects of aging on macrophage function, a live imaging phagocytosis assay was used (methods detailed in Section 2.12). Briefly, flies with endogenously marked macrophage cells were injected with small volumes of fluorescently labeled heat-killed bacteria. Colocalization events were then quantified in imaging software FIJI. This technique allowed for *in vivo*, real-time analysis of changes in sessile macrophage function.

6.6.1 Changes to macrophage function with age as measured by hemolectin-GFP

Macrophage function was first assayed in a conventional fly background using cells endogenously marked with *hml-GFP*. Here, hml-GFP was used based on fluorophore color. Abdomen-associated sessile macrophage cells show a significant increase in phagocytic function with age (Figure 6.24 A-D). Thorax-associated sessile macrophage cells show a small nonsignificant increase in phagocytic function with age (Figure 6.24 E-H). Results indicate that prior to midlife (Figure 6.1 A) phagocytic function increase in marked macrophage cells.

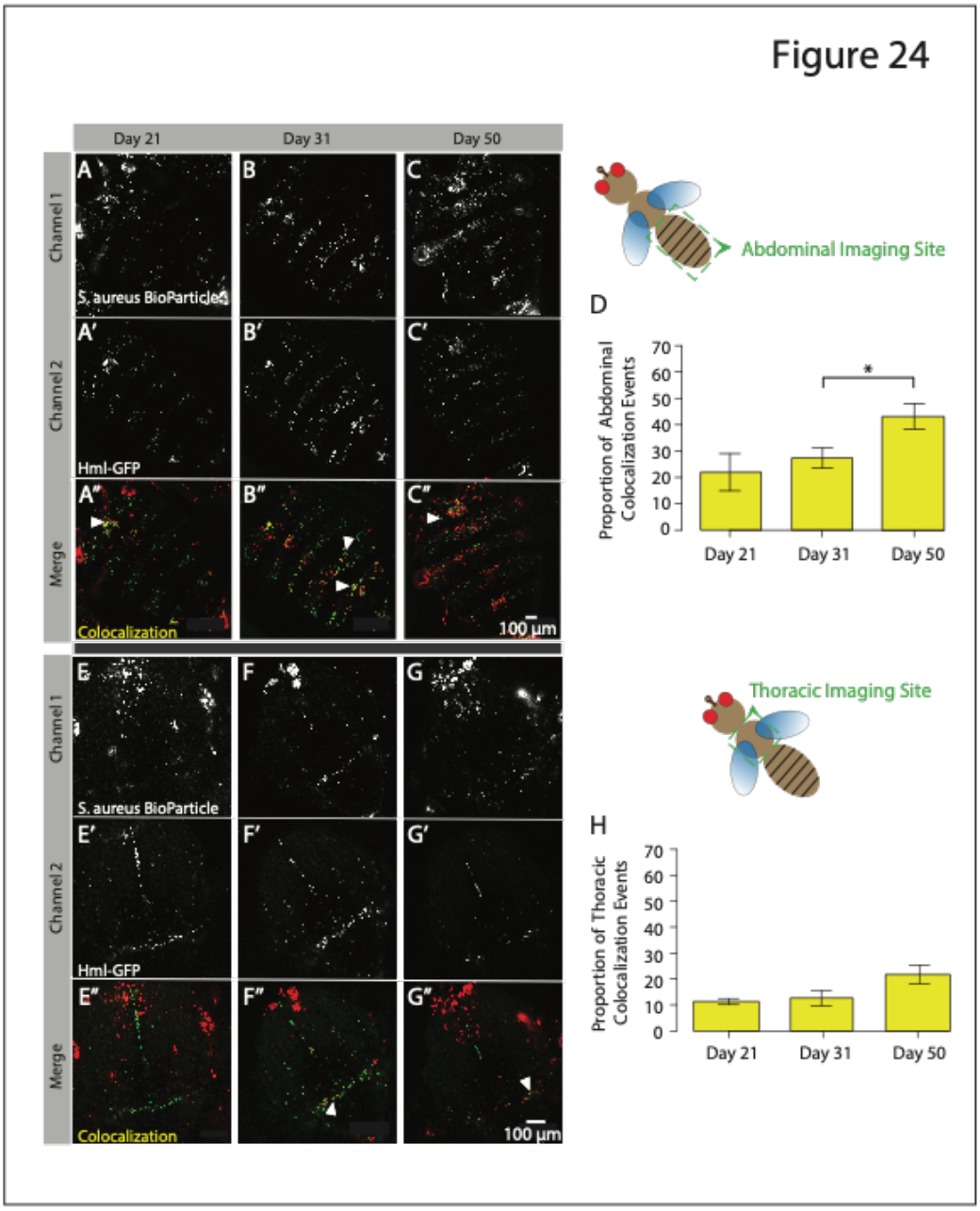

Figure 6.24: Abdominal macrophage function increases in late-life conventional flies endogenously marked with Hemolectin-GFP

Confocal images depict the abdomen and thorax of endogenously marked female flies at 21, 31, and 50 days of adulthood. Representative max intensity projections from live imaging (A-C, E-G) show *Staphylococcus aureus* Alexa Fluor594 BioParticles and Hml-GFP marked sessile macrophages associated with the dorsal fly cuticle, labelled as Channel 1 and Channel 2 respectively. Colocalization between macrophages and *S. aureus* Bioparticles are shown in yellow (A"-C", E"-G"). All flies were scored as non-Smurf prior to imaging. Contrast uniformly increased for clarity using the *Enhanced True Color Contrast* function (Fiji). White arrows in merged images point to colocalization events. y-axis equation = (BioParticle+Hml-GFP)/Hml-GFP. Bar graphs show quantification of phagocytosing cells in the fly abdomen (D) and thorax (H). Two experimental replicates with n = 6-11 flies per time point. p-value <0.05 = *, in One-way ANOVA/Kruskal-Wallis Test, only significant changes shown. Error bars show mean and SEM. Hml-GFP = w*[1118]; HmlΔGal4,UAS-2xeGFP*.

6.6.2 Changes to macrophage function with age in the absence of bacteria

6.6.2.1 Antibiotic fed flies endogenously marked with hemolectin-dsRed

Macrophage function was next assayed in antibiotic fed flies and ethanol fed controls. Macrophage cells were endogenously marked with *hml-dsRed*. Here, *hml-dsRed* was used as part of a cohesive experiment tied to sessile macrophage counts and other bacteria-related data from Section 6.4. In control flies, all dorsal cuticle associated macrophages showed a significant decrease in phagocytic function with age (Figure 6.25 A"-D", Figure 6.26 A"-D", Figure 6.27 A, C). In antibiotic fed flies, abdomen-associated sessile macrophage function significantly decreased with age (Figure 6.25 E"-G", Figure 6.26 E"-G", Figure 6.27 B); thorax-associated sessile macrophage function also showed a small nonsignificant decrease in phagocytic function with age (Figure 6.27 D). These results indicate that phagocytic function in *hml-dsRed* marked sessile macrophage cells is maintained for longer in the abdomen by antibiotic feeding.

6.6.2.2 Antibiotic fed flies endogenously marked with serpent-mCherry

Macrophage function was next assayed in antibiotic fed and ethanol control flies, this time endogenously marked with *srp-mCherry*. Here, *srp-mCherry* was used as part of a cohesive experiment tied to sessile macrophage counts and other bacteria-related data from Section 6.4. In control flies, all dorsal cuticle associated macrophages showed unchanged phagocytic function with age (Figure 6.28 A"-C", Figure 6.29 A"-C", Figure 6.30 A, C). Similarly, all dorsal cuticle associated macrophages showed unchanged phagocytic function with age in antibiotic fed flies (Figure 6.28 D"-E", Figure 6.29 D"-E", Figure 6.30 B, D). These results indicate that phagocytic function in *srp-mCherry* marked sessile macrophage cells is unaffected by aging or the absence of bacteria.

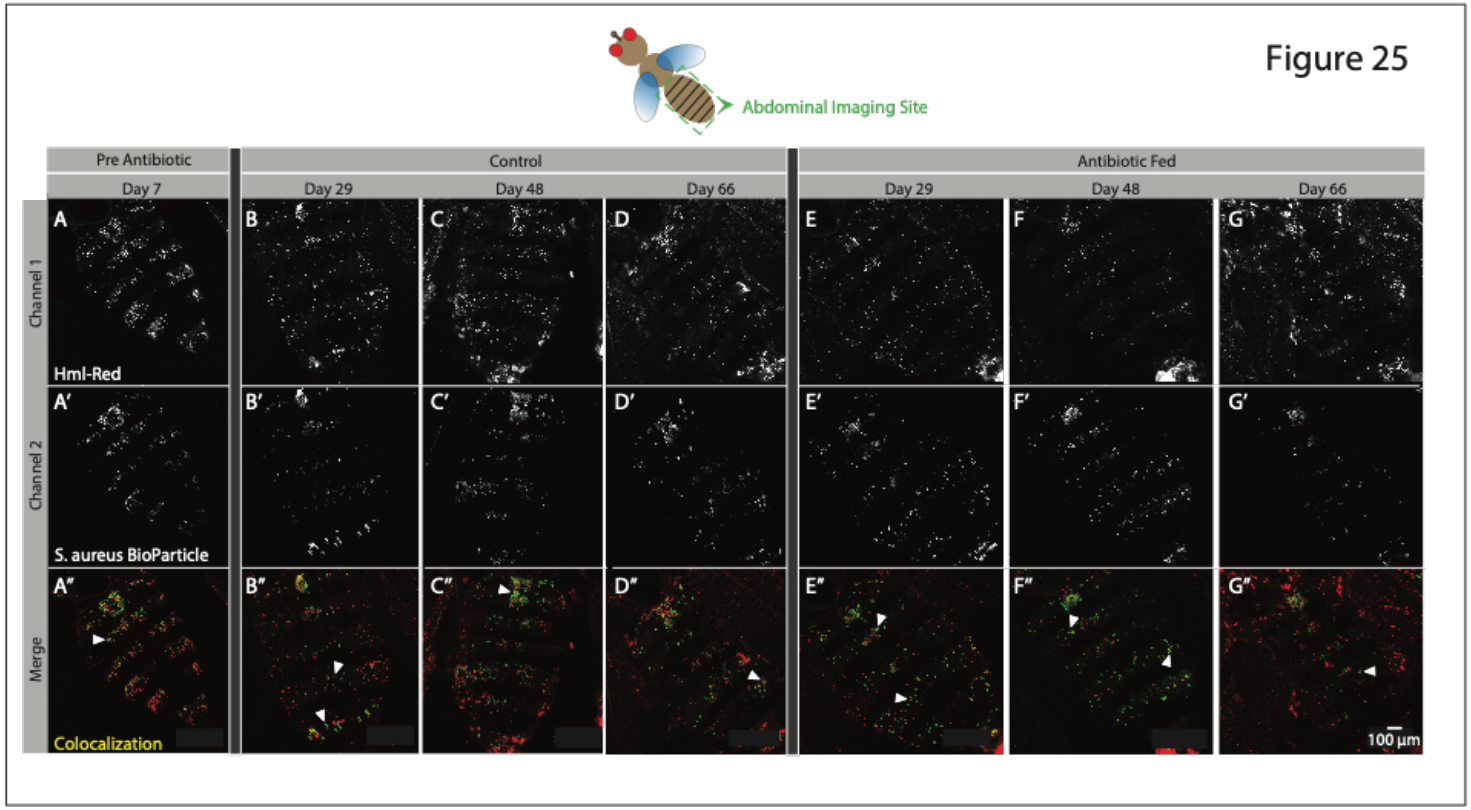

Figure 6.25: Confocal microscopy of changes in abdominal macrophages function assayed through live imaging colocalization assay - Antibiotic-fed flies marked with Hemolectin-dsRed

Confocal images depict the abdomen of antibiotic-fed female flies at 7, 29, 48, and 66 days of adulthood. Representative max intensity projections from live imaging (A-G) show Hml-Red marked sessile macrophages associated with the dorsal fly cuticle and *Staphylococcus aureus* Alexa Fluor488 BioParticles, labelled as Channel 1 and Channel 2 respectively. Colocalization between macrophages and *S. aureus* Bioparticles are shown in yellow (A"-G"). All flies were scored as non-Smurf prior to imaging. Antibiotic cocktail diet fed from 10 days of adulthood (E-G) and ethanol-control diet (B-D). Contrast uniformly increased for clarity using the *Enhanced True Color Contrast* function (Fiji). White arrows in merged images point to colocalization events. Hml-Red = *w[1118]; HmlΔ-dsRed/+*.

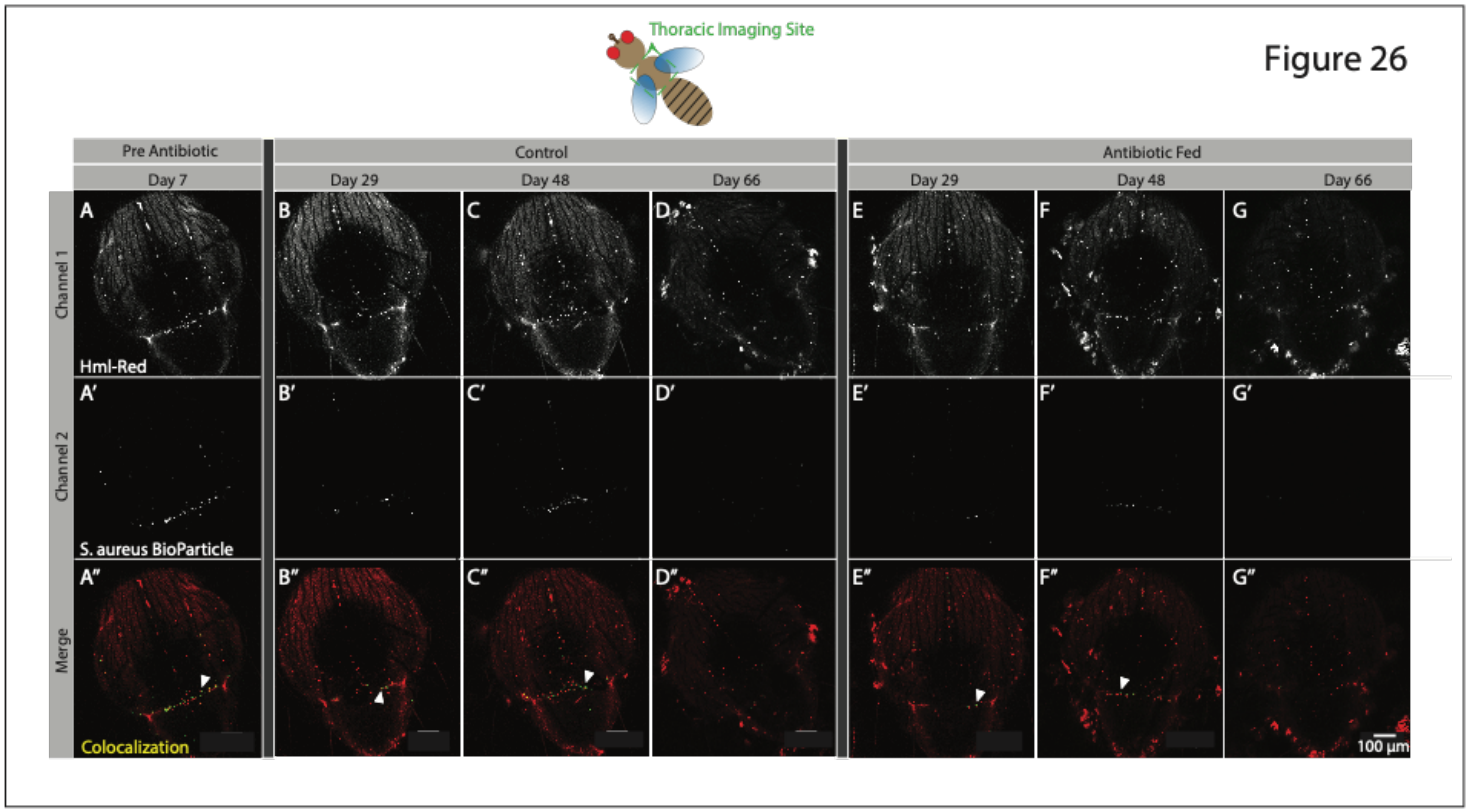

Figure 6.26: Confocal microscopy of changes in thoracic macrophage function assayed through live imaging colocalization assay - Antibiotic-fed flies marked with Hemolectin-dsRed

Confocal images depict the thorax of antibiotic-fed female flies at 7, 29, 48, and 66 days of adulthood. Representative max intensity projections from live imaging (A-G) show Hml-Red marked sessile macrophages associated with the dorsal fly cuticle and *Staphylococcus aureus* Alexa Fluor488 BioParticles, labelled as Channel 1 and Channel 2 respectively. Colocalization between macrophages and *S. aureus* Bioparticles are shown in yellow (A"-G"). All flies were scored as non-Smurf prior to imaging. Antibiotic cocktail diet fed from 10 days of adulthood (E-G) and ethanol-control diet (B-D). Contrast uniformly increased for clarity using the *Enhanced True Color Contrast* function (Fiji). White arrows in merged images point to colocalization events. Hml-Red = *w[1118]; HmlΔ-dsRed/+*.

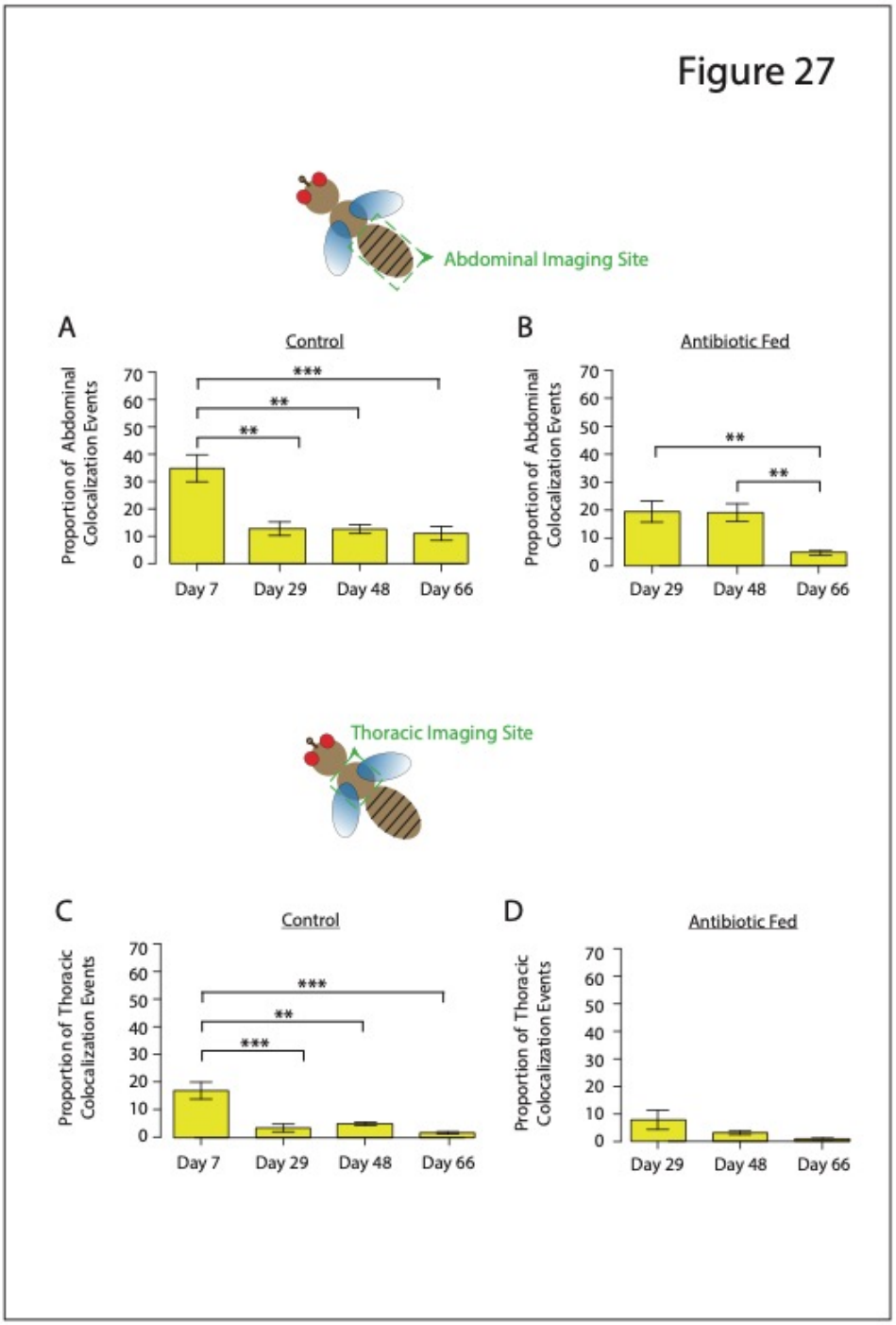

Figure 6.27: Macrophages marked by Hemolectin-dsRed show steady decline in function with age even after antibiotic treatment

Quantification of live imaging colocalization events in antibiotic fed flies. Bar graphs show quantification of phagocytosing cells in the fly abdomen (A-B) and thorax (C-D) at regular intervals throughout fly lifespan. n = 5-7 flies/condition/time point. p-value <0.01 = **, <0.001 = ***, in One-way ANOVA/Kruskal-Wallis Test, only significant changes shown. Error bars show mean and SEM. Hml-Red = *w[1118]; HmlΔ-dsRed/+*.

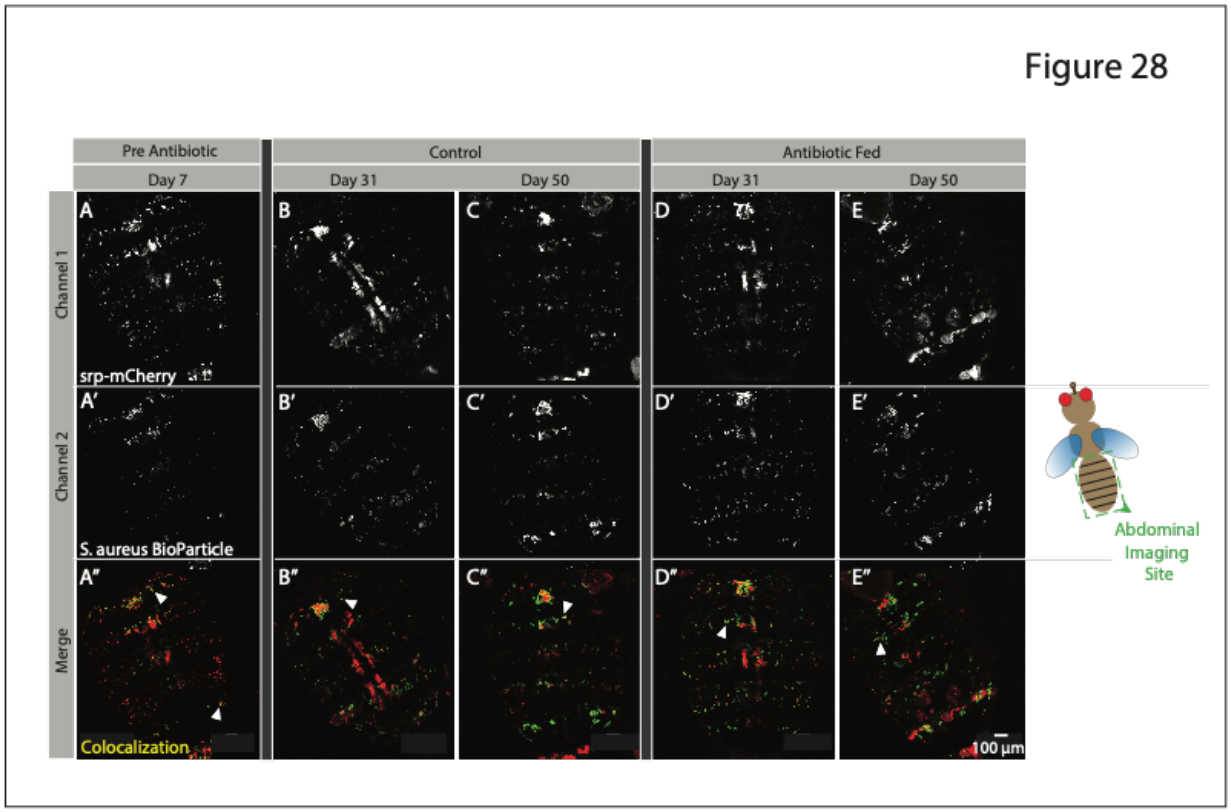

Figure 6.28: Confocal microscopy of changes in abdominal macrophage function assayed through live imaging colocalization assay - Antibiotic-fed flies marked with serpent-mCherry

Confocal images depict the abdomen of antibiotic-fed female flies at 7, 31, and 50 days of adulthood. Representative max intensity projections from live imaging (A-E) show srp-mCherry marked sessile macrophages associated with the dorsal fly cuticle and *Staphylococcus aureus* Alexa Fluor488 BioParticles, labelled as Channel 1 and Channel 2 respectively. Colocalization between macrophages and *S. aureus* Bioparticles are shown in yellow (A"-E"). All flies were scored as non-Smurf prior to imaging. Antibiotic cocktail diet fed from 10 days of adulthood (D-E) and ethanol-control diet (B-C). Contrast uniformly increased for clarity using the *Enhanced True Color Contrast* function (Fiji). White arrows in merged images point to colocalization events. srp-mCherry = *w[1118];; srpHemo-3xmCherry/+*.

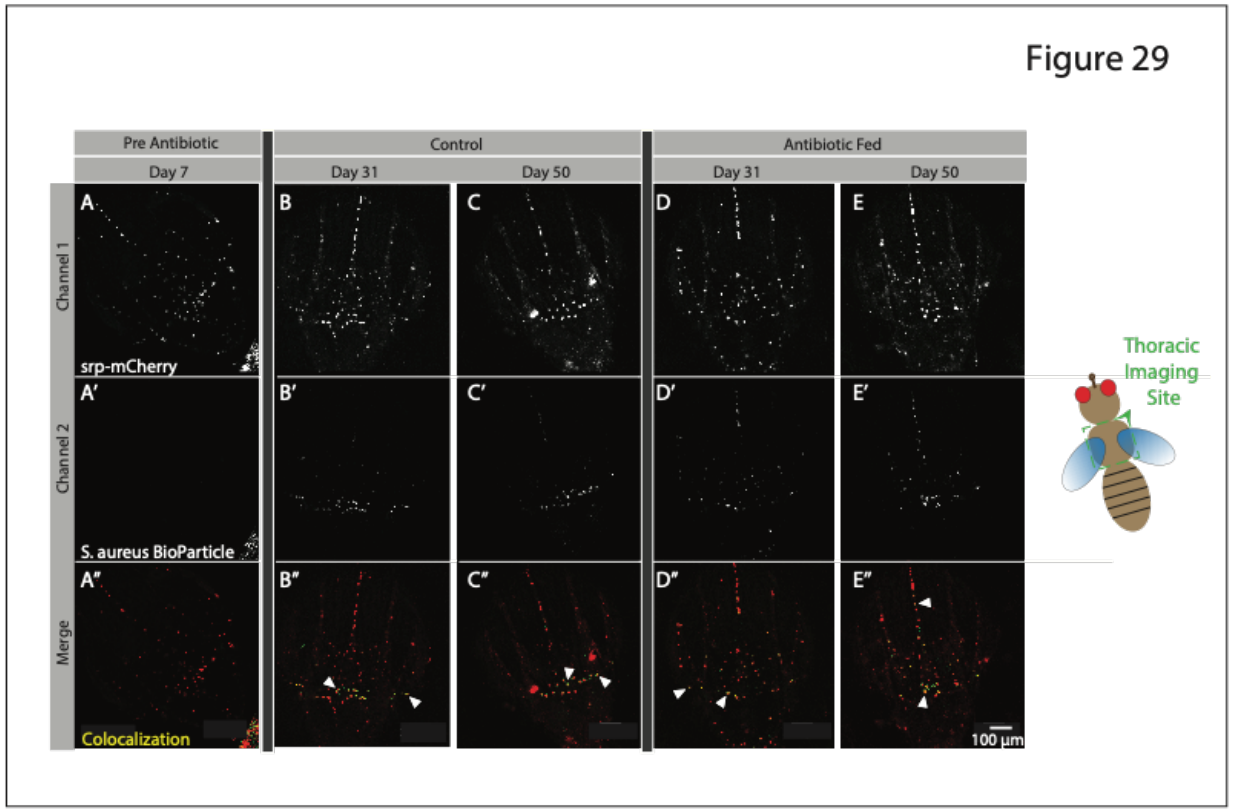

Figure 6.29: Confocal microscopy of changes in thoracic macrophage function assayed through live imaging colocalization assay - Antibiotic-fed flies marked with serpent-mCherry

Confocal images depict the thorax of antibiotic-fed female flies at 7, 31, and 50 days of adulthood. Representative max intensity projections from live imaging (A-E) show srp-mCherry marked sessile macrophages associated with the dorsal fly cuticle and *Staphylococcus aureus* Alexa Fluor488 BioParticles, labelled as Channel 1 and Channel 2 respectively. Colocalization between macrophages and *S. aureus* Bioparticles are shown in yellow (A"-E"). All flies were scored as non-Smurf prior to imaging. Antibiotic cocktail diet fed from 10 days of adulthood (D-E) and ethanol-control diet (B-C). Contrast uniformly increased for clarity using the *Enhanced True Color Contrast* function (Fiji). White arrows in merged images point to colocalization events. srp-mCherry = *w[1118];; srpHemo-3xmCherry/+*.

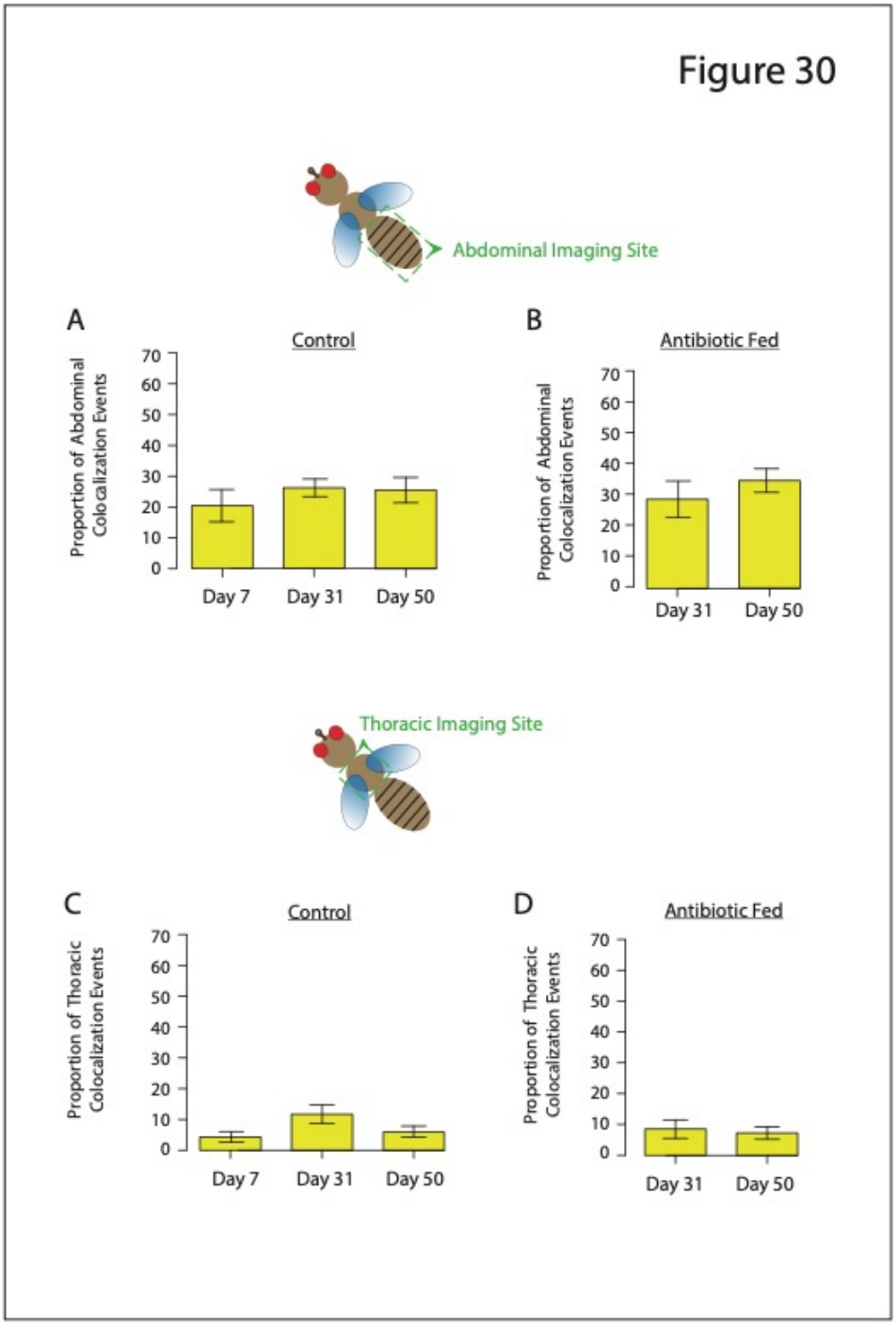

Figure 6.30: Macrophages marked with serpent-mCherry show no change in function with age even after antibiotic treatment

Quantification of live imaging colocalization events in antibiotic fed flies. Bar graphs show quantification of phagocytosing cells in the fly abdomen (A-B) and thorax (C-D) at regular intervals throughout fly lifespan. n = 5-7 flies/condition/time point. No significant changes, in One-way ANOVA/Kruskal-Wallis Test. Error bars show mean and SEM. srp-mCherry = w[1118];; srpHemo-3xmCherry/+.

6.6.2.3 Axenic flies endogenously marked with hemolectin-dsRed

Macrophage function was finally assayed in axenic and conventionally reared flies. Macrophage cells were endogenously marked with *hml-dsRed*. Similar to Section 6.6.2.1, *hml-dsRed* was used to corroborate macrophage function findings. In axenic flies, all dorsal cuticle associated macrophages showed unchanged phagocytic function with age (Figure 6.31 A"-C", Figure 6.32 A"-C", Figure 6.33 A, C). In conventional flies, all dorsal cuticle associated macrophages also showed unchanged phagocytic function with age (Figure 6.31 D"-F", Figure 6.32 D"-F", Figure 6.33 B, D). Axenic results indicate that phagocytic function in *hml-dsRed* marked sessile macrophage cells is unaffected by aging of the absence of bacteria.

6.6.2.4 Axenic flies endogenously marked with serpent-mCherry

Macrophage function was finally assayed in axenic and conventionally reared flies, this time endogenously marked with *srp-mCherry*. Similar to Section 6.6.2.2, *srp-mCherry* was used to corroborate macrophage function findings. In axenic flies, abdomen-associated sessile macrophages showed a significant decrease in phagocytic function with age (Figure 6.34 A"-C", Figure 6.36 A). Thorax-associated sessile macrophages showed a significant increase in phagocytic function at midlife, followed by a significant decrease in phagocytic function later in life (Figure 6.35 A"-C", Figure 6.36 C). In conventional flies, all dorsal cuticle associated macrophages show unchanged phagocytic function with age (Figure 6.34 D"-F", Figure 6.35 D"-F", Figure 6.36 B, D). These results indicate that phagocytic function in *srp-mCherry* marked sessile macrophage cells is affected by the absence of bacteria, showing changes with age not seen in conventionally reared flies.

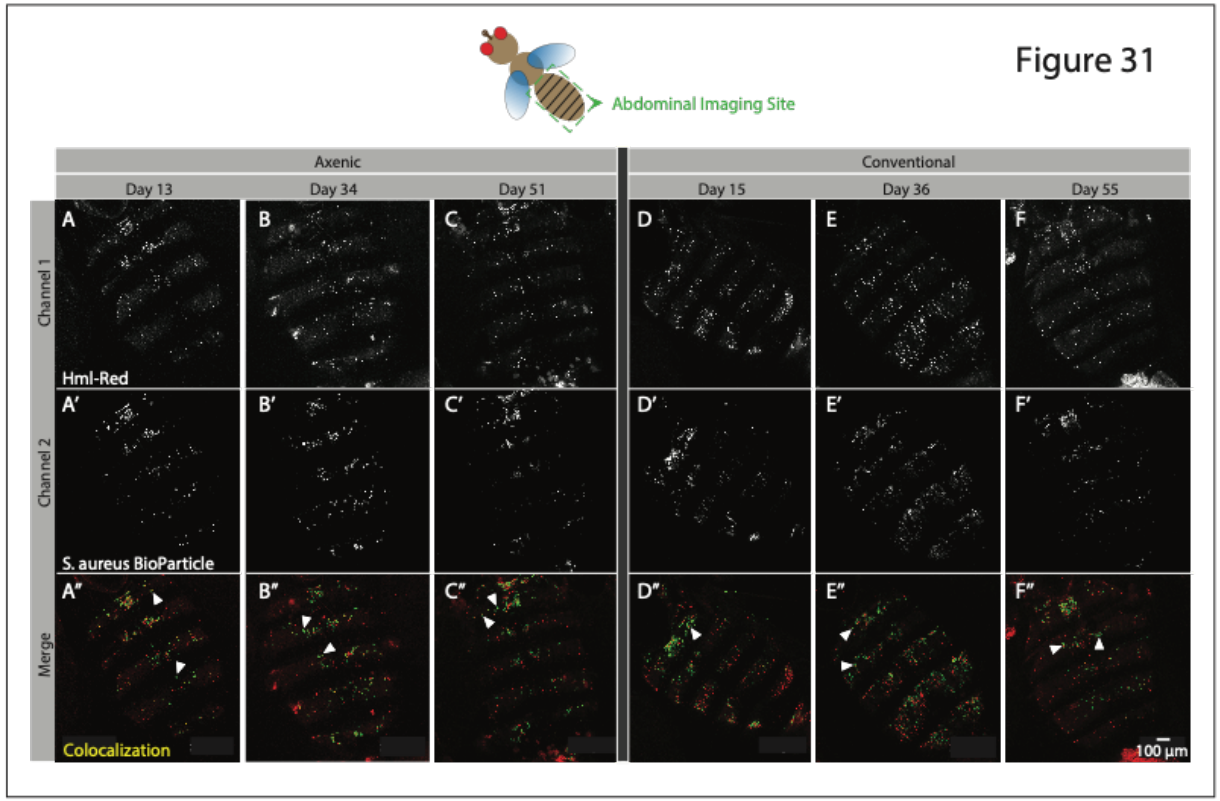

Figure 6.31: Confocal microscopy of changes in abdominal macrophage function assayed through live imaging colocalization assay - Axenic flies marked with Hemolectin-dsRed

Confocal images depict the abdomen of axenic and conventional female flies at 13, 34, and 51 days of adulthood. Representative max intensity projections from live imaging (A-F) show Hml-Red marked sessile macrophages associated with the dorsal fly cuticle and *Staphylococcus aureus* Alexa Fluor488 BioParticles, labelled as Channel 1 and Channel 2 respectively. Colocalization between macrophages and *S. aureus* Bioparticles are shown in yellow (A"-F"). Axenic flies developed and maintained on sterile media throughout adulthood (A-C) and conventionally reared controls (D-F). All flies were scored as non-Smurf prior to imaging. Contrast uniformly increased for clarity using the *Enhanced True Color Contrast* function (Fiji). White arrows in merged images point to colocalization events. Hml-Red = *w[1118]; HmlΔ-dsRed/+*.

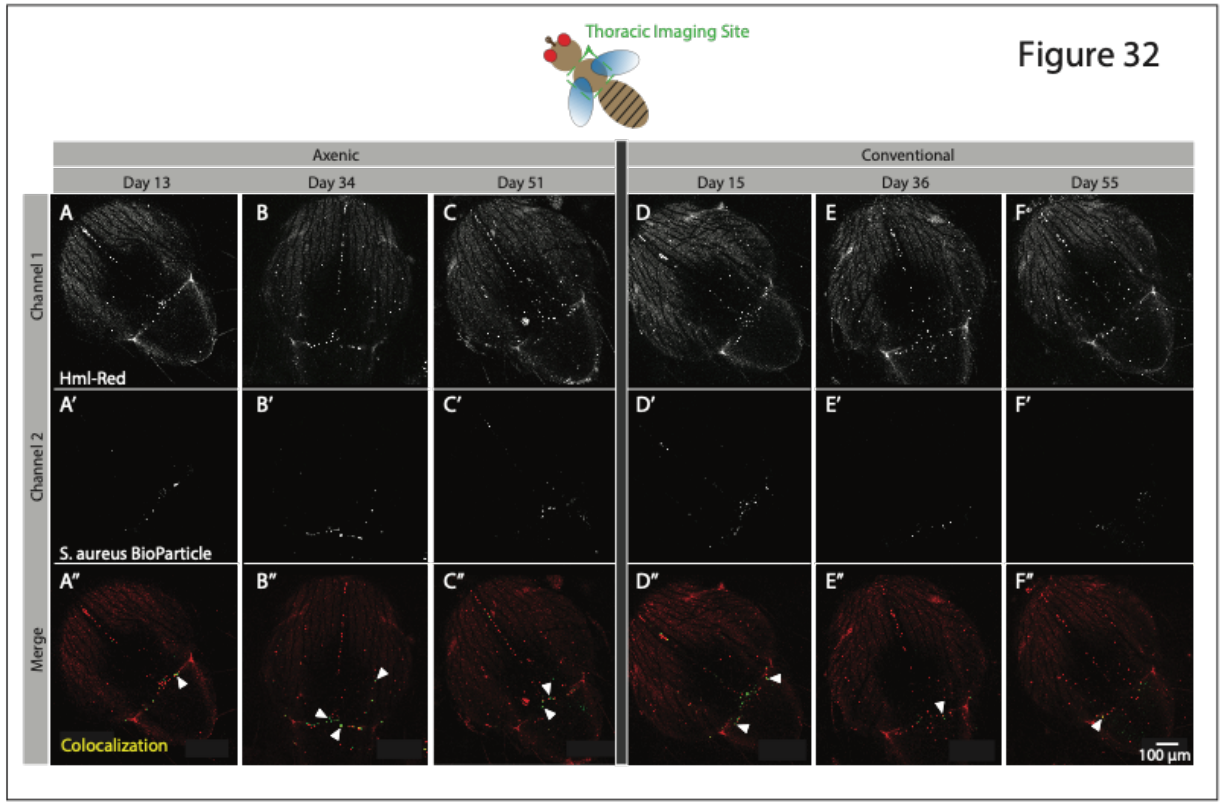

Figure 6.32: Confocal microscopy of changes in thoracic macrophage function assayed through live imaging colocalization assay - Axenic flies marked with Hemolectin-dsRed

Confocal images depict the thorax of axenic and conventional female flies at 13, 34, and 51 days of adulthood. Representative max intensity projections from live imaging (A-F) show Hml-Red marked sessile macrophages associated with the dorsal fly cuticle and *Staphylococcus aureus* Alexa Fluor488 BioParticles, labelled as Channel 1 and Channel 2 respectively. Colocalization between macrophages and *S. aureus* Bioparticles are shown in yellow (A”-F”). Axenic flies developed and maintained on sterile media throughout adulthood (A-C) and conventionally reared controls (D-F). All flies were scored as non-Smurf prior to imaging. Contrast uniformly increased for clarity using the *Enhanced True Color Contrast* function (Fiji). White arrows in merged images point to colocalization events. Hml-Red = *w[1118]; HmlΔ-dsRed/+*.

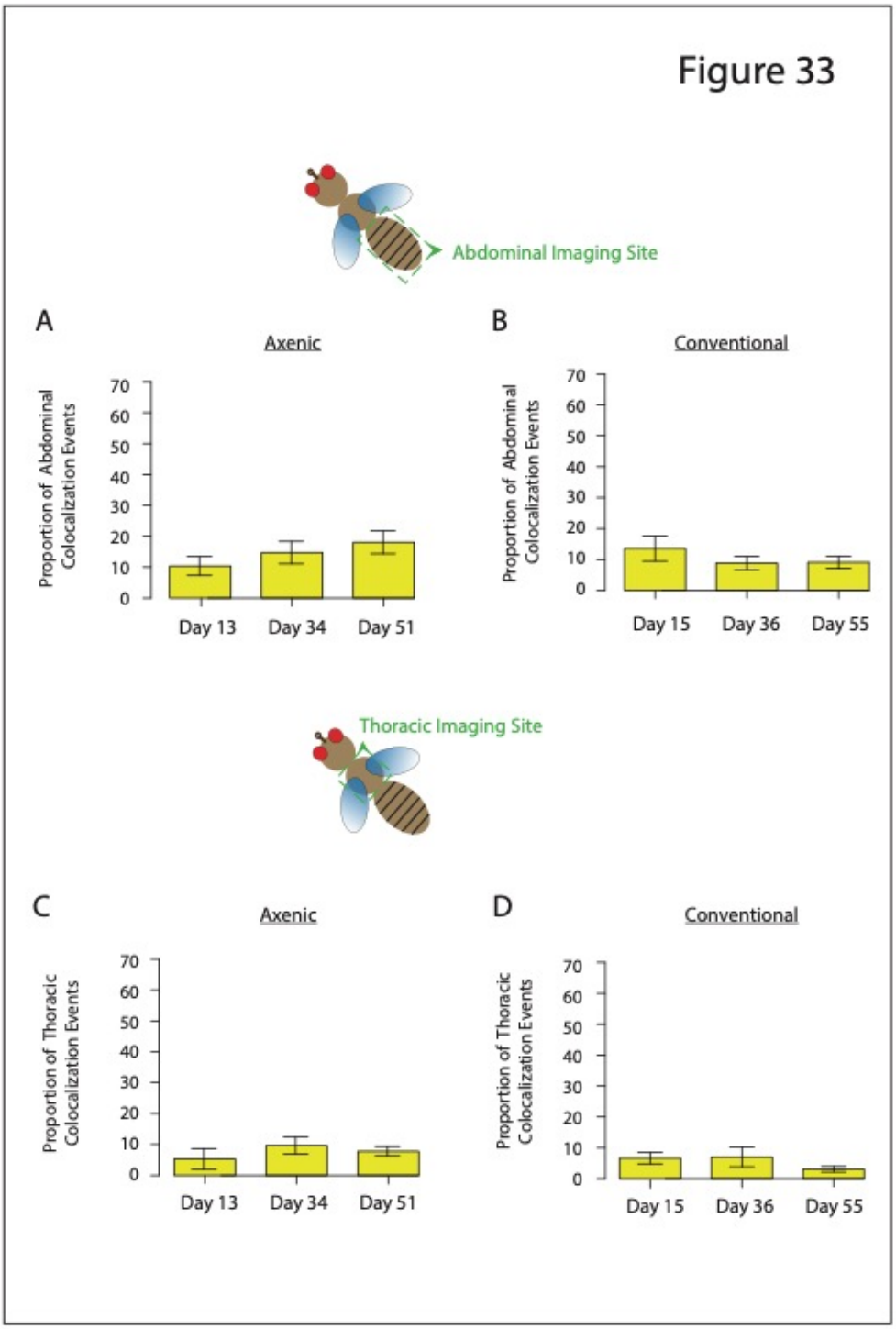

Figure 6.33: Macrophages marked with Hemolectin-dsRed show no change in function with age in entirely germ-free flies

Quantification of live imaging colocalization events in axenic and conventional control flies. Bar graphs show quantification of phagocytosing cells in the fly abdomen (A-B) and thorax (C-D) at regular intervals throughout fly lifespan. n = 5-6 flies/condition/time point. No significant changes, in One-way ANOVA/Kruskal-Wallis Test. Error bars show mean and SEM. Hml-Red = *w[1118]; HmlΔ-dsRed/+*.

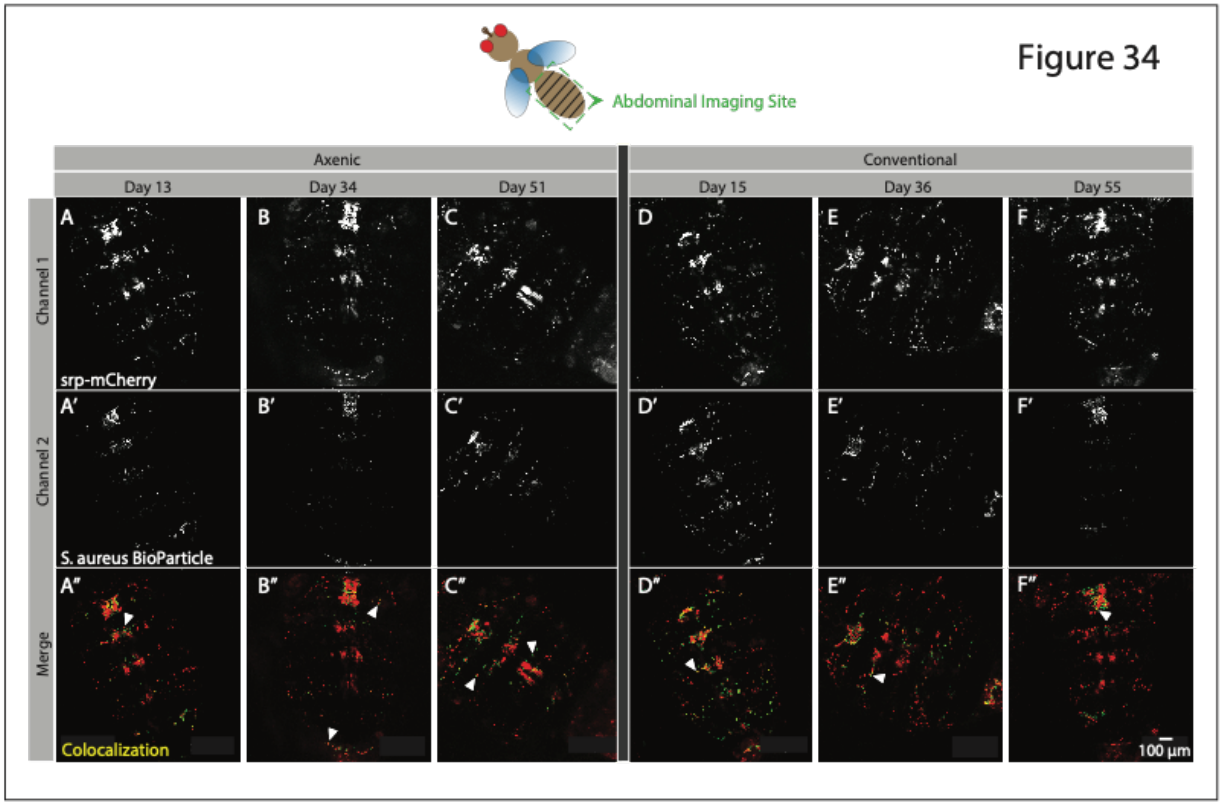

Figure 6.34: Confocal microscopy of changes in abdominal macrophage function assayed through live imaging colocalization assay - Axenic flies marked with serpent-mCherry

Confocal images depict the abdomen of axenic and conventional female flies at 13, 34, and 51 days of adulthood. Representative max intensity projections from live imaging (A-F) show srp-mCherry marked sessile macrophages associated with the dorsal fly cuticle and *Staphylococcus aureus* Alexa Fluor488 BioParticles, labelled as Channel 1 and Channel 2 respectively. Colocalization between macrophages and *S. aureus* Bioparticles are shown in yellow (A”-F”). Axenic flies developed and maintained on sterile media throughout adulthood (A-C) and conventionally reared controls (D-F). All flies were scored as non-Smurf prior to imaging. Contrast uniformly increased for clarity using the *Enhanced True Color Contrast* function (Fiji). White arrows in merged images point to colocalization events. srp-mCherry = *w[1118];; srpHemo-3xmCherry/+*.

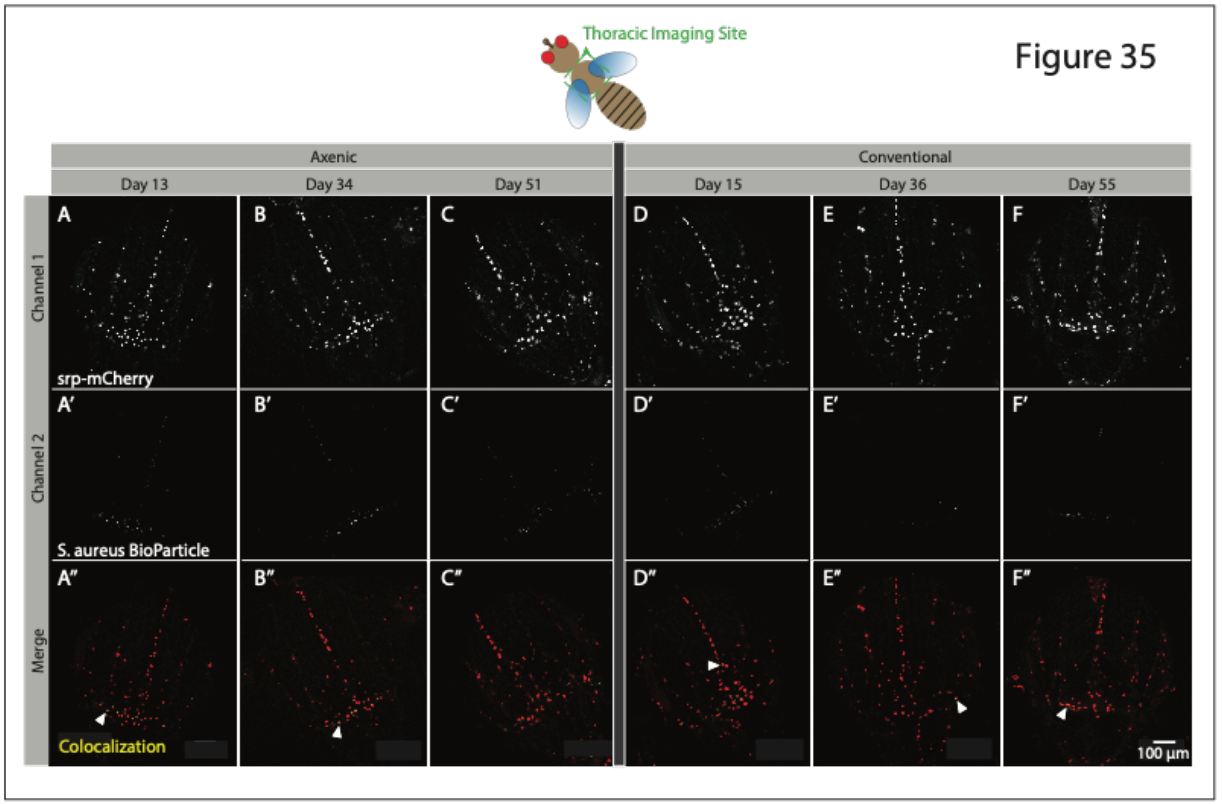

Figure 6.35: Confocal microscopy of changes in thoracic macrophage function assayed through live imaging colocalization assay - Axenic flies marked with serpent-mCherry

Confocal images depict the thorax of axenic and conventional female flies at 13, 34, and 51 days of adulthood. Representative max intensity projections from live imaging (A-F) show srp-mCherry marked sessile macrophages associated with the dorsal fly cuticle and *Staphylococcus aureus* Alexa Fluor488 BioParticles, labelled as Channel 1 and Channel 2 respectively. Colocalization between macrophages and *S. aureus* Bioparticles are shown in yellow (A"-F"). Axenic flies developed and maintained on sterile media throughout adulthood (A-C) and conventionally reared controls (D-F). All flies were scored as non-Smurf prior to imaging. Contrast uniformly increased for clarity using the *Enhanced True Color Contrast* function (Fiji). White arrows in merged images point to colocalization events. srp-mCherry = *w[1118];; srpHemo-3xmCherry/+*.

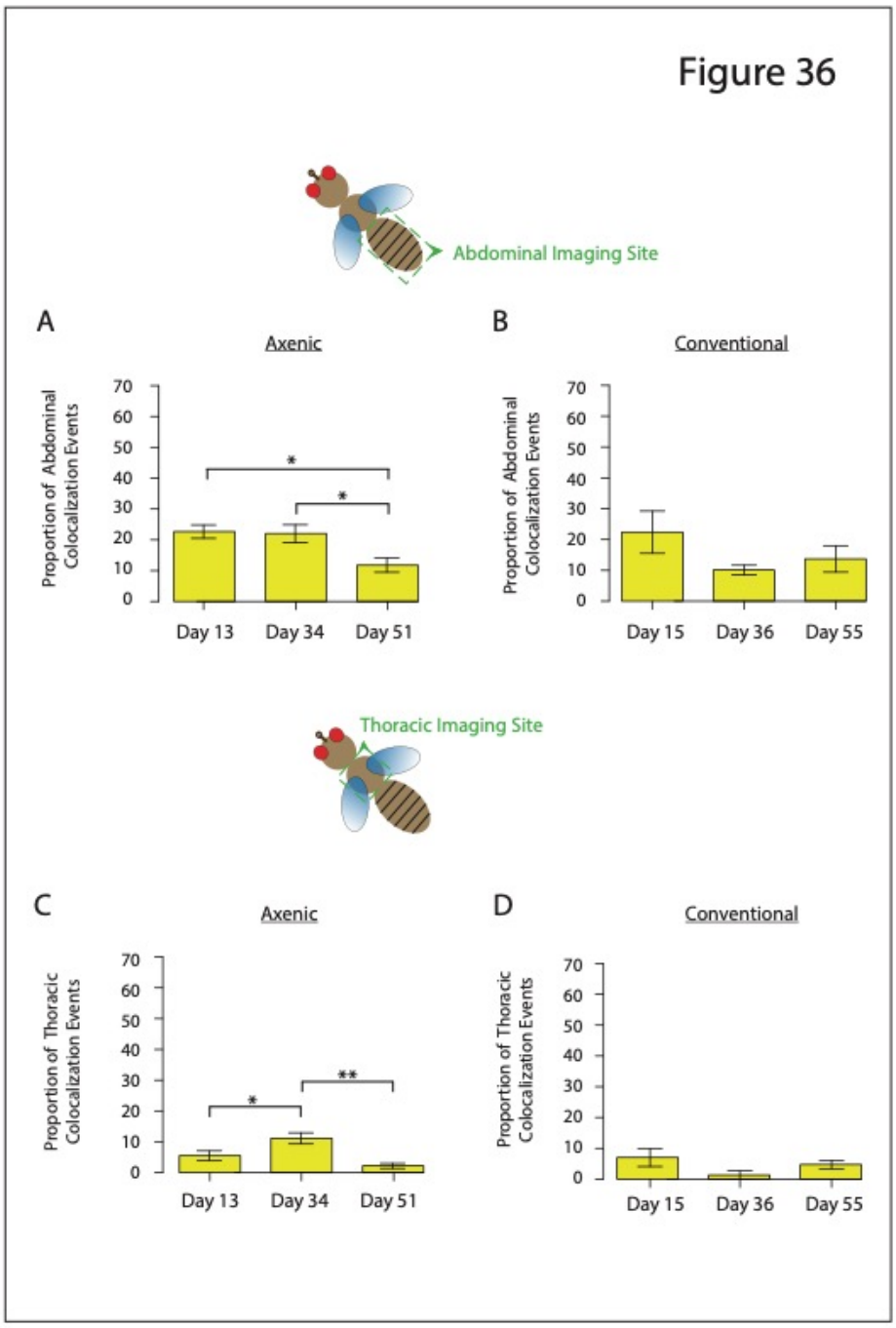

Figure 6.36: Macrophages marked with serpent-mCherry show a decline in function with age in entirely germ-free flies

Quantification of live imaging colocalization events in axenic and conventional control flies. Bar graphs show quantification of phagocytosing cells in the fly abdomen (A-B) and thorax (C-D) at regular intervals throughout fly lifespan. n = 5-6 flies/condition/time point. p-value <0.05 = *, <0.01 = **, in One-way ANOVA/Kruskal-Wallis Test, only significant changes shown. Error bars show mean and SEM. srp-mCherry = *w[1118];; srpHemo-3xmCherry/+*.

6.7 Discussion

6.7.1 Overview

Taken together, data from this chapter show that intestinal barrier dysfunction impacts macrophage number – in some cases this change is independent of bacteria. Subpopulations of phagocytic cells may be present in the adult and change in proportion with age, complicating data interpretation. Finally age-related decreases in macrophage function are not always recorded, but where they are they are delayed in the absence of bacteria. The following questions remain after data analysis and will be further discussed as part of my data interpretation (1) Does immune dysregulation of macrophage cells occur after dysbiosis or barrier dysfunction? (2) How does the viability/function of macrophages change with age and in Smurfs.

6.7.2 How are pre-Smurf and Smurf flies impacting macrophage decline with age?

Data presented in this chapter show that age-associated loss of barrier function is correlated with changes in circulating as well as sessile macrophage populations. This presents the question, what specific aspects of barrier dysfunction are responsible for changes seen in macrophage number/function? Chapter data show that systemic immune activation, but not intestinal immune activation, significantly increases the number of *hml-GFP* marked sessile macrophages in both pre-Smurf and Smurf flies. This raises the question of whether other stress/damage signals, known to be impacted by ageing and/or gut decline, could have a role here. For example, the role of the JNK pathway could be tested through construction of the following transgenic line: *TIGS>Hml Red; UAS-Hep [CA]*. Key assays conducted in this chapter i.e., macrophage counts, phagocytic assays, etc. could then be repeated to assess the impact of JNK signaling on these readouts. Similarly, the effects of cell adhesion (or rather the breakdown of cell adhesion in Smurf

flies) could be addressed with construction of the following line: *UAS-ssk RNAi, Hml-dsRed; TIGS* and, again, repeating key assays in conventional and axenic flies to see how macrophages are impacted by epithelial junction knockdown.

6.7.2.1 Distress signals from the aging gut may drive macrophage changes

Chapter data show that differences in macrophage cells are largely post-Smurf, rather than age-related. For this reason, a post-Smurf timeline becomes more important. This thesis has already discussed several potential signals that may be important in regulating macrophages – in response to intestinal decline. As mentioned in the previous section, multiple signals are known to be impacted by age-related decline. For example: reactive oxygen species, responses to apoptosis i.e., reaper, JNK, Jak/STAT, IMD pathway activity. To establish which of these may be relevant in this context readouts of these signals could be measured in dissected gut samples from *hml-dsRed /GFP* and *srp-mCherry* lines over an aging time course and in Smurf flies. Where there is an indication that any of the signals listed above are candidates for the "gut damage" signal, a respective *UAS-RNAi* for our target gene of interest could be used to inhibit the signal from the gut or to block receipt of the signal in the macrophage cells.

6.7.3 Microbiota impact on macrophage decline

My data suggests that bacteria may not be responsible for observed age-related macrophage changes. In fact, bacterial presence seems to facilitate macrophage phagocytosis for longer. Indicating that bacteria-mediated mechanisms may be necessary for maintenance of macrophage function with age. Constitutive immune activity, however, seems to be a catalyst in macrophage dysregulation. Since we know that immune activation drives a "leaky gut" phenotype, are microbes leaking out of the gut and driving

macrophage decline? If so, how would this impact macrophage efficacy? Unpublished data (conducted by former Clark Lab student, Ellie Hughes) shows that a commensal bacterial infection, via injection, can induce an immune response. Further, published work by Salazar and colleagues shows an increased bacterial concentration in adult fly circulation, following barrier dysfunction (Salazar et al., 2018). Indicating that bacteria can, and indeed do, escape the gut following loss of barrier function.

6.7.4 Are macrophage changes in Smurfs due to cell migration or changes in cell gene expression?

Differences in the number of macrophages detected through the adult fly cuticle may be linked to an increase in cell numbers through the production of new cells, the migration of circulating cells to the tissue-associated population, or to marker overexpression. In other words, an increase in fluorescence could be recorded as an increase in macrophage number in Smurfs. Distinguishing between these possibilities is challenging. However, several experiments are possible that could provide some indication of how best to interpret these data. For example, to discern whether macrophage cell number changes are a product of new cells or cell migration, could be looked at indirectly through live imaging followed by extraction of total hemocytes from the same fly allowing comparison of the size of the two pools. However, what's really needed is a before/after comparison across the Smurf boundary which is impossible given that the fly needs to be sacrificed for the total cell counts.

The question of whether marker expression is changing is also difficult to address. Quantitative PCR could be used to test for changes in whole fly expression in each condition to give an initial idea. Whether expression in hemocytes specifically changes could be tested using FACS to sort and count the cell population followed by qPCR to

measure marker expression which could then be normalized to cell number. This would tell us whether expression is in fact changing. If it is, however, the impact of that on the cell counts is hard to address.

6.7.5 Does macrophage function only decline following barrier loss?

In contrast to previous reports, the data presented here do not show a consistent decline in macrophage function, as measured by phagocytic ability, with age. However, these experiments were limited to non-Smurf flies, leaving open the possibility of macrophage dysfunction associated with barrier loss. This could be addressed through ex vivo phagocytosis experiments with fluorescent-labelled bacteria i.e., *srp-mCherry* line and GFP labelled-*E.Coli* or *hml-GFP* line and mCherry labelled-*L.plantarum*. This ex vivo technique would allow for Smurf macrophage viability and clearance function to be tested – as there were technical challenges associated with the blue dye during phagocytosis assay live-imaging. Modifications of this technique could include microinjection of flies with above mentioned fluorescent bacteria, followed by macrophage extraction or "bleeding". This would allow for comparisons between gut versus systemic impacts on macrophage function to be measured. For example, macrophage uptake could be visualized and recorded on an Axiovert Apotome microscope, followed by analysis of video data to determine rate of engulfment between different conditions. This would allow a much more detailed assessment of changes to phagocytic function beyond the current recording of numbers of successful phagocytic events.

6.7.6 Important subpopulation consideration for differential changes in macrophages

Existing evidence corroborates the existence of different subpopulations of macrophages in the adult fly (Sanchez Bosch et al., 2019, Clark et al., 2011). My data show that different

patterns of localization are associated with different endogenous macrophage markers. *srp-mCherry* localizes mostly around the dorsal vein, whereas *hml-dsRed* and *hml-GFP* localize more uniformly around the body cavity, with a slight concentration around the cardia (or fly 'heart'). For this reason, experimental assays looked at sessile macrophages associated with the abdomen and thorax separately. Microenvironments highlighted by (Sanchez Bosch et al., 2019), mean that minute changes may have otherwise been missed had findings been analyzed together as just 'dorsal cuticle' macrophage counts. This is an important point, my data consider the anatomy that is individual to the thorax and abdomen, respectively. For example, most of the fat body is in the fly abdomen, while respiratory airways and muscle predominate in the thorax (Demerec, 1994b). To better discern if/how subpopulations of macrophages are behaving, macrophage cells from *hml-GFP/+; srp-mCherry/+* could be extracted from the whole fly to quantify changes in cell ratio with age and in Smurf flies. Ex vivo phagocytosis experiments could also help discern changes in function in different subpopulations with age and barrier loss.

6.7.7 Summary

Due to the complex nature of this work, my data offers more questions than answers. Could immune activation with age be a product of decline in hemocyte function due to barrier loss? Can we disrupt receipt of a gut damage signal in macrophages and prevent the dysregulation observed in Smurfs? Could blocking damage signals during aging prevent changes in macrophage number/function and extend lifespan? One finding, however, consistently stands out – it is the loss of barrier function, not age, not bacteria, that drives consistent decline.

Chapter 7: Thesis Discussion

7.1 Summary of thesis findings

This thesis aimed to understand the consequences of age-associated inflammation on the gut. Throughout the course of this doctorate, work uncovered that while inflammation can drive dysbiosis and ultimately fly death – there is an intermediate link, barrier dysfunction. The following is a summarized list of findings presented in this thesis that help support the conclusions summarized in Figure 7.1.

- Immune activation drives dysbiosis largely via its impact on barrier permeability
- Immune activation alone is sufficient to drive barrier loss and mortality
- Current tools are limited to properly address tissue specificity
- Immune activation, the microbiota, age, and barrier status all impact the macrophage population and impact different subsets/markers in different ways. The consequences of this for immune and metabolic activities of macrophages and so for age-related decline remain to be determined.

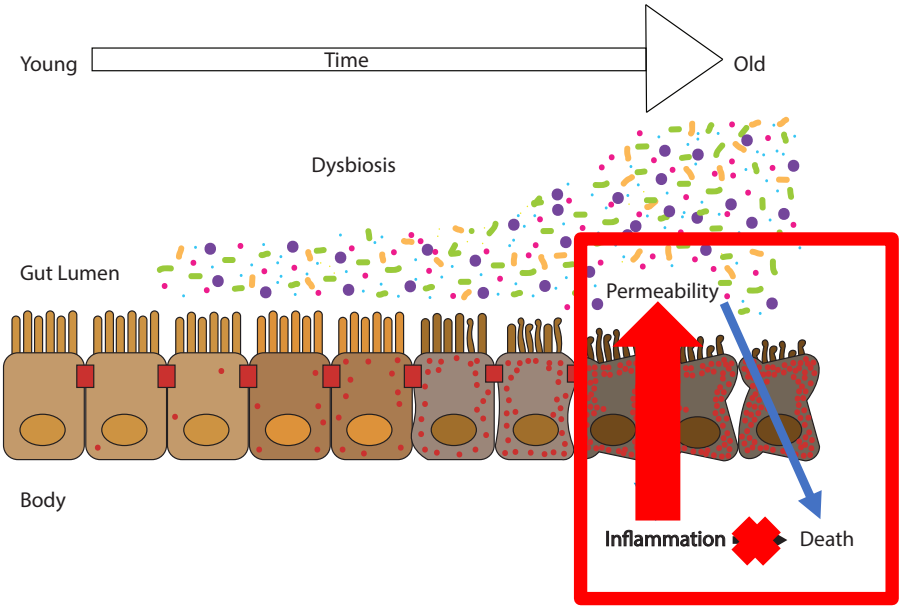

Figure 7.1: Representation of age-associated intestinal decline

In contrast to Figure 1.1, thesis data show inflammation (or immune activation) drives gut permeability (or barrier dysfunction). Loss of intestinal barrier function triggers dysbiosis and results in fly death, regardless of chronological age.

7.2 Implications of thesis findings for the field

The data presented in this thesis offers an alternative hypothesis for the role of immune activation, hereafter referred to as 'inflammation' in age-related intestinal decline. Previously published works have repeatedly shown that bacterial imbalance, immune dysfunction, and loss of epithelial homeostasis are precursors to death in the fly. Further, published works suggest a potential timeline for when the above-mentioned aging hallmarks occur. Typically, this sequence of events starts with immune dysfunction, followed by dysbiosis, resulting in loss of intestinal stem cell homeostasis and fly death (Figure 7.2).

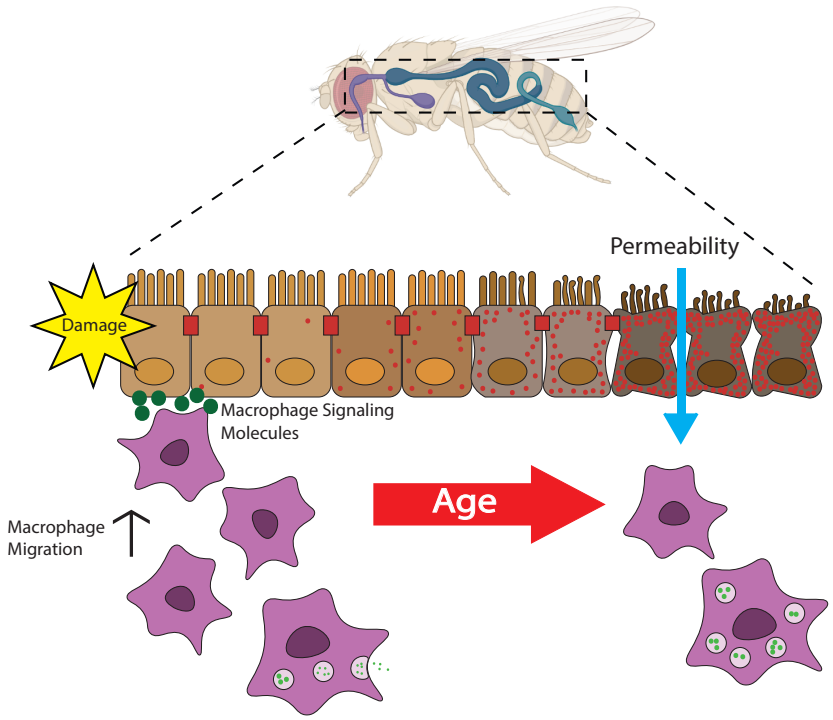

Figure 7.2: Current understanding of age-associated intestinal decline

Schematic depiction of themes covered during this thesis, specifically pertaining to "gut damage" associated with age-related decline – shown here as permeability or barrier dysfunction. *Drosophila* icon was generated using templates in BioRender.com.

Interventions at any of these steps typically are sufficient to rescue, and in some cases extend, lifespan. This oversimplified interpretation is not meant to take away from the complexity of this work, but to give a reference point for how these thesis findings fit into the breadth of currently published literature. These thesis findings offer a new interpretation for how immune-induced gut decline impacts fly health. However, there are many questions that arise from the data presented herein; many of which are inherently due to the interconnected networks and complex dynamics between immunity, microbiota, gut health, and aging. The remainder of this discussion section will consider the larger implications of findings from this thesis, with a focus on how presented data contribute to understandings of key areas of interplay i.e., loss of intestinal barrier dysfunction as a key driver of bacterial growth.

Here data have shown that immune activation sufficiently drives barrier dysfunction, without 'help' from bacteria. The larger questions presented because of this finding include, how, from a mechanistic standpoint, is immune activation driving intestinal barrier loss? The relationship between barrier loss and other aspects of intestinal homeostasis remains unclear and need to be looked at carefully. Thesis data have also shown that barrier loss is consistently and effectively a driver of dysbiosis in the fly. This presents several questions pertaining to why and how epithelial barrier loss enables bacterial overgrowth. Specifically, why do only specific bacterial species benefit from immune activation alone? Why, in contrast, do most bacterial species and/or strains seem to respond to increased barrier permeability? In the context of currently published literature, this measurement of intestinal barrier status is often missing. Importantly, disregarding barrier status limits what can be learned about the mechanisms driving dysbiosis. This thesis highlights this point further by showing that the macrophage population in adult flies may be more complex than previously appreciated. Macrophage cells appear to be affected by age-related changes in the gut and by immune activation in complex ways. Perhaps echoing the complex immune cell subsets observed in mammalian systems? While many of these complex questions can still best be answered in the *Drosophila* model system, these thesis findings further highlight the need for new tools in the field if we are to truly address questions regarding tissue specificity. Collectively the field must ask whether true tissue specificity is possible, and whether it is biologically relevant and worth the investment of time and resources.

7.3 Wider implications and translational nature of thesis findings

Several studies from multiple model organisms have highlighted intestinal barrier permeability as a key feature of aging and a driver for microbial dysbiosis and age-related inflammation. This work has covered diverse organisms from worms to zebrafish (Dambroise et al., 2016) and from mice (Thevaranjan et al., 2018) to non-human primates (Mitchell et al., 2017). There is also strong evidence that age-related inflammation is a driver of health decline across multiple tissues and organ systems.

Recently published work in centenarians suggests inflammatory status is a better predictor of successful aging than telomere length (Arai et al., 2015). This finding is of great interest to the field as inflammation is widely considered to be a consistent biological precursor of aging. From their findings Arai et al. suggest that immune suppression is a major determinant of longevity. There are prominent health conditions associated with both inflammation and aging (Buford, 2017). Many of these conditions span an array of organ systems, the deleterious effects of which stem from impaired inflammatory resolution. Collectively the field is starting to build a narrative that links inflammation, gut health, and aging. These factors are interconnected, starting with predominantly environmental risk factors which facilitate chronic inflammation and microbial imbalance. Ultimately culminating in age-associated inflammatory conditions.

7.3.1 Studies of intestinal permeability in higher vertebrates

In higher order species permeability has been largely studied as it relates to chronic disease i.e., rheumatoid arthritis and in patients with other co-morbidities such as intensive care unit (ICU) patients (Otani and Coopersmith, 2019, Martel et al., 2022). It is well documented that leaky gut is present and prevalent in ICU patients (Iacob and Iacob, 2019). Thus far, however, work has largely focused on correlative measures associated

with leaky gut microbial translocation. This places endotoxemia as an important instigator of immune activation. Although current work provides context for age-related barrier dysfunction, we are still lacking in-depth understanding of key mechanisms driving gut epithelial changes.

7.3.1.1 Gut permeability in humans

Patients which have been admitted to the ICU are the predominate population of humans of humans in which intestinal permeability has been studied (Otani and Coopersmith, 2019). Researchers have found that ICU patients experiencing sever septic illness or bacterial infection are more susceptible to intestinal permeability. Endotoxemia further exacerbates a cycle of systemic inflammation and worsening barrier permeability. This crosstalk aspect of gut-originating systemic immunity is clearly illustrated in patients suffering from rheumatoid arthritis (RA) (Matei et al., 2021). In RA patients' higher serum levels of intestinal content markers simultaneously presents as increased severity of the auto-immune disease (Matei et al., 2021). There are interventions associated with mitigating impacts of endotoxemia in humans by reinforcing the gut barrier e.g., reintroduction of dietary fiber, exercise, dietary fish oil (Martel et al., 2022). Although these interventions decrease plasma levels of permeability markers, even the healthiest of aged humans continue to experience loss of barrier function with age.

7.3.1.2 Gut permeability in non-human primates

Work conducted by the Kavanagh Lab in small cohorts of young versus old female vervet monkeys (*Chlorocebus aethiops sabeus*) provided a necessary control for gut permeability research. Further, high fat diet and increased sugar uptake are external factors responsible of increased microbial translocation and endotoxemia. Because obesity is a prevalent

human disease, it "confounds" aging and intestinal barrier function studies in humans. Studies from Kavanagh and colleagues allowed for characterization of aging gut phenotypes without comorbidities and other pharmacological studies typically conduced in the intensive care unit (Mitchell et al., 2017, Wilson et al., 2018).

Mitchell et al. created a baseline for the aging intestine in higher vertebrates, further corroborating the Smurf phenotype in a monkey model of aging. The authors generate results from intestinal motility assays (like the T.U.R.D assay in flies), intestinal permeability assays using oral administration of fluorescein-isothiocyanate conjugated dextran 40KD (like the Smurf assay in flies), and gross fecal analysis used as an umbrella approach for measuring bacterial load (Mitchell et al., 2017).

Wilson et al. found that barrier dysfunction increases with age as measured by microbial translocation - assayed as endotoxin in circulation. Data showed no change in bacterial composition but did suggest an increase in bacterial abundance and immune markers (Wilson et al., 2018), both hallmarks of a leaky gut in *Drosophila* (Rera et al., 2012). Wilson et al. took finding from Mitchell et al. further by hypothesizing that the barrier dysfunction observed with old age would be improved with SBI oral dosing. SBI (or serum bovine immunoglobulins) is a clinically used non-absorbable protein product that captures pathogen generated immunoglobulins. This study shows that SBI at old age is ineffective and does nothing to repair intestinal barrier function (Wilson et al., 2018); much like other pharmacological drugs aimed at sequestering endotoxins (Sandler et al., 2014). Thus, indicating that a more targeted intervention is necessary, on that can only be developed upon understanding the mechanism behind immune-induced barrier dysfunction.

7.3.1.3 Gut permeability in murine models

Work pertaining to immune dysfunction and gut permeability in colitis patients is also recapitulated in colitogenic mice models. For example, Burrello et al. have shown the importance of immune cells in mediating intestinal homeostasis (Burrello et al., 2018). Colitogenic mice were administered fecal microbiota transplantation (FMT), providing changes to the composition of intestinal microbiota. Ecological shift in intestinal microbiota were sufficient to induce differential responses from gut associated immune cells. Burrello and colleagues' findings suggest that pathogen detection via immune cells was altered, such that greater expression of interleukin-10 (IL-10) was observed. Data suggest that IL-10 participates in tolerance mechanisms aimed at maintaining intestinal homeostasis as it regards to immune and microbe dynamics (Burrello et al., 2018). Taken together, Burrello et al. suggest that FMT instigates increased IL-10 secretion from immune cells, resolving dysbiosis induced inflammation, ultimately facilitating intestinal restoration and homeostasis.

7.3.2 Filling the gaps in mammalian gut permeability studies

Discussion of mammalian works provides further corroboration of the effects of barrier dysfunction on intestinal disease. It is known that gastrointestinal infections, as well as inflammatory bowel disease (IBD) (i.e., Ulcerative colitis and Chron's disease) are the consequence of immune-induced breakdown of intestinal barriers. These diseases are associated with genetic and environmental factors which lead to intestinal barrier dysfunction (Martel et al., 2022). Studies in human subjects have further shown that bacterial DNA increases in the blood of IBD patients compared with healthy patients.

Importantly, however, healthy aged humans still experience leaky gut and chronic low-grade inflammation. With age, serum levels of zonulin increase in concentration, even in healthy aged cohorts (Qi et al., 2017, Buford, 2017). Zonulin is a human analog of zonula occludens toxin (Zot) – an enterotoxin associated with *Vibrio cholera* (Sturgeon and Fasano, 2016, Fasano, 2020). Like Zot, human zonulin modulates epithelial tight junctions and induces leaky gut (Fasano et al., 1991). Still, what is the role of gut barrier disruption in chronic inflammation with age? And can aging be delayed by treatments aimed at maintaining or restoring diseased gut barrier loss, e.g., fiber, probiotics, vitamin D, and other targeted drugs? There first must be an understanding of the sequence of events to best create a plan for preventative treatment. *Drosophila* and its respective tools are tailormade for foundational work of this nature.

7.3.3 Precedent for the importance of Drosophila studies in translation research

The vertebrate research community has only just started to study barrier permeability from a from a pathophysiology of aging perspective. Up until now, this hallmark phenotype has only been characterized at the center of chronic disease (Wilson et al., 2018). In other words, even though intestinal barrier dysfunction occurs across model systems, the leaky gut has only been characterized as a predictor of death in invertebrate models.

7.3.3.1 From flies to mice

Findings from foundational work in the fly by Clark et al. have been further corroborated in murine models (Clark et al., 2015, Thevaranjan et al., 2018). Tumor necrosis factor (TNF) is a pro-inflammatory cytokine, which when upregulated, increases intestinal permeability and results in immune cell decline. Thevaranjan et al. observe that old mice show increased permeability at the colon and increased bacterial products in circulation.

Germ-free old mice show a decrease in IL-6 levels with age and under LPS (lipopolysaccharide found on the outer membrane of gram-negative bacteria) injection, macrophage function does not decline under germ-free conditions (Thevaranjan et al., 2018). Taken together, these findings indicate that not only in barrier permeability a harbinger of death in the fly, but also that it remains a conserved predictive phenotype in higher vertebrates.

7.3.3.2 From flies to humans

The work conducted throughout the course of this thesis provides foundational insight and techniques that could be used, and have been used, in a medical setting. Angarita and colleagues have made use of the Smurf assay (detailed in Section 2.3) to detect loss of barrier integrity in ICU patients (Angarita et al., 2019). Physicians amended this non-invasive assay, still using the same FD&C Blue Dye No. 1, expanding its utility to a clinical setting where loss of barrier integrity is largely regarded as fundamental to pathogenesis of disease as well as age-induced decline i.e., sepsis/multiple organ failure.

7.4 Final questions and the directions for future work

The data presented in this thesis highlights the role of age-related inflammation as a driver of intestinal barrier permeability, as well as a consequence of it. This leaves us with several questions: 1) What is the initial instigator of age-related intestinal inflammation? 2) By what mechanism(s) does inflammation drive barrier permeability? 3) Can these mechanisms provide a target for antiaging therapies?

Factors responsible for initiating chronic inflammation with age have not been fully defined, in large part because of the complexities involving microbes, organ-organ communication, immune pathway crosstalk, etc. While there are other theories regarding

aging, we are looking at how extrinsic factors – mainly loss of barrier function – are responsible, in part, for the changes being seen with age. Results in humans are sparse and conflicting.

Importantly, in the context of human health understanding the underlying drivers of age-related decline enables the targeted development of potential therapies. Given the complex interplay between the immune system, intestinal epithelium and microbial populations, studies in similar model organisms such as the fly have a key role to play in defining these underlying mechanisms.

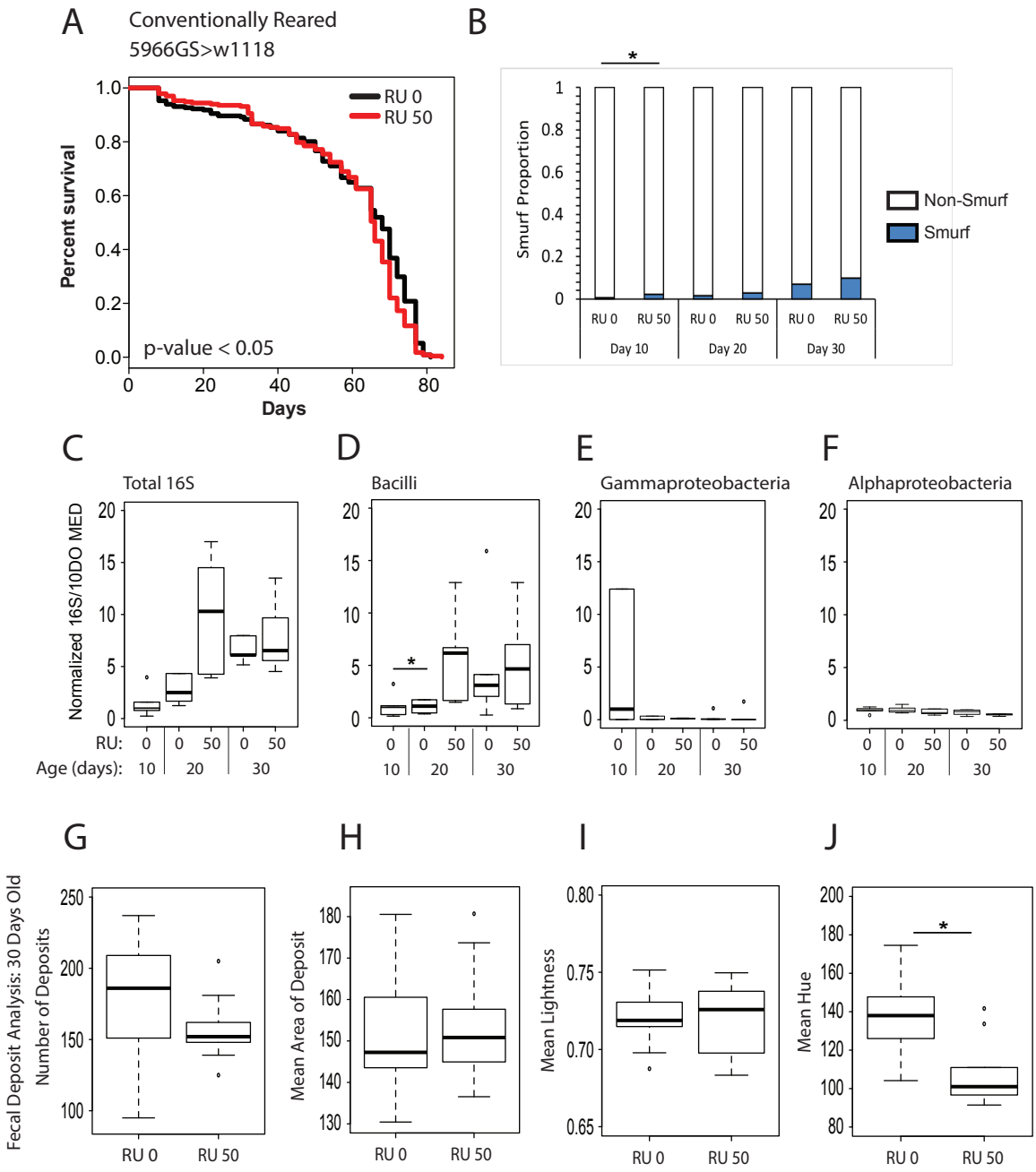

Appendix 1:
Conventionally Reared *5966-GS > w[1118]* Negative Control Data

A.) Fly lifespan was not affected by RU treatment. Survival curves for *5966-GS > w^{1118}*, female flies fed 50 µg/ml of RU486 (RU 50), or equal volume of ethanol (RU 0), from day 10 of adulthood. n = >200 flies/condition. No significant difference in log rank test.

B.) Smurf proportions were not affected by RU treatment. Smurf status was assayed at regular intervals throughout the lifespan at day 10, 20, and 30. Stacked bar graphs show female flies fed 50 µg/ml of RU486 (RU 50), or equal volume of ethanol (RU

0), from day 10 of adulthood. n = >200 flies/condition. p-value <0.05 = * in Binomial Test, only significant changes shown.

C.) Whole fly internal bacterial load was not affected by RU treatment. Bacterial levels assayed by RT-qPCR of 16S with universal primers in non-Smurf female flies fed 50 μg/ml of RU486 (RU 50), or equal volume of ethanol (RU 0), from day 10 of adulthood. n = 5 replicates of five surface-sterilized flies. No significant difference in Wilcoxon Test.

D.) *Bacilli* proportions were not affected by RU treatment. Bacterial levels assayed by taxon-specific RT-qPCR of the16S rRNA gene in non-Smurf female flies fed 50 μg/ml of RU486 (RU 50), or equal volume of ethanol (RU 0), from day 10 of adulthood. n = 5 replicates of five surface-sterilized flies. p-value <0.05 = * in Wilcoxon Test, only significant changes shown.

E.) *Gammaproteobacteria* proportions were not affected by RU treatment. Bacterial levels assayed by taxon-specific RT-qPCR of the16S rRNA gene in non-Smurf female flies fed 50 μg/ml of RU486 (RU 50), or equal volume of ethanol (RU 0), from day 10 of adulthood. n = 5 replicates of five surface-sterilized flies. No significant difference in Wilcoxon Test.

F.) *Alphaproteoacteria* proportions were not affected by RU treatment. Bacterial levels assayed by taxon-specific RT-qPCR of the16S rRNA gene in non-Smurf female flies fed 50 μg/ml of RU486 (RU 50), or equal volume of ethanol (RU 0), from day 10 of adulthood. n = 5 replicates of five surface-sterilized flies. No significant difference in Wilcoxon Test.

G.) Number of quantified fly excrements were not affected by RU treatment. T.U.R.D assay completed in n = 10 replicate groups of ten female non-Smurf flies at 30-days old, fed 50 μg/ml of RU486 (RU 50), or equal volume of ethanol (RU 0), from day 10 of adulthood. Boxplots display the first and third quartile, with the horizontal bar at the median. No significant difference in Wilcoxon Test.

H.) Area of quantified fly excrements were not affected by RU treatment. T.U.R.D assay completed in n = 10 replicate groups of ten female non-Smurf flies at 30-days old, fed 50 μg/ml of RU486 (RU 50), or equal volume of ethanol (RU 0), from day 10 of adulthood. Boxplots display the first and third quartile, with the horizontal bar at the median. No significant difference in Wilcoxon Test.

I.) Concentration of fly excrements were not affected by RU treatment. T.U.R.D assay completed in n = 10 replicate groups of ten female non-Smurf flies at 30-days old, fed 50 μg/ml of RU486 (RU 50), or equal volume of ethanol (RU 0), from day 10 of adulthood. Boxplots display the first and third quartile, with the horizontal bar at the median. No significant difference in Wilcoxon Test. Lightness = dye concentration/diuresis

J.) Fly excrements were made moderately more acidic by RU treatment. T.U.R.D assay completed in n = 10 replicate groups of ten female non-Smurf flies at 30-days old, fed 50 μg/ml of RU486 (RU 50), or equal volume of ethanol (RU 0), from day 10 of adulthood. Boxplots display the first and third quartile, with the horizontal bar at the median. p-value <0.05 = *, in Mann-Whitney U Test, only significant changes shown. Hue = biological correlate of pH.

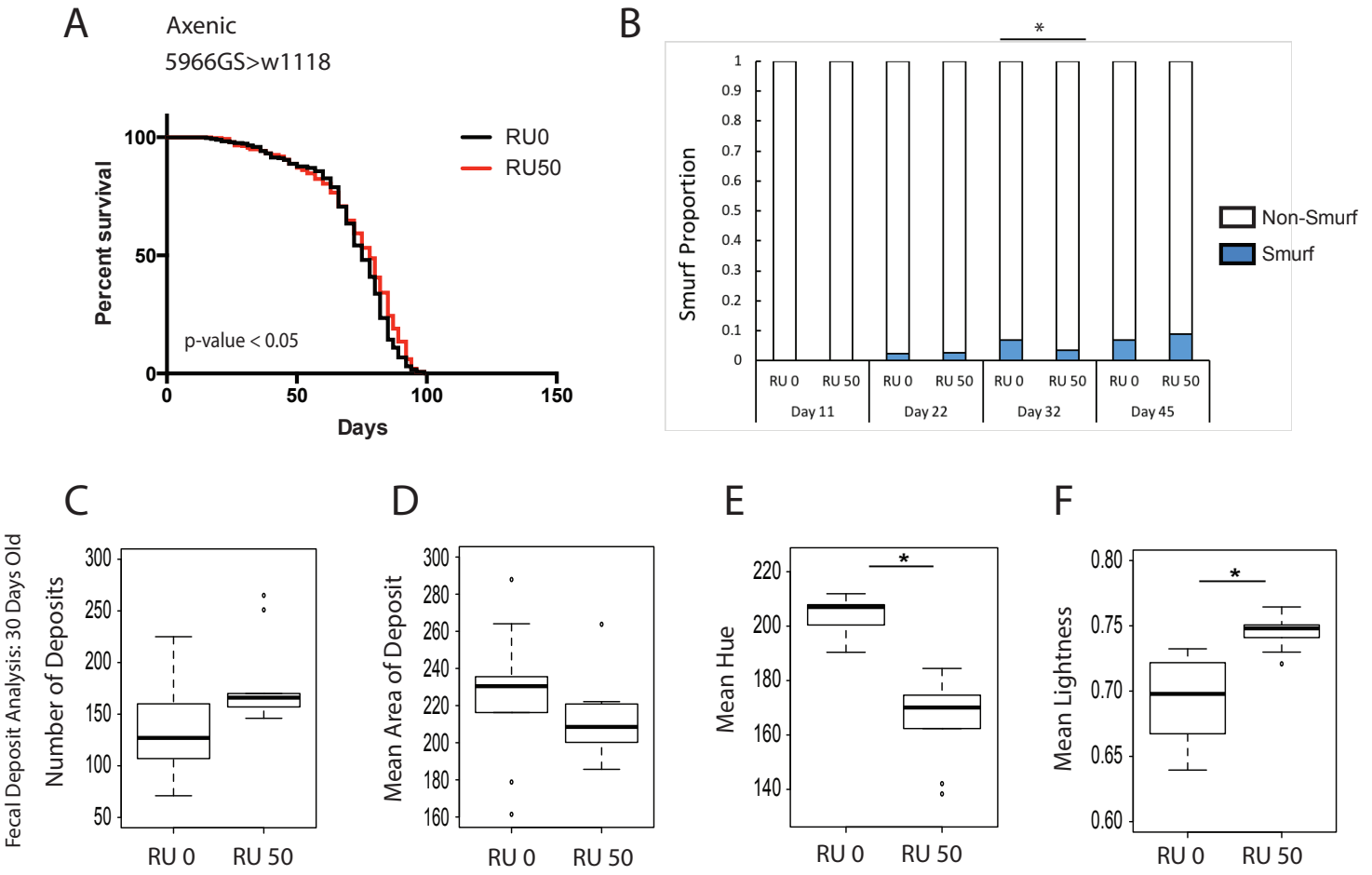
A
Axenic
5966GS>w1118
Percent survival
Days
RU0
RU50
p-value < 0.05
B
Smurf Proportion
Non-Smurf
Smurf
RU 0
RU 50
Day 11
Day 22
Day 32
Day 45
C
Fecal Deposit Analysis: 30 Days Old
Number of Deposits
D
Mean Area of Deposit
E
Mean Hue
F
Mean Lightness

Appendix 2: Axenic Developed and Reared *5966-GS > w[1118]* Negative Control Data

A.) Axenic fly lifespan was not affected by RU treatment. Survival curves for *5966-GS > w^{1118}*, female flies fed 50 µg/ml of RU486 (RU 50), or equal volume of ethanol (RU 0), from day 10 of adulthood. n = >200 flies/condition. No significant difference in log rank test.

B.) Axenic Smurf proportions were not affected by RU treatment. Smurf status was assayed at regular intervals throughout the lifespan at day 11, 21, 32, and 45. Stacked bar graphs show female flies fed 50 µg/ml of RU486 (RU 50), or equal volume of ethanol (RU 0), from day 10 of adulthood. n = >200 flies/condition. p-value <0.05 = * in Binomial Test, only significant changes shown.

C.) Number of quantified axenic fly excrements were not affected by RU treatment. T.U.R.D assay completed in n = 10 replicate groups of ten female non-Smurf flies at 30-days old, fed 50 µg/ml of RU486 (RU 50), or equal volume of ethanol (RU 0), from day 10 of adulthood. Boxplots display the first and third quartile, with the horizontal bar at the median. No significant difference in Wilcoxon Test.

D.) Area of quantified axenic fly excrements were not affected by RU treatment. T.U.R.D assay completed in n = 10 replicate groups of ten female non-Smurf flies at 30-days old, fed 50 µg/ml of RU486 (RU 50), or equal volume of ethanol (RU 0), from day 10 of adulthood. Boxplots display the first and third quartile, with the horizontal bar at the median. No significant difference in Wilcoxon Test.

E.) Axenic fly excrements were made moderately more acidic by RU treatment. T.U.R.D assay completed in n = 10 replicate groups of ten female non-Smurf flies at 30-days old, fed 50 µg/ml of RU486 (RU 50), or equal volume of ethanol (RU 0), from day 10 of adulthood. Boxplots display the first and third quartile, with the horizontal bar at the median. p-value <0.05 = *, in Mann-Whitney U Test, only significant changes shown. Hue = biological correlate of pH.

F.) Axenic fly excrements were made moderately more dilute by RU treatment. T.U.R.D assay completed in n = 10 replicate groups of ten female non-Smurf flies at 30-days old, fed 50 µg/ml of RU486 (RU 50), or equal volume of ethanol (RU 0), from day 10 of adulthood. Boxplots display the first and third quartile, with the horizontal bar at the median. p-value <0.05 = *, in Mann-Whitney U Test, only significant changes shown. Lightness = dye concentration/diuresis

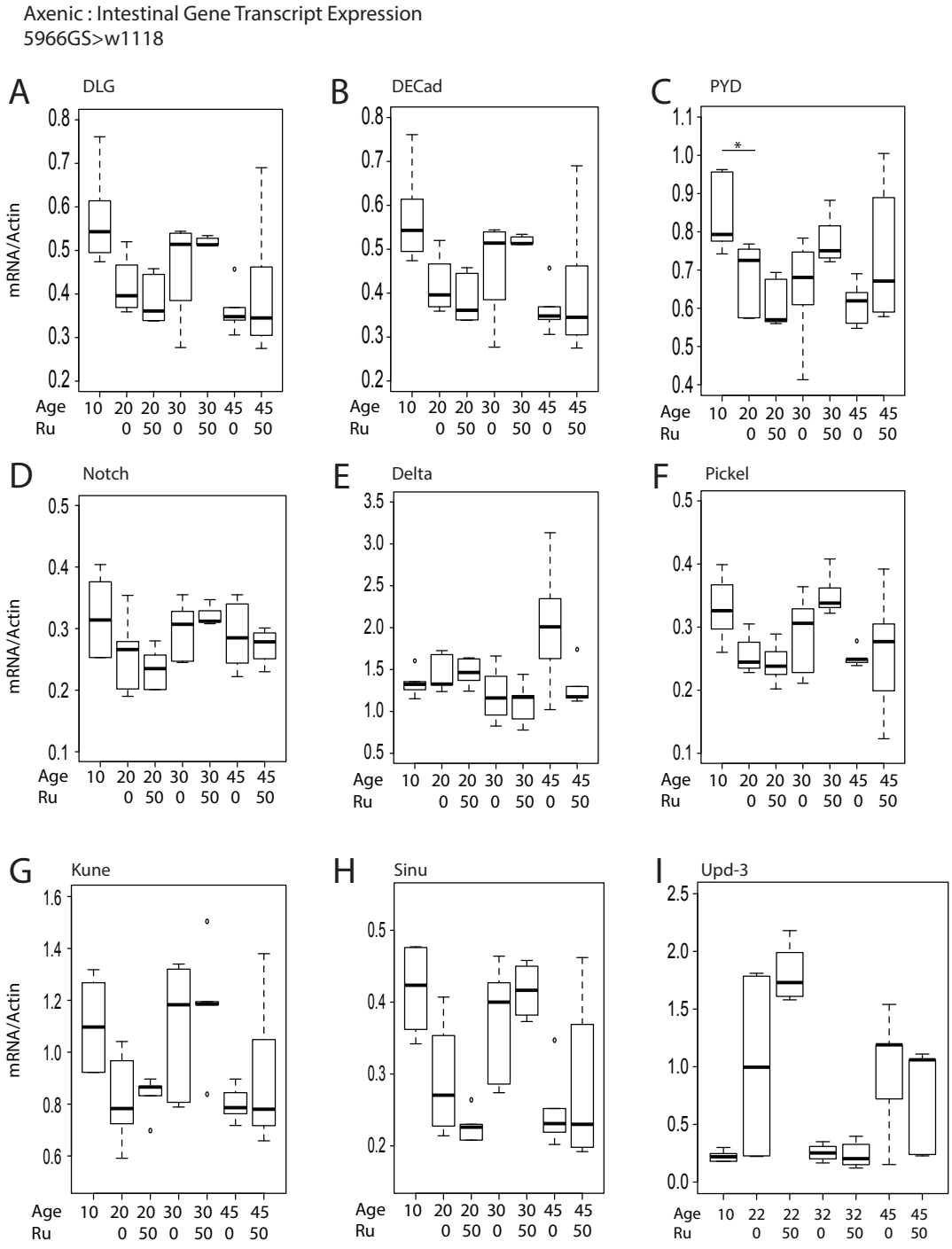

Appendix 3: Axenic Developed and Reared *5966-GS > w[1118]* Negative Control Data – mRNA Transcript Expression

Quantified mRNA levels remain unchanged by RU treatment. Gene expression assayed by RT-qPCR from dissected intestines; non-Smurf axenic female flies, fed 50 µg/ml of RU486 (RU 50), or equal volume of ethanol (RU 0), from day 10 of adulthood. Boxplots display the first and third quartile, with the horizontal bar at the median. n = 6 replicates of five intestines. p-value <0.05 = * in Wilcoxon Test, only significant changes shown.

A.) Discs Large -1 (DLG)
B.) *Drosophila* E-Cadherin (DE-cad) – Epithelial Cell Adherens Junction Component
C.) Polychaetoid (PYD) – Epithelial Cell Adherens Junction Component
D.) Notch – Enteroblast Marker
E.) Delta – Intestinal Stem Cell Marker/ Notch Ligand
F.) Pickel – Epithelial Cell Septate Junction Component
G.) Kune-Kune (Kune) – Epithelial Cell Septate Junction Component
H.) Sinuous (Sinu) – Epithelial Cell Septate Junction Component
I.) Unpaired-3 (Upd-3) – Cytokine Ligand, Activates Jak/STAT Pathway

References

AGAISSE, H., PETERSEN, U.-M., BOUTROS, M., MATHEY-PREVOT, B. & PERRIMON, N. 2003. Signaling Role of Hemocytes in Drosophila JAK/STAT-Dependent Response to Septic Injury. *Developmental Cell,* 5**,** 441-450.

AKHTAR, I., STEWART, F. A., HÄRLE, A., DROSTE, A. & BELLER, M. 2021. Visualization of endogenous gut bacteria in Drosophila melanogaster using fluorescence in situ hybridization. *PLOS ONE,* 16**,** e0247376.

ALCARAZ, J. 2016. *Microbiota and immune contributions to age-related intestinal decline.* Master of Science, University of California, Los Angeles.

AMCHESLAVSKY, A., JIANG, J. & IP, Y. T. 2009. Tissue Damage-Induced Intestinal Stem Cell Division in Drosophila. *Cell Stem Cell,* 4**,** 49-61.

AMCHESLAVSKY, A., LINDBLAD, J. L. & BERGMANN, A. 2020. Transiently "Undead" Enterocytes Mediate Homeostatic Tissue Turnover in the Adult Drosophila Midgut. *Cell Reports,* 33**,** 108408.

ANDERSON, J. M. & VAN ITALLIE, C. M. 2008. Tight junctions. *Current Biology,* 18**,** R941-R943.

ANDJELKOVIĆ, A., KEMPPAINEN, K. K. & JACOBS, H. T. 2016. Ligand-Bound GeneSwitch Causes Developmental Aberrations in Drosophila that Are Alleviated by the Alternative Oxidase. *G3 Genes|Genomes|Genetics,* 6**,** 2839-2846.

ANGARITA, S. A. K., DUARTE, S., RUSSELL, T. A., RUCHALA, P., ELLIOTT, I. A., WHITELEGGE, J. P. & ZARRINPAR, A. 2019. Quantitative Measure of Intestinal Permeability Using Blue Food Coloring. *Journal of Surgical Research,* 233**,** 20-25.

ARAI, Y., MARTIN-RUIZ, C. M., TAKAYAMA, M., ABE, Y., TAKEBAYASHI, T., KOYASU, S., SUEMATSU, M., HIROSE, N. & VON ZGLINICKI, T. 2015. Inflammation, But Not Telomere Length, Predicts Successful Ageing at Extreme Old Age: A Longitudinal Study of Semi-supercentenarians. *EBioMedicine,* 2**,** 1549-1558.

AYYAZ, A., LI, H. & JASPER, H. 2015. Hemocytes control stem cell activity in the Drosophila intestine. *Nature cell biology,* 17**,** 736-748.

BÄCKHED, F., FRASER, CLAIRE M., RINGEL, Y., SANDERS, MARY E., SARTOR, R. B., SHERMAN, PHILIP M., VERSALOVIC, J., YOUNG, V. & FINLAY, B. B. 2012. Defining a Healthy Human Gut Microbiome: Current Concepts, Future Directions, and Clinical Applications. *Cell Host & Microbe,* 12**,** 611-622.

BAKULA, M. 1969. The persistence of a microbial flora during postembryogenesis of Drosophila melanogaster. *J Invertebr Pathol,* 14**,** 365-74.

BELMONTE, R. L., CORBALLY, M. K., DUNEAU, D. F. & REGAN, J. C. 2019. Sexual Dimorphisms in Innate Immunity and Responses to Infection in Drosophila melanogaster. *Front Immunol,* 10**,** 3075.

BEUTLER, B. 2004. Inferences, questions and possibilities in Toll-like receptor signalling. *Nature,* 430**,** 257-263.

BIAGI, E., NYLUND, L., CANDELA, M., OSTAN, R., BUCCI, L., PINI, E., NIKKÏLA, J., MONTI, D., SATOKARI, R., FRANCESCHI, C., BRIGIDI, P. & DE VOS, W. 2010. Through Ageing, and Beyond: Gut Microbiota and Inflammatory Status in Seniors and Centenarians. *PLoS ONE,* 5**,** e10667.

BISCHOFF, S. C. 2016. Microbiota and aging. *Current Opinion in Clinical Nutrition and Metabolic Care,* 19**,** 26-30.

BITEAU, B., HOCHMUTH, C. E. & JASPER, H. 2008. JNK Activity in Somatic Stem Cells Causes Loss of Tissue Homeostasis in the Aging Drosophila Gut. *Cell Stem Cell,* 3**,** 442-455.

BITEAU, B., KARPAC, J., SUPOYO, S., DEGENNARO, M., LEHMANN, R. & JASPER, H. 2010. Lifespan Extension by Preserving Proliferative Homeostasis in Drosophila. *PLoS Genetics,* 6**,** e1001159.

BONFINI, A., LIU, X. & BUCHON, N. 2016. From pathogens to microbiota: How Drosophila intestinal stem cells react to gut microbes. *Developmental & Comparative Immunology,* 64**,** 22-38.

BONNAY, F., COHEN-BERROS, E., HOFFMANN, M., KIM, S. Y., BOULIANNE, G. L., HOFFMANN, J. A., MATT, N. & REICHHART, J. M. 2013. big bang gene modulates gut immune tolerance in Drosophila. *Proceedings of the National Academy of Sciences,* 110**,** 2957-2962.

BOSCO-DRAYON, V., POIDEVIN, M., IVO, NARBONNE-REVEAU, K., ROYET, J. & CHARROUX, B. 2012. Peptidoglycan Sensing by the Receptor PGRP-LE in the Drosophila Gut Induces Immune Responses to Infectious Bacteria and Tolerance to Microbiota. *Cell Host & Microbe,* 12**,** 153-165.

BRODERICK, N. A. 2016. Friend, foe or food? Recognition and the role of antimicrobial peptides in gut immunity and Drosophila –microbe interactions. *Philosophical Transactions of the Royal Society B: Biological Sciences,* 371**,** 20150295.

BRODERICK, N. A., BUCHON, N. & LEMAITRE, B. 2014. Microbiota-induced changes in drosophila melanogaster host gene expression and gut morphology. *mBio,* 5**,** e01117-14.

BRUMMEL, T., CHING, A., SEROUDE, L., SIMON, A. F. & BENZER, S. 2004. Drosophila lifespan enhancement by exogenous bacteria. *Proceedings of the National Academy of Sciences,* 101**,** 12974-12979.

BUCHON, N., BRODERICK, N. A., CHAKRABARTI, S. & LEMAITRE, B. 2009a. Invasive and indigenous microbiota impact intestinal stem cell activity through multiple pathways in Drosophila. *Genes & Development,* 23**,** 2333-2344.

BUCHON, N., BRODERICK, N. A., KURAISHI, T. & LEMAITRE, B. 2010. DrosophilaEGFR pathway coordinates stem cell proliferation and gut remodeling following infection. *BMC Biology,* 8**,** 152.

BUCHON, N., BRODERICK, N. A., POIDEVIN, M., PRADERVAND, S. & LEMAITRE, B. 2009b. Drosophila Intestinal Response to Bacterial Infection: Activation of Host Defense and Stem Cell Proliferation. *Cell Host & Microbe,* 5**,** 200-211.

BUCHON, N., SILVERMAN, N. & CHERRY, S. 2014. Immunity in Drosophila melanogaster — from microbial recognition to whole-organism physiology. *Nature Reviews Immunology,* 14**,** 796-810.

BUFORD, T. W. 2017. (Dis)Trust your gut: the gut microbiome in age-related inflammation, health, and disease. *Microbiome,* 5.

BURRELLO, C., GARAVAGLIA, F., CRIBIÙ, F. M., ERCOLI, G., LOPEZ, G., TROISI, J., COLUCCI, A., GUGLIETTA, S., CARLONI, S., GUGLIELMETTI, S., TAVERNITI, V., NIZZOLI, G., BOSARI, S., CAPRIOLI, F., RESCIGNO, M. & FACCIOTTI, F. 2018. Therapeutic faecal microbiota transplantation controls intestinal inflammation through IL10 secretion by immune cells. *Nature Communications,* 9.

CHAKRABARTI, S., DUDZIC, J. P., LI, X., COLLAS, E. J., BOQUETE, J.-P. & LEMAITRE, B. 2016. Remote Control of Intestinal Stem Cell Activity by Haemocytes in Drosophila. *PLOS Genetics,* 12**,** e1006089.

CHAKRABARTI, S., LIEHL, P., BUCHON, N. & LEMAITRE, B. 2012. Infection-Induced Host Translational Blockage Inhibits Immune Responses and Epithelial Renewal in the Drosophila Gut. *Cell Host & Microbe,* 12**,** 60-70.

CHANDLER, J. A., MORGAN LANG, J., BHATNAGAR, S., EISEN, J. A. & KOPP, A. 2011. Bacterial Communities of Diverse Drosophila Species: Ecological Context of a Host–Microbe Model System. *PLoS Genetics,* 7**,** e1002272.

CHEN, H., ZHENG, X. & ZHENG, Y. 2014. Age-Associated Loss of Lamin-B Leads to Systemic Inflammation and Gut Hyperplasia. *Cell,* 159**,** 829-843.

CHEN, J., SAYADIAN, A.-C., LOWE, N., LOVEGROVE, H. E. & ST JOHNSTON, D. 2018. An alternative mode of epithelial polarity in the Drosophila midgut. *PLOS Biology,* 16**,** e3000041.

CHEN, X., LEE, K.-A., HA, E.-M., LEE, K. M., SEO, Y. Y., CHOI, H. K., KIM, H. N., KIM, M. J., CHO, C.-S., LEE, S. Y., LEE, W.-J. & YOON, J. 2011. A specific and sensitive method for detection of hypochlorous acid for the imaging of microbe-induced HOCl production. *Chemical Communications,* 47**,** 4373.

CHO, I. & BLASER, M. J. 2012. The human microbiome: at the interface of health and disease. *Nature Reviews Genetics,* 13**,** 260-270.

CHU, H. & MAZMANIAN, S. K. 2013. Innate immune recognition of the microbiota promotes host-microbial symbiosis. *Nat Immunol,* 14**,** 668-675.

CLAESSON, M. J., CUSACK, S., O'SULLIVAN, O., GREENE-DINIZ, R., DE WEERD, H., FLANNERY, E., MARCHESI, J. R., FALUSH, D., DINAN, T., FITZGERALD, G., STANTON, C., VAN SINDEREN, D., O'CONNOR, M., HARNEDY, N., O'CONNOR, K., HENRY, C., O'MAHONY, D., FITZGERALD, A. P., SHANAHAN, F., TWOMEY, C., HILL, C., ROSS, R. P. & O'TOOLE, P. W. 2010. Composition, variability, and temporal stability of the intestinal microbiota of the elderly. *Proceedings of the National Academy of Sciences,* 108**,** 4586-4591.

CLAESSON, M. J., JEFFERY, I. B., CONDE, S., POWER, S. E., O'CONNOR, E. M., CUSACK, S., HARRIS, H. M. B., COAKLEY, M., LAKSHMINARAYANAN, B., O'SULLIVAN, O., FITZGERALD, G. F., DEANE, J., O'CONNOR, M., HARNEDY, N., O'CONNOR, K., O'MAHONY, D., VAN SINDEREN, D., WALLACE, M., BRENNAN, L., STANTON, C., MARCHESI, J. R., FITZGERALD, A. P., SHANAHAN, F., HILL, C., ROSS, R. P. & O'TOOLE, P. W. 2012. Gut microbiota composition correlates with diet and health in the elderly. *Nature,* 488**,** 178-184.

CLARK, REBECCA I., SALAZAR, A., YAMADA, R., FITZ-GIBBON, S., MORSELLI, M., ALCARAZ, J., RANA, A., RERA, M., PELLEGRINI, M., JA, WILLIAM W. & WALKER, DAVID W. 2015. Distinct Shifts in Microbiota Composition during Drosophila Aging Impair Intestinal Function and Drive Mortality. *Cell Reports,* 12**,** 1656-1667.

CLARK, REBECCA I., WOODCOCK, KATIE J., GEISSMANN, F., TROUILLET, C. & DIONNE, MARC S. 2011. Multiple TGF-beta Superfamily Signals Modulate the Adult Drosophila Immune Response. *Current Biology,* 21**,** 1672-1677.

COGNIGNI, P., BAILEY, A. P. & MIGUEL-ALIAGA, I. 2011. Enteric Neurons and Systemic Signals Couple Nutritional and Reproductive Status with Intestinal Homeostasis. *Cell Metabolism,* 13**,** 92-104.

COPELAND, J. M., CHO, J., LO, T., HUR, J. H., BAHADORANI, S., ARABYAN, T., RABIE, J., SOH, J. & WALKER, D. W. 2009. Extension of Drosophila Life Span by RNAi of the Mitochondrial Respiratory Chain. *Current Biology,* 19**,** 1591-1598.

CORBY-HARRIS, V., PONTAROLI, A. C., SHIMKETS, L. J., BENNETZEN, J. L., HABEL, K. E. & PROMISLOW, D. E. L. 2007. Geographical Distribution and Diversity of Bacteria Associated with Natural Populations of Drosophila melanogaster. *Applied and Environmental Microbiology,* 73**,** 3470-3479.

COSTA, A., JAN, E., SARNOW, P. & SCHNEIDER, D. 2009. The Imd Pathway Is Involved in Antiviral Immune Responses in Drosophila. *PLOS ONE,* 4**,** e7436.

DAMBROISE, E., MONNIER, L., RUISHENG, L., AGUILANIU, H., JOLY, J. S., TRICOIRE, H. & RERA, M. 2016. Two phases of aging separated by the Smurf transition as a public path to death. *Scientific Reports,* 6**,** 23523.

DANTOFT, W., DAVIS, M. M., LINDVALL, J. M., TANG, X., UVELL, H., JUNELL, A., BESKOW, A. & ENGSTRÖM, Y. 2013. The Oct1 homolog Nubbin is a repressor of NF-κB-dependent immune gene expression that increases the tolerance to gut microbiota. *BMC Biology,* 11**,** 99.

DANTOFT, W., LUNDIN, D., ESFAHANI, S. S. & ENGSTRÖM, Y. 2016. The POU/Oct Transcription Factor Pdm1/nub Is Necessary for a Beneficial Gut Microbiota and Normal Lifespan of Drosophila. *Journal of Innate Immunity,* 8**,** 412-426.

DEMEREC, M. (ed.) 1994a. *Biology of Drosophila* New York, USA: Cold Spring Harbor Laboratory Press

DEMEREC, M. (ed.) 1994b. *Biology of Drosophila,* New York, USA: Cold Spring Harbor Laboratory Press.

DOUPÉ, D. P., MARSHALL, O. J., DAYTON, H., BRAND, A. H. & PERRIMON, N. 2018. Drosophila intestinal stem and progenitor cells are major sources and regulators of homeostatic niche signals. *Proceedings of the National Academy of Sciences,* 115**,** 12218-12223.

DUBREUIL, R. R. 2004. Copper cells and stomach acid secretion in the Drosophila midgut. *The International Journal of Biochemistry & Cell Biology,* 36**,** 742-752.

DUNEAU, D. F., KONDOLF, H. C., IM, J. H., ORTIZ, G. A., CHOW, C., FOX, M. A., EUGENIO, A. T., REVAH, J., BUCHON, N. & LAZZARO, B. P. 2017. The Toll pathway underlies host sexual dimorphism in resistance to both Gram-negative and Gram-positive bacteria in mated Drosophila. *BMC Biol,* 15**,** 124.

DUTTA, D., ADAM, PHILIP, GLÄSSE, C., REVAH, J., KORZELIUS, J., PATEL, P. H., BRUCE & BUCHON, N. 2015. Regional Cell-Specific Transcriptome Mapping Reveals Regulatory Complexity in the Adult Drosophila Midgut. *Cell Reports,* 12**,** 346-358.

EARLY, A. M., SHANMUGARAJAH, N., BUCHON, N. & CLARK, A. G. 2017. Drosophila Genotype Influences Commensal Bacterial Levels. *PLOS ONE,* 12**,** e0170332.

ERKOSAR, B., STORELLI, G., DEFAYE, A. & LEULIER, F. 2013. Host-Intestinal Microbiota Mutualism: "Learning on the Fly". *Cell Host & Microbe,* 13**,** 8-14.

EVANGELOU, A., IGNATIOU, A., ANTONIOU, C., KALANIDOU, S., CHATZIMATTHAIOU, S., SHIANIOU, G., ELLINA, S., ATHANASIOU, R., PANAGI, M., APIDIANAKIS, Y. & PITSOULI, C. 2019. Unpredictable Effects of the Genetic Background of Transgenic Lines in Physiological Quantitative Traits. *G3 (Bethesda),* 9**,** 3877-3890.

FASANO, A. 2020. All disease begins in the (leaky) gut: role of zonulin-mediated gut permeability in the pathogenesis of some chronic inflammatory diseases. *F1000Research,* 9**,** 69.

FASANO, A., BAUDRY, B., PUMPLIN, D. W., WASSERMAN, S. S., TALL, B. D., KETLEY, J. M. & KAPER, J. B. 1991. Vibrio cholerae produces a second enterotoxin, which affects intestinal tight junctions. *Proceedings of the National Academy of Sciences,* 88**,** 5242-5246.

FAST, D., DUGGAL, A. & FOLEY, E. 2018a. Monoassociation with Lactobacillus plantarum Disrupts Intestinal Homeostasis in Adult Drosophila melanogaster. *mBio,* 9.

FAST, D., KOSTIUK, B., FOLEY, E. & PUKATZKI, S. 2018b. Commensal pathogen competition impacts host viability. *Proceedings of the National Academy of Sciences,* 115**,** 7099-7104.

FAST, D., PETKAU, K., FERGUSON, M., SHIN, M., GALENZA, A., KOSTIUK, B., PUKATZKI, S. & FOLEY, E. 2020. Vibrio cholerae-Symbiont Interactions Inhibit Intestinal Repair in Drosophila. *Cell Rep,* 30**,** 1088-1100 e5.

FERGUSON, M., PETKAU, K., SHIN, M., GALENZA, A., FAST, D. & FOLEY, E. 2020. Differential effects of commensal bacteria on progenitor cell adhesion, division symmetry and tumorigenesis in the Drosophila intestine. *bioRxiv***,** 799981.

FRANC, N. C., DIMARCQ, J.-L., LAGUEUX, M., HOFFMANN, J. & EZEKOWITZ, R. A. B. 1996. Croquemort, A Novel Drosophila Hemocyte/Macrophage Receptor that Recognizes Apoptotic Cells. *Immunity,* 4**,** 431-443.

GÁLIKOVÁ, M., DIRCKSEN, H. & NÄSSEL, D. R. 2018. The thirsty fly: Ion transport peptide (ITP) is a novel endocrine regulator of water homeostasis in Drosophila. *PLOS Genetics,* 14**,** e1007618.

GERMANI, F., BERGANTINOS, C. & JOHNSTON, L. A. 2018. Mosaic Analysis in Drosophila. *Genetics,* 208**,** 473-490.

GERVAIS, L. & BARDIN, A. J. 2017. Tissue homeostasis and aging: new insight from the fly intestine. *Current Opinion in Cell Biology,* 48**,** 97-105.

GHOSH, S., SINGH, A., MANDAL, S. & MANDAL, L. 2015. Active Hematopoietic Hubs in Drosophila Adults Generate Hemocytes and Contribute to Immune Response. *Developmental Cell,* 33**,** 478-488.

GOTO, A., KUMAGAI, T., KUMAGAI, C., HIROSE, J., NARITA, H., MORI, H., KADOWAKI, T., BECK, K. & KITAGAWA, Y. 2001. A Drosophila haemocyte-specific protein, hemolectin, similar to human von Willebrand factor. *Biochemical Journal,* 359**,** 99.

GUILLOU, A., TROHA, K., WANG, H., FRANC, N. C. & BUCHON, N. 2016. The Drosophila CD36 Homologue croquemort Is Required to Maintain Immune and Gut Homeostasis during Development and Aging. *PLOS Pathogens,* 12**,** e1005961.

GUO, L., KARPAC, J., TRAN, SUSAN L. & JASPER, H. 2014. PGRP-SC2 Promotes Gut Immune Homeostasis to Limit Commensal Dysbiosis and Extend Lifespan. *Cell,* 156**,** 109-122.

GUPTA, D. 2008. Peptidoglycan Recognition Proteins—Maintaining Immune Homeostasis and Normal Development. *Cell Host & Microbe,* 3**,** 273-274.

GYOERGY, A., ROBLEK, M., RATHEESH, A., VALOSKOVA, K., BELYAEVA, V., WACHNER, S., MATSUBAYASHI, Y., SÁNCHEZ-SÁNCHEZ, B. J., STRAMER, B. & SIEKHAUS, D. E. 2018. Tools Allowing Independent Visualization and Genetic Manipulation of

Drosophila melanogaster Macrophages and Surrounding Tissues. *G3: Genes|Genomes|Genetics,* 8**,** 845.

HA, E.-M., OH, C.-T., BAE, Y. S. & LEE, W.-J. 2005. A Direct Role for Dual Oxidase inDrosophilaGut Immunity. *Science,* 310**,** 847-850.

HAN, G., LEE, H. J., JEONG, S. E., JEON, C. O. & HYUN, S. 2017. Comparative Analysis of Drosophila melanogaster Gut Microbiota with Respect to Host Strain, Sex, and Age. *Microbial Ecology,* 74**,** 207-216.

HEDENGREN, M., BENGTÅSLING, DUSHAY, M. S., ANDO, I., EKENGREN, S., WIHLBORG, M. & HULTMARK, D. 1999. Relish, a Central Factor in the Control of Humoral but Not Cellular Immunity in Drosophila. *Molecular Cell,* 4**,** 827-837.

HEINTZ, C. & MAIR, W. 2014. You Are What You Host: Microbiome Modulation of the Aging Process. *Cell,* 156**,** 408-411.

HETRU, C. & HOFFMANN, J. A. 2009. NF-κB in the Immune Response of Drosophila. *Cold Spring Harbor Perspectives in Biology,* 1**,** a000232.

HOLZ, A., BOSSINGER, B., STRASSER, T., JANNING, W. & KLAPPER, R. 2003. The two origins of hemocytes in <em>Drosophila</em&gt. *Development,* 130**,** 4955.

HORN, L., LEIPS, J. & STARZ-GAIANO, M. 2014. Phagocytic ability declines with age in adult Drosophila hemocytes. *Aging Cell,* 13**,** 719-728.

HUR, J. H., BAHADORANI, S., GRANIEL, J., KOEHLER, C. L., ULGHERAIT, M., RERA, M., JONES, D. L. & WALKER, D. W. 2013. Increased longevity mediated by yeast NDI1 expression in Drosophila intestinal stem and progenitor cells. *Aging,* 5**,** 662-681.

IACOB, S. & IACOB, D. G. 2019. Infectious Threats, the Intestinal Barrier, and Its Trojan Horse: Dysbiosis. *Front Microbiol,* 10**,** 1676.

IATSENKO, I., BOQUETE, J. P. & LEMAITRE, B. 2018. Microbiota-Derived Lactate Activates Production of Reactive Oxygen Species by the Intestinal NADPH Oxidase Nox and Shortens Drosophila Lifespan. *Immunity,* 49**,** 929-942 e5.

IATSENKO, I., KONDO, S., MENGIN-LECREULX, D. & LEMAITRE, B. 2016. PGRP-SD, an Extracellular Pattern-Recognition Receptor, Enhances Peptidoglycan-Mediated Activation of the Drosophila Imd Pathway. *Immunity,* 45**,** 1013-1023.

IZUMI, Y., FURUSE, K. & FURUSE, M. 2019. Septate junctions regulate gut homeostasis through regulation of stem cell proliferation and enterocyte behavior in Drosophila. *Journal of Cell Science,* 132**,** jcs232108.

IZUMI, Y., FURUSE, K. & FURUSE, M. 2020. A novel membrane protein Hoka regulates septate junction organization and stem cell homeostasis in the Drosophila gut. Cold Spring Harbor Laboratory.

IZUMI, Y., YANAGIHASHI, Y. & FURUSE, M. 2012. A novel protein complex, mesh-ssk, is required for septate junction formation indrosophilamidgut. *Journal of Cell Science,* 125**,** 4923-4933.

JIANG, H., GRENLEY, M. O., BRAVO, M. J., BLUMHAGEN, R. Z. & EDGAR, B. A. 2011. EGFR/Ras/MAPK signaling mediates adult midgut epithelial homeostasis and regeneration in Drosophila. *Cell Stem Cell,* 8**,** 84-95.

JIANG, H., PATEL, P. H., KOHLMAIER, A., GRENLEY, M. O., MCEWEN, D. G. & EDGAR, B. A. 2009. Cytokine/Jak/Stat Signaling Mediates Regeneration and Homeostasis in the Drosophila Midgut. *Cell,* 137**,** 1343-1355.

JONUSAITE, S., DONINI, A. & KELLY, S. P. 2016. Occluding junctions of invertebrate epithelia. *Journal of Comparative Physiology B,* 186**,** 17-43.

KABIL, H., KABIL, O., BANERJEE, R., HARSHMAN, L. G. & PLETCHER, S. D. 2011. Increased transsulfuration mediates longevity and dietary restriction in *Drosophila*. *Proceedings of the National Academy of Sciences,* 108**,** 16831-16836.

KAMAREDDINE, L., NAJJAR, H., SOHAIL, M. U., ABDULKADER, H. & AL-ASMAKH, M. 2020. The Microbiota and Gut-Related Disorders: Insights from Animal Models. *Cells,* 9**,** 2401.

KAMAREDDINE, L., ROBINS, W. P., BERKEY, C. D., MEKALANOS, J. J. & WATNICK, P. I. 2018. The Drosophila Immune Deficiency Pathway Modulates Enteroendocrine Function and Host Metabolism. *Cell Metabolism,* 28**,** 449-462.e5.

KIM, E.-K. 2020. Bacterial Nucleoside Catabolism Controls Quorum Sensing and Commensal-to-Pathogen Transition in the Drosophila Gut.

KIM, E. K., KIM, S. H., NAM, H. J., CHOI, M. K., LEE, K. A., CHOI, S. H., SEO, Y. Y., YOU, H., KIM, B. & LEE, W. J. 2012. Draft Genome Sequence of Commensalibacter intestini A911T, a Symbiotic Bacterium Isolated from Drosophila melanogaster Intestine. *Journal of Bacteriology,* 194**,** 1246-1246.

KOEHLER, C. L., PERKINS, G. A., ELLISMAN, M. H. & JONES, D. L. 2017. Pink1 and Parkin regulate Drosophila intestinal stem cell proliferation during stress and aging. *Journal of Cell Biology,* 216**,** 2315-2327.

KURAISHI, T., BINGGELI, O., OPOTA, O., BUCHON, N. & LEMAITRE, B. 2011. Genetic evidence for a protective role of the peritrophic matrix against intestinal bacterial infection in Drosophila melanogaster. *Proceedings of the National Academy of Sciences,* 108**,** 15966-15971.

LEE, H.-Y., LEE, S.-H., LEE, J.-H., LEE, W.-J. & MIN, K.-J. 2019. The role of commensal microbes in the lifespan of Drosophila melanogaster. *Aging,* 11**,** 4611-4640.

LEE, K.-A., KIM, S.-H., KIM, E.-K., HA, E.-M., YOU, H., KIM, B., KIM, M.-J., KWON, Y., RYU, J.-H. & LEE, W.-J. 2013a. Bacterial-Derived Uracil as a Modulator of Mucosal Immunity and Gut-Microbe Homeostasis in Drosophila. *Cell,* 153**,** 797-811.

LEE, K.-A., KIM, S.-H., KIM, E.-K., HA, E.-M., YOU, H., KIM, B., KIM, M.-J., KWON, Y., RYU, J.-H. & LEE, W.-J. 2013b. Bacterial-Derived Uracil as a Modulator of Mucosal Immunity and Gut-Microbe Homeostasis in Drosophila. *Cell,* 153**,** 797-811.

LEE, Y. S., NAKAHARA, K., PHAM, J. W., KIM, K., HE, Z., SONTHEIMER, E. J. & CARTHEW, R. W. 2004. Distinct Roles for Drosophila Dicer-1 and Dicer-2 in the siRNA/miRNA Silencing Pathways. *Cell,* 117**,** 69-81.

LEOPOLD, P. & PERRIMON, N. 2007. Drosophila and the genetics of the internal milieu. *Nature,* 450**,** 186-188.

LESCH, C., GOTO, A., LINDGREN, M., BIDLA, G., DUSHAY, M. S. & THEOPOLD, U. 2007. A role for Hemolectin in coagulation and immunity in Drosophila melanogaster. *Developmental & Comparative Immunology,* 31**,** 1255-1263.

LESPERANCE, D. N. & BRODERICK, N. A. 2020. Microbiomes as modulators of Drosophila melanogaster homeostasis and disease. *Current Opinion in Insect Science,* 39**,** 84-90.

LEWIS, E. B. 1960. A new standard of food medium. *Drosophila Information Service,* 34**,** 117-118.

LI, H., QI, Y. & JASPER, H. 2013. Dpp Signaling Determines Regional Stem Cell Identity in the Regenerating Adult Drosophila Gastrointestinal Tract. *Cell Reports,* 4**,** 10-18.

LI, H., QI, Y. & JASPER, H. 2016. Preventing Age-Related Decline of Gut Compartmentalization Limits Microbiota Dysbiosis and Extends Lifespan. *Cell Host & Microbe,* 19**,** 240-253.

LIANG, J., BALACHANDRA, S., NGO, S. & O'BRIEN, L. E. 2017. Feedback regulation of steady-state epithelial turnover and organ size. *Nature,* 548**,** 588-591.

LIM, S. Y., YOU, H., LEE, J., LEE, J., LEE, Y., LEE, K.-A., KIM, B., LEE, J.-H., JEONG, J., JANG, S., KIM, B., CHOI, H., HWANG, G., CHOI, M. S., YOON, S.-E., KWON, J. Y., LEE, W.-J., KIM, Y.-J. & SUH, G. S. B. 2021. Identification and characterization of GAL4 drivers that mark distinct cell types and regions in the Drosophila adult gut. *Journal of Neurogenetics,* 35**,** 33-44.

LIU, Q. & JIN, L. H. 2017. Organ-to-Organ Communication: A Drosophila Gastrointestinal Tract Perspective. *Front Cell Dev Biol,* 5**,** 29.

LOCH, G., ZINKE, I., MORI, T., CARRERA, P., SCHROER, J., TAKEYAMA, H. & HOCH, M. 2017. Antimicrobial peptides extend lifespan in Drosophila. *PLOS ONE,* 12**,** e0176689.

LOUDHAIEF, R., BRUN-BARALE, A., BENGUETTAT, O., NAWROT-ESPOSITO, M.-P., PAURON, D., AMICHOT, M. & GALLET, A. 2017. Apoptosis restores cellular density by eliminating a physiologically or genetically induced excess of enterocytes in the Drosophila midgut. *Development,* 144**,** 808-819.

MACKENZIE, D. K., BUSSIÈRE, L. F. & TINSLEY, M. C. 2011. Senescence of the cellular immune response in Drosophila melanogaster. *Experimental Gerontology,* 46**,** 853-859.

MAEDA, K., TAKEMURA, M., UMEMORI, M. & ADACHI-YAMADA, T. 2008. E-cadherin prolongs the moment for interaction between intestinal stem cell and its progenitor cell to ensure Notch signaling in adultDrosophilamidgut. *Genes to Cells,* 13**,** 1219-1227.

MAIER, T., GÜELL, M. & SERRANO, L. 2009. Correlation of mRNA and protein in complex biological samples. *FEBS Letters,* 583**,** 3966-3973.

MARRA, A., HANSON, M. A., KONDO, S., ERKOSAR, B. & LEMAITRE, B. 2021. Drosophila Antimicrobial Peptides and Lysozymes Regulate Gut Microbiota Composition and Abundance. *mBio,* 12**,** e0082421.

MARTEL, J., CHANG, S. H., KO, Y. F., HWANG, T. L., YOUNG, J. D. & OJCIUS, D. M. 2022. Gut barrier disruption and chronic disease. *Trends Endocrinol Metab,* 33**,** 247-265.

MARTIN, J. L., SANDERS, E. N., MORENO-ROMAN, P., JARAMILLO KOYAMA, L. A., BALACHANDRA, S., DU, X. & O'BRIEN, L. E. 2018. Long-term live imaging of the Drosophila adult midgut reveals real-time dynamics of division, differentiation and loss. *eLife,* 7.

MATEI, D. E., MENON, M., ALBER, D. G., SMITH, A. M., NEDJAT-SHOKOUHI, B., FASANO, A., MAGILL, L., DUHLIN, A., BITOUN, S., GLEIZES, A., HACEIN-BEY-ABINA, S., MANSON, J. J., ROSSER, E. C., KLEIN, N., BLAIR, P. A. & MAURI, C. 2021. Intestinal barrier dysfunction plays an integral role in arthritis pathology and can be targeted to ameliorate disease. *Med,* 2**,** 864-883.e9.

MATHUR, D., BOST, A., DRIVER, I. & OHLSTEIN, B. 2010. A Transient Niche Regulates the Specification of Drosophila Intestinal Stem Cells. *Science,* 327**,** 210-213.

MATOVA, N. & ANDERSON, K. V. 2006. Rel/NF-κB double mutants reveal that cellular immunity is central to Drosophila host defense. *Proceedings of the National Academy of Sciences,* 103**,** 16424.

MCCLURE, C. D., HASSAN, A., AUGHEY, G. N., BUTT, K., ESTACIO-GÓMEZ, A., DUGGAL, A., YING SIA, C., BARBER, A. F. & SOUTHALL, T. D. 2022. An auxin-inducible, GAL4-compatible, gene expression system for Drosophila. *eLife,* 11.

MEHROTRA, S., BANSAL, P., OLI, N., PILLAI, S. J. & GALANDE, S. 2020. Defective Proventriculus Regulates Cell Specification in the Gastric Region of Drosophila Intestine. *Front Physiol,* 11**,** 711.

MICCHELLI, C. A. & PERRIMON, N. 2006. Evidence that stem cells reside in the adult Drosophila midgut epithelium. *Nature,* 439**,** 475-479.

MIGUEL-ALIAGA, I., JASPER, H. & LEMAITRE, B. 2018. Anatomy and Physiology of the Digestive Tract of Drosophila melanogaster. *Genetics,* 210**,** 357-396.

MITCHELL, E. L., DAVIS, A. T., BRASS, K., DENDINGER, M., BARNER, R., GHARAIBEH, R., FODOR, A. A. & KAVANAGH, K. 2017. Reduced intestinal motility, mucosal barrier function, and inflammation in aged monkeys. *The journal of nutrition, health & aging,* 21**,** 354-361.

NEYEN, C., RUNCHEL, C., SCHUPFER, F., MEIER, P. & LEMAITRE, B. 2016. The regulatory isoform rPGRP-LC induces immune resolution via endosomal degradation of receptors. *Nat Immunol,* 17**,** 1150-1158.

NGO, S., LIANG, J., SU, Y. H. & O'BRIEN, L. E. 2020. Disruption of EGF Feedback by Intestinal Tumors and Neighboring Cells in Drosophila. *Curr Biol,* 30**,** 1537-1546 e3.

NICHOLSON, L., SINGH, G. K., OSTERWALDER, T., ROMAN, G. W., DAVIS, R. L. & KESHISHIAN, H. 2008. Spatial and Temporal Control of Gene Expression in Drosophila Using the Inducible GeneSwitch GAL4 System. I. Screen for Larval Nervous System Drivers. *Genetics,* 178**,** 215-234.

OHLSTEIN, B. & SPRADLING, A. 2006. The adult Drosophila posterior midgut is maintained by pluripotent stem cells. *Nature,* 439**,** 470-474.

OSTERWALDER, T., YOON, K. S., WHITE, B. H. & KESHISHIAN, H. 2001. A conditional tissue-specific transgene expression system using inducible GAL4. *Proceedings of the National Academy of Sciences,* 98**,** 12596-12601.

OTANI, S. & COOPERSMITH, C. M. 2019. Gut integrity in critical illness. *Journal of Intensive Care,* 7.

PAIS, I. S., VALENTE, R. S., SPORNIAK, M. & TEIXEIRA, L. 2018. Drosophila melanogaster establishes a species-specific mutualistic interaction with stable gut-colonizing bacteria. *PLOS Biology,* 16**,** e2005710.

PETERSEN, U. M., KADALAYIL, L., REHORN, K. P., HOSHIZAKI, D. K., REUTER, R. & ENGSTRÖM, Y. 1999. Serpent regulates Drosophila immunity genes in the larval fat body through an essential GATA motif. *The EMBO Journal,* 18**,** 4013.

PETKAU, K., FERGUSON, M., GUNTERMANN, S. & FOLEY, E. 2017. Constitutive Immune Activity Promotes Tumorigenesis in Drosophila Intestinal Progenitor Cells. *Cell Reports,* 20**,** 1784-1793.

PICKARD, J. M., MAURICE, C. F., KINNEBREW, M. A., ABT, M. C., SCHENTEN, D., GOLOVKINA, T. V., BOGATYREV, S. R., ISMAGILOV, R. F., PAMER, E. G., TURNBAUGH, P. J. & CHERVONSKY, A. V. 2014. Rapid fucosylation of intestinal epithelium sustains host–commensal symbiosis in sickness. *Nature,* 514**,** 638-641.

PINAL, N., CALLEJA, M. & MORATA, G. 2019. Pro-apoptotic and pro-proliferation functions of the JNK pathway of Drosophila: roles in cell competition, tumorigenesis and regeneration. *Open Biology,* 9**,** 180256.

POIRIER, L., SHANE, A., ZHENG, J. & SEROUDE, L. 2008. Characterization of theDrosophilaGene-Switch system in aging studies: a cautionary tale. *Aging Cell,* 7**,** 758-770.

QI, Y., GOEL, R., KIM, S., RICHARDS, E. M., CARTER, C. S., PEPINE, C. J., RAIZADA, M. K. & BUFORD, T. W. 2017. Intestinal Permeability Biomarker Zonulin is Elevated in Healthy Aging. *Journal of the American Medical Directors Association,* 18**,** 810.e1-810.e4.

RAKOFF-NAHOUM, S., PAGLINO, J., ESLAMI-VARZANEH, F., EDBERG, S. & MEDZHITOV, R. 2004. Recognition of Commensal Microflora by Toll-Like Receptors Is Required for Intestinal Homeostasis. *Cell,* 118**,** 229-241.

REEDY, A. R., LUO, L., NEISH, A. S. & JONES, R. M. 2019. Commensal microbiota induced redox signaling activates proliferative signals in the intestinal stem cell microenvironment. *Development,* 146**,** dev171520.

REGAN, J. C., BRANDÃO, A. S., LEITÃO, A. B., MANTAS DIAS, Â. R., SUCENA, É., JACINTO, A. & ZAIDMAN-RÉMY, A. 2013. Steroid Hormone Signaling Is Essential to Regulate Innate Immune Cells and Fight Bacterial Infection in Drosophila. *PLoS Pathogens,* 9**,** e1003720.

REN, C., WEBSTER, P., FINKEL, S. E. & TOWER, J. 2007. Increased Internal and External Bacterial Load during Drosophila Aging without Life-Span Trade-Off. *Cell Metabolism,* 6**,** 144-152.

RERA, M., BAHADORANI, S., CHO, J., CHRISTOPHER, ULGHERAIT, M., JAE, WILLIAM, LO, T., D & DAVID 2011. Modulation of Longevity and Tissue Homeostasis by the Drosophila PGC-1 Homolog. *Cell Metabolism,* 14**,** 623-634.

RERA, M., CLARK, R. I. & WALKER, D. W. 2012. Intestinal barrier dysfunction links metabolic and inflammatory markers of aging to death in Drosophila. *Proceedings of the National Academy of Sciences,* 109**,** 21528-21533.

RESNIK-DOCAMPO, M., KOEHLER, C. L., CLARK, R. I., SCHINAMAN, J. M., SAUER, V., WONG, D. M., LEWIS, S., D'ALTERIO, C., WALKER, D. W. & JONES, D. L. 2016. Tricellular junctions regulate intestinal stem cell behaviour to maintain homeostasis. *Nature Cell Biology,* 19**,** 52-59.

RESNIK-DOCAMPO, M., SAUER, V., SCHINAMAN, J. M., CLARK, R. I., WALKER, D. W. & JONES, D. L. 2018. Keeping it tight: The relationship between bacterial dysbiosis, septate junctions, and the intestinal barrier in Drosophila. *Fly,* 12**,** 34-40.

RIDLEY, E. V., WONG, A. C. N., WESTMILLER, S. & DOUGLAS, A. E. 2012. Impact of the Resident Microbiota on the Nutritional Phenotype of Drosophila melanogaster. *PLoS ONE,* 7**,** e36765.

RIZK, A., PAUL, G., INCARDONA, P., BUGARSKI, M., MANSOURI, M., NIEMANN, A., ZIEGLER, U., BERGER, P. & SBALZARINI, I. F. 2014. Segmentation and quantification of subcellular structures in fluorescence microscopy images using Squassh. *Nature Protocols,* 9**,** 586-596.

ROGER, L. C. & MCCARTNEY, A. L. 2010. Longitudinal investigation of the faecal microbiota of healthy full-term infants using fluorescence in situ hybridization and denaturing gradient gel electrophoresis. *Microbiology,* 156**,** 3317-3328.

ROH, S. W., NAM, Y.-D., CHANG, H.-W., KIM, K.-H., KIM, M.-S., RYU, J.-H., KIM, S.-H., LEE, W.-J. & BAE, J.-W. 2008. Phylogenetic Characterization of Two Novel Commensal Bacteria Involved with Innate Immune Homeostasis in Drosophila melanogaster. *Applied and Environmental Microbiology,* 74**,** 6171-6177.

ROMAN, G. & DAVIS, R. L. 2002. Conditional expression of UAS-transgenes in the adult eye with a new gene-switch vector system. *genesis,* 34**,** 127-131.
ROMAN, G., ENDO, K., ZONG, L. & DAVIS, R. L. 2001. P{Switch}, a system for spatial and temporal control of gene expression in Drosophila melanogaster. *Proceedings of the National Academy of Sciences,* 98**,** 12602-12607.
ROOS, S., ENGSTRAND, L. & JONSSON, H. 2005. Lactobacillus gastricus sp. nov., Lactobacillus antri sp. nov., Lactobacillus kalixensis sp. nov. and Lactobacillus ultunensis sp. nov., isolated from human stomach mucosa. *International Journal of Systematic and Evolutionary Microbiology,* 55**,** 77-82.
RYU, J.-H., KIM, S.-H., LEE, H.-Y., BAI, J. Y., NAM, Y.-D., BAE, J.-W., LEE, D. G., SHIN, S. C., HA, E.-M. & LEE, W.-J. 2008a. Innate Immune Homeostasis by the Homeobox Gene Caudal and Commensal-Gut Mutualism in Drosophila. *Science,* 319**,** 777-782.
RYU, J. H., KIM, S. H., LEE, H. Y., BAI, J. Y., NAM, Y. D., BAE, J. W., LEE, D. G., SHIN, S. C., HA, E. M. & LEE, W. J. 2008b. Innate Immune Homeostasis by the Homeobox Gene Caudal and Commensal-Gut Mutualism in Drosophila. *Science,* 319**,** 777-782.
SALAZAR, A. M., RESNIK-DOCAMPO, M., ULGHERAIT, M., CLARK, R. I., SHIRASU-HIZA, M., JONES, D. L. & WALKER, D. W. 2018. Intestinal Snakeskin Limits Microbial Dysbiosis during Aging and Promotes Longevity. *iScience,* 9**,** 229-243.
SANCHEZ BOSCH, P., MAKHIJANI, K., HERBOSO, L., GOLD, K. S., BAGINSKY, R., WOODCOCK, K. J., ALEXANDER, B., KUKAR, K., CORCORAN, S., JACOBS, T., OUYANG, D., WONG, C., RAMOND, E. J. V., RHINER, C., MORENO, E., LEMAITRE, B., GEISSMANN, F. & BRÜCKNER, K. 2019. Adult Drosophila Lack Hematopoiesis but Rely on a Blood Cell Reservoir at the Respiratory Epithelia to Relay Infection Signals to Surrounding Tissues. *Developmental Cell,* 51**,** 787-803.e5.
SANDLER, N. G., ZHANG, X., BOSCH, R. J., FUNDERBURG, N. T., CHOI, A. I., ROBINSON, J. K., FINE, D. M., COOMBS, R. W., JACOBSON, J. M., LANDAY, A. L., DOUEK, D. C., TRESSLER, R., READ, S. W., WILSON, C. C., DEEKS, S. G., LEDERMAN, M. M. & GANDHI, R. T. 2014. Sevelamer Does Not Decrease Lipopolysaccharide or Soluble CD14 Levels But Decreases Soluble Tissue Factor, Low-Density Lipoprotein (LDL) Cholesterol, and Oxidized LDL Cholesterol Levels in Individuals With Untreated HIV Infection. *Journal of Infectious Diseases,* 210**,** 1549-1554.
SCOTT, K. P., GRATZ, S. W., SHERIDAN, P. O., FLINT, H. J. & DUNCAN, S. H. 2013. The influence of diet on the gut microbiota. *Pharmacological Research,* 69**,** 52-60.
SHIN, M., FERGUSON, M., WILLMS, R. J., JONES, L. O., PETKAU, K. & FOLEY, E. 2019. Immune Regulation of Intestinal Stem Cell Proliferation and Differentiation in Drosophila. Cold Spring Harbor Laboratory.
SILVERMAN, N. & MANIATIS, T. 2001. NF-κB signaling pathways in mammalian and insect innate immunity. *Genes & Development,* 15**,** 2321-2342.
SILVERMAN, N., ZHOU, R., ERLICH, R. L., HUNTER, M., BERNSTEIN, E., SCHNEIDER, D. & MANIATIS, T. 2003. Immune Activation of NF-κB and JNK Requires Drosophila TAK1. *Journal of Biological Chemistry,* 278**,** 48928-48934.
SINENKO, S. A. & MATHEY-PREVOT, B. 2004. Increased expression of Drosophila tetraspanin, Tsp68C, suppresses the abnormal proliferation of ytr-deficient and Ras/Raf-activated hemocytes. *Oncogene,* 23**,** 9120-9128.
SLACK, E., HAPFELMEIER, S., STECHER, B., VELYKOREDKO, Y., STOEL, M., LAWSON, M. A. E., GEUKING, M. B., BEUTLER, B., TEDDER, T. F., HARDT, W.-D., BERCIK, P., VERDU,

E. F., MCCOY, K. D. & MACPHERSON, A. J. 2009. Innate and Adaptive Immunity Cooperate Flexibly to Maintain Host-Microbiota Mutualism. *Science,* 325**,** 617-620.
SOMMER, F. & BÄCKHED, F. 2013. The gut microbiota — masters of host development and physiology. *Nature Reviews Microbiology,* 11**,** 227-238.
SOMPAYRAC, L. M. 2016. *How the Immune System Works*, Wiley-Blackwell.
SONG, W., VEENSTRA, A., JAN & PERRIMON, N. 2014. Control of Lipid Metabolism by Tachykinin in Drosophila. *Cell Reports,* 9**,** 40-47.
SOUSA-VICTOR, P., AYYAZ, A., HAYASHI, R., QI, Y., MADDEN, D. T., LUNYAK, V. V. & JASPER, H. 2017. Piwi Is Required to Limit Exhaustion of Aging Somatic Stem Cells. *Cell Reports,* 20**,** 2527-2537.
STRAND, M. & MICCHELLI, C. A. 2011. Quiescent gastric stem cells maintain the adult Drosophila stomach. *Proceedings of the National Academy of Sciences,* 108**,** 17696-17701.
STRAND, M. & MICCHELLI, C. A. 2013. Regional Control of Drosophila Gut Stem Cell Proliferation: EGF Establishes GSSC Proliferative Set Point & Controls Emergence from Quiescence. *PLoS ONE,* 8**,** e80608.
STURGEON, C. & FASANO, A. 2016. Zonulin, a regulator of epithelial and endothelial barrier functions, and its involvement in chronic inflammatory diseases. *Tissue Barriers,* 4**,** e1251384.
TEPASS, U., TANENTZAPF, G., WARD, R. & FEHON, R. 2001. Epithelial Cell Polarity and Cell Junctions inDrosophila. *Annual Review of Genetics,* 35**,** 747-784.
THAISS, C. A., LEVY, M., SUEZ, J. & ELINAV, E. 2014. The interplay between the innate immune system and the microbiota. *Current Opinion in Immunology,* 26**,** 41-48.
THAISS, C. A., ZMORA, N., LEVY, M. & ELINAV, E. 2016. The microbiome and innate immunity. *Nature,* 535**,** 65-74.
THEVARANJAN, N., PUCHTA, A., SCHULZ, C., NAIDOO, A., SZAMOSI, J. C., VERSCHOOR, C. P., LOUKOV, D., SCHENCK, L. P., JURY, J., FOLEY, K. P., SCHERTZER, J. D., LARCHÉ, M. J., DAVIDSON, D. J., VERDÚ, E. F., SURETTE, M. G. & BOWDISH, D. M. E. 2018. Age-Associated Microbial Dysbiosis Promotes Intestinal Permeability, Systemic Inflammation, and Macrophage Dysfunction. *Cell Host & Microbe,* 23**,** 570.
TRICOIRE, H., BATTISTI, V., TRANNOY, S., LASBLEIZ, C., PRET, A.-M. & MONNIER, V. 2009. The steroid hormone receptor EcR finely modulates Drosophila lifespan during adulthood in a sex-specific manner. *Mechanisms of Ageing and Development,* 130**,** 547-552.
ULGHERAIT, M., RANA, A., RERA, M., GRANIEL, J. & DAVID 2014. AMPK Modulates Tissue and Organismal Aging in a Non-Cell-Autonomous Manner. *Cell Reports,* 8**,** 1767-1780.
VOGEL, C. & MARCOTTE, E. M. 2012. Insights into the regulation of protein abundance from proteomic and transcriptomic analyses. *Nature Reviews Genetics,* 13**,** 227-232.
WANG, F. & XIA, Q. 2018. Back to homeostasis: Negative regulation of NF-κB immune signaling in insects. *Developmental & Comparative Immunology,* 87**,** 216-223.
WAYLAND, M. T., DEFAYE, A., ROCHA, J., JAYARAM, S. A., ROYET, J., MIGUEL-ALIAGA, I., LEULIER, F. & COGNIGNI, P. 2014. Spotting the differences: Probing host/microbiota interactions with a dedicated software tool for the analysis of faecal outputs in Drosophila. *Journal of Insect Physiology,* 69**,** 126-135.

WERNER, T., LIU, G., KANG, D., EKENGREN, S., STEINER, H. & HULTMARK, D. 2000. A family of peptidoglycan recognition proteins in the fruit fly Drosophila melanogaster. *Proceedings of the National Academy of Sciences,* 97**,** 13772-13777.

WILSON, Q. N., WELLS, M., DAVIS, A. T., SHERRILL, C., TSILIMIGRAS, M. C. B., JONES, R. B., FODOR, A. A. & KAVANAGH, K. 2018. Greater Microbial Translocation and Vulnerability to Metabolic Disease in Healthy Aged Female Monkeys. *Scientific Reports,* 8.

WONG, C. N. A., NG, P. & DOUGLAS, A. E. 2011. Low-diversity bacterial community in the gut of the fruitfly Drosophila melanogaster. *Environmental Microbiology,* 13**,** 1889-1900.

WOODCOCK, KATIE J., KIERDORF, K., POUCHELON, CLARA A., VIVANCOS, V., DIONNE, MARC S. & GEISSMANN, F. 2015. Macrophage-Derived upd3 Cytokine Causes Impaired Glucose Homeostasis and Reduced Lifespan in Drosophila Fed a Lipid-Rich Diet. *Immunity,* 42**,** 133-144.

WU, S.-C., LIAO, C.-W., PAN, R.-L. & JUANG, J.-L. 2012. Infection-Induced Intestinal Oxidative Stress Triggers Organ-to-Organ Immunological Communication in Drosophila. *Cell Host & Microbe,* 11**,** 410-417.

XU, C., TANG, H. W., HUNG, R. J., HU, Y., NI, X., HOUSDEN, B. E. & PERRIMON, N. 2019. The Septate Junction Protein Tsp2A Restricts Intestinal Stem Cell Activity via Endocytic Regulation of aPKC and Hippo Signaling. *Cell Rep,* 26**,** 670-688 e6.

YOUNES, S., AL-SULAITI, A., NASSER, E. A. A., NAJJAR, H. & KAMAREDDINE, L. 2020. Drosophila as a Model Organism in Host-Pathogen Interaction Studies. *Front Cell Infect Microbiol,* 10**,** 214.

ZAIDMAN-RÉMY, A., HERVÉ, M., POIDEVIN, M., PILI-FLOURY, S., KIM, M.-S., BLANOT, D., OH, B.-H., UEDA, R., MENGIN-LECREULX, D. & LEMAITRE, B. 2006. The Drosophila Amidase PGRP-LB Modulates the Immune Response to Bacterial Infection. *Immunity,* 24**,** 463-473.

ZHAI, Z., BOQUETE, J.-P. & LEMAITRE, B. 2017. A genetic framework controlling the differentiation of intestinal stem cells during regeneration in Drosophila. *PLOS Genetics,* 13**,** e1006854.